USGS
science for a changing world

Geological Field Trips in Southern Idaho, Eastern Oregon, and Northern Nevada

Edited by Kathleen M. Haller and Spencer H. Wood

Open-File Report 2004-1222

U.S. Department of the Interior
U.S. Geological Survey

Geological Field Trips in Southern Idaho, Eastern Oregon, and Northern Nevada

Edited by Kathleen M. Haller, and Spencer H. Wood

Contents

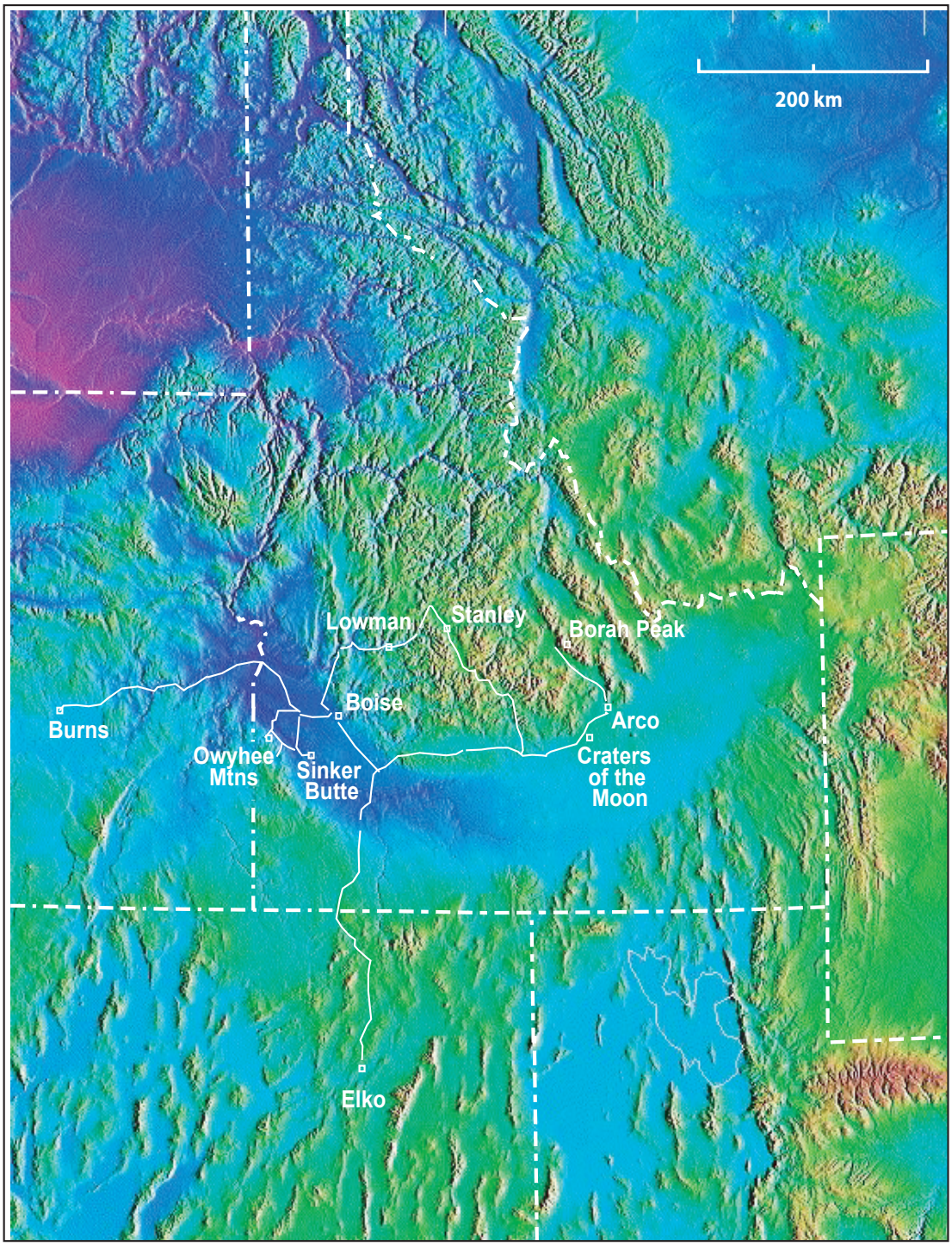

Field-trip routes shown on a digital elevation model (DEM) image (NGSDEM99, National Geodetic Survey, by D.A. Smith and D.R. Roman).

Introduction

This guidebook was produced for the joint Cordilleran (100th Annual) and the Rocky Mountain (56th Annual) Section Meeting of the Geological Society of America in Boise, Idaho, May 1–7, 2004. We are most fortunate in assembling people who have done recent investigations in Idaho, eastern Oregon, and Nevada to write this guidebook and lead the trips. The trips and the guidebook involved authors, leaders, and editors hailing from many universities of the Cordilleran and Rocky Mountain region, the Oregon Department of Mines and Geology, the Idaho Geological Survey, the National Park Service,

the U.S. Bureau of Land Management, and the U.S. Geological Survey. We hope that this cooperative effort to provide new geoscience information will be useful to educators, researchers, government, students, and all those who are interested in the earth and water that underlies this region.

The following provides general locations of the field trips offered in conjunction with the meeting:

The Rattlesnake Tuff and other Miocene silicic volcanism in eastern Oregon. Stops for this field trip are along a circular route (Highways 20, 395, and 26) in the vicinity of Vale and John Day, Oregon. The focus of the trip is the extensive middle to late Miocene rhyolitic ash-flow tuffs that erupted after the main stages of Columbia River Basalt volcanism to the north and Steens Basalt volcanism to the south including the youngest voluminous ash-flow tuff, the 70-Ma Rattlesnake Tuff.

The western margin of North America after the Antler orogeny: Mississippian through Late Permian History in the Basin and Range, Nevada (Cosponsored by the Paleontological Society). Field-trip stops are near Elko and Carlin, Nevada. This trip focuses on the evidence for several Late Paleozoic deformation events that occurred *between* the Antler and Sonoma orogenies. Stops are at field localities that constrain the kinematics of folding and thrusting and the precise timing of angular unconformities that mark the deformation events.

Fire and ice in central Idaho: Modern and Holocene fires, debris flows, and climate in the Payette River Basin, and Quaternary and glacial geology in the Sawtooth Mountains. The first part of this trip, addressing the fire and debris-flow history of the area, follows the South Fork Payette River from Banks to Stanley, Idaho. Storm events following recent fires in the South Fork Payette basin have both produced new deposits and have exposed Holocene fire-related debris-flow and flood sediments and other alluvial fan-building deposits that yield insights into Holocene environmental change. The last two parts of the trip, addressing the glacial history, continue southeast of Stanley along Highway 75 to near Sun Valley, Idaho. Stops address glacial-moraine characteristics and sediment cores from the southeastern Sawtooth Mountains and Stanley Basin that provide evidence of late Pleistocene alpine glaciation. A combination of these glacial records with reconstructions of regional equilibrium line elevations produces late-glacial paleoclimatic inferences for the area.

Owyhee Mountains to the Boise foothills: Geology across and under the western Snake River Plain. This trip traverses the Snake River Plain from the Owyhee front, south of Marsing, Idaho, to the Boise foothills, east of Boise, Idaho and addresses the history of Neogene Lake Idaho along the edges of the western Snake River Plain as recorded in the sedimentary record. The transgressional phase of the last filling of Lake Idaho is marked by an angular unconformity; in the Boise foothills stops are at localities of prodelta muds, Gilbert-deltas, and oolite beds, and finally at the Table Rock Quarries.

Basalt emergent volcanoes and maars, Sinker Butte-Snake River Canyon, Idaho. This trip is at Sinker Butte, which is about 60 miles south of Boise, Idaho. The trip focuses on the sequence of basaltic hydrovolcanic deposits that were erupted from a large emergent Snake River Plain volcano and are now spectacularly well exposed in the walls of the Snake River Canyon. Stops are at localities where deposits having subaqueous and subaerial origins are represented and include the complete sequence of deposits produced at this volcanic center. Volcanism ended with strombolian scoria, spatter, and lava flows.

Twenty years after the Borah Peak Earthquake: Field Guide to Surface-rupturing Earthquakes along the Lost River Fault, Idaho. Following U.S. Highway 93 from Arco to Challis, Idaho, this trip focuses on the character of the historical rupture and the paleoseismic evidence for prehistoric events along this famous normal-fault system. Several stops are along the 34-km-long spectacular surface ruptures from the 1983 (M 7.3) Borah Peak earthquake. Stops north and south of the surface rupture explain the chronology of prehistoric earthquakes along the 140-km-long fault.

Geology of the Craters of the Moon 30' x 60' map area and new perspectives on basaltic volcanism of the eastern Snake River Plain, Idaho. This field trip is in and near Craters of the Moon National Monument, near Arco, Idaho. It focuses on the Holocene and late Pleistocene volcanism confirmed by new $^{40}Ar/^{39}Ar$ ages; geologic mapping of the area around the margins of the Craters of the Moon lava field provides new insights about the processes of basaltic volcanism in Craters of the Moon National Monument.

Miocene Snake River Plain Rhyolites of the Owyhee Front, Owyhee County, Idaho. This trip examines the many forms of rhyolite beautifully exposed along the north side of the Owyhee Mountains, south of Boise, from near Marsing to Walters Ferry, Idaho. This group of rhyolite units seems to have been erupted over a short time after the western Snake River Plain graben started to form and range between 11.7 and 10.6 Ma in age. Stops focus on examining features of rhyolite lava flows, rhyolite spatter, clastigenic units, ignimbrites, domes, and feeder dikes, as well as other features of the western Snake River Plain.

The editors thank the many individuals who served as reviewers for this impressive group of field trip guides.

Kathy Haller, U.S. Geological Survey, Denver, Colorado
Spencer Wood, Boise State University, Boise, Idaho
May 2004

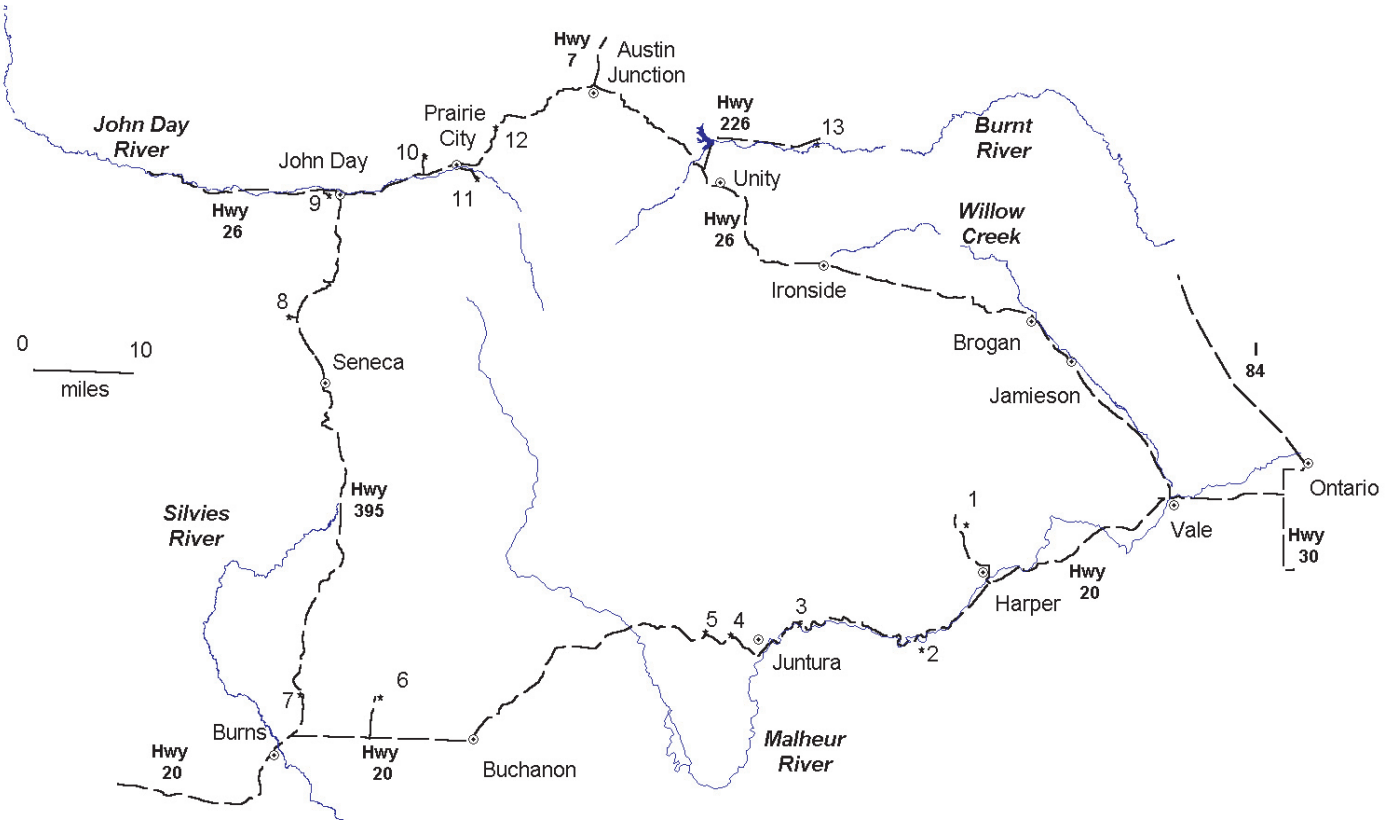

Figure 1. Sketch map of field-trip route. Trip begins at the intersection of Highway 26 and Highway 20, in the town of Vale, Oregon. We will overnight in Burns.

The Rattlesnake Tuff and Other Miocene Silicic Volcanism in Eastern Oregon

By Martin Streck[1] and Mark Ferns[2]

Regional Context of Miocene Silicic Volcanism

Two separate (well maybe not so separate) problems arise when we consider the middle Miocene rhyolite lava flows and ash-flow tuffs exposed along the field-trip route. First, what is the relationship between the older (~15.5 Ma) rhyolites (Dinner Creek Ash-flow Tuff and Littlefield Rhyolite) and the time correlative flood basalts of Columbia River Basalt Group to the north and Steens Basalt to the south? It now is clear that the Columbia River Basalt, the Steens Basalt, and the older rhyolites are part of a larger, bimodal magmatic province (Hooper and others, 2002). Plume-related and back-arc spreading models for the origin of the Columbia River Basalt must account for the very large volumes of silicic magmas that were generated in the southern half of this larger magmatic province. Additionally, genetic models must account for subsequent calc-alkaline volcanism, extension, and rapid subsidence along the Oregon-Idaho graben (Cummings and others, 2000).

Our second problem arises when we consider the younger (7–10 Ma) and equally extensive ash-flow tuffs that erupted from buried vents located to the west near Burns. How do they relate to the initial middle Miocene magmatism? The Burns area ash-flow tuffs (Devine Canyon, Prater Creek, and Rattlesnake ash-flow tuffs) are the largest ash-flow tuffs erupted from a westward-younging belt of rhyolite eruptive centers that culminates at Newberry Caldera (MacLeod and others, 1975). Oldest rhyolites in the west belt are Stockade Mountain and Duck Butte (10.4 Ma), located on the west flank of the Oregon-Idaho graben, just north of the Steens escarpment (MacLeod and others, 1975; Johnson and Grunder, 2000). The general westward-progression of rhyolitic magmatism is complicated by older, enigmatic, small rhyodacite domes near the town of Buchanan (~14 Ma, ~40 km east of Burns) and at Horsehead Mountain (15.5 Ma), west of Burns (MacLeod and others, 1975; MacLean, 1994). Small rhyolite and rhyodacite domes at Double Mountain (8.1 Ma) and ash flow tuffs at Kern Basin (12.6 Ma) record recurrent silicic eruptions on the east end of the trend, within the Oregon-Idaho graben proper (Ferns and others, 1993; Cummings and others, 2000).

The Rattlesnake Tuff

The 7.05-Ma Rattlesnake Tuff covers about 9,000 km^2 but reconstructed original coverage was between 30,000 and 40,000 km^2. Travel distances are among the farthest recorded (Wilson and others, 1995) and were in excess of 150 km from the inferred source near the center of the tuff's distribution based on existing outcrops. Eruption products are mostly (>99 percent) high-silica rhyolites that contain colored glass shards and pumice clasts with narrow and distinct ranges in major element composition but typically large ranges in incompatible trace elements (Streck and Grunder, 1997). Although volumetrically minor, a wide compositional spectrum is indicated by dacite pumices (<1 percent) and quenched basaltic inclusions (<<0.1 percent) that are almost exclusively found in dacite and dacite/rhyolite banded pumices (Streck and Grunder, 1999). Data are most consistent with the following petrogenetic scenarios in the evolution of the Rattlesnake Tuff magmatic system: (1) partial melting of mafic crust yielded rhyolitic melts that were compositionally close to observed, least-evolved high-silica rhyolites (Streck, 2002); (2) fractional crystallization dominated processes led to chemical gradients observed among five compositionally and mineralogically distinct rhyolitic magmas (Streck and Grunder, 1997); and (3) primitive tholeitic magmas stalled beneath rhyolites, evolved to enriched basaltic andesitic magmas (preserved in inclusions) and yielded dacitic compositions after mixing with least-evolved rhyolites (Streck and Grunder, 1999).

Thickness of tuff outcrops is remarkably uniform, ranging between 15 and 30 m for the most complete sections. Only 13 percent of the area is covered with tuff thicker than 30 m, to a maximum of approximately 70 m. Excellent preservation makes it possible to distinguish multiple welding and crystallization facies; in addition, rheomorphic tuff can be found within a radius of 40-60 km from the inferred source (Streck and Grunder, 1995).

[1]Department of Geology, Portland State University, Portland, OR 97207, streckm@pdx.edu

[2]Oregon Department of Geology and Mineral Industries, Portland OR 97207, mark.ferns@state.or.us

Based on vitric unaltered tuff, the entire welding range is subdivided into five mappable facies of welding that are (with associated bulk densities and porosities): nonwelded (<1.5 g/cm^3; >36 percent), incipiently welded (1.50-1.65 g/cm^3; 36-30 percent), partially welded with pumice (1.65-2.05 g/cm^3; 30-12 percent), partially welded with fiamme (2.05-2.30 g/cm^3; 12-2 percent), and densely welded (2.30-2.34 g/cm^3; <2 percent). In the partially welded zone, deformation of pumices precedes one of matrix shards and leads to fiamme composed of dense glass while the shard matrix has a remaining porosity of 12 percent or less.

Degree of welding generally decreases with distance from the source. Densely welded tuff is rare beyond approximately 70 km from the source, and partially welded tuff with fiamme is rare beyond approximately 130 km. A regional change in welding only is observed subtly in the highest welding degrees because strong local variations are often prevail. Local variations complicate simple welding scenarios that imply loss of temperature during travel and/or reduced tuff thickness with distance leads to less welding.

Strong local variations in welding are most dramatic near the source, where observed welding degrees encompasses the entire range. For example, at constant thickness (20±3 m) and over a distance of 1 to 3 km, nonrheomorphic outcrops can grade from an entirely nonwelded to incipiently welded vitric section to a mostly densely welded and crystallized section, where incipiently or less welded tuff is constrained to an approximately 1-m-thick basal zone and presumably a comparably thick top zone (now eroded). This is evident even though crystallization subsequent to welding reduces the vitric tuff proportion. Such strong local variations are interpreted to be the result of threshold-governed welding that imply combined parameters that control welding (T, P, P_{H2O}) create welding conditions that are significantly modified by slight variations in thickness and/or accumulation rate.

ROAD LOG

Mileage Inc.	Cum.	
0	0	Intersection of U.S. Highways 26 and 20 in Vale, Ore. (fig. 1).
2.6	2.6	Double Mountain (fig. 2), a rhyolite dome dated at about 8.1 Ma is visible to the southwest. Double Mountain is one of a number of small, late Miocene silicic centers erupted in

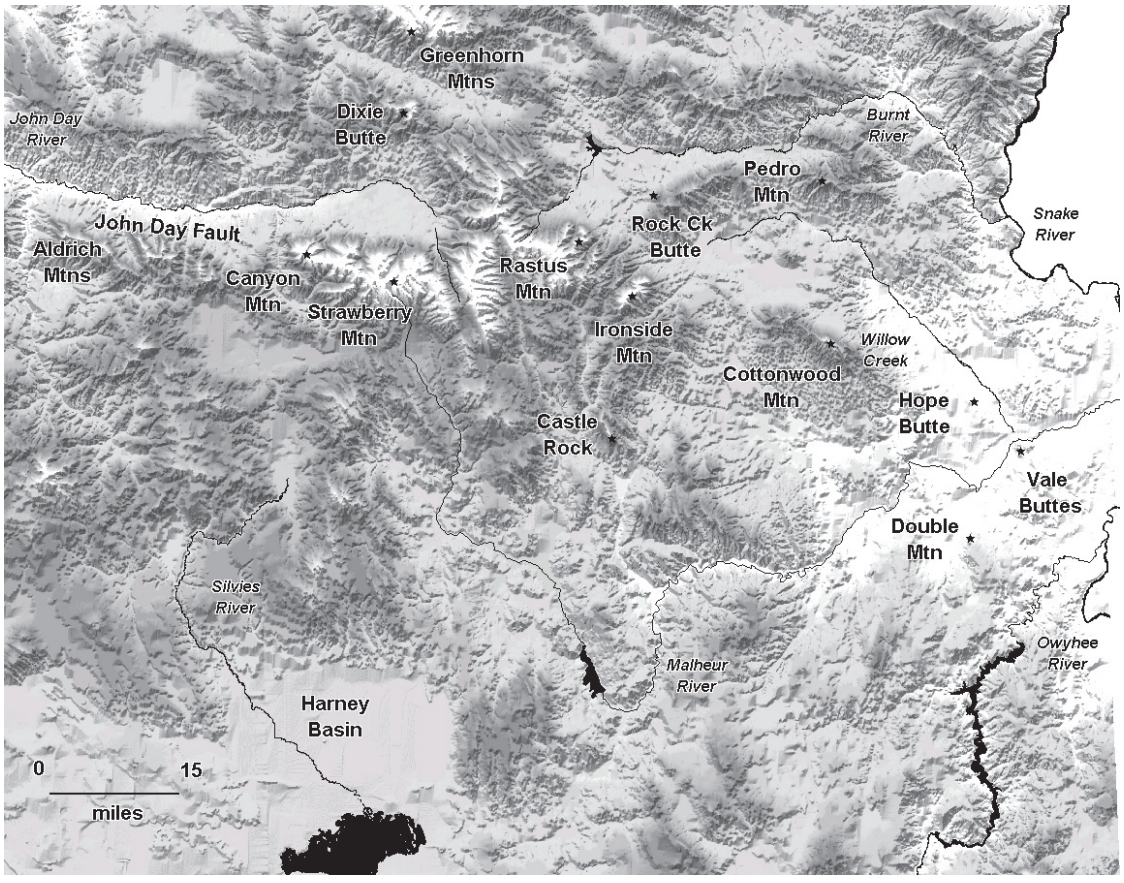

Figure 2. Main physiographic features along the field-trip route.

the central part of the Oregon–Idaho graben between 12 and 8 Ma (fig. 3).

4.0 6.6 Thick flow cropping out along the canyon walls of the Malheur River to the north is a late Miocene, hypersthene-bearing andesite. Referred to as the Vines Hill Andesite by Lees (1994), who reported an $^{40}Ar/^{39}Ar$ radiometric age of 10.25±0.94 Ma. Age is very similar to post Columbia River Basalt Group andesites near La Grande, which have yielded $^{40}Ar/^{39}Ar$ ages of 10.4 Ma (Ferns and others, 2002b).

4.5 11.1 Light-colored exposures are part of the Late Miocene–Pliocene Lake Idaho deposits.

1.2 12.3 Freshwater limestone is exposed overlying the Vines Hill andesite to the northwest. Note the exposures of cross-bedded gravels and sandstones along the highway east of the Vines Hill summit. The highway crosses several poorly expressed north-trending, down to the east faults between 12.3-13.2 mi that juxtapose gravel, limestone, and andesite.

0.9 13.2 Bar ditch exposures of fossiliferous freshwater limestone.

1.2 14.4 An older late Miocene sedimentary sequence is exposed beneath olivine basalt flows to the northwest. Rough radiometric ages from several olivine basalt flows indicate that they erupted at about 7.5 Ma.

0.7 15.1 Highway crosses through the very small town of Little Valley. Active hot springs come up along faults in this area.

2.8 17.9 Light-colored outcrops to the north and south are part of the Bully Creek Formation (Kittleman and others, 1965, 1967). The formation is made up of interbedded fine-grained tuffaceous sediments, diatomite, and interbedded ash-flow tuffs. These fine-grained sediments are unconformable across an older faulted sequence of interbedded arkosic sandstones, palagonitic tuffs, and calc-alkaline lava flows.

3.9 21.8 Turn to the right at Harper junction and cross the abandoned railroad line. TURN RIGHT and proceed to Harper, following the paved road.

0.4 22.3 TURN RIGHT and follow the paved road through Harper, which winds around and turns to the north.

5.6 27.9 If weather conditions allow, turn off of the paved road, proceed through the gate, and follow the dirt road to the cliff-forming outcrops to the north.

Stop 1. Tuff of Bully Creek

The ash-flow tuff prominently exposed here is the lower of two ash-flows mapped by Brooks and O'Brien, (1992a, 1992b) within the Bully Creek Formation. The upper ash-flow tuff, which is locally welded, displays the high Zr (1,200 ppm) signature that is characteristic for the Devine Canyon ash-flow tuff. The lower ash-flow tuff, named by Ferns and others (1993) as the tuff of Bully Creek, is a gray massive ash-rich, phenocryst-poor (<5 percent) tuff that at this location contains entrained and deformed clasts of diatomite and small pumices (~2 cm). Note the centimeter-wide subtle "lineations" across outcrop that are most likely gas-escape pipes. Also, note the fine-grained and glassy, thus excellently preserved, fall-out ash deposit at the base. We do not know whether this ash-flow tuff erupted from a nearby source or, like the Devine Canyon ash-flow tuff, is the distal deposit of a larger eruption, possibly near Burns(?). The ash-rich nature and small pumice size suggest the latter. Lees (1994) reports a $^{40}Ar/^{39}Ar$ age of 10.33±1.59 Ma from the olivine basalt flow that caps the ridge to the east. A question to consider here—Is there evidence in this outcrop for subaqueous flow into a shallow lake?

Mileage
Inc. Cum.

0.7 28.6 Return to the paved road and turn south, following the road back through Harper and onto Highway 20.

6.0 34.6 Turn right on Highway 20 and proceed west towards Burns.

3.0 37.6 Rounded yellow hills to the south are interbedded siltstones, sandstones, and palagonitic tuffs. Here Highway 20 crosses onto a bench formed by a resistant basalt sill. The basalt sill is more than 200-m thick and extends three-fourths of the way up the hill to the south. In places, the margins of the sill are marked by pepperite breccias, indicating intrusion into wet sediments.

1.5 39.1 Eroded hills to the north and south are erosional remnants of middle Miocene sediments. Radiometric ages from interbedded basalt and basaltic andesite flows record an extensive period of subsidence, sedimentation, and synvolcanic calc-alkaline volcanism starting at about 14.5 Ma. Synvolcanic hot spring activ-

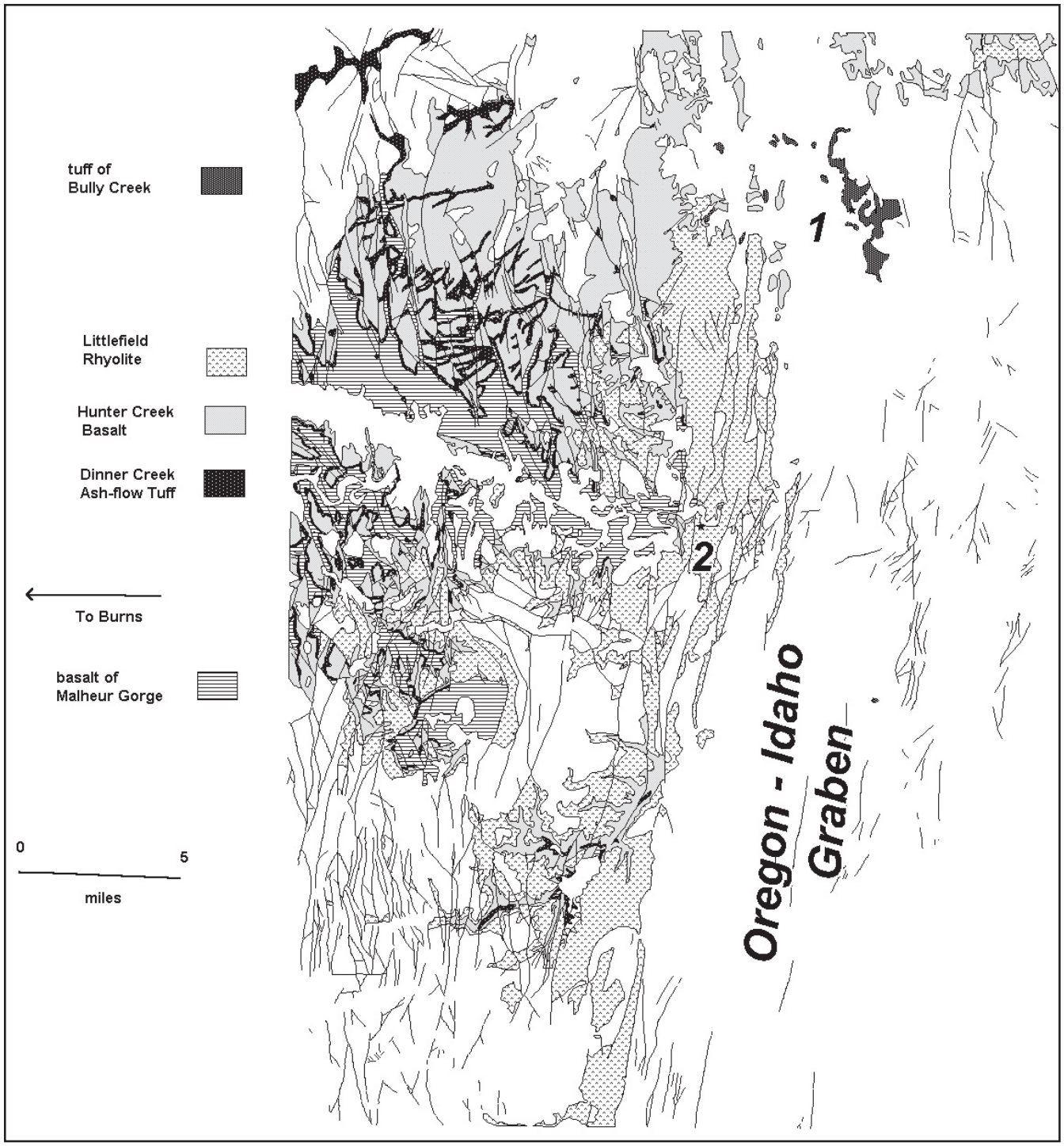

Figure 3. Geologic map of the lower Malheur River after Ferns and others (1993). Locations of Stops 1 and 2 are shown.

ity resulted in extensive areas of epithermal mineralization.

1.0 40.1 Red weathering exposures along the road to the south are part of the outcrops of Littlefield Rhyolite (Kittleman and others, 1965, 1967), which is made up of several very large rhyolite lava flows (fig. 3).

1.0 41.1 U.S. Highway 26 crosses one of the boundary faults to the Oregon-Idaho graben and enters into canyon lands cut by the Malheur River.

Exposures to the north and south are all large rhyolite lava flows.

2.0 43.1 TURN LEFT WITH CAUTION—BE ALERT FOR ONCOMING TRAFFIC onto old Highway 26, which follows along the south side of the Malheur River. We will follow the old highway to a point where all the vehicles can comfortably park; this is Stop 2.

Stop 2. Littlefield Rhyolite

Here the Malheur River cuts through silicic and mafic units that make up the Hog Creek sequence (Hooper and others, 2002). Thin ash-flow tuffs, including the Dinner Creek Ash-flow Tuff (Kittleman and others, 1965, 1967) and the tuff of Namorf (Ferns and O'Brien, 1992), and thick rhyolite lava flows, Littlefield Rhyolite (Kittleman and others, 1965, 1967), mark a transition from mafic to silicic volcanism. Base of the section here is marked by the Hunter Creek Basalt (Kittleman and others, 1967), a series of glassy, aphanitic mafic lava flows that are chemically and petrographically indistinguishable from flows of the Grande Ronde Basalt. The tuff of Namorf (Ferns and O'Brien, 1992), marked by yellow outcrops farther up the hill is perhaps the most inconspicuous ash-flow tuff in the Hog Creek sequence. This ash-rich, phenocryst-poor tuff here is partially welded and glassy. The ash-flow tuff underlies a vitrophyre flow breccia that locally marks the base of one of the large rhyolite lava flows that make up the Littlefield Rhyolite. We will take a closer look at very large basal flow lobes exposed in a side canyon.

The Littlefield Rhyolite is the westernmost example of the enigmatic, very large rhyolite lava flows that erupted during the middle Miocene in southeast Oregon and southwest Nevada. At least 3 separate flows are exposed in the cliff to the south forming a unit that extends over 850 km^2 representing about 100 km^3 of magma. Individual flows are typically glassy with small plagioclase and clinopyroxene phenocrysts. Individual flows can be traced over very large distances. Lees (1994) suggests that the glassy matrix is actually composed of super-welded glass shards, implying that the Littlefield Rhyolite is a series of rheomorphic ash-flow tuffs. Outcrop pattern suggests that the Littlefield Rhyolite may have erupted from linear vents along the western margin of the Oregon-Idaho graben.

Mileage
Inc. Cum.

0.4 43.5 PROCEED WITH CAUTION and turn left onto U.S. Highway 26, heading west toward Burns.

2.9 46.4 The basalt of Malheur Gorge (Evans, 1990; Hooper and others, 2002) is exposed on both sides of the river through here. For all intents and purposes, aphyric flows in the upper part of the basalt of Malheur Gorge cannot be distinguished from Grande Ronde Basalt.

5.5 51.9 Differential weathering of mappable units along the Malheur River has allowed geologists working here to clearly identify faults. The Dinner Creek Ash-flow Tuff is a prominent ledge former that can be easily identified at a distance. The Dinner Creek is nearly always overlain by the Hunter Creek Basalt, which characteristically weathers to form rounded hills mantled by fist-sized blocky talus. The overlying Littlefield Rhyolite typically forms prominent cliffs.

2.0 53.9 Hunter Creek Basalt to the left typically forms hackly-jointed exposures. Note the thin collonade beneath the thick, hackly jointed entabulature.

0.6 54.5 Evans (1990) notes that the Malheur River follows a northwest-trending graben structure. Erosional remnants of diatomaceous sediments and interbedded, partially welded ash-flow tuffs are exposed to the south. Geochemical analyses indicate that one of the ash-flow tuffs is the Devine Canyon Tuff.

0.6 55.1 Much more densely welded exposures of the older Dinner Creek Ash-flow Tuff form prominent cliff bands along the hills to the north and south of the river. Here the Dinner Creek serves as an excellent marker horizon that allows ready identification of faults.

9.3 64.4 Pull out to the right; this is Stop 3.

Stop 3. Dinner Creek Welded Ash-Flow Tuff

The Dinner Creek Welded Ash-flow Tuff (15.2 Ma; Hooper and others, 2002) is an important marker unit that separates the upper, rhyolite-dominated Hog Creek Formation from the basalt of Malheur Gorge. The Dinner Creek Tuff forms distinctive ledges that can be easily traced on both sides of the Malheur River. Mafic lava flows exposed below the Dinner Creek include a lower package of plagioclase phyric flows petrographically similar to the Steens Basalt and an upper package of aphanitic flows that, like the Hunter Creek Basalt, are petrographically and chemically similar to the Grande Ronde Basalt. The Dinner Creek Tuff is rhyolitic in composition and phenocryst poor. The tuff thickens toward a presumed vent area at or near Castle Rock (Rytuba and Vander Meulen, 1991). Based on distribution of mapped outcrops

correlated with the Dinner Creek, the ash-flow covered some 4,000 km^2.

The Dinner Creek Tuff is typically welded and marked by a basal vitrophyre. Devitrified zones are marked by irregular ovoid cavities and spherulites. This locality is somewhat atypical, as many of the cavities are filled with chalcedonic quartz. The tuff is about 20-m thick of which the lowest most 1–2 m consists of the non- to densely welded vitric base.

Mileage Inc.	Cum.	
3.3	67.7	Oasis Café in Juntura.
3.3	71.0	Turn right onto dirt road and drive about 0.1 mi up to the first rim (tilted); this is Stop 4.

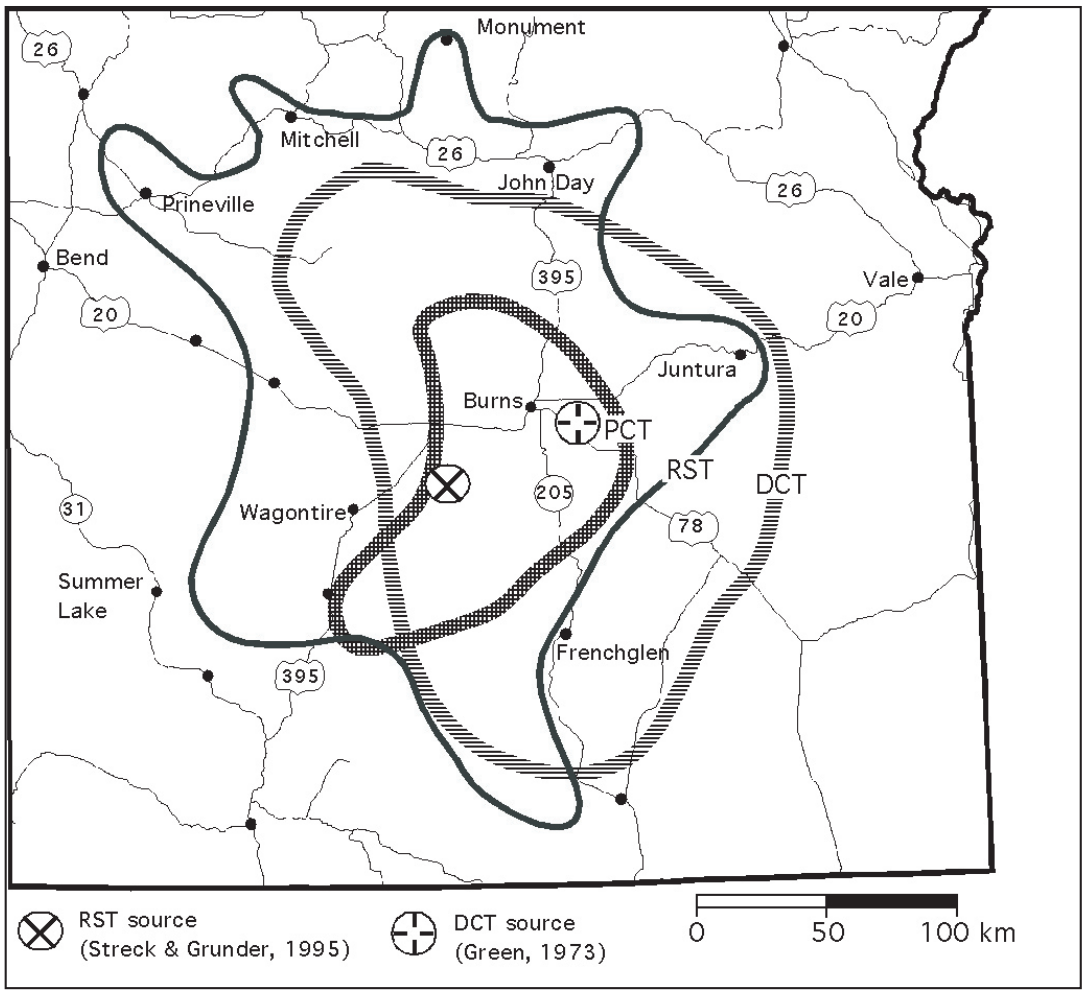

Figure 4. Inferred outlines and source areas of Harney Basin Tuffs. RST, Rattlesnake Tuff; PCT, Prater Creek Tuff; DCT, Devine Canyon Tuff. Outlines for DCT and PCT modified from Green (1973) and Walker (1979), respectively.

Stop 4. Devine Canyon Tuff

The Devine Canyon Tuff is crystal rich and originally covered more than 18,600 km^2 of southeastern Oregon, with a total volume of approximately 195 km^3 (Greene, 1973) (fig. 4). It is characterized by 10–30 percent phenocrysts of alkali feldspar and quartz, with sparse clinopyroxene. It varies from nonwelded to densely welded; most commonly it occurs as greenish-gray stony devitrified tuff. Thickness is about 30 m near the type section about 0.5 km northeast of the confluence with Poison Creek and corresponds to observed maximal thicknesses (Greene, 1973). $^{40}Ar/^{39}Ar$ age of 9.68±0.03 Ma was obtained from sanidine separates (Deino and Grunder, unpublished). At this location, the tuff is nearly densely welded, vitric and exhibits its crystal-rich nature. Tuff cliff is 4–5-m thick.

Mileage Inc.	Cum.	
8.9	79.9	OPTIONAL STOP (along road): diatomite and altered tuff with huge sanidines (~1 cm in diameter).
0.7	80.6	Park along road: Stop 5 is at Drinkwater Pass on descending side westward.

Stop 5. Diatomite and Devine Canyon Tuff

Here, Devine Canyon Tuff is non- to partially welded and vitric; it sits on top of diatomite. The tuff is excellently preserved and such fresh looking non-welded tuff of Devine Canyon Tuff is rather uncommon. Approximate thickness is 10 m.

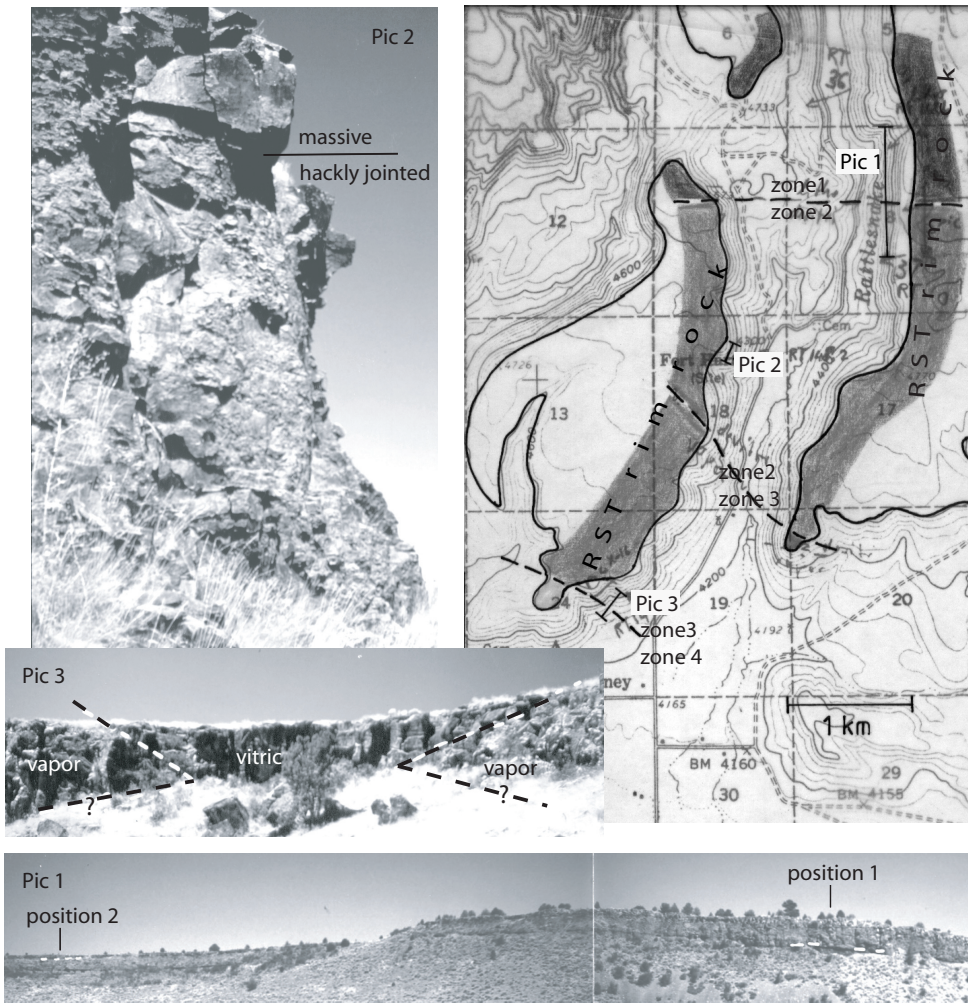

Figure 5. Overview of local facies changes. Zone 1: tuff dominated by thick lithophysal tuff underlying pervasively devitrified tuff and overlying (inferred, not exposed here) lower non- to densely welded vitric tuff. Zone 2: tuff dominated by pervasively devitrified tuff (Pic 2) overlying lower vitric tuff and underlying upper vitric tuff. Zone 3: tuff section consists of partially welded (with pumice) tuff that is vitric or vapor phase altered. Zone 4: vitric incipiently welded tuff. Picture 1: at position 1, densely welded vitrophyre exposed below white dashed line and section is topped with float of upper vitric tuff and at position 2, entire section below white dashed line is lithophysal tuff. Picture 2 shows pervasively devitrified tuff throughout in two facies, hackly jointed and massive. Picture 3: in middle of picture, tuff consists entirely of vitric tuff (vitric) that splits into a lower and upper vitric tuff separated by vapor phase tuff (vapor) further to the right and left, dashed lines indicate position of sharp interfaces between vitric and vapor phase tuff (analogous to the one seen in fig. 13 in Streck and Grunder, 1995).

Mileage Inc.	Cum.	
15.8	96.4	Stinkwater Pass.
0.3	96.7	Lithic-rich hydrovolcanic surge deposits.
5.4	102.1	Town of Buchanan.
3.0	105.1	Rims to right are Rattlesnake Tuff.
7.7	112.8	TURN RIGHT ON Rattlesnake Road.
4.9	117.7	PULL OUT to the right, this is part of Stop 6.

Stop 6. Strong Local Facies Changes in the Rattesnake Tuff

From the distance here and as we drive out of the canyon, we will observe how the Rattlesnake Tuff can drastically change in facies over a distance of 1–3 km without an apparent strong change in thickness (fig. 5). Local and strong facies changes are typical for the Rattlesnake Tuff (see above, Streck and Grunder, 1995) and complicate simple distance driven welding and alteration (high temperature) trends. Across from parking (Zone 2 and position 1 in fig. 5), Rattlesnake Tuff is 17-m thick and prominent outcrop cliff consists mostly of pervasively devitrified tuff underlain by 1.5 m densely welded vitric tuff (black vitrophyre) and capped by float of upper vitric, partially welded tuff. Just north of here (Zone 1, position 2 in fig. 5), outcrop is equally thick but most of section consists now of lithophysal tuff overlain by pervasively devitrified tuff—an analogue of this section with a more complete stratigraphy, but with similar proportional thicknesses of each zone, will be observed at Stop 7. As we drive back and out of Rattlesnake Creek, the first facies change is where thick middle pervasively devitrified section is lost (transition Zone 2-Zone 3 in fig. 5) and replaced by tuff that is partially welded with pumice and has a vapor phase altered zone as upper part (see fig. 13 in Streck and Grunder, 1995). And finally, this gives way to a incipiently welded, vitric tuff at mouth of canyon where the cliff is still 12-m high (Zone 4 in fig. 5).

Constraints on lower tuff boundaries at Stop 6 (*e.g.*, lower vitrophyre), flat lying tuff cliffs, and flat-topped rim rock topography indicate that facies changes are not associ-

ated with great topographic variations over the distance from Stop 6 to mouth of canyon. This suggests that tuff did not change thickness by more that a factor of about two. As mentioned above, Streck and Grunder (1995) interpreted this type of local facies change mostly as a function of the time span the tuff stayed hot above a critical welding temperature. Change in alteration facies is, in turn, largely a function of welding degree, temperature, and amount of vapor.

Mileage Inc.	Cum.	
5.8	123.5	Back on Highway 20.
9.8	133.3	TURN RIGHT at intersection with 395.
3.4	136.7	Pull out to the right, Stop 7.

Stop 7. Rattlesnake Tuff Type Section

This is the type locality of the Rattlesnake Ash-flow Tuff (Walker, 1979), herein referred to as Rattlesnake Tuff (RST). It is named for the original type locality on Rattlesnake Creek (John Day Valley), about 100 km north from here. Total thickness of the tuff at Stop 7 is 22 m. It is a highly zoned section and distance to inferred source is 51 km. The underlying pale-orange to buff-colored, fine-grained, poorly consolidated tuffaceous sedimentary sequence is a ubiquitous slope-forming unit throughout the Harney Basin.

The lowermost white 1-m-thick deposit likely is a precursory fallout deposit to the Rattlesnake Tuff (Streck and Grunder, 1997) resting on a soily substrate (fig. 6). It consists almost entirely of clear glass shards (note: later today we will observe tuff sections at Stops 9 and 11 that consist entirely of this type of glass shard matrix). The fallout deposit is conformably overlain by 0.5 m of nonwelded vitric RST with "mixed" shard matrix (clear and brown rhyolitic glass shards) and 7 to 10 percent white pumice up to 2 cm in diameter. In some places, the transition from the lower deposit to the nonwelded tuff is nearly gradational, and the transition may be overemphasized by the change from white to mixed shard matrix. Bubble wall shards can be seen in both nonwelded and layered deposit. The nonwelded zone grades abruptly to 0.5 m of partially welded vitric tuff, overlain by 1 m of black vitrophyre. The more than 19-m-thick capping cliff-forming unit is entirely lithophysal tuff. The lower 4 m of this section are divided into a perlitic black matrix base and upper part with spherulitic matrix. The upper 15 m are entirely lithophysae in a devitrified matrix and are capped by float of pevasively devirtrified tuff. Just across the highway (east) from this location, float on top of cliff-forming RST also includes upper vitric partially welded tuff indicating proximity to the inferred original top of the unit.

Continue from Stop 7 northward on 395. Highway 395 drives into Poison Creek canyon with excellent exposures of Harney Basin ignimbrite stratigraphy. Lowermost cliff is Devine Canyon Tuff (DCT) separated from the overlying Prater Creek Tuff (PCT) by poorly exposed tuff and tuffaceous sedimentary rocks. The sequence is capped by the Rattlesnake Tuff (RST). The bulk of the ignimbrites is composed of high-silica rhyolites that range from the slightly peralkaline DCT to the peralkaline/metaluminous RST and form important regional stratigraphic and structural markers.

Intercalated-tuffaceous sediments appear to thin until they are completely missing about 40–60 km from here, southward and northward. In the south, the Rattlesnake Tuff directly overlies the Devine Canyon Tuff that also is evident at Stop 8. Similarly, sediments thin westward suggesting

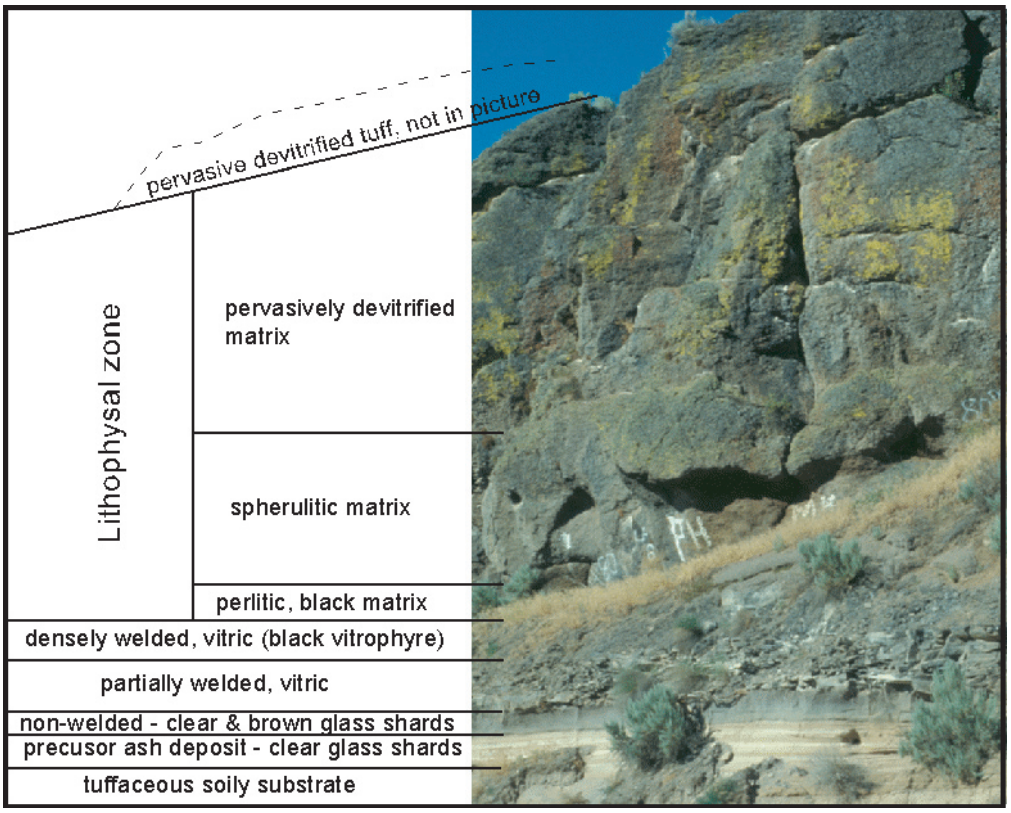

Figure 6. Outcrop stratigraphy of Rattlesnake Tuff at Stop 7.

an active basin existed between about 9 and 7 Ma around Burns extending into what is now the southern termination of the Blue Mountain uplift (Walker and Robinson, 1990).

The Prater Creek Tuff is mainly a devitrified, crystal-poor ash-flow tuff. Exposures of the type section (designated by Walker, 1979) can be seen from U.S. Highway 395 on the walls of Poison Creek where the maximum thickness is 12 m; lithologic variations can be seen in reference sections in Prater Creek, about 5 km east of Poison Creek. The type section consists chiefly of pale grayish-red, devitrified tuff with grayish-pink gas cavities up to about 2 cm in diameter. Flattened, devitrified-pumice fragments are present throughout but are not abundant. Alkali feldspar and quartz are sparse, and the tuff contains rare lithic fragments (Walker, 1979). Devitrified whole-rock tuff gave an age of 8.48±0.05 Ma (Deino and Grunder, unpublished).

Mileage Inc.	Cum.	
1.1	137.8	Prater Creek Tuff rim on left.
2.0	139.8	PULL OUT to the left for OPTIONAL STOP to view Harney Basin Tuff stratigraphy and to inspect partially welded Devine Canyon Tuff with pumices in size up to 30 cm.
10.8	150.6	Mermaid rhyolite flow.
5.5	156.1	Aldrich (left), Canyon (center), and Strawberry Mountains (right) in background (fig. 2). Topographic highs are related to the eroded volcanic edifices of the Strawberry volcanics and to the upthrown side of a high-angle fault. It is thought to be a fairly young reverse fault that substantially displaces the 7.05 Ma Rattlesnake Tuff. The fault trends east-west along the John Day Valley.
18.9	175	Town of Seneca.
7.4	182.4	TURN LEFT at intersection with Izee-Paulina road.
0.3	182.5	Gravel pit in Devine Canyon Tuff, entrance on south side of Izee-Paulina road.
0.8	183.3	Park on either side and walk up dirt road to the north towards open forest. Small cliff outcrop about 30 m past the fence. Small outcrop is Stop 8.

Small cliff outcrop is vitric non- to incipiently welded Rattlesnake Tuff. Tuff also is pumiceous, even though the distance to inferred source is 98 km and thus, the tuff has lost its biggest pumices (average maximum pumice size is 12.3 cm; near the source it reaches >50 cm). Tuff is mostly vitric and displays variously colored glass shards from dark brown to white (clear under microscope) (see fig. 2 in Streck and Grunder, 1997). All shard populations are high-silica rhyolite and coincide lithologically and chemically with high-silica pumice populations (Streck and Grunder, 1997). This mixed-shard matrix observed here is the northernmost exposure of this overall dark, "salt and pepper" appearance. From here northward, the glass matrix consists also of mixed shards, however, darker populations are lost leading to a lighter appearance in outcrop. Similar light tuff is observed closer to the vent only as basal parts of tuff sections, as was observed in basalt part of section at Stop 7.

Before driving back to intersection with U.S. Highway 395, note low subdued hills to the west. These are the erosional tuff remnants of mostly Devine Canyon Tuff as observed at Stop 6. Thus, younger Rattlesnake overlie the older Devine Canyon at this location.

On the way back to U.S. Highway 395, optional Stop at gravel pit exposing vitric, partially welded Devine Canyon Tuff similar to what we observed at Stops 4 and 5. Distance to Stop 5 is about 100 km (figs. 1, 2, and 4).

Mileage Inc.	Cum.	
4.1	187.4	Canyon Mountain ahead (ophiolite complex) As you drive towards John Day—you pass by outcrops of serpentinite after the main decline into the valley when road is on river level.
14.2	201.6	Intersection of U.S. Highway 395 with U.S. Highway 26 in John Day (side trip to Stop 9 from intersection 395 and 26).
1.1	202.7	Intersection of Highway 26 and 47B-Turn left on 47B.
0.5	203.2	Intersection 47B and 47—Turn left on 47.
1.2	204.4	Rattlesnake Tuff outcrop on left: Stop 9.

Stop 9. Thick Distal Rattlesnake Tuff

At Stop 9 we can see an approximately 22-m-thick section of Rattlesnake Tuff in contact with underlying substrate material, a conglomerate consisting of a variety of lithologies eroded from the Aldrich, Canyon, and Strawberry Mountains (side note: the Canyon Mountain ophiolitic complex was exposed at the time since its lithologies can be found as pebbles and cobbles in the conglomerate). This location is 118 km from the inferred RST source. Lithological zonations at Stop 9 include a 1-m-thick nonwelded zone, overlain by about 8 m of partially welded tuff (lower part, about half, "with pumice" and upper half "with fiamme" thus exhibiting higher welding, fig. 7). Lower vitric tuff is overlain by pervasively devitrified tuff (6–8-m thick) and capped by a 2-m-thick vapor phase zone (*i.e.*, porous devitrified tuff). This section illustrates that

only the degree of welding of the thickest tuff sections are systematic indicators of distance-dependent decrease in welding. The highest welding degree of this deposit is "partially welded with fiamme" and not densely, although tuff sections with similar thickness exhibit densely welded zones if closer to the source. No black vitrophyre (*i.e.*, dense welding) was observed beyond a distance of about 70 km. Therefore, an overall temperature decrease and/or volatile loss with distance is indicated very subtly. Another feature to observe here, in comparison to Stop 8, is that this section consists of a matrix characterized by shards that mostly represent the most evolved rhyolite compositions, thus it lacks dark brown coloration.

Mileage Inc.	Cum.	
2.8	207.2	Back at intersection of U.S. Highways 26 and 395 in John Day, continue east on U.S. Highway 26 towards Prairie City.
5.0	213.2	On north side of road, exposures are mainly mafic lavas and one tuff near the base, which will be observed at Stop 10. The tuff likely is the Mascall ignimbrite. For discussion later at Stop 10, note stratigraphic sequence.
0.9	214.1	Lowest most cliffs are more outcrops of Mascall ignimbrite.
1.4	215.5	Crossing John Day River, lower rims on the left (north), about 10-m-thick Mascall ignimbrite.
1.1	216.6	TURN Left (north) on country road, side trip to Stop 10.
1.9	218.5	Mascall outcrop (cliff) on E side a few meters up the slope is Stop 10.

Stop 10. Lithic Rich Tuff—Mascall Ignimbrite

Exposed is a lithic and pumice-rich partially welded vitric tuff. The tuff is correlative based on lithological characteristics with the Mascall ignimbrite of Davenport (1971) found in the Paulina Basin 80 km west southwest from here. The ignimbrite was named for its occurrence near the base of the Mascall formation. The Mascall formation was established by Merriam (1901) for a sedimentary sequence near the Mascall Ranch and in the vicinity of Picture Gorge, proper. The tuff was dated by K-Ar yielding an age of 15.8±1.4 Ma that is consistent with mammalian fossils of Barstovian age found above the ignimbrite (Davenport, 1971). Mineral phases in the Mascall ignimbrite are anorthoclase, magnetite, green clinopyroxene, and zircon, and bulk composition is high-silica rhyolite with 75 weight percent SiO_2 (Davenport, 1971). The Mascall ignimbrite is characterized by abundant (5–10 percent) lithic obsidian clasts, which distinguish this tuff from the Rattlesnake Tuff that is otherwise lithologically similar. Widespread occurrence of abundant obsidian clasts may suggest that pyroclastic eruptions leading to the Mascall ignimbrite reworked previous dome material that predated the voluminous Mascall eruption. Chemical analysis to evaluate this hypothesis is currently underway. Although Mascall ignimbrite outcrops occur sparsely, their spacing of about 100 km apart indicate that the Mascall ignimbrite also was an originally widespread tuff unit resulting from a voluminous, likely-caldera forming eruption. Petrography and composition indicate affinities to Harney Basin tuffs and thus an original source for the Mascall ignimbrite may lie well to the south.

The correlation of this outcrop and outcrops nearby (see above and below) with the Mascall ignimbrite has significant stratigraphic implications. The thick section of mafic lava flows, which has been visible in the bluffs north of U.S. Highway 26 east of John Day, cannot be

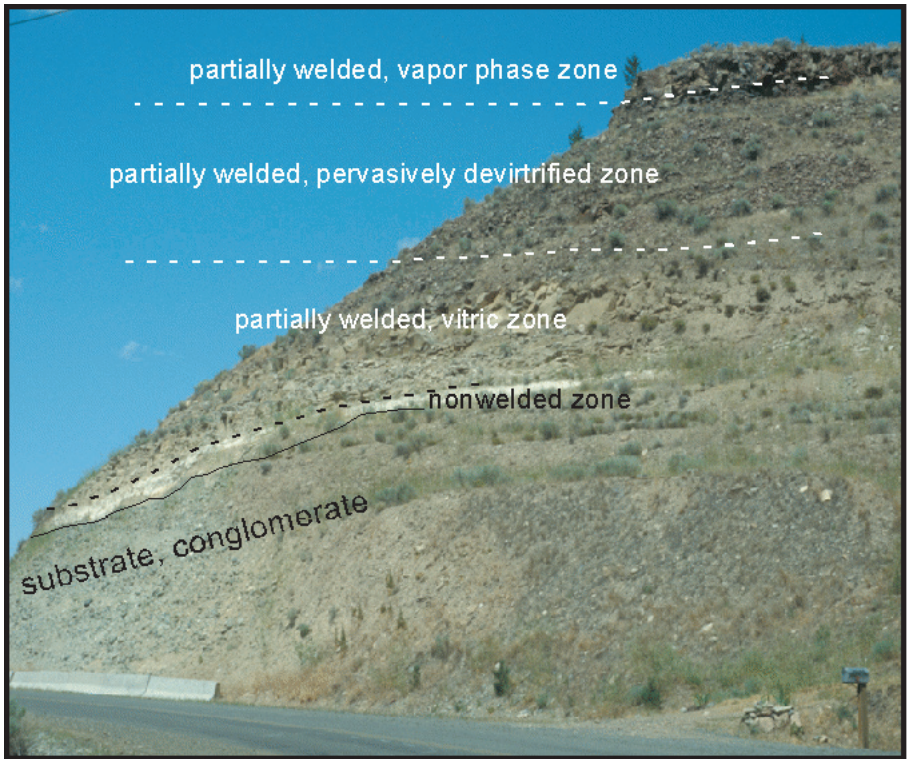

Figure 7. Outcrop stratigraphy of Rattlesnake Tuff at Stop 9.

Picture Gorge Basalt flows because of their post-Mascall age (Mascall formation overlies unconformably the Picture Gorge basalts at Picture Gorge). Much of the area north and west from here was previously mapped as Columbia River Basalt (Thayer and Brown, 1964; Brooks and others, 1984). However, chemical analyses may imply that this area is underlain mainly by younger calc-alkaline flows (see analyses in Brooks and others, 1984) that more properly belong in the Strawberry Volcanics of Thayer and Brown (1964). Very limited geochemical analyses from mafic lavas flows north of here in apparently the same stratigraphic position as the post-Mascall flows present here, do not correlate with chemistries of any of the Picture Gorge flows.

RETURN TO U.S. Highway 26 and continue east towards Prairie City.

Mileage Inc.	Cum.	
2.5	221	U.S. Highway 26 cuts into Mascall ignimbrite, which also is exposed as cliff on north side of road.
3.0	224	Intersection Main Street and U.S. Highway 26 in Prairie City: Side trip to Stop 11 from this intersection; TURN RIGHT onto Main Street and continue.
0.4	224.4	TURN Left into Bridge Street at intersection of Main Street and Bridge Street; continue on Bridge Street that will turn into country road #62 after next intersection; Stop 11 (along country road #62).
4.2	228.6	Park in turn out next to outcrop on south side of road. Light outcrops are Stop 11.

Stop 11. Non-Welded Rattlesnake Tuff

Outcrop is 4-m thick and consists entirely of nonwelded Rattlesnake Tuff. Distance to inferred source is 133 km and thus pumices are small. Average maximum size is 4 cm. This outcrop is extraordinary for the nonwelded nature, yet excellent preservation. Outcrop is entirely glassy and shards are mostly clear and, if juxtaposed with matrix of Stop 8, a strong color contrast is apparent that reflects the change in proportions among shard populations. Material from this outcrop was used for welding experiments of Grunder and Druitt and Quane and Russell (both submitted to JVGR's special volume on welding).

TRACK BACK TO intersection Main Street and U.S. Highway 26 in Prairie City, continue on U.S. Highway 26 eastward.

Mileage Inc.	Cum.	
6.4	235.0	Stacked sequence of olivine basalt flows and underlying lithic ash-flow tuff is exposed in the hills immediately to the north of U.S. Highway 26. Although the olivine basalt flows generally are considered to be part of the Picture Gorge Basalt, not enough work has been done on them to confirm that correlation. Presence of an underlying ash-flow tuff here is troubling.
0.2	235.2–235.5	**OPTIONAL STOP.** Oligocene(?) ignimbrite. Directly along east side of road, small outcrops of biotite and amphibole bearing welded tuff. Presence of biotite and amphibole in the tuff here suggests that it may be an Oligocene ash-flow tuff. Oligocene–early Miocene tuffs elsewhere in the region, at Tower Mountain and near Unity Reservoir (Ferns and others, 2001), generally contain hydrous mineral phases, in contrast to the middle Miocene ash-flow tuffs, which generally do not. Radiometric dates are needed before this conundrum can be resolved. The overlying olivine basalt flows appear more similar to the early calc-alkaline mafic eruptions associated with the Powder River Volcanic Field (Ferns and others, 2001; 2002a) than to the Picture Gorge Basalt. The olivine basalt flows may represent early stages of Strawberry Volcanics magmatism.
4.4	239.9	TURN OUT on right shoulder for Stop 12.

Stop 12. Early Oligocene Dacite at the Fireside Inn—33 Ma

Here we will look at one of the older Oligocene bimodal volcanic centers exposed in northeast Oregon. Early Oligocene silicic eruptions produced distinctive, coarse-textured porphyritic dacites and rhyolites that, unlike most of the later middle Miocene ash-flow tuffs, contain hydrous mineral phases such as biotite and hornblende. The road cut exposes a dacite dome and dome breccia that is cut by several porphyritic basalt dikes. Although this particular dome has not been dated, nearby porphyritic dacites have yielded radiometric ages of about 33.6 Ma (Ferns and others, 1982) and 33.7 Ma (Urbanczyk, 1990). Similarly aged granodiorite intrusions to the southeast (Hooper and others, 1995) and possibly to the west are associated with porphyry copper mineralization. Somewhat younger (~25–28 Ma) eruptions of rhyolitic ash-flow tuffs accompanied formation of large calderas at Tower Mountain (Ferns and others, 2001).

Mileage Inc.	Cum.	
2.1	242.0	Some of the oldest (~42 Ma) Tertiary volcanic rocks exposed in northeast Oregon form columnar jointed outcrops on the north side of U.S. Highway 26, just east of the Dixie Mountain pass. Andesite breccias of similar age are exposed on the side of Dixie Mountain to the north, filling an eroded surface of older pre-Tertiary rocks. Pre-Tertiary rocks exposed along U.S. Highway 26 to the east are parts of a serpentinite-matrix mélange.
0.9	244.1	Prominent outcrops of basaltic andesite exposed along the road here are part of the Slide Creek Basalt (Robyn, 1979) the basal member of the Strawberry Volcanics. Age of the Slide Creek generally is considered to be about 15 Ma.
4.0	248.1	Continue east on U.S. Highway 26, through Austin Junction, bypassing the turn off to Baker City and Sumpter. The Greenhorn Mountains, which form the high ridge to the northwest, are part of a serpentinite-matrix mélange.
0.7	248.8	Diatomite and tuffaceous sediments are exposed beneath a basalt flow. Although generally considered to be part of the Slide Creek Basalt, this flow may be younger than the Slide Creek. The diatomite beds locally contain abundant leaf fossils and may be similar in age to Bully Creek Formation.

Strawberry Volcanics

The Strawberry Volcanics, originally defined by Thayer (1957) is one of the largest, most diverse, and most poorly mapped units in eastern Oregon. Although generally considered to be middle Miocene in age and representative of a post-Columbia River Basalt Group calc-alkaline complex (Robyn, 1979), areas now mapped as Strawberry Volcanics contain both older late Oligocene–early Miocene rhyolite and dacites (Walker and Robinson, 1990) and younger late Miocene–Pliocene mafic lavas. Much of the area was heavily forested when first mapped. Subsequent large forest fires have considerably reduced the amount of concealing ground cover, making this region an ideal candidate for future mapping and study.

Mileage Inc.	Cum.	
4.2	253.0	Red-weathering basaltic andesite flow with abundant, large plagioclase phenocrysts. Not clear where this flow lies in respect to the diatomite section.
2.8	255.8	Platy andesite flow.
3.7	259.5	Tuffaceous sediments are exposed beneath andesite flows as U.S. Highway 26 descends into the upper end of the Burnt River valley.
1.8	261.3	Aphyric basalt flow; overlies tuffaceous sediments and, to the south, ash-flow tuff.
2.1	263.4	Badlands topography with erosional remnants of basalt flows overlying tuffaceous sediments. Thick ash flow is exposed in ditch beneath basalt flow to south.
1.5	264.9	Intersection of Highway 245 and U.S. Highway 26. Side trip to Stop 13 (optional). Proceed left onto Highway 245 and continue 2.6 miles to Unity Reservoir. Note: Cumulative mileage does not include this side trip.

Stop 13. Unity Reservoir

Ridge to north of reservoir is a fault block capped by what appears to be an older Oligocene ash-flow tuff. According to Reef (1983), there are three ignimbrite units exposed in the upper part of the fault block (fig. 8)—a lower pumiceous tuff, an overlying, densely welded vitric tuff; and a capping, partially welded lithic tuff. All three seem to be associated with basal vitrophyres. The lower two tuffs contain biotite crystals. A thick rhyolite dome truncates the ash-flow tuffs to the northwest. The ash-flow tuff rests atop a series of thick rhyodacite lahars and tuff breccias. A rhyodacite clast in the tuff breccia has a K/Ar age of 19.5 Ma (Fiebelkorn and others, 1983). Fossilized palm boles have been found in the top of an ash-flow further to the east.

Mileage Inc.	Cum.	
0.1	265.0	An uplifted block of pre-Tertiary basement rocks is exposed to the south. West flank of the uplift is unconformably overlain by flows of the Strawberry Volcanics. The uplift, the exposed front of which forms Bullrun Rock and Rastus Mountain, is cored by mineralized Oligocene porphyry intrusions (Hooper and others, 1995).
3.1	268.1	Town of Unity—The Waterhole and the High Country Café.
1.8	269.9	Rock Creek Butte, at 12:30, is a slab of peridotite in another uplifted block of basement

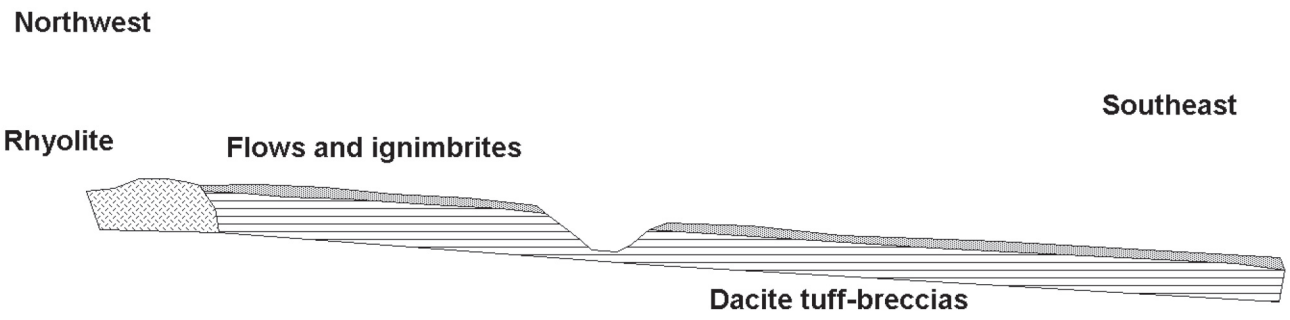

Figure 8. Stratigraphic section at Stop 13 at Unity Reservoir.

rock. Rock Creek Butte marks a pre-Tertiary terrane boundary.

4.8	274.7	Columnar jointed porphyritic lava flow, not known whether it is Miocene or older in age.
1.3	276.0	The thick ash-flow tuff exposed along the road here is mapped as Dinner Creek Tuff. Note that exposures here are much thicker than those seen along the Malheur River.
0.9	276.9	The prominent butte to the south is Ironside Mountain. Formed by dacite and rhyolite flows filling a small, oval depression above Jurassic sediments. Although considered to be a complex folded fault structure (Thayer and Brown, 1973) it might be a collapsed central vent structure related to the eruption of middle Miocene ash flows.
0.2	277.1	Jurassic volcaniclastic sediments of the Weatherby Formation (Brooks, 1979) exposed along the highway.
0.5	277.6	Highway crosses onto younger Pliocene lava flows first mapped by Brooks and others (1976). Flows are alkalic lavas and part of the Keeney Creek.
1.2	278.8	Eldorado Pass. Late Miocene to Pliocene, fluvial and lacustrine sediments are exposed that underlie the Keeney Creek Formation.
6.9	285.7	Rounded hill to east is a Pliocene cinder cone that still retains a cone form.
0.6	286.3	Town of Ironside, high ground in distance is Pedro Mountain, a late Jurassic–early Cretaceous intrusion. Intrusion was emplaced along a pre-Tertiary terrane boundary. Pedro Mountain is cut by a swarm of north-trending Columbia River Basalt dikes. Geochemical analyses indicate the dikes are all Grande Ronde Basalt. Black double butte in the middle ground is another one of the small Keeney Creek vents.
6.9	293.2	High ridge to the south is Cottonwood Mountain, which is made up of pre-Tertiary rocks, Malheur Gorge Basalt flows, and capping Littlefield Rhyolite flows. Hooper and others (2002) consider the upper basalt of Malheur Gorge to be correlative with the Grande Ronde Basalt. Small hill to the left is Cow Valley Butte, a small, undated, granitic intrusion assumed to be of late Jurassic–early Cretaceous age.
4.0	297.2	At Cow Creek, more basalt of Malheur Gorge flows exposed to right.
6.2	303.4	Underlying exposures of Jurassic sediments, Weatherby Formation (Brooks, 1979).
1.4	304.8	Pliocene Keeney Creek Formation flows to east.
2.3	307.1	A large displacement fault runs along the foot of Cottonwood Mountain to the southwest; in places it cuts alluvial fans. This may well be an active Holocene fault.
2.1	309.2	Town of Brogan.
2.4	311.6	Low hills are eroded remnants of late Miocene and Pliocene sediments. Sediments can be traced eastward into the western Snake River Plain. Generally considered that they were deposited in the large Pliocene Lake Idaho.
3.7	315.3	Town of Jamieson.
0.8	316.1	Rounded butte to the right at 2:30 is Hope Butte. Top of the butte is underlain by hot spring sinter deposits. Hot spring activity was accompanied by mercury and gold mineralization.

0.9	317	Vale Buttes comes into view at 11:30. The buttes are a hydrothermally hardened mass of Pliocene sandstone and siltstone. Several active hot springs vent into the river from the west side of the buttes. Alteration zones are marked by mercury and gold mineralization.
15.5	332.5	Intersection of U.S. Highways 26 and 20.

END of road log

References

Brooks, H.C., 1979, Geologic map of the Huntington and part of the Olds Ferry quadrangles, Baker and Malheur Counties, Oregon: Oregon Department of Geology and Mineral Industries Geologic Map Series GMS-13, scale 1:62,500.

Brooks, H.C., McIntyre, J.R., and Walker, G.W., 1976, Geology of the Oregon part of the Baker 1 degree x 2 degree quadrangle: Oregon Department of Geology and Mineral Industries Geological Map Series GMS-7, scale 1:250,000.

Brooks, H.C., Ferns, M.L., and Avery, D.G., 1984, Geology and gold deposits of the southwest quarter of the Bates quadrangle, Grant County, Oregon: Oregon Department of Geology and Mineral Industries Geological Map Series GMS-35, scale 1:24,000.

Brooks, H.C., and O'Brien, J.P., 1992a, Geology and mineral resources map of the Westfall quadrangle, Malheur County, Oregon: Oregon Department of Geology and Mineral Industries Geologic Map Series GMS-71, scale 1:24,000.

Brooks, H.C., and O'Brien, J.P., 1992b, Geology and mineral Resources map of the Little Valley quadrangle, Malheur County, Oregon: Oregon Department of Geology and Mineral Industries Geologic Map Series GMS-72, scale 1:24,000.

Cummings, M.L., Evans, J.G., Ferns, M.L., and Lees, K.R., 2000, Stratigraphic and structural evolution of the middle Miocene syn-volcanic Oregon-Idaho graben: Geological Society of America Bulletin, v. 112, p. 668–682.

Davenport, R.E., 1971, Geology of the Rattlesnake and older ignimbrites in the Paulina basin and adjacent area, central Oregon: Corvallis, Oregon State University, unpublished Ph.D. thesis, 132 p.

Evans, J.G., 1990, Geology and mineral resources map of the Jonesboro quadrangle, Malheur County, Oregon: Oregon Department of Geology and Mineral Industries Geological Map Series GMS-66, scale 1:24,000.

Ferns, M.L., Brooks, H.C., and Ducette, J., 1982, Geology and mineral resources map of the Mt Ireland quadrangle, Baker and Grant Counties, Oregon: Oregon Department of Geology and Mineral Industries Geologic Map Series GMS-22, scale 1:24,000.

Ferns, M.L., and O'Brien, J.P., 1992, Geology and mineral resources map of the Namorf quadrangle, Malheur County, Oregon: Oregon Department of Geology and Mineral Industries Geologic Map Series GMS-74, scale 1:24,000.

Ferns, M.L., Brooks, H.C., Evans, J.G., and Cummings, M.L., 1993, Geologic map of the Vale 30' x 60' quadrangle, Malheur County, Oregon and Owyhee County, Idaho: Oregon Department of Geology and Mineral Industries Geologic Map Series GMS-77, scale 1:100,000.

Ferns, M.L., Madin, I.P., and Taubeneck, W.H., 2001, Reconnaissance geologic map of the La Grande 30' x 60' quadrangle, Baker, Grant, Umatilla, and Union Counties, Oregon: Oregon Department of Geology and Mineral Industries Reconnaissance Map Series RMS-1, scale 1:100,000.

Ferns, M.L., McConnell, V.S., and Madin, I.P., 2002a, Geology of the surface and subsurface of the southern Grande Ronde Valley and lower Catherine Creek drainage, Union County, Oregon: Oregon Department of Geology and Mineral Industries Open File Report O-02-02.

Ferns, M.L., McConnell, V.S., and Van Tassell, J., 2002b, Geology of the Imbler quadrangle, Union County, Oregon: Oregon Department of Geology and Mineral Industries Geology Map Series GMS-114, scale 1:24,000.

Fiebelkorn, R.B., Walker, G.W., MacLeod, N.S., McKee, E.H., and Smith, J.G., 1983, Index to K-Ar determinations for the State of Oregon: Isochron/West, v. 37, p. 3–60.

Greene, R.C., 1973, Petrology of the welded tuff of Devine Canyon, southeastern Oregon: U.S. Geological Survey Professional Paper 792, 26 p.

Hooper, P.R., Housemann, M.D., Beane, J.E., Caffrey, G.M., Enght, K.R., Scrivner, J.V., and Watkinson, A.J., 1995, Geology of the northern part of the Ironside Mountain inliern, northeastern Oregon, *in* Vallier, T.L., and Brooks, H.C., eds., Petrology and tectonic evolution of pre-Tertiary rocks of the Blue Mountains region: U.S. Geological Survey Professional Paper 1438, p. 415–457.

Hooper, P.R., Binger, G.B., and Lees, K.R., 2002, Ages of the Steens and Columbia River flood basalts and their relationship to extension-related calc-alkalic volcanism in eastern Oregon: Geological Society of America Bulletin, v. 114, p. 43–50.

Johnson, J. A., and Grunder, A.L., 2000, The making of intermediate composition magma in a bimodal suite—Duck Butte eruptive center, Oregon, USA: Journal of Volcanology and Geothermal Research, v. 95, p. 175–195.

Kittleman, L.R., Green, A.R., Haddock, G.H., Hagood, A.R., Johnson, A.M., McMurray, J.M., Russell, R.G., and Weeden, D.A., 1965, Cenozoic stratigraphy of the Owyhee region, south-eastern Oregon: University of Oregon Museum of Natural History Bulletin, 45 p.

Kittleman, L.R., Green, A.R., Haddock, G.H., Hagood, A.R., Johnson, A.M., McMurray, J.M., Russell, R.G., and Weeden, D.A., 1967, Geologic map of the Owyhee region, Malheur County, Oregon: University of Oregon Museum of Natural History Bulletin, scale 1:125,000.

Lees, K.R., 1994, Magmatic and tectonic changes through time in the Neogene volcanic rocks of the Vale area, Oregon, northwestern U.S.A.: Milton Keynes, U.K., Open University, unpublished Ph.D. thesis, 283 p.

MacLean, J.W., 1994, Geology and geochemistry of Juniper Ridge, Horsehead Mountain and Burns Butte—Implications for the petrogenesis of silicic magmas on the High Lava Plains, southeastern Oregon: Corvallis, Oregon State University, unpublished M.S. thesis, 141 p.

MacLeod, N.S., Walker, G.W., and McKee, E.H., 1975, Geothermal significance of eastward increase in age of Upper Cenozoic rhyolitic domes in southeastern Oregon: U.S. Geological Survey Open-File Report 75-348, 21 p.

Merriam, J.C., 1901, A contribution to the geology of the John Day Basin: University of California Publications in Geological Sciences 2, p. 269–314.

Robyn, T.L., 1979, Miocene volcanism in eastern Oregon—An example of calc-alkaline volcanism unrelated to subduction: Journal of Volcanological and Geothermal Research, v. 5, p. 149–161.

Reef, J.W., 1983, The Unity Reservoir rhyodacite tuff-breccia and associated volcanic rocks, Baker County, Oregon: Pullman, Washington State University, unpublished M.S. thesis, 128 p.

Rytuba, J.J., and Vander Meulen, D.B., 1991, Hot-spring precious-metal systems in the Lake Owyhee volcanic field, Oregon-Idaho, *in* Raines, G.L., Lisle, R.E., Schafer, R.W., and Wilkinson, W.H., eds., Geology and ore deposits of the Great Basin: Reno, Geological Society of Nevada, Symposium Proceedings, April 1–5, 1990, v. 2, p. 1085–1096.

Streck, M.J., 2002, Partial melting to produce high-silica rhyolites of a young bimodal suite—Compositional constraints among rhyolites, basalts, and metamorphic xenoliths: International Journal of Earth Sciences, v. 91, p. 583–593.

Streck, M.J., and Grunder, A.L., 1995, Crystallization and welding variations in a widespread ignimbrite sheet—The Rattlesnake Tuff, eastern Oregon: Bulletin of Volcanology, v. 57, p. 151–169.

Streck, M.J., and Grunder, A.L., 1997, Compositional gradients and gaps in high-silica rhyolites of the Rattlesnake Tuff, Oregon: Journal of Petrology, v. 38, p. 133–163.

Streck, M.J., and Grunder, A.L., 1999, Enrichment of basalt and mixing of dacite in the rootzone of a large rhyolite chamber—Inclusions and pumices from the Rattlesnake Tuff, Oregon: Contributions to Mineralogy and Petrology, v. 136, p. 193–212.

Thayer, T.P., 1957, Some relations of later Tertiary volcanology and structure in eastern Oregon: International Geological Congress, Volcanologia del Cenozoico, v. 1, p. 231–245.

Thayer, T.P. and Brown, C.E., 1964, Pre-Tertiary orogenic and plutonic intrusive activity in central and northeastern Oregon: Geological Society of America Bulletin, v. 75, p. 1255–1261.

Thayer, T.P. and Brown, C.E., 1973, Ironside Mountain, Oregon—A Late Tertiary volcanic and structural enigma: Geological Society of America Bulletin, v. 84, p. 489–497.

Urbanczyk, K.M., 1990, Geology of the eastern part of the Clarno Formation, northeast Oregon: Pullman, Washington State University, unpublished Ph.D. thesis, 263 p.

Walker, G.W., 1979, Revisions to the Cenozoic stratigraphy of Harney Basin, Oregon: U.S. Geological Survey Bulletin 1475, 35 p.

Walker, G.W., Robinson, P.T., 1990, Cenozoic tectonism and volcanism of the Blue Mountains region, *in* Walker G.W., ed., Geology of the Blue Mountains region of Oregon, Idaho, and Washington: U.S. Geological Survey Professional Paper 1437, p. 119–135.

Wilson, C.J.N., Houghton, B.F., Kamp, P.J.J., and McWilliams, M.O., 1995, An exceptionally widespread ignimbrite with implications for pyroclastic flow emplacement: Nature, v. 378, p. 605–607.

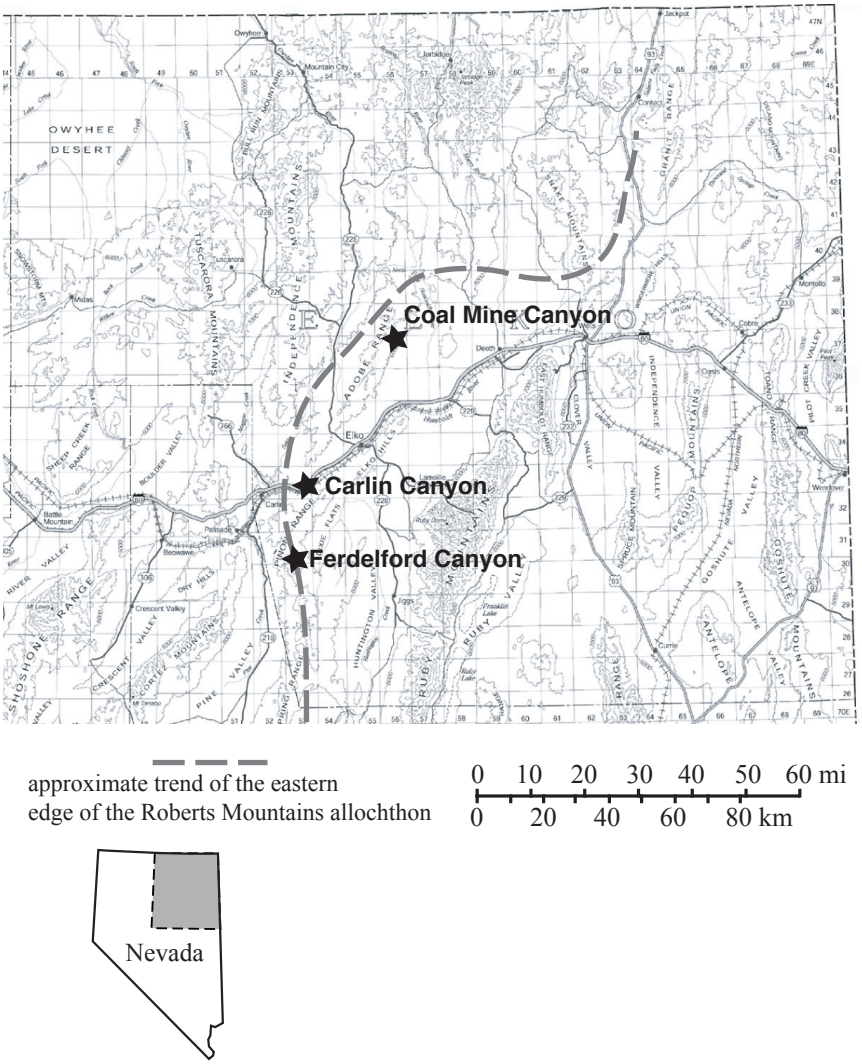

Figure 1. Map of northern Nevada showing the location of areas described in the road log.

The Western Margin of North America After the Antler Orogeny: Mississippian Through Late Permian History in the Basin and Range, Nevada

By James H. Trexler, Jr.[1], Patricia H. Cashman[1], Walter S. Snyder[2], and Vladimir I. Davydov[2]

Overview

This field trip will examine the evidence for Mississippian, Pennsylvanian and Permian deformation events in north-central Nevada. These events are notable for their timing—*after* the Antler orogeny and well *before* the Sonoma orogeny (both as traditionally defined)—and, locally, for their intensity. On this trip, we will demonstrate that these deformation events are linked to unconformities that separate genetically related stratigraphic packages in the upper Paleozoic section. These unconformities can be recognized over wide areas, can be correlated at a regional scale, are synchronous (within the resolution of biostratigraphy), and are accompanied by marked facies changes. In each case, the subunconformity rocks or their correlatives have a deformation history not recorded in the overlying rocks. These unconformities are, therefore, important stratigraphic markers with tectonic significance. We refer to these as tectonostratigraphic boundaries.

On the first day, we will drive from Boise to Elko, with a possible Stop along Nevada State Highway 225 in the northern Adobe Range (approximately 4 mi west of Elko) to see Mississippian rocks of the Antler foreland and Permian overlap strata. On the second day, we will see mid-Mississippian deformation at Ferdelford Canyon in the Piñon Range, and mid-Mississippian, mid-Pennsylvanian and early Permian deformations at Carlin Canyon in the southern Adobe Range. Here, the deformations have distinctive fold styles and geometries, as well as different ages. On the third day, we will drive through a thick succession of Early Mississippian foreland basin strata structurally overlain by Roberts Mountains allochthon, all depositionally overlapped by Middle (?) Permian strata.

Our interpretations are the product of a truly multidisciplinary study and would not have been possible without the full participation of sedimentologists, biostratigraphers, and structural geologists. Complete documentation of the map relationships, age control, stratigraphic revisions, and structural analyses in this study is beyond the scope of this guidebook paper, but is presented in two recent publications: Trexler and others (2003) and Trexler and others (2004). Reprints of these papers will be provided to field-trip participants.

[1]Department of Geological Sciences, University of Nevada, Reno, NV 89557, trexler@mines.unr.edu

[2]Department of Geology and Geophysics, Boise State University, Boise, ID 83725

Background

The conventional tectonic interpretation of the evolution of western North America is that there were two major orogenies in Paleozoic time; however, this does not explain the numerous local and regional-scale tectonic events recorded in Late Paleozoic rocks. The Late Devonian Antler orogeny and the Permo-Triassic Sonoma orogeny are both characterized as the eastward emplacement of oceanic facies sedimentary and volcanic rocks over continental margin sedimentary rocks (Roberts, 1951; Roberts and others, 1958; Silberling and Roberts, 1962). Many syntheses (*e.g.*, Burchfiel and Davis, 1972, 1975; Speed and Sleep, 1982) propose that a long-lived subduction zone oriented down-to-the-northwest, possibly accompanied by slab roll-back to the east (*e.g.*, Dickinson, 2000), was responsible for the east-directed Antler and Sonoma orogenies and all activity in between. This model is not robust in predicting the angular unconformities, disconformities, and deformation documented by many workers in upper Paleozoic rocks (*e.g.*, Dott, 1955; Johnson and Visconti, 1992; Schwarz and others, 1994; Snyder and others, 1997; Silberling and others, 1997; Ketner, 1998; Schiappa and others, 1999; Trexler and Giles, 2000). In this study, our objective has been to constrain tectonic models by determining the timing, extent, and kinematics of these short-lived upper Paleozoic tectonic events.

Our work throughout Nevada has shown that there are a number of regional unconformities from middle Mississippian through Permian time, and that they all represent genetically important breaks in the stratigraphic record (fig. 2) (Snyder, 2000; Trexler and others, 2003, 2004). These unconformities are tectonically generated and are nearly isochronous (to the resolution of Upper Paleozoic biostratigraphic control, ±~1 to 5 m.y.). More importantly, these unconformities can be correlated laterally to "event horizons" (*e.g.*, lithofacies shifts) that have the same origin. This feature makes them useful far beyond the areas of actual uplift, deformation, and erosion.

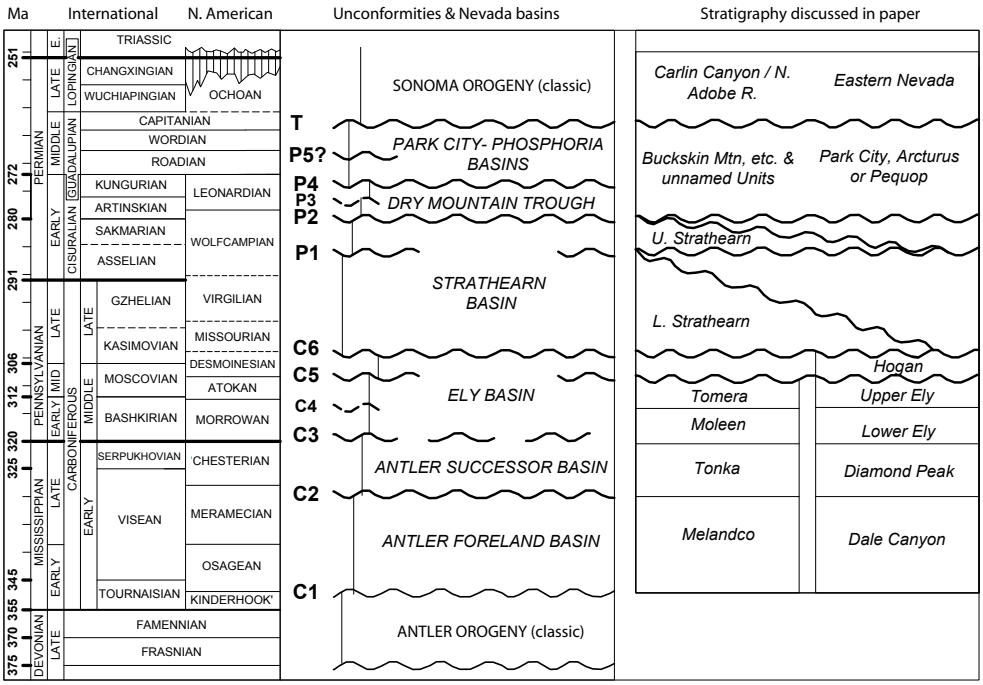

Figure 2. Regional stratigraphy of northern Nevada, showing the major tectonostratigraphic boundaries discussed in the text.

We have adopted a numbering scheme for the regional unconformities, using a system much like that used for the Mesozoic section on the Colorado plateau (Pipiringos and O'Sullivan, 1978; Peterson and Pipiringos, 1979). They are numbered sequentially from oldest to youngest within each time period (fig. 2). For the upper Paleozoic, we use the time periods C = Carboniferous, P = Permian (Snyder, 2000; Trexler and others, 2003, 2004). Our reassessment of the late Paleozoic stratigraphy in Nevada uses these unconformities and their correlative event horizons as natural breaks that separate packages of genetically related strata.

We have revised the regional stratigraphy based on our recognition of widespread unconformities in the Upper Paleozoic record. In many cases, these unconformities occur within existing mapped formations (Trexler and others, 2003, 2004). Each unconformity is, by definition, a boundary of at least formation rank; it, therefore, requires stratigraphic revision where it breaks an existing formation. Some of the unconformities can be mapped laterally into areas where the underlying rocks are deformed; these we have identified as key stratigraphic markers with tectonic significance. Some unconformities can also be traced laterally into areas where they are conformable surfaces with minor or no hiatus. Even in these cases, a signal may exist in the form of a facies change forced by the same tectonic disruption. Correlation of the unconformities with their correlative conformable surfaces is made possible by detailed biostratigraphy.

This unconformity-based analysis documents several widespread deformation and uplift events in the upper Paleozoic *between* the Antler and Sonoma orogenies. There are three of primary importance:

(1) The Mississippian C2 unconformity records Meramecian deformation of Antler foreland basin deposits, overlapped by Chesterian strata. It is particularly well developed in the Piñon Range.
(2) The Pennsylvanian C6 unconformity (recognized by Dott, 1955) truncates thrust-related deformation in rocks as young as Atokan and is overlain by middle Missourian strata.
(3) The early Permian P1 unconformity post-dates folding in the Virgilian (and older) section and is covered by Wolfcampian (upper Asselian-lower Sakmarian) sedimentary rocks. The latter two deformation events are visible at Carlin Canyon.

Recognition and widespread correlation of tectonic boundaries would not be possible without biostratigraphic age control. We are fortunate in this part of the section to have high-resolution biostratigraphy provided by small foraminifera and fusulinids. These fossils provide age resolution on the order of ±1 m.y.

Part 1: Deformation of the Antler foreland in the northern Piñon Range

Unconformity-bounded stratigraphic packages in the Mississippian and Pennsylvanian–A quick summary

Mississippian and Pennsylvanian-Early Permian strata in the Carlin area are characterized by genetic stratigraphic packages that were deposited in response to tectonic deformation, uplift, erosion, and subsidence. The angular unconformities between these packages provide an opportunity to determine the kinematics of deformation at each stage of this history (fig. 2).

Continental margin strata and Antler foreland onlap sequence – C1

The Antler orogeny, commonly defined as Late Devonian obduction of ocean-margin strata onto the Paleozoic miogeocline, is thought to be the first collisional disruption of the western margin of North America. Nonetheless, it is difficult to ascertain what structural features formed as a result of this collision. This is because there are several overprinting

events that are contractional and roughly coaxial, and there is a general lack of overlap strata that would constrain the age of structures. The Roberts Mountains thrust (separating allochthonous rocks from the miogeocline section, and often thought of as the "Antler thrust") can be shown to have several episodes of motion. Its age is constrained only as older than Permian based on dated overlap strata. The age of folding in the Roberts Mountains allochthon likewise is difficult to pin down; the oldest overlap strata are Permian rocks. The principal signal of the Antler orogeny is the foreland basin that resulted from loading by the allochthon. Sediments that filled this basin document its geometry and setting (Poole, 1974; Poole and Sandberg, 1977).

Middle Mississippian deformation and overlap strata – C2

In late Osagean or Meramecian time, the Antler foreland was deformed by a contractional event that also affected miogeoclinal rocks (Trexler and others, 2003). This deformation has been documented throughout the Piñon Range and south to the Diamond Mountains (*e.g.*, Silberling and others, 1997); the stratigraphic signal is ubiquitous throughout the Great Basin. In the Carlin area, this boundary is an angular unconformity with an overlap unit (Tonka Formation) that constrains the deformation to be pre-Chesterian. We will discuss this boundary in detail on the Ferdelford Canyon leg of the trip.

Pennsylvanian disruption – C3, C4, C5

Each of these boundaries is best expressed elsewhere in the region and will not be discussed in detail on this trip. However, at Carlin Canyon two of these boundaries are lithostratigraphic breaks, probably caused by deformation elsewhere; C3 is the Tonka-Moleen contact, and C4 is the Moleen-Tomera contact. The C5 contact was removed here by erosion on the C6 boundary.

Missourian deformation and overlap – C6

The C6 boundary is the centerpiece of the story at Carlin Canyon. All strata older than Missourian are dramatically deformed. The oldest overlap unit is the mid-late Pennsylvanian Strathearn Formation (lower member).

Early Permian regional event – P1

The P1 boundary at Carlin Canyon subtly truncates the lower member of the Strathearn Formation, cutting down to the east. Upper Strathearn Formation overlaps both lower Strathearn and deformed Pennsylvanian rocks. The characteristics of the lower and upper Strathearn here are so similar that mapping the boundary is very difficult except where deformation of the lower member is more pronounced. We initially recognized the boundary here based on biostratigraphy. The best expression of this event documented to date is near Beaver Peak in the Tuscarora Mountains, where lower Strathearn is caught up in thrusting; this deformation is depositionally overlapped by upper Strathearn (Theodore and others, 1998; Berger and others, 2001).

ROAD LOG—ELKO TO CARLIN

Mileage Cum.	Inc.	
0.0	0.0	Begin this leg of the trip in Elko at the intersection of Interstate 80 and Nevada State Route 225. Drive west along the Humboldt River valley on Interstate 80.
5.0	5.0	The view to the south is the mouth of the South Fork of the Humboldt River, where it flows north out of a deep canyon to enter the main Humboldt River valley. The deep canyon was cut (presumably) by Pleistocene outwash from Ruby Mountains glaciation.

HISTORICAL NOTE: The "Hastings Cutoff" used by some California-bound settlers followed the South Fork of the Humboldt River. It was supposed to be a shortcut to the main trail west. The Hastings Cutoff left the main trail in Utah and crossed the Great Salt Desert to rejoin the main trail here, saving miles but adding weeks to the trek. The ill-fated party of immigrants including the Donner family passed here in September of 1849, well behind schedule. They intended to cross the Sierra before early winter snows sealed the passes. They were already too late.

8.5-9.5	3.5-4.5	Grindstone Mountain is the ridge to the south (left) with the microwave tower on top. Here, the Mississippian-Pennsylvanian section is structurally duplicated. The structural break occurs at the topographic step one-third of the way up the north slope. The lower section is mostly Morrowan-Atokan Moleen and Tomera Formations. Above the step, the upper slope is Tonka Formation overlain (with an angular unconformity) by cyclothemic Morrowan-Atokan Ely Formation. Mapping by Smith and Ketner (1998) shows the lower, north block as being down-dropped along a north-dipping normal fault, but the fact that the two sections have very different lithostratigraphy argues against a simple normal fault interpretation. This problem has not been resolved.
12.5	3.0	The hoodoos on the right with horizontal bedding are mapped by Smith and Ketner (1978) as Eocene conglomerate. Behind (stratigraphically beneath) a buttress unconformity are

		subvertical beds of the Moleen – Tomera Formations. Stratigraphic "tops" are toward the northwest, and the bedding is locally overturned. The southward continuation of this northwest-vergent overturned anticline-syncline pair can be seen along strike on the south side of the Humboldt River in the bluffs directly ahead to the west.
14.0	2.5	"The amphitheater" is on the right. This dramatic cliff of Pennsylvanian-Permian limestone will be the main subject of a Stop on the Carlin Canyon leg of the field trip.
15.0	1.0	Cross the Humboldt River and enter the highway tunnel. When you exit the tunnel, look to the right to see the C6 unconformity, pictured in many textbooks as a classical angular unconformity.
16.3	1.3	University of Nevada, Reno, Fire Science Academy is on the right. Continue west.
18.8	2.5	East Carlin exit. Leave the freeway here and follow Route 221 into Carlin. Alternatively, stay on the freeway to the Central Carlin exit. We will begin the Carlin Canyon segment here at the east Carlin exit. This ends the segment.

FERDELFORD CANYON

Mileage Cum.	Inc.	
0.0	0.0	Begin this trip segment at the four-way Stop intersection just south of the main Carlin exit of Interstate 80. This intersection is in the center of Carlin, Nevada. Turn onto, or continue on, Route 221 west out of town. Note the very conservative speed limits in town.
1.4	1.4	Turn left at the Stop sign, onto state Route 278 south toward Eureka. Drive south on Route 278, following the Humboldt River and the route of the original transcontinental railroad toward Palisade.

HISTORICAL NOTE: Clarence King and the U.S. Geological Survey 40th Parallel Survey came through this country in 1868 (fig. 3), about the time that the transcontinental railroad was being built. King returned to the area in 1872 to inventory gold mines for the U.S.G.S., visiting, among others, the Bullion Mine just east of Piñon Peak. The infamous Diamond Rush of the early 1870s was just getting under way, and King soon played a role in exposing the hoax.

At this point you are more or less on the modern "Carlin Trend" of disseminated gold deposits. Most of the large mines operated by Newmont and Barrick are to the northwest in the Tuscarora Mountains. The active Rain Mine (Newmont) and the inactive Bullion Mine are to the southeast in the northern Piñon Range. According to Dr. Tommy Thompson, Director of the Center for Research in Economic Geology at the University of Nevada, Reno:

> *"The Carlin trend is the largest gold-producing district in the U.S., and in April 2002, passed the 50 million ounce production threshold. Due to this prominence Nevada ranks third, behind South Africa and Australia, in world-wide annual gold production. Gold occurs in arsenian pyrite and arsenian marcasite in deposits localized by shelf carbonates that have suffered decarbonatization and silicification. Structural controls are prominent in all deposits as well.*
>
> *Research by the Ralph J. Roberts Center for Research in Economic Geology (CREG) has demonstrated that the gold deposits are Eocene in age (36–42 Ma), commonly localized in close proxim-*

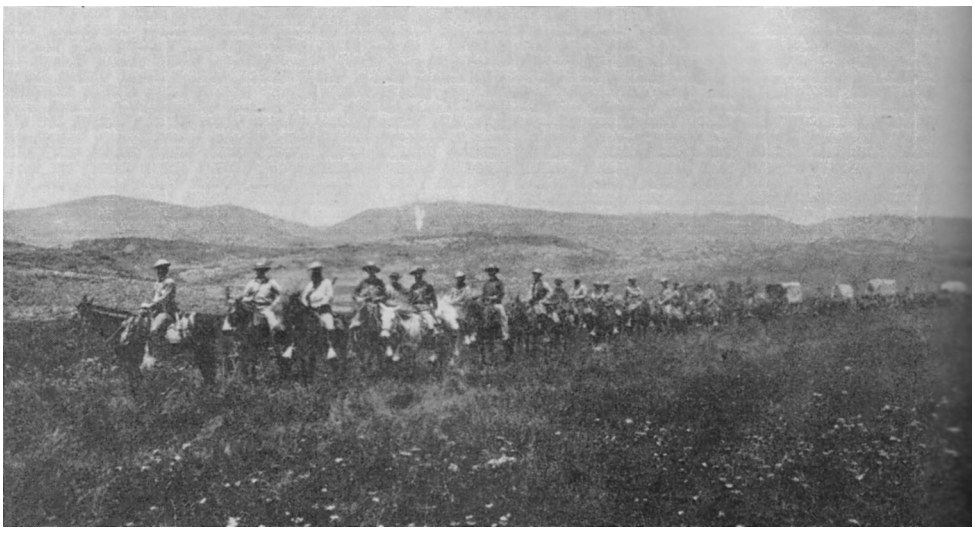

Figure 3. The 40th Parallel (King) Survey crosses Nevada in 1868. Photo by T.H. O'Sullivan.

ity to igneous rocks of the same age. Stable isotope analyses by CREG researchers have demonstrated that the deeper Carlin-type gold deposits have a significant component of magmatic waters related to their formation."

Mileage Cum.	Inc.	
2.6	1.2	Cross the railroad track and the Humboldt River. Volcanic flows forming the canyon walls are the Miocene Palisade Canyon Rhyolite.
10.4	7.8	Intersection with a road that goes right to the townsite of Palisade. Route 278 departs from the river and the railroad here to follow the tributary drainage of Pine Creek and Pine Valley southward.

HISTORICAL NOTE: Palisade Canyon of the Humboldt River proved to be a relatively minor barrier to construction of the transcontinental railroad (fig. 4), allowing the railroad to maintain grade from the Carson Desert all the way up the Humboldt River to its headwaters. From Elko, the original route runs northeast to Wells, and then north past the Goose Creek Mountains to Promontory Utah, where the Central Pacific and Union Pacific met in 1868.

The bluffs through which Pine Creek flows are in the Miocene Humboldt Formation. Piñon Peak, the sharp tree-covered peak on the southern skyline, is underlain by Devonian Devils Gate and Nevada Formations. These limestones and dolomites are the upper part of the North American miogeocline and are in the footwall to all thrusting in the area.

15.7	5.3	Turn left to drive up Ferdelford Canyon on a graded dirt road. This turn is obscure, but can be recognized because it is opposite the Brown Ranch, on the right side of the highway. As you drive up this canyon you are going down section. The steep sage-covered hillsides are Miocene Humboldt Formation, which rarely crops out.
18.5	2.8	Cross the cattle guard at the "Tomera Ranches" sign. Conglomerate outcrops in the

Figure 4. First construction train steams through Palisade Canyon in 1868. Photo by Alfred Hart.

bluffs ahead are the late Mississippian Tonka Formation. Fossil beds just uphill on the left date this Tonka as Chesterian. Bedding in the Tonka here dips gently north.

19.3 0.8 The cottonwoods on the right mark the site of the Webb Ranch, after which Webb Creek and the Webb Formation were named. Original ranch buildings stood on this site until the late 1980s.

19.7 0.5 Follow the graded road where it turns south (right), crosses Ferdelford Creek and climbs a side canyon up Webb Creek.

20.5 0.8 The lower Mississippian Melandco Formation crops out in road cuts here. We will Stop to look at it on the way down the hill. It is shale and chert-litharenite turbidite beds with some heterolithic conglomerate. The Devonian Webb Formation is poorly exposed in fault-bounded blocks a little further up the canyon.

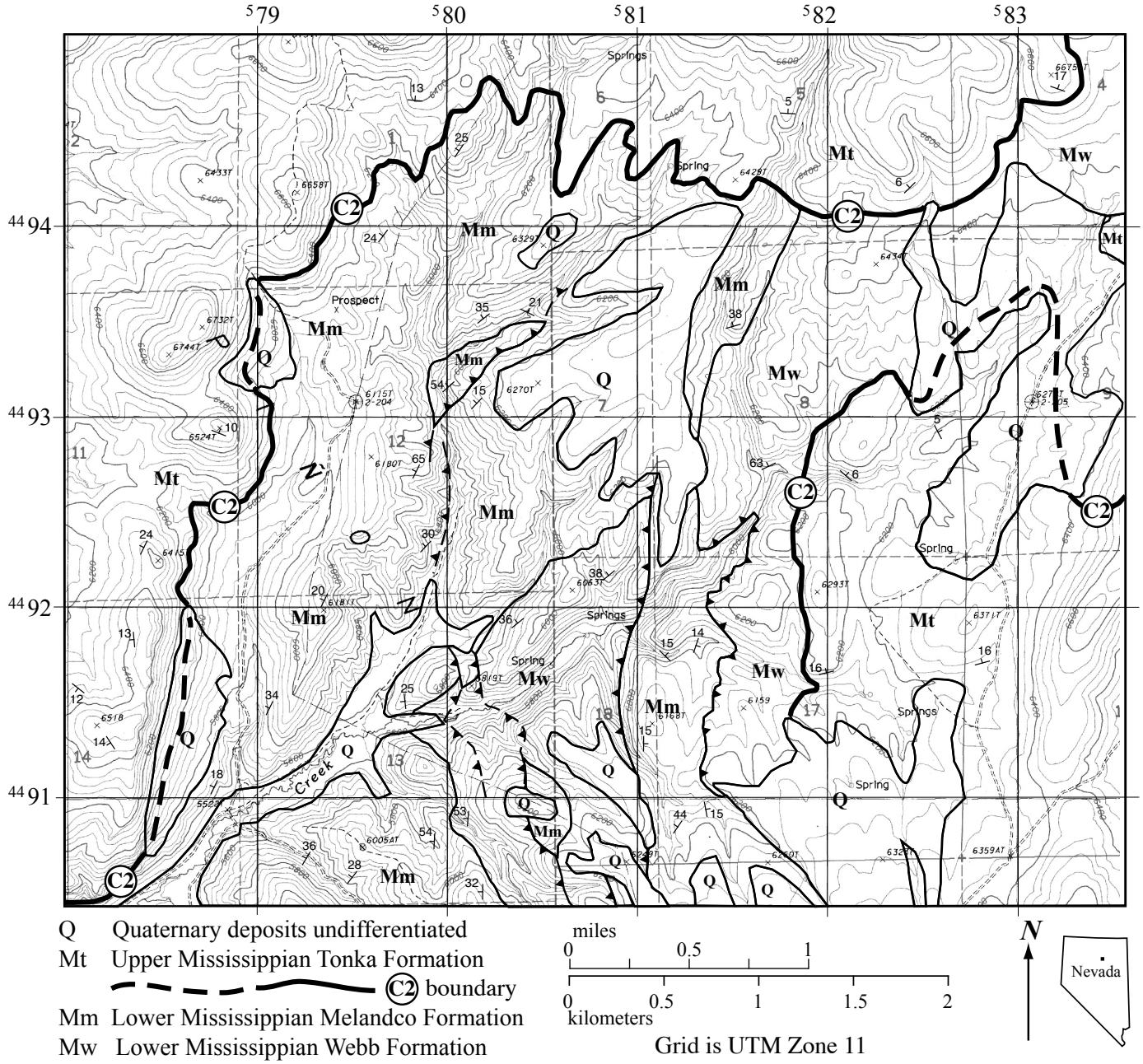

Figure 5. Map of part of the Raven's Nest quadrangle by R. Tosdal, as published in Trexler and others (2003).

21.0 0.5 Devonian Woodruff Formation crops out in the road cut on the right. We will Stop and look at these road cuts on the way down the hill.

21.6 0.6 The road climbs up and reaches an old pediment at a maintained fence line. Turn acutely north and proceed in vehicle or on foot (depending on road conditions, there is a year-round seep here) north on the faint jeep track that will take you about 0.5 miles to the end of the ridge. This short detour is not counted in the road log mileage.

Stop 1. View point on the ridge, overlooking the canyon to the north. The view to the north is the map area in figure 5. The rocks along the skyline to the north are late Mississippian (Chesterian) Tonka Formation. They are gently folded, but generally flat-lying. The base of the Tonka is the C2 boundary, regionally constrained to be upper Meramecian to lowest Chesterian. The rocks beneath the C2 boundary are Late Devonian Woodruff, earliest Mississppian Webb, and Mississippian Melandco Formations. These are deformed and repeated by east-vergent folds and east-directed thrust faults; this deformation is truncated by the C2 unconformity (fig. 6). For a more complete discussion of the mid-Mississippian deformation event, see Silberling and others (1997) and Trexler and others (2003).

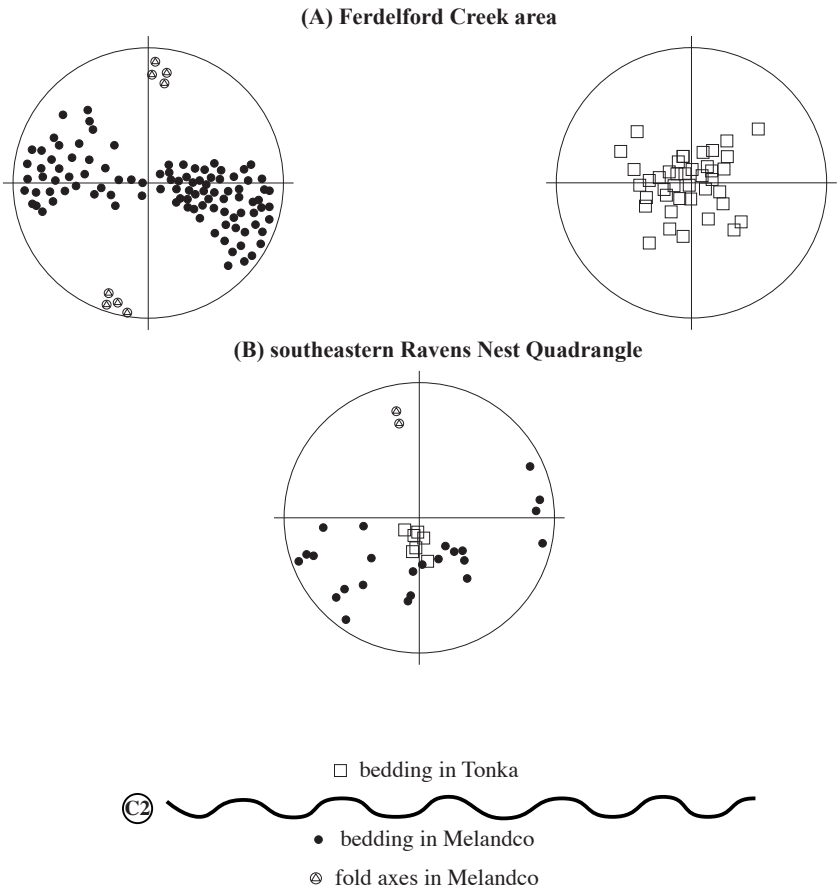

Figure 6. Stereogram of fold axes and poles to bedding above and below the C2 unconformity (Tonka and Melandco Formations, respectively) in the southeast part of the Raven's Nest 7.5 minute quadrangle. The Melandco Formation is folded around north-south axes and the Tonka Formation is not. This deformation therefore occurred in mid-Mississippian time; see text for discussion of age control. Data are from mapping by Tosdal (as published in Trexler and others, 2003).

ECONOMIC GEOLOGY NOTE (Dr. Tommy Thompson): The Rain Mine is visible to the northeast. The Rain Mine is localized along the N. 40–50° W.-striking, 80–45° SW.-dipping, dextral Rain fault. The orebodies are hosted in hydrothermal breccias localized within the hanging wall of the Rain fault, and within the Mississippian Webb Formation immediately overlying the contact with the Devonian Devils Gate Limestone. The orebodies were mined in open pit (1.17 Moz gold) and in underground stopes (265 Koz gold). The open pit concentrations were 1.8 g/t Au while the underground grades average 7.7 g/t Au.

STRATIGRAPHIC NOTE: Several earlier maps have shown the fine-grained rocks of the Webb and Melandco here as "Chainman Shale" and the coarser Melandco as "Diamond Peak Formation". We have abandoned both "Chainman" and "Diamond Peak" in this area (but not entirely, see Trexler and others, 2003) because the names are ambiguous—they have been applied to different age rocks in different places. In some areas these units, as originally named, contain one or more tectonostratigraphic boundaries. As we will see on this trip, formation designation based on gross lithostratigraphy obscures stratigraphic and structural relationships. Previous workers have recognized the significance of deformation here (Jansma and Speed, 1990; Silberling and others, 1997; Tosdal, unpublished mapping and in Trexler and others, 2003).

Another problem in this area concerns the black shale and argillite underlying the Melandco Formation. Devonian Woodruff and Mississippian Webb are particularly difficult to tell apart; many workers have relied on scanty fossil data to differentiate these two on the basis of age. Although both are mapped in the area (Smith and Ketner, 1978), work by geologists in the Rain Mine pit (see economic geology note above) documents Webb Formation conformably on Devonian Devil's Gate Formation. These problems are not resolved.

Return south to the graded dirt road. Turn right and return

down the canyon. Continue cumulative mileage as you drive down the canyon.

Mileage Cum.	Inc.	
22.2	0.6	Park for Stop 2.

Stop 2. Look at the Woodruff Formation in outcrop. The Woodruff Formation is black argillite and siltstone, rarely exposed. Age control is based on radiolaria preserved in ellipsoidal phosphatic nodules. These radiolaria have been dated at this locality as Famennian (latest Devonian) (P. Noble, written communication, 2003).

The Woodruff and Webb Formations are considered by many workers to be the initial foredeep mudrocks deposited in the Antler foreland basin, recording the initiation of foreland basin subsidence and, therefore, dating the Antler Orogeny. The C1 boundary lies beneath the Webb (or Woodruff) and above the rocks of the carbonate miogeocline. As stated above in the note on the Rain Mine, there the Webb lies conformably on the Devonian Devil's Gate Limestone, tying it depositionally to the carbonate miogeocline.

Continue back down the canyon the way you came up. Cumulative mileage continues.

Mileage Cum.	Inc.	
22.8	0.6	Park for Stop 3.

Stop 3. Look at the Melandco Formation in outcrop. The Melandco is made up of heterolithic conglomerate, litharenite, and mudrock. Here, the section is mostly mudrock with 1- to 5-m intervals of conglomerate that are matrix rich to matrix supported. Clast types in the conglomerates include chert, litharenite, quartzite, limestone, and rare volcanic rocks. (This is in contrast to the overlying Tonka conglomerates, which contain none of the less resistant clast types.) The Melandco contains graded beds generally less than 1-m thick. These beds typically preserve characteristics of density-modified flow or turbidity current deposits. Scours and bases of channels indicate east and southeast flow directions. The Melandco is not fossiliferous here and rarely is elsewhere, but regionally it is constrained to Osage to early Meramec in age. These beds have been interpreted as Antler foreland submarine fan deposits, with the sediment source being the Antler highland to the west (Poole, 1974; many others).

STRATIGRAPHIC NOTE: We have chosen to call these rocks "Melandco", and not "Chainman", as they have often been mapped. The term "Chainman" is not appropriate, because the type Chainman, in the Ely area, is significantly younger in age (Chesterian), and lies above the regional C2 boundary. The term "Melandco" in its type area was originally applied to foreland basin submarine fan rocks of this age east of Elko in the Snake Mountains, and thus is appropriate here both in age and in lithology. This unit also could legitimately be called "Dale Canyon Formation" (Silberling and others, 1997), the equivalent unit in age and tectonic significance to the south in the Eureka area.

Continue to the main canyon bottom, and turn left to go back down Ferdelford Creek.

Mileage Cum.	Inc.	
23.8	1.0	A large float block of Tonka Formation conglomerate sits on the right side of the road. We will Stop in Carlin Canyon later today to look at the Tonka in detail.

Rejoin Route 278 and retrace route northward to Carlin. This ends the segment.

CARLIN CANYON

Mileage Cum.	Inc.	
0.0	0.0	Interstate 80 freeway onramp at East Carlin.

ROUTE NOTE: Because we must use I-80 to travel between stops in this segment, we will need to do some doubling back in order to visit the next few stops in a logical—chronological—order. We do not advocate stopping on the Interstate to look at road-cut outcrops. It is dangerous and probably illegal.

Drive east on the frontage road on the south side of the interstate. Follow Bureau of Land Management (BLM) signs to Carlin Canyon.

As we drive east from Carlin toward Carlin Canyon, the Ordovician Vinini, upper Devonian Woodruff, and lower Mississippian Webb Formations underlie the monotonous low-relief slopes to the north and south. The steep slopes at the entrance to the canyon are held up by Mississippian conglomerates. The Webb is mapped in fault contact with the lower Mississippian Melandco Formation. This is a steep fault that is apparently reverse on the north side of the highway; on the south side, map relations indicate Webb is thrust over Mississippian rocks, but the timing of thrusting is not known.

Mileage Cum.	Inc.	
1.8	1.8	The bridge across the highway to the left goes

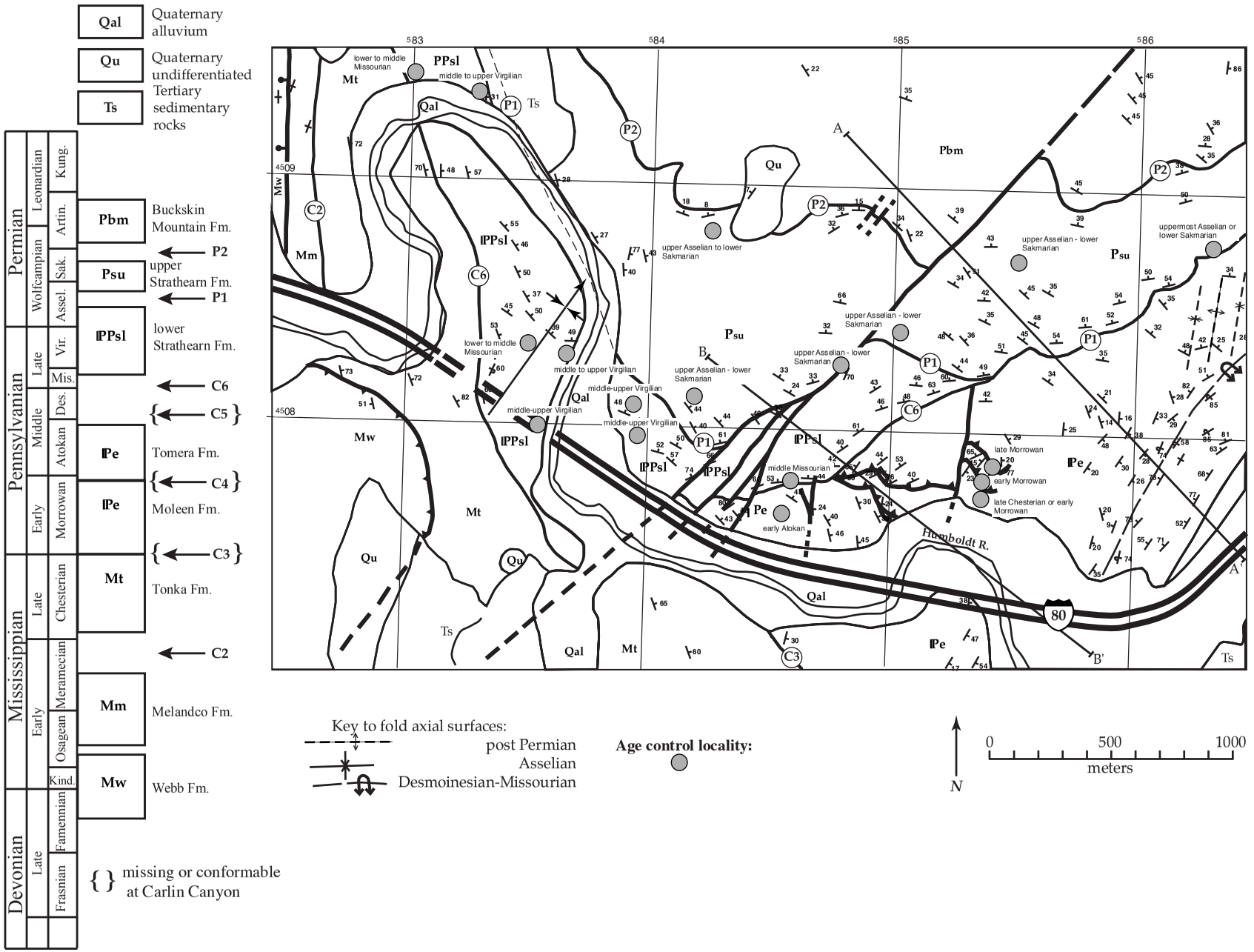

Figure 7. Map and stratigraphy of the Carlin Canyon area, as published in Trexler and others (2004).

to the University of Nevada, Reno, Fire Science Academy; continue straight.

The wetlands to the right are part of Newmont Mining's wetland mitigation project. As we approach the tunnel portals in the canyon, we are on the map in figure 7.

3.4 1.6 **Stop 4.** The view to the north, across the freeway, shows the C2 unconformity (fig. 8). The subvertical beds on the right are the lowest Tonka Formation, which is in angular unconformity over the Melandco Formation to the left. We will be able to walk back to examine this contact from the next stop.

3.6 0.2 Cross beneath I-80 to the north side of the freeway.

3.9 0.3 **Stop 5.** BLM wayside Stop (view of the C6 unconformity a short distance up-river to the north); park on the left side of the road in the gravel lot. We will look at the C2 unconformity at the west end of Carlin Canyon, and at the Tonka Formation. Begin by walking up the abandoned freeway ramp to the west.

The Melandco Formation here is predominantly heterolithic conglomerate and coarse litharenite, with rubble intervals that are mudrock and argillite. Clast counts document a number of different clast types, including friable quartzarenite, which might have a source in the Harmony Formation. The conglomerates generally lack recognizable fabric other than crude bedding-plane-parallel long-axis orientation of clasts. These strata are interpreted as density-modified flow and high-density turbidity current deposits and are thought to be primary Antler foreland basin fill. Paleocurrent indicators (elsewhere) as well as abundant radiolarian chert clasts document a western source in the Antler orogenic highlands.

The C2 boundary is marked by a change in attitude from vertical beds of the Melandco to steeply east-dipping beds of the Tonka (fig. 8). This angular unconformity can be mapped south throughout the Piñon Range, the Diamond Mountains, and the northern Fish Creek Mountains, a distance of over 150 km.

The Tonka Formation comprises clean chert-quartzite conglomerate and litharenite, interbedded with calcareous silt-

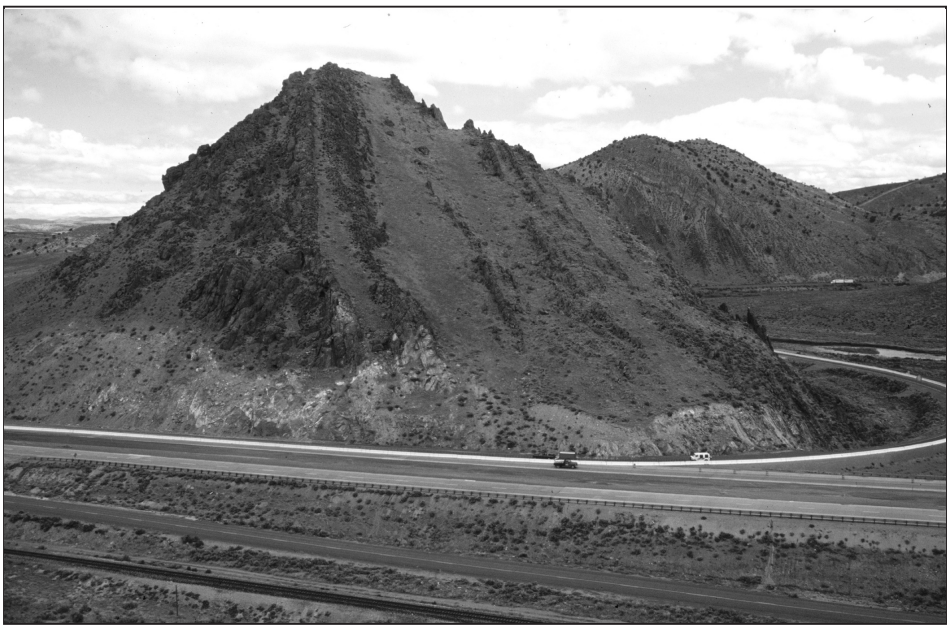

Figure 8. West end of Carlin Canyon, looking north. The C2 boundary is the angular unconformity in the foreground, and the C6 boundary can be seen in the background to the right. See text for discussion.

stone and sandy limestone. The conglomerate and litharenite preserve channel geometries, trough cross-bedding, bar foresets, and other features consistent with fluvial processes. The siltstones and carbonates are sandy and fossiliferous, lenticular bodies, interpreted as overbank deposits and lagoonal facies. The overall setting for the Tonka is interpreted as marginal-marine deltaic. Fossils in the Tonka range through the Chesterian in age. The pronounced shift in depositional environment, as well as the angular unconformity, emphasize the importance of the C2 boundary.

This Stop gives an excellent view of the C6 boundary unconformity a short distance to the north. Subvertical beds of Tonka Formation are truncated by steeply dipping beds of the lower (Missourian) member of the Strathearn Formation. Note that the geometric relationships are the same as the C2 boundary unconformity, suggesting progressive, and probably coaxial, deformation. Considerable section is missing here that is not missing at the east end of the canyon: upper Tonka, Moleen and Tomera Formations have all been removed by erosion under the C6 unconformity.

Mileage Cum.	Inc.	
4.3	0.4	**Stop 6.** The gray beds are the base of Strathearn Formation in angular unconformity (C6) over reddish Tonka conglomerate and litharenite.

The C6 unconformity is hidden at road level, but is exposed in outcrops on the steep hillside to the north. There, the lowest Strathearn is a red-stained paleosol containing fragments of the underlying Tonka. Relief on the Tonka is limited at map scale here, but at outcrop scale the surface is irregular. These characteristics indicate that the Tonka – Strathearn contact here is an uncomformity. Note that although this contact was initially described as an unconformity (Dott, 1955), some subsequent workers have interpreted it to be a fault (*e.g.*, Jansma and Speed, 1990). We have examined the contact closely and have not found evidence for significant faulting along it. Locally, there has been a small amount of slip, probably as flexural slip during later folding.

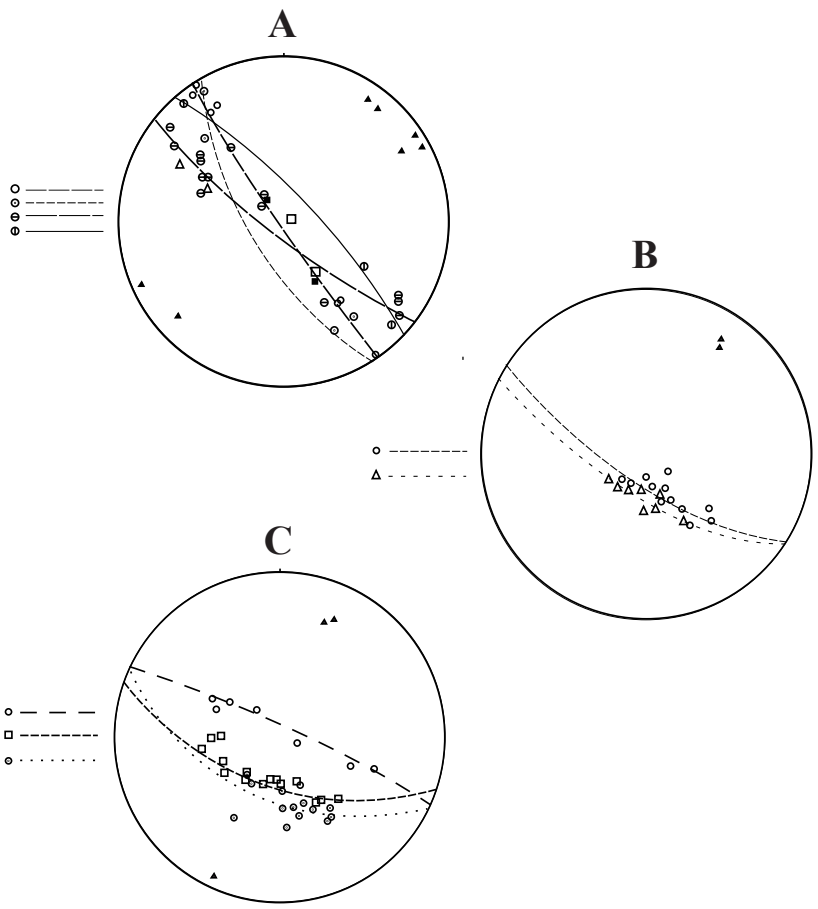

Figure 9. Stereograms of the three different fold sets in the Carlin Canyon map area. All are lower hemisphere, equal-area plots, with poles to bedding shown as circles, squares, or open triangles. Different symbols represent individual mesoscopic or macroscopic folds. Fold axes for individual folds are shown as filled triangles.
(A) Pennsylvanian (C6) deformation, characterized by asymmetric to overturned folding, and northwest-directed thrust faulting. Stereogram shows poles to bedding in macroscopic, mesoscopic and hanging-wall folds, with individual fold axes plotted. Fold axes most commonly trend east-northeast (050°-065°). Note: The subsequent deformation has not been rotated out for most of these folds, because the overlying Strathearn Formation is not preserved. However, the three folds where subsequent tilt has been removed do not differ systematically from the other folds on this stereogram, indicating that subsequent rotation is not significant here. (Fold axis orientations, presented as plunge/trend: 11/037, 08/039, 04/056, 04/063, 18/059, 02/246, 12/228.)
(B) Lower Permian (P1) deformation, characterized by open, upright folds. The tilt of the overlying upper Strathearn has been removed, and the P1 fold axes plunge gently toward 030°-032°. (Fold axis orientations, presented as plunge/trend: 16/032, 13/030.)
(C) Post-Permian deformation, characterized by open, upright folds. The fold axes plunge gently toward 020°-026°. (Fold axis orientations, presented as plunge/trend: 21/026, 25/020, 05/205.)

Continue upriver on the old highway. Cliffs on the left (east) are the upper (lower Permian) member of the Strathearn. Bedding strike in these rocks is parallel to the highway (see fig. 7).

Mileage Cum.	Inc.	
5.3	1.0	**Stop 7.** Lower Strathearn, across the river to the right, is folded below the unconformity with the upper Strathearn; the unconformity is under the river here. Bedding in the lower Strathearn is folded into a broad syncline and strikes directly down the hill toward us, and upper Strathearn behind us is unaffected. This is the P1 unconformity. See figure 9 for structural data from this area. Return toward East Carlin via the old highway (back the way you came).
10.6	5.3	East Carlin freeway ramps. Turn right, and immediately right again to get on Interstate 80 east toward Elko. Continue cumulative mileage.
14.1	3.5	Enter the freeway tunnel eastbound.
15.1	1.0	Tonka railroad siding is on the right; this is the type section of the Tonka Formation (Dott, 1955). This was an unfortunate choice of type locality, because the section is duplicated in at least one place by thrusting.
16.2	1.1	Just beyond the second bridge over the river, pull off the freeway to the right into the small dirt pullout where a graded dirt road goes through a gate to follow the railroad (the gate may be locked). Pull well off this busy, high-speed highway. Walk through or climb over the gate, and climb up to one of several vantage points looking north across the railroad, river, and Interstate 80 at the south-facing cliff-face, a locality we refer to as "the amphitheater."

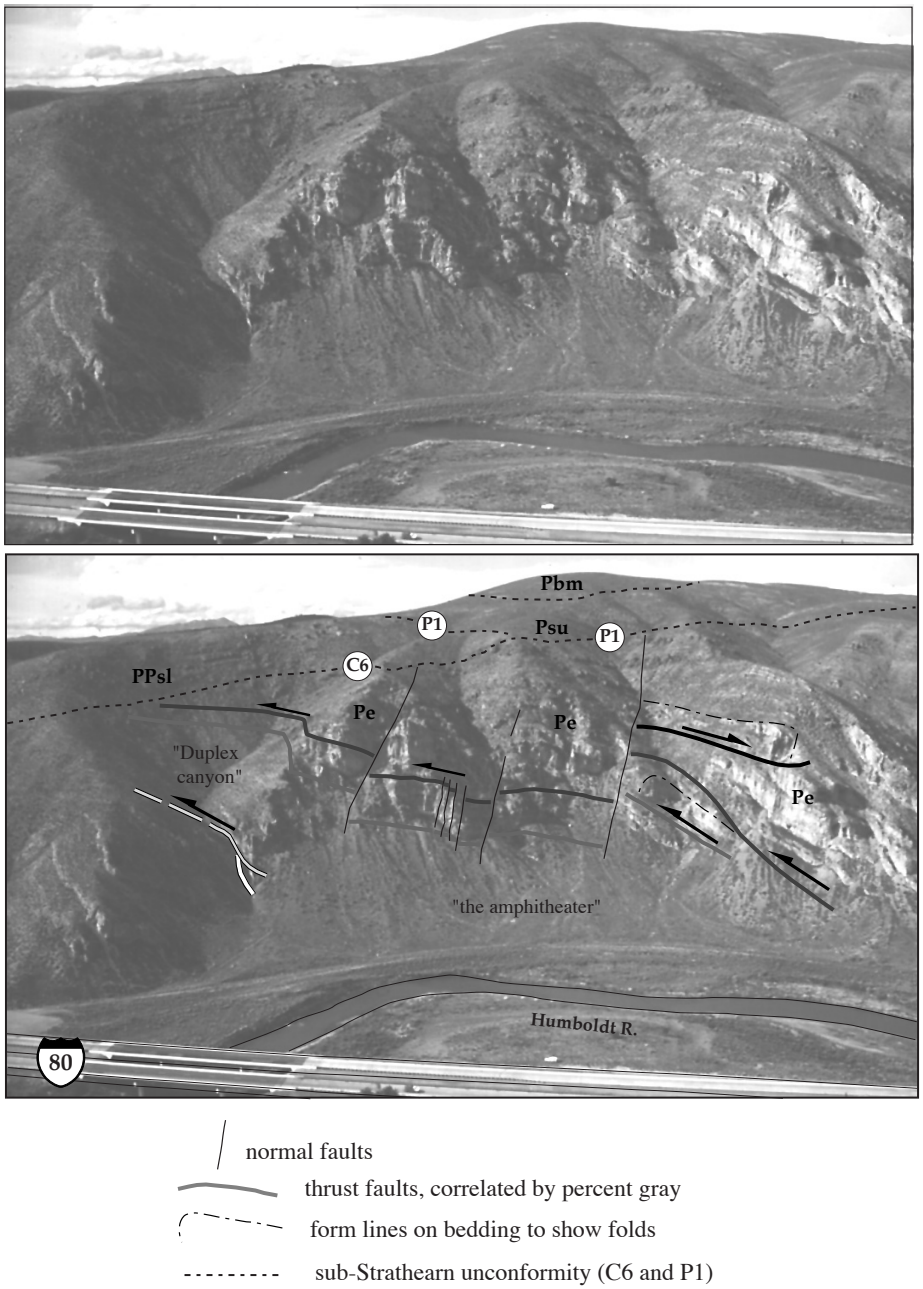

Figure 10. Annotated photograph of "the amphitheater": a view to the north at the south-facing wall in the eastern part of Carlin Canyon. A discussion of the structure displayed here is in the text.

Stop 8. Strata of "the amphitheater" display the structures developed during Missourian thrusting and folding here at Carlin Canyon (fig. 10). In order to understand this structure, we have mapped the entire cliff face using a total station posi-

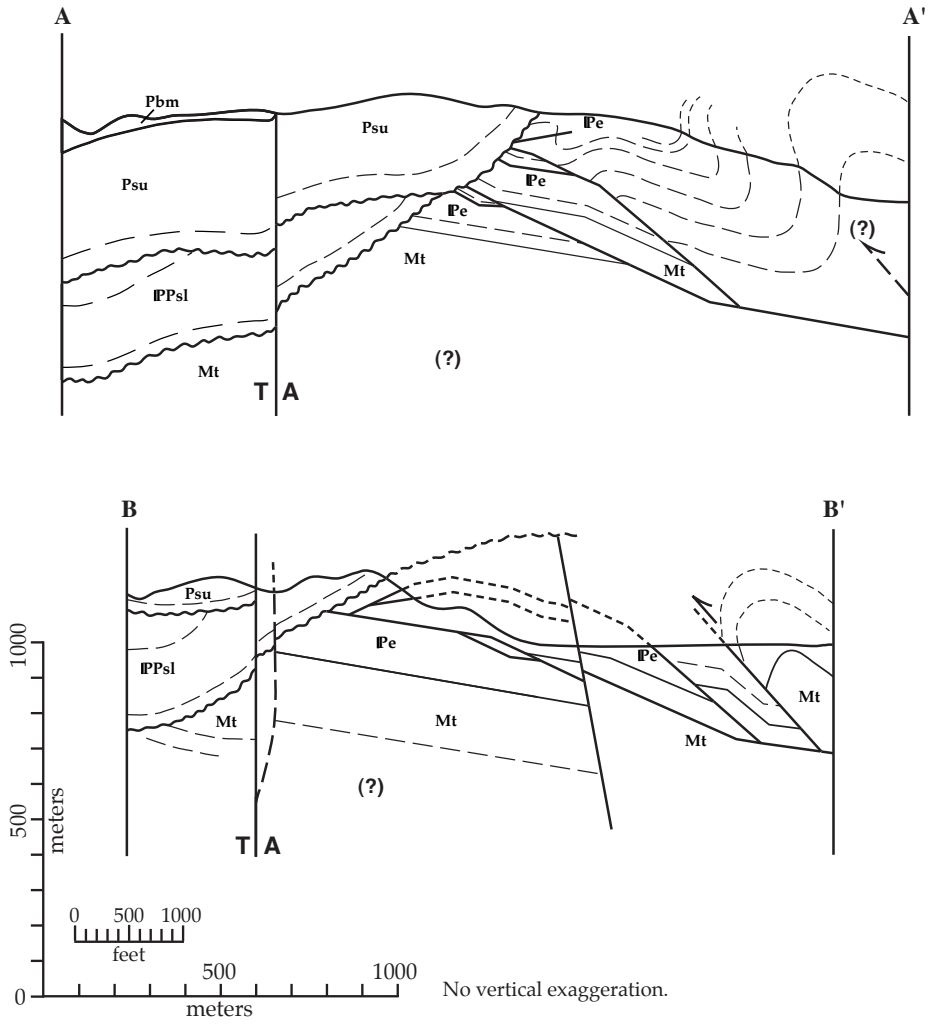

Figure 11. Cross sections through the Carlin map area. See map (fig. 7) for locations.

tioned at this vantage point. This detailed mapping, combined with fusulinid biostratigraphy, enabled us to work out the complex structure. The photo for figure 10 was taken at the top of the hill directly behind you to the south. See figure 11 for our interpretation of this structure in cross-section.

Units in the cliff are the Moleen and Tomera Formations and are Morrowan through Atokan in age. These strata are thrust faulted and folded, and eroded along an unconformity (P1) that is near the skyline as viewed from here. Overlying the unconformity here is the upper Strathearn; it is the highest carbonate one can see from this vantage point. The Permian Buckskin Mountain Formation overlies the Strathearn and caps the mountain to the north. Note that the lower member of the Strathearn (which underlies the upper Strathearn at Stop 7, and overlies the Tonka along the C6 unconformity at Stop 6) is not present here. It has been removed by erosion along the P1 boundary unconformity prior to the deposition of the upper Strathearn.

The Missourian deformation at Carlin Canyon is dominated by northwest-vergent folding and several northwest-directed thrust faults. In the cliff face, you can see two minor thrusts that step up-section in the footwall toward the northwest (fig. 10). These faults have northwest-vergent hanging wall anticlines with amplitudes of tens of meters. In the canyon we call Duplex Canyon at the west end of "the amphitheater" several more thrusts are exposed. These, too, are northwest directed, as shown by footwall truncations (upsection toward the northwest) and ramp anticlines in the hanging walls. A southeast-vergent thrust with hanging-wall anticline can be seen high in the wall at the east end of the amphitheater. The fold is coaxial with the northwest-vergent folds, so this structure appears to be a local back thrust, accommodating the same northwest-southeast shortening as the northwest-vergent fold-thrust system. A marker horizon ("Chaetetes horizon" of Dott, 1955) crops out at the base of the exposure at the west end of "the amphitheater", and high on the slope out of sight to the east of the amphitheater. The stratigraphic separation across these thrusts is, therefore, several hundred meters. A large northwest-vergent overturned anticline-syncline pair just east of the amphitheater accommodates more northwest-southeast shortening; the subvertical bedding (described at Mile 12.5 Elko to Carlin road log) forms the common limb of this fold pair.

Although all three folding events recorded at Carlin Canyon have northeast-plunging axes, they can be distinguished based on details of fold style and geometry (Trexler and others, 2004). The Missourian, sub-C6 deformation, is characterized by northwest-verging overturned folds and thrusts described in the preceding paragraph. Fold axes appear to trend about 060°. Sub-P1 (earliest Permian) folds (*e.g.*, at Stop 7) are open and upright with axes plunging gently toward 030°-035°. Post-Permian deformation consists of open 020°- to 025°-trending folds in the few exposures where we have seen it. Work in progress by UNR graduate student Tristan Ashcroft will further define this deformation.

Carefully get back on the freeway and continue east on Interstate 80.

Mileage Cum.	Inc.	
18.9	2.7	To the right, on a point bar of the Humboldt River adjacent to the black railroad bridge, you may see a long-lived example of local folk art. Many generations of lawn flamingoes have appeared in various configurations here for at least 15 years.
22.1	3.2	Exit at Hunter (exit 292). Maggie Creek Ranch is on the right. If you wish to return to west-bound I-80, cross over the freeway and get back on. This ends the segment.

Part 2: Thrust Faults, Unconformities, and Reactivation of the Roberts Mountain Allochthon

During this segment of the trip, we (1) continue the themes of upper Paleozic tectonism and widespread unconformities raised during Part 1, (2) highlight the depositional environment for these Antler foreland basin (C1–C2) strata (Stop 10), (3) examine deformed C1–C2 strata overlapped unconformably by post-P4 units (Stop 11), and (4) see pre-P4 structural reactivation of the Roberts Mountains allochthon (Stop 13). At the last stop, we also will have a chance to discuss the nature of the Antler orogeny and the mechanics of deformation of bedded chert.

The Northern Adobe Range is structurally dominated by the Adobe syncline (Ketner and Ross, 1990). The syncline is cored by Triassic rocks, and is, therefore, a Mesozoic-Cenozoic structure. We will look at Mississippian and Permian strata on the eastern limb, traverse across the axis of the syncline, and see Late Devonian, Mississippian and Permian strata on the western limb. If road conditions permit, we will continue west/northwest along the road and exit onto Nevada State Highway 225 and return to Boise; otherwise, we will return to Elko and then to Boise.

Figure 12. Stop 11, basal conglomerate of Permian (Guadalupian) age overlying Early Mississippian Melandco Formation. Note fragments of Melandco in carbonate matrix (inset).

ROAD LOG—COAL MINE CANYON

Please note that the mileages for this portion of the road log are approximate, because we had to estimate them from aerial photographs. There should be no cumulative error.

Mileage Cum.	Inc.	
0.0	0.0	Begin this part of the trip at the East Elko Interchange of Interstate 80. Drive east on I-80 along the Humboldt River valley.
11.2	11.2	Turn off I-80 at the Ryndon exit (second exit from the start). Turn north and go under the interstate, bear west on the north side of the Interstate, then turn north on the well-graded gravel road. Don't worry about getting lost in this small residential development, just head north and you will be on the right road.
19.7	8.5	Intersection of the Coal Mine Canyon road and a dude ranch driveway; the dude ranch itself is approximately 1 mi north of this intersection. Turn left (west) on the unmarked Coal Mine Canyon road.
22.9	3.2	Make a 90° right turn (north) into Coal Mine Canyon; there are several houses near the road.
25.5	2.5	**Stop 9.** Here, we will discuss the Mississippian conglomerates that are near prominent white cliffs (Eocene Elko Formation), where the road begins to enter the narrower part of the canyon. Stop where there is a good view of the conglomerates (mapped as "Pennsylvanian-Mississippian Diamond Peak Formation") that cap the Adobe Range.

The "Diamond Peak" nomenclature is difficult to use in this part of the Great Basin because Mississippian conglomerates here can be either part of the Antler foreland basin (C1 to C2) or Antler successor basin (C2 to C3) sections. The former is part of the Melandco, the latter, part of the Tonka (as originally defined by Dott, 1955). The sharp contact between

the underlying fine-grained strata and these conglomerates reflects either an abrupt shift from distal mudrocks to submarine channel facies of the Melandco, or the C2 unconformity with Tonka overlapping the finer-grained Melandco. The lack of age control and the massive nature of these conglomerates hamper the interpretation. These are the same conglomerates viewed at the informal Stop on Nevada State Highway 225 approximately 3 mi west of Elko.

Mileage Cum.	Inc.	
26.8	1.3	**Stop 10.** This is the Melandco Formation, characterized by sandstone horizons and polymict debris flows within shale and siltstone. The purpose of this Stop is to demonstrate the basinal facies of the Melandco, the true Antler foreland basin (C1 to C2, our terminology), for contrast with the deposits of the Antler successor basin (C2 to C3), seen yesterday. Recall that the Melandco (C1 to C2) units in Carlin Canyon were inner submarine-fan conglomerate and litharenite, which differs from this mudrock-dominated submarine fan section. The fine-grained sections are not exposed, making accurate fan models impossible.
27.3	0.5	**Stop 11.** The structure of the northern Adobe Range is dominated by the Adobe Range syncline, in the core of which lie Triassic strata. It is, therefore, clearly a Mesozoic structure. Stop 3 is on the southeast limb of the syncline.

Here, the Middle Permian (P4-P5/Tr1) unconformably overlies deformed Melandco. We are still in Melandco along the road, but the ridge to the north-northwest is capped by Permian siliciclastic and mixed siliciclastic-carbonate units. As initially mapped (Ketner and Ross, 1990), the contact between the two is interpreted to be a thrust fault. However, we now know that it is an unconformity, and that the base of the Permian is a conglomerate including clasts from the underlying Melandco (fig. 12). As you walk up the hill, note the polydeformed nature of the Melandco below the contact with the Permian.

The unconformable nature of this Mississippian-Permian contact brings into question many of the other contacts in this area that have been mapped as low-angle faults. For example, the Mississippian-Permian contact on the northwest limb of the Adobe Range syncline also has been mapped as a thrust fault (Ketner and Ross, 1990). However, we have remapped a small portion of the area (near the head of Coal Canyon) and found similar relationships to those in Carlin Canyon, although the age of deformation is not as tightly constrained; interbedded black chert, argillite and siltstone of the Roberts Mountains allochthon (Ordovician Vinini Formation and Silurian Slaven Chert, Ketner and Ross, 1990) are tightly folded, with axes uniformly trending northeast. These are in thrust contact over homoclinal black mudstone that has been designated Mississippian "Chainman Shale" (we would call it Melandco) by Ketner and Ross (1990). Both the thrust contact and the tight folding are overlain by a Permian mixed carbonate/siliciclastic unit along what we interpret to be a depositional contact. The precise ages of these units within the Mississippian has not been determined; the Permian has yielded a Guadalupian brachiopod. The age of the thrusting here can, therefore, be dated only as post-"Mississippian" and pre-Guadalupian (Middle Permian). (Note: Although we don't know the age of the "Chainman" within the Mississippian, this siliciclastic sediment was deposited in the Antler foreland basin and was derived from the Antler allochthon. These rocks subsequently have been faulted against the Antler allochthon along a pre-Middle Permian fault.)

Our map of this area differs from the published map in that the Permian is everywhere in depositional contact on the underlying rocks and, therefore, overlaps the post-Melandco thrust fault. Our interpretation is based on the lack of penetrative deformation near the contact and on the consistent gentle dips in the basal Permian where it overlies both upper and lower thrust plates. This Late Paleozoic thrust, unconformity and overlying Permian section are tightly folded by Mesozoic deformation elsewhere in this area.

The deformation within the Melando could be associated with any one, or several, of the C2 through P4 events. However, it seems likely that this pre-Middle Permian deformation may correlate with that seen in Carlin Canyon. Although we have no direct data to support this interpretation at this time, the C6 and/or C5 deformation displayed at Carlin Canyon is the most intense post-Mississippian/pre-Middle Permian deformation yet documented in Nevada. It is thus the most viable candidate for the similar-age, relatively intense deformation here in the northern Adobe Range.

Mileage Cum.	Inc.	
28.0	0.7	**Stop 12.** This is the Triassic overlap; the fossil hunters in the group may find Triassic ammonoids here. We have no experience with this Triassic unit, and therefore quote directly from the map unit description of Ketner and Ross (1990):

"Shale and limestone (Lower Triassic) – A slope and basin deposit consisting of olive-drab shale, thin-bedded limestone with graded beds and sole marks, slump deposits, and bouldery olistostromes derived from the Gerster Formation. (The Gerster is an autochthonous Permian shelf limestone unit of eastern Nevada and western Utah.) Thickness estimated to be more than 2000 ft (610 m). The Triassic unit contains many dioritic sills a few meters thick and traceable for as far as 1.5 mi (2 km) parallel to

bedding. Some of the sills contain smoothly rounded boulders of quartzite similar to the Eureka Quartzite, and of marble. Formation was dated by ammonoids and conodonts."

Ketner and Ross (1990) map the basal contact of these Triassic rocks as a low-angle fault rather than as an unconformity, because (1) they map tectonic slices of older Paleozoic units along the contact between the Permian and the Triassic, and (2) there appears to be an abrupt change in depositional setting between the Permian units—which locally contain evaporites and which they interpret to be shallow-water deposits—and the fine-grained, deep-water turbidites of the Triassic.

Alternatively, since we interpret many of the other "low-angle fault" contacts in this region to be unconformities, the Permian-Triassic contact here also may be an unconformity. This would simplify the post-Triassic deformation in this area but would not change the basic interpretation—that there was large-scale Mesozoic folding and thrust faulting. In addition, it would enlarge the geographic extent of yet another Late Paleozoic unconformity in north-central Nevada.

Mileage Cum.	Inc.	
30.0	2.0	**Stop 13.** There are several items of interest at this stop. The spectacular outcrops across the small gully are chevron-folded Late Devonian and Early Mississippian bedded chert. These deformed strata comprise a mappable, tectonostratigraphic unit (MDw) that lies structurally on top of younger Mississippian Melandco. This bedded chert succession is usually considered to be part of the Roberts Mountains allochthon, but it could also be part of the Rodeo Creek Formation or equivalent parautochthonous units of the outer continental shelf. These are well represented west of here, along the Carlin trend.

The nature of the folds within MDw suggests deformation occurred not long after deposition—it could correlate with the classic Antler orogeny, or other Mississippian or Early Pennsylvanian event(s); the nature of the deformation and possible interpretations will be discussed on the outcrop.

LOGISTICAL NOTE: Depending on recent weather conditions, we may have to turn around and retrace the route to Elko. There is a creek crossing 6.4 mi ahead that a van cannot cross if the creek has moderate-flow levels.

Mileage Cum.	Inc.	
35.9	5.9	Sharp left (west) turn toward creek.
36.4	0.5	Creek crossing.
36.9	0.5	Sharp (almost 90 degree) turn to the west.
37.7	0.8	90 degree turn to the south.
38.4	0.7	Nevada State Highway 225 (highway from Boise and Mountain Home to Elko).

This is the end of this segment.

Follow Highway 225 north through Mountain Home to Interstate 84, east on I-84 to Boise; approximately 185 mi total travel from where you enter Highway 225 to Boise (total approximately 220 mi from Boise to Elko). Note: Highway 225 turns into Idaho State Highway 51.

Acknowledgments

Many colleagues and students, over many years, have contributed to our understanding of the area traversed by this field trip. Bob Dott's seminal work in the area (1955) put us on the right track, and continues to be a reference bible. Geologic insights and age control have been provided by Norm Silberling, Scott Ritter, Bruce Wardlaw, John Groves, Tamra Schiappa, Paula Noble, CJ Northrup, Jennifer Titcze, Dustin Sweet, Ted Theodore, and Keith Ketner. Land access has been kindly provided by the Maggie Creek Ranch.

References

Berger, V.I., Singer, D.A., and Theodore, T.G., 2001, Sedimentology of the Pennsylvanian and Permian Strathearn Formation, northern Carlin Trend, Nevada: U.S. Geological Survey Open-File Report 01-402, 99 p.

Burchfiel, B.C., and Davis, G.A., 1972, Structural framework and evolution of the southern part of the Cordilleran orogen, Western United States: American Journal of Science, v. 272, p. 97–118.

Burchfiel, B.C., and Davis, G.A., 1975, Nature and controls of Cordilleran orogenesis, Western United States; extensions of an earlier synthesis: American Journal of Science, v. 275-A, p. 363–396.

Dickinson, W.R., 2000, Geodynamic interpretation of Paleozoic tectonic trends oriented oblique to the Mesozoic Klamath-Sierran continental margin: Geological Society of America Special Paper 347, p. 209–245.

Dott, R.H., 1955, Pennsylvanian stratigraphy of the Elko and northern Diamond Ranges, northeast Nevada: American Association of Petroleum Geologists Bulletin, v. 39, p. 2211–2305.

Jansma, P.E., and Speed, R.C., 1990, Omissional faulting during Mesozoic regional contraction at Carlin Canyon, Nevada: Geological Society of America Bulletin, v. 102, p. 417–427.

Johnson, J.G., and Visconti, R., 1992, Roberts Mountains thrust relationships in a critical area, northern Sulphur Springs Range, Nevada: Geological Society of America Bulletin, v. 104, p. 1208–1220.

Ketner, K.B., 1998, The nature and timing of tectonism in the western facies terrane of Nevada and California—An outline of evidence and interpretations derived from geologic maps of key areas: U.S. Geological Survey Professional Paper 1592, 19 p.

Ketner, K.B., and Ross, R.J., 1990, Geologic map of the northern Adobe Range, Elko County, Nevada: U.S. Geological Survey Miscellaneous Investigations I-2081, scale 1:24,000.

Pipiringos, G.N., and O'Sullivan, R.B., 1978, Principal unconformities in Triassic and Jurassic rocks, western interior United States—A preliminary survey: U.S. Geological Survey Professional Paper 1035-A, p. A1–A29.

Peterson, F., and Pipiringos, G.N., 1979, Stratigraphic relations of the Navajo Sandstone to Middle Jurassic formations, southern Utah and northern Arizona: U.S. Geological Survey Professional Paper 1035-B, p. B1–B43.

Poole, F.G., 1974, Flysch deposits of the Antler foreland basin, Western United States, *in* Dickinson, W.R., ed., Tectonics and sedimentation: Society of Economic Paleontologists and Mineralogists Special Publication 22, p. 58–82.

Poole, F.G., and Sandberg, C.A., 1977, Mississippian paleogeography and tectonics of the Western United States, *in* Stewart, J.H., Stevens, C.H., and Fritsche, A.E., eds., Paleozoic paleogeography of the Western United States: Tulsa, Oklahoma, Society of Economic Paleontologists and Mineralogists, Pacific Section, Pacific Coast Paleogeography Symposium 1, p. 67–85.

Roberts, R.J., 1951, Geology of the Antler Peak quadrangle, Nevada: U.S. Geological Survey Geologic Quadrangle Map GQ-10, scale 1:62,500.

Roberts, R.J., Hotz, P.E., Gilluly, J., and Ferguson, H.G., 1958, Paleozoic rocks of north-central Nevada: American Association of Petroleum Geologists Bulletin, v. 42, p. 2813–2857.

Schiappa, T.A., Snyder, W.S., and Trexler, J.H., Jr., 1999, Tectonic signatures within the Pennsylvanian-Early Permian Tippipah Limestone, Nevada Test Site: Geological Society of America, Abstracts with Programs, v. 31, no. 4, p. A-54.

Schwarz, D.L., Carpenter, J.A., and Snyder, W.S., 1994, Reexamination of critical geological relations in the Carlin Canyon area, Elko County, Nevada, *in* Dobbs, S.W., and Taylor, W.J., eds., Structural and stratigraphic investigations and petroleum potential of Nevada, with special emphasis south of the Railroad Valley producing trend: Reno, Nevada Petroleum Society, p. 255–272.

Silberling, N.J., Nichols, K.M., Trexler, J.H., Jr., Jewell, P.W., and Crosbie, R.A., 1997, Overview of Mississippian depositional and paleotectonic history of the Antler foreland, eastern Nevada and western Utah, *in* Link, P.K., and Kowalis, B.J., eds., Geological Society of America Fieldtrip Guidebook: Provo, Brigham Young University, v. 42, p. 161–196.

Silberling, N.J., and Roberts, R.J., 1962, Pre-Tertiary Stratigraphy and structure of northwestern Nevada: Geological Society of America Special Paper 58, 58 p.

Smith, J.F., and Ketner, K.B., 1978, Geologic map of the Carlin-Piñon Range area, Elko and Eureka Counties, Nevada: U.S. Geological Survey Miscellaneous Investigation I-1028, scale 1:62,500.

Snyder, W.S., Trexler, J.H., Jr., and Cashman, P.H., 1997, A newly recognized tectonic event in Nevada: Geological Society of America Abstracts with Programs, v. 29.

Snyder, W.S., 2000, The upper Paleozoic continental margin of western North America—A tectonostratigraphic framework: Geological Society of America Abstracts with Programs, v. 32, p. 466.

Speed, R.C., and Sleep, N., 1982, Antler orogeny and foreland basin—A model: Geological Society of America Bulletin, v. 93, p. 815–828.

Theodore, T.G., Armstrong, A.K., Harris, A.G., Stevens, C.H., and Tosdal, R.M., 1998, Geology of the northern terminus of the Carlin trend, Nevada—Links between crustal shortening during the late Paleozoic Humboldt orogeny and northeast-striking faults, *in* Tosdal, R.M., ed., Contributions to the gold metallogeny of northern Nevada: U.S. Geological Survey Open-File Report 98-338, p. 69–105.

Trexler, J.H., Jr., and Giles, K., 2000, The Antler orogeny in the Great Basin—A review of the data: Geological Society of America Abstracts with Programs, v. 32, no. 7, p. A–382.

Trexler, J.H., Jr., Cashman, P.H., Cole, J.C., Snyder, W.S., Tosdal, R.M., and Davydov, V.I., 2003, Widespread effects of mid-Mississippian deformation in the Great Basin of western North America: Geological Society of America Bulletin, v. 115, p. 1278–1288.

Trexler, J.H., Jr., Cashman, P.H., Snyder, W.S., and Davydov, V.I., 2004, Upper Paleozoic tectonism in Nevada; timing, kinematics, and tectonic significance: Geological Society of America Bulletin, in press.

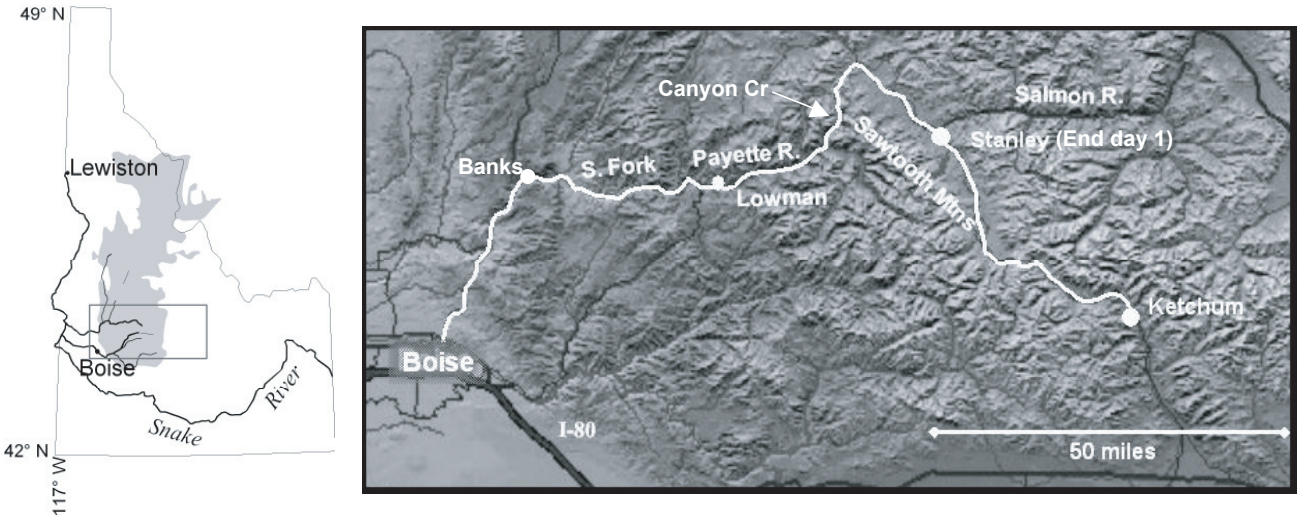

Figure 1. Map showing approximate location of the field-trip area within the State of Idaho and enlargement of field-trip route to right of state map. Gray shading on the state map shows the outline of the Idaho batholith. The trip will depart from Boise, travel up the main stem Payette River, turn east at Banks up the South Fork Payette Canyon, and continue up Canyon Creek into the Stanley Basin, ending day one in Stanley. Day two of the trip will examine glacial features near lakes on the eastern side of the Sawtooth Mountains and continue over Galena summit into the town of Ketchum.

Fire and Ice in Central Idaho: Modern and Holocene Fires, Debris Flows, and Climate in the Payette River Basin, and Quaternary and Glacial Geology in the Sawtooth Mountains

By Jennifer L. Pierce[1], Grant A. Meyer[1], Glenn D. Thackray[2], Spencer H. Wood[3], Kari Lundeen[4], Jennifer A. Borgert[5], and Eric Rothwell[3]

Introduction

This 2-day trip will highlight recent fire and storm-related debris flows in the Payette River region, Holocene records of fires and fire-related sedimentation events preserved in alluvial fan stratigraphic sequences, and geomorphology and geology of alpine glaciations in the spectacular Sawtooth Mountains and Stanley Basin of central Idaho. Storm events and associated scour following recent fires in the South Fork Payette basin have exposed Holocene fire-related debris-flow deposits, flood sediments, and other alluvial fan-building deposits that yield insights into Holocene environmental change. Moraine characteristics and sediment cores from the southeastern Sawtooth Mountains and Stanley Basin provide evidence of late Pleistocene alpine glaciation. A combination of these glacial records with reconstructions of regional equilibrium line elevations produces late-glacial paleoclimatic inferences for the area.

Day one of the trip will examine recent and Holocene fire-related deposits along the South Fork Payette River; day two will focus on alpine glaciation in the Sawtooth Mountains (fig. 1). A description of the scope, methods, results and interpretation of the South Fork Payette fire study is given below. Background information on late Pleistocene alpine glaciation in the eastern Sawtooth Mountains is presented with the material for day 2 of the trip.

The road log for day 1 of the trip begins at Banks, Idaho, and ends in Stanley, Idaho. Stop locations are shown on figure 2. At Stop 1, we will provide an introduction to interpretation of alluvial fan stratigraphic sections, and discuss the Boise Ridge fault. At Stops 2–4 (Hopkins Creek, Deadwood River, and Jughead creek), we will examine recent debris-flow deposits and Holocene alluvial fan stratigraphic sections. At Stop 5 (Helende Campground), we will look at a series of well-preserved Holocene and Pleistocene terraces and at Stop 6 (Canyon Creek), we will briefly inspect fire-related deposits in higher-elevation alluvial fan stratigraphic sections.

The road log for day 2 begins at Stanley, Idaho, and ends in Sun Valley, Idaho. Stop locations are shown on figure 2. Stop 1, at Redfish Lake, will focus on regional equilibrium line altitude reconstructions and on the general pattern of late Pleistocene glaciation on the eastern flank of the Sawtooth Mountains. Stop 2 will be at Pettit Lake, where we will examine the moraine sequence and discuss relative weathering criteria and moraine groupings. At Stop 3, near Alturas Lake, we will discuss lake sediment coring, moraine chronology, and implications for latest Pleistocene paleoclimatic inferences. Stop 4 will be a brief stop at Galena Summit for an overview of the Sawtooth Mountains and a discussion of ice accumulation patterns. The trip will end at a set of moraines in the Trail Creek valley, near Sun Valley, where we will examine moraine morphology and weathering rind data that constrain the moraine ages.

South Fork Payette Fire Study

Introduction

Fire is an important agent of geomorphic change in forested mountain landscapes (Swanson, 1981; Wells, 1987; Parrett, 1988; Benda and Dunne, 1997; McNabb and Swanson, 1990; Meyer and others, 1995; Meyer and Wells, 1997; Cannon and others, 1998; Cannon and Reneau, 2000). Greatly increased surface runoff and decreased slope stability after severe fires often produce floods, debris flows, and massive sediment transport. In recent years, a number of "catastrophic" fires have burned through conifer forests of the Western

[1]University of New Mexico, Department of Earth and Planetary Science, Albuquerque, NM 87131, jpierce@unm.edu, gmeyer@unm.edu

[2]Department of Geosciences, Idaho State University, Pocatello, ID 83209-8072, thacglen@isu.edu

[3]Geosciences Department, Boise State University, Boise, ID 83725, EricRothwell@mail.boisestate.edu

[4]Connecticut Department of Environmental Protection, Hartford, CT 06106, kari.lundeen@po.state.ct.us

[5]Retec, Inc., St. Paul, MN, JBorgert@retec.com

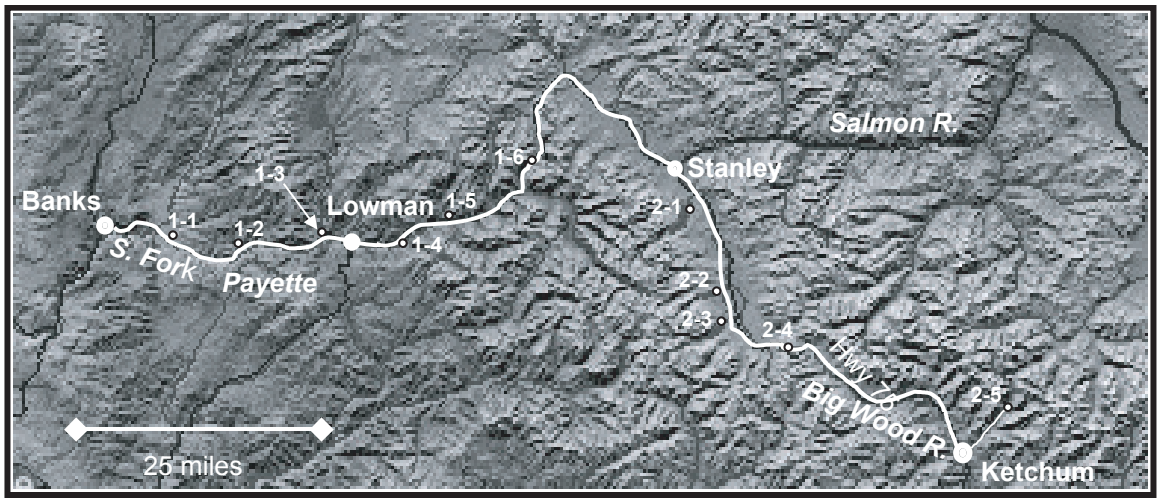

Figure 2. Approximate locations of field-trip stops. Stops on the first day of the trip along the South Fork Payette River focus on fire-related deposits in alluvial-fan stratigraphy, and include Stop 1-1 (Garden Valley fault), 1-2 (Hopkins Creek), 1-3 (Deadwood River), 1-4 (Jughead creek), and 1-5 (Helende Campground). The second day of the trip examines evidence of late Pleistocene alpine glaciation in the southeastern Sawtooth Mountains at Redfish Lake (2-1), Petit Lake (2-2) Lost Boots marsh (2-3), Galena Summit (2-4), and concludes with a study of moraine characteristics along Trail Creek (2-5) outside of Ketchum, Idaho.

United States, promoting concerns about soil erosion, accelerated sedimentation and other impacts to aquatic ecosystems, and hazards to human development. In 2002, wildfires burned over 7 million acres across the United States (National Interagency Fire Center, 2003), from the moist fir and hemlock forests of the Pacific Northwest, to the dry ponderosa pine forests of Arizona and New Mexico.

Fire data for the past 30 years reveal that although the annual acreage burned has not increased, the total number of large, severe fires has increased, and three of the largest fires ever recorded in the United States have occurred in the last 12 years (National Interagency Fire Center, 2003). In many ponderosa pine (*Pinus ponderosa)* forests in the Western United States, fire suppression, logging, and grazing are thought to have caused unprecedented increases in tree densities in post-settlement times (Cooper, 1960; Swetnam and Baisan, 1996; Covington and Moore, 1994; Arno and others, 1995; Fule and others, 1997). The resulting buildup of fuels due to fire suppression, and decrease in the availability of fine fuels for frequent surface fires due to grazing may account for the increase in fire size and severity (Swetnam, 1993; Covington and Moore, 1994; Grissino-Mayer and Swetnam, 2000; Kipfmueller and Baker, 2000), and a corresponding apparent increase in fire-related erosional events. Likewise, in central Idaho, tree-ring records show that although fire frequency decreased significantly within the 1900s, fire severity and magnitude increased in ponderosa pine and Douglas-fir *(Pseudotsuga menziesii)* forests late in the century (Steele and others, 1986; Barrett, 1988; Barrett and others, 1997).

In many ponderosa pine forests, recent stand-replacing fires contrast with frequent, low-intensity fires during presettlement times, as shown by tree-ring fire-scar studies. Climate is a primary control on fire regimes, however, and using the prefire suppression record to define reference conditions and management goals for the warmer and drier present may not be justifiable. The tree-ring fire-scar records begin during the Little Ice Age (LIA), a time of widespread minor glacial advances and generally cooler climate ca. 1200-1900 AD (*e.g.*, Grove, 1988; Luckman, 2000; Grove, 2001; Esper and others, 2002). Following the LIA, marked warming occurred in the late 1800s–early 1900s and the late 20th century (Jones and others, 1999; Mann and others, 1999). Geothermal data from boreholes provide a record of past fluctuations in surface temperatures. Temperature reconstructions from these data show a 1° C increase in temperature over the last 5 centuries, with half of that increase occurring during the last century (Pollack and others, 1998). Therefore, at least some of the observed increase in magnitude and severity of fires may be the result of a warming climate and severe droughts.

With the exception of data reported by Meyer and others (1995), little is known about changes in fire regimes and rates of slope erosion, how those changes relate to climate, and whether or not recent catastrophic fires truly are extraordinary in Holocene times. Fires and fire-related floods and debris flows are recorded in alluvial fans as burned soil surfaces and charcoal-rich deposits. Although alluvial-fan deposition is discontinuous in both space and time, fan deposits provide records of events in specific small basins, contain datable materials and, unlike lakes, are ubiquitous in mountain landscapes. The episodic nature of deposition on alluvial fans can be offset by compiling the records from tens to hundreds of individual stratigraphic sections, yielding a detailed history for the region.

On this trip, we will view the effects of recent large debris-flow and flood events in the South Fork Payette River region, in both burned and unburned mountain drainage

basins. Depositional and erosional features yield evidence of flow processes and geomorphic controls. Deposits also provide analogs to aid in interpretation of Holocene fan stratigraphy. We will examine a number of the dated alluvial-fan stratigraphic sections that are being used to develop a detailed record of fire-related sedimentation events in the South Fork Payette region and to estimate long-term sediment yields at selected locations. We also will consider how changes in the magnitude and frequency of fire-related sedimentation may relate to regional climate change. Insights are gained through comparison and contrast of the Payette record with similar data from the cooler, high-elevation lodgepole-pine forests of Yellowstone National Park (Meyer and others, 1995).

Study Area

The Idaho batholith

The Idaho batholith covers approximately 41,000 km^2 in central Idaho and western Montana (fig. 1) and is part of a chain of large intrusive bodies that extend inland along western North America (Hyndman, 1983; Clayton and Megahan, 1986). Limited dating using K-Ar and Rb-Sr methods indicates that the large southern Atlanta lobe of the batholith was intruded between about 95 and 65 Ma (Armstrong, 1974; Kiilsgaard and others, 2001). The batholith in the South Fork Payette study area is composed mainly of biotite granodiorite and muscovite-biotite granite (McCarthy and Kiilsgaard, 2001). Fission-track data suggest the Atlanta lobe of the batholith lay at a shallow depth and was relatively unaffected by tectonism during most the Cenozoic, despite active Basin and Range extension around its margins, and was then unroofed by rapid denudation over the last 10 Ma (Sweetkind and Blackwell, 1989). The batholith is intruded by Eocene stocks and batholiths ranging in composition from gabbro to younger granite that likely are related to the Eocene Challis Volcanics (Kiilsgaard and others, 2001). Shallow emplacement and rapid cooling of these Eocene plutons caused widespread (>10,000 km^2) meteoric-hydrothermal alteration of the batholith granitic rock (Criss and Taylor, 1983). Tertiary rhyolitic to andesitic dikes ranging in width from a few centimeters up to approximately 100 m cross cut all plutonic rocks and generally are more resistant than the weathered batholith granite. The majority of these dikes strike northeast, likely associated with the northeast-trending pattern of regional faults in the central Idaho area (Kiilsgaard and others, 2001).

The batholith granitic rock in the Payette River region is highly weathered and altered, and surface and road-cut exposures show decomposed granite to depths of over 10 m. Drill cores from the Arrowrock Reservoir site on the Middle Fork Boise River reveal biotite oxidation and feldspar hydrolysis to depths of over 600 m (J.L. Clayton, 2003, written commun.). The present suite of hot springs along the South Fork Payette River, however, represents nonmagmatic, fracture-controlled hydrothermal systems (Druschel and Rosenberg, 2001).

A belt of north-south trending, late-Cenozoic normal faults runs along the west side of the Idaho batholith (Hamilton, 1962). The east-facing escarpments and west-dipping footwall blocks of these faults contrast with predominantly west-facing escarpments and east-dipping footwall blocks of faults east of the batholith (Wood and Clemens, 2002). The Boise Ridge fault forms a prominent east-facing escarpment across the lower South Fork Payette valley.

Geomorphology

The South Fork Payette River canyon is deeply incised within a lower-relief upland and features steep slopes (20–40°) and high local relief (~500 m) (figs. 2 and 3). Broad trough valleys with floors mantled by till and outwash deposits characterize the glaciated headwaters (Stanford, 1982). Below the last-glacial terminal position near Grandjean, the valley floor has a generally narrower but variable width. Fluvial-terrace surfaces with tread-surface heights between 1 and 20 m above current bankfull level are common except within the canyon between Lowman and Gallagher Creek, and fluvial gravels locally exist as high as 185 m above the current channel. Bedrock strath surfaces predominate in constrained reaches of more resistant bedrock, whereas in broader segments bordered by floodplain or fluvial terraces, small valley-side alluvial fans store some of the sediment produced from tributary basins. Granular disintegration of weathered Idaho batholith granitic rocks has produced abundant grussy colluvium on unglaciated slopes along the canyon. Soils on hillslopes in the South Fork Payette area are coarse textured and typically have A and oxidized C horizons underlain by weathered granitic bedrock (Clayton, 1979). Soils on hillsides are poorly developed due to high erosion rates and lack significant accumulations of clay and other fine-grained material (Clayton, 1979); however, fines are locally abundant in areas of strongly altered bedrock.

Between Lowman and the Gallagher Creek area, the South Fork Payette River enters a higher gradient canyon, with steep valley walls and few preserved terrace surfaces. Below Gallagher Creek, the valley is characterized by high bedrock strath terrace surfaces about 20 m, 15 m, and 10 m above the incised modern channel. At Garden Valley, abrupt widening of the valley floor to about 2 km likely is related to late Cenozoic movement on the Boise Ridge fault (Wood, 2004).

Climate and Vegetation

Pacific-derived moisture from winter cyclonic storms accounts for most of the annual precipitation, whereas occasional localized convective storms occur during summer months. Annual rainfall data show that between 1896 and 2002, 39 percent of mean-annual precipitation in the study area occurred between November and February, while only 13 percent of the mean-annual precipitation fell between June

Figure 3. Looking west along South Fork Payette River, note steep valley slopes within the canyon, with higher elevations in the distance typified by more moderate relief. The mixed ponderosa pine and Douglas-fir forests on the north-facing slopes versus the sparsely forested rangeland on south-facing slopes reflect the strong aspect control on vegetation in this area.

and August. At Lowman, the mean annual temperature is –5° C, and about 60 percent of the total precipitation comes as snowfall. Mean-annual precipitation in the study area varies from approximately 60 cm at lower elevations to approximately 80–100 cm or more at higher elevations. Snowmelt produces a majority of the runoff, but rapid thaws and large storms sometimes generate major winter floods (Meyer and others, 2001). A pronounced summer dry period is conducive to frequent fires, especially at lower elevations.

The South Fork Payette study area includes several different climatic and ecologic zones determined largely by elevation and aspect. On south-facing slopes in the lower basin (below ~900 m), the valley vegetation is typified by shrubs, grasses, forbs, and sparse ponderosa pines. At elevations between 900–1,400 m, open ponderosa pine forests cover south-facing slopes and mixed pine, and Douglas-fir forests are found on north-facing and wetter sites. Higher elevations above about 2,200 m are typified by ponderosa pine and Douglas-fir forests on south-facing slopes and mixed spruce, Douglas-fir and pine forests on north-facing slopes (fig. 3). Palmer Drought Severity Index (PDSI) calculated for the study area (climate region 4) shows that drought severity has increased over the period of instrumental record (statistically significant at the 95 percent confidence interval) between 1895 and 2002, with extended periods of drought from 1928–1937, 1987–1995, and 1999–2003. During the same period, mean summer temperature (June–August) in Idaho climate division 4 increased by approximately 0.3° C (fig. 4). The periods 1901–1925 and 1951–1975 were generally wetter periods with cooler summers, and relatively small areas burned in the Boise National Forest (~140 and 170 km^2, respectively). In contrast, 1926–1950 and 1976–1996 are periods when large areas burned (~1,270 and 1,650 km^2) and include prolonged droughts with generally warmer summers.

Recent Fires, Storms, and Erosional Events

From July 15–27, 1989, lightning ignited 335 fires in the Boise and Payette National Forests. The Lowman fire ultimately burned over 186 km^2 of ponderosa pine and Douglas-fir forest until it was put out by cooler temperatures and higher humidity in the early fall of 1989. Eight years later, between December 20, 1996, and January 4, 1997, the South Fork Payette basin received approximately 11 inches of rain on melting snow. This event caused widespread flooding and culminated in numerous slope failures in colluvial hollows on New Year's Day (Meyer and others, 2001).

A previous study documenting the colluvial failures resulting from the 1997 storm in the South Fork Payette area showed that of the 246 failures inventoried, approximately 75 percent occurred in areas burned in 1989, and about 25 percent occurred on unburned but unforested south-facing slopes (Shaub, 2001). The majority of the colluvial failures (92 percent) occurred below 1,588-m elevation, which may indicate a threshold for frozen ground at the time of this event (Shaub, 2001). These colluvial failures led to sediment-charged sheetfloods and debris flows in tributary channels of the South Fork Payette, incision of tributary fans, and damage to roads and buildings.

Fire-Related Geomorphic Processes

Fire promotes sedimentation events such as debris flows and floods via two distinct sets of processes (Meyer and Pierce, 2003). Saturation-induced failures result when infiltration of heavy rainfall, snowmelt, or rainfall on areas with high-saturation antecedent conditions cause failure of colluvium. Fire increases the likelihood of failure because of diminished root strength after decay. The difficulty of measuring root cohesion and its importance relative to other factors in slope stability (*e.g.*, Schmidt and others, 2001) makes it difficult to positively identify fire as the primary cause of failure. Reduced infiltration, typically caused by post-fire water repel-

lency and(or) surface-sealing of soils (Robichaud, 2000), provides an additional mechanism for generating major sedimentation events following fire. Greatly increased overland flow picks up abundant sediment through sheetwash, rilling, and gully erosion, such that sediment-charged flows ranging from flash floods to debris flows are produced through progressive sediment bulking (Meyer and Wells, 1997; Cannon and others, 2003). Post-fire surface runoff typically is generated by high-intensity precipitation, as in summer convective storms, and can readily erode the cohesionless grussy colluvium of the Idaho batholith (Megahan and Molitor, 1975).

Sedimentation on Alluvial Fans

The range of possible depositional processes on alluvial fans includes debris flow, hyperconcentrated flow, sheetflood, and streamflow. Deposit facies produced by these flow types have been recognized and defined by previous studies based on their sedimentology and morphology. Debris flows are non-Newtonian fluids with high sediment concentrations, where the water and fine sediment move together in a single fluid slurry. Characteristic features of debris-flow deposits include very poor sorting, marginal levees, a lack of internal stratification and a fine-grained matrix between clasts. The matrix may flow out on deposition, or may have later been washed out of the deposit (Pierson and Costa, 1987; Costa, 1984, 1988; Blair and McPherson, 1994; Meyer and Wells, 1997). Noncohesive debris flows contain low percentages of silt and clay. This lack of fines can reflect the character of available sediment in the basin and is a common characteristic of the grussy, generally clay-poor regolith in the South Fork Payette region. Hyperconcentrated flows also are non-Newtonian flows that are transitional between Newtonian water flow (streamflow of Pierson and Costa, 1987) and debris flows. Hyperconcentrated flows have a measurable but low yield strength from particle interactions, and turbulence is damped relative to water flows (Pierson and Costa, 1987). Poorly sorted deposits that are unstratified or weakly stratified with internal grading patterns and a sand and pebble-dominated texture often characterize hyperconcentrated flows deposits in the South Fork Payette region. Streamflows are Newtonian highly turbulent flows with sediment concentrations that are too low to produce a yield strength and leave stratified deposits (Pierson and Costa, 1987). Sheetfloods are unconfined streamflows that spread over fan surfaces (Blair and McPherson, 1994; Meyer and Wells, 1997). Sheetflood deposits typically contain well-developed, graded surface-

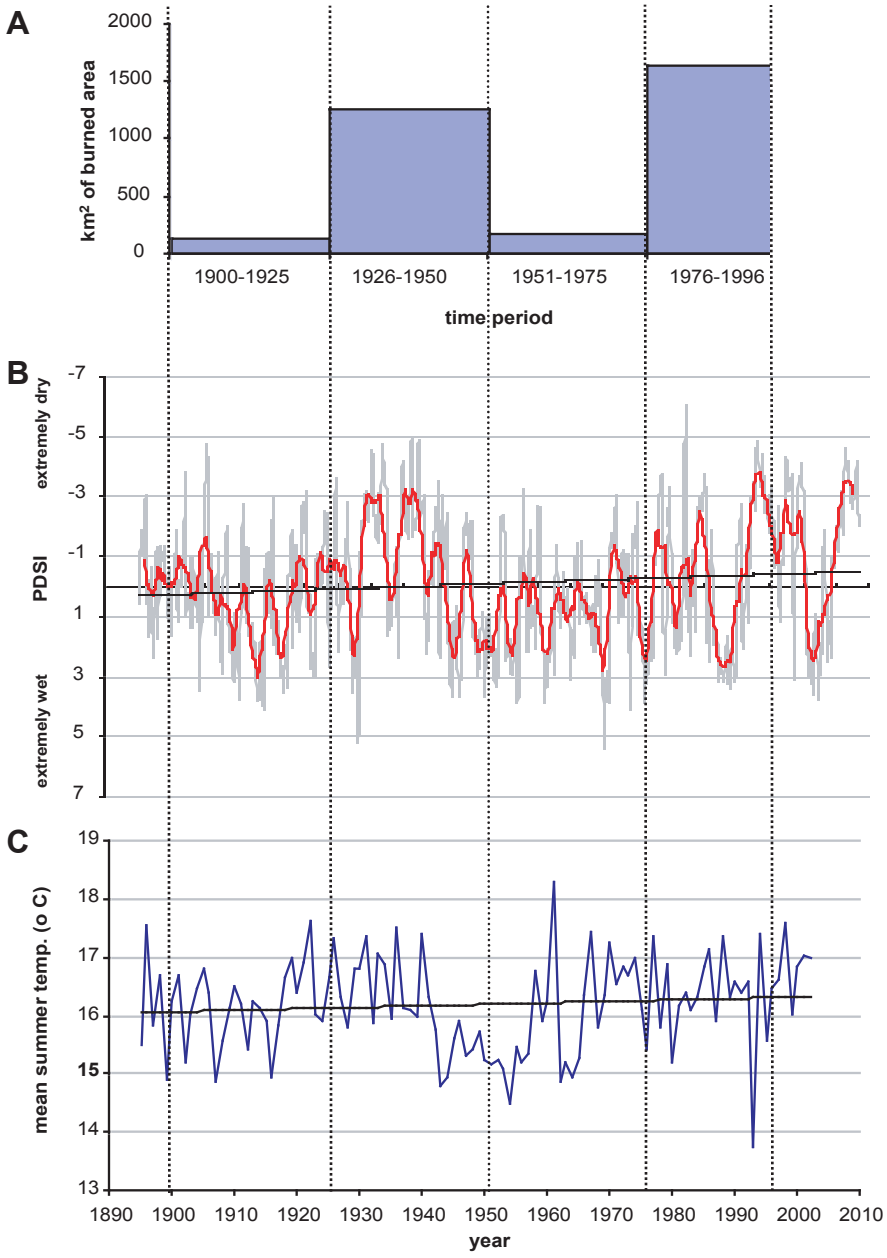

Figure 4. (A) Approximate number of square kilometers of area burned in the Boise National Forest between 1900–1997 (Strom and others, 1998) is shown as a bar graph. (B) Palmer Drought Severity Index (PDSI; top graph) for Idaho division 4, where the light gray lines show monthly PDSI values; and the black line shows a 20-month moving average of PDSI values. (C) Idaho division 4 mean summer (June–August) temperature from 1895–2003. Trendlines show increase in mean summer temperatures (~0.3° C) and a decrease in PDSI (~0.8 units) over the 20th century.

parallel stratification, and are better sorted than debris flows or hyperconcentrated flow deposits. Streamflows confined within fan channels often generate coarse, imbricated deposits. Streamflow and sheetflood deposits are relatively well sorted and clast supported with features such as sorting and clast imbrication indicating suspension- and traction-transport processes.

Methods

We described alluvial-fan stratigraphy and sampled charcoal for ^{14}C dating from sites in the South Fork Payette and North Fork Boise River basins of central Idaho. Field examination of deposit sedimentary structures, sorting, clast size and content, proportions of sand, silt, and clay in the fine (<2 mm) fraction of the deposit, boundary characteristics, color, and the presence of buried soils were used to determine variations in deposit characteristics. Fire-related deposits were distinguished based on the presence of abundant angular charcoal fragments or dark mottles of charcoal or charred material. Buried burned-soil surfaces are characterized by discrete, laterally extensive layers approximately 0.5–5-cm thick, composed predominantly of fine charred organic material representing the forest litter layer. In the South Fork Payette area, these incipient buried soils usually do not display distinct soil development other than a thin, weak A horizon (sometimes with silt enrichment) underlying the charred organic layer. If the burned surface is not disturbed by bioturbation and erosion before deposition of overlying sediment, this indicates that the depositional event occurred soon after a fire, and thus is likely related to fire.

Individual units within alluvial fan stratigraphic sections also were differentiated by deposit characteristics and thickness. Debris-flow units with abundant coarse angular charcoal that generally are coarser grained than other units in a stratigraphic section and comprise at least 20 percent of the thickness of the section are classified as “major events.” These deposits most likely represent high-severity burns. Deposits that are clearly related to fire, but do not meet the above criteria are classified as “small events.”

Dating Methods

Charcoal samples were radiocarbon dated at the NSF-Arizona Laboratory using accelerator mass spectrometry (AMS). To avoid dating samples of inner heartwood and bark from older trees that have “inbuilt” ages significantly older than the fires that burned them (Gavin, 2001), small twigs,

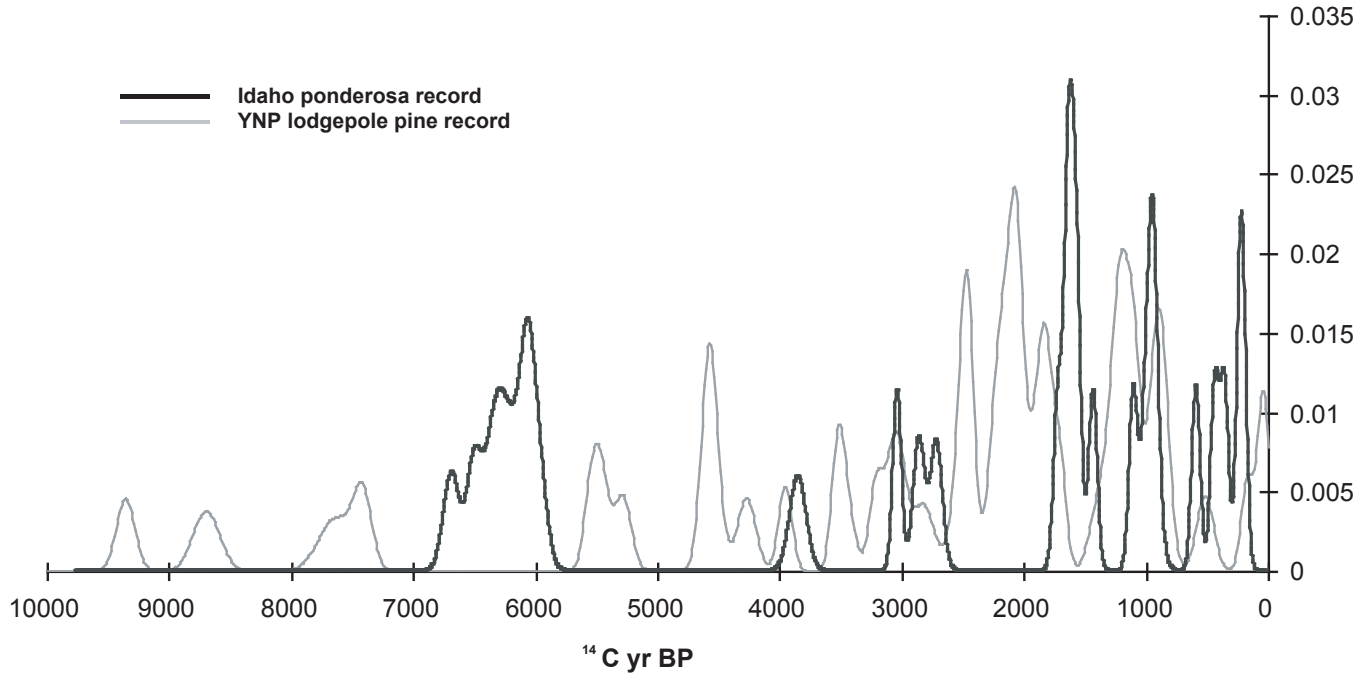

Figure 5. Probability distributions of 26 individual radiocarbon ages and their analytical uncertainty for alluvial-fan sites from the South Fork Payette Idaho study area (black line). Yellowstone (YNP) data (gray line) are from Meyer and others (1995). Preliminary data in the Idaho ponderosa record show peaks during the “Little Ice Age” (LIA) between about 750–50 cal yr BP when fire-related sedimentation in YNP is at a minimum. Both records show the probability of fire-related events at one maximum centered about 1,000 ^{14}C yr BP, which corresponds with Medieval Climatic Anomaly (MCA) between about 750–1,050 cal yr BP. Most of the fire-related events in the Idaho study area that occurred during the MCA were major fire-related debris-flow events (criteria described in text), while the LIA is characterized by frequent but minor fire-related sedimentation events in Idaho.

cone fragments, needles, and seeds were selected where possible. Individual charcoal fragments were selected for dating to avoid mixing of charcoal ages; rootlets were removed manually and acid and base washes were used to remove soluble organic contaminants. Identification of charcoal macrofossils was used when possible to determine the type of vegetation burned, and to aid in paleoclimatic interpretation.

Inverted dates (those with ages significantly older than underlying age(s) in a sequence) can be caused by bioturbation, deep burning of roots, reworking of older charcoal from existing soils or deposits, or large inbuilt ages. Analysis of radiocarbon dates within their stratigraphic context and careful selection and handling of samples limits error from these sources. For multiple ages obtained within the same deposit, the youngest age was assumed to have the least inbuilt age and to be the most accurate. Radiocarbon ages (^{14}C yr BP) were calibrated to calendar years (cal yr BP) using the program CALIB 4.3 (*e.g.*, Stuiver and Reimer, 1993).

Preliminary Results and Interpretation

Figure 5 summarizes preliminary sample results from ten dated alluvial fan sections. These results show several periods of frequent fire-related sedimentation in the South Fork Payette area at ca. 200–600 cal yr BP, 900–1,000 cal yr BP, 1,300–1,600 cal yr BP, 2,800–3,100 cal yr BP, and 6,600–7,400 cal yr BP. The majority of these events produced relatively minor sheetflood and small debris-flow deposits, consistent with the limited erosional response typical of low- to mixed-severity fires (Lavee and others, 1995). The relatively frequent fire-related events 200–600 cal yr BP occurred during the Little Ice Age in the South Fork Payette region. This and most of the other peak periods of fire-related sedimentation frequency in Idaho correspond to times of relatively few fire-related sedimentation events in Yellowstone National Park (fig. 5). Minima in fire-related sedimentation in the high-elevation Yellowstone forests occur during relatively cool, wet periods, when fire spread is inhibited by fuel moisture (Meyer and others, 1995). In the more xeric Idaho study area, these may be times when effectively wetter conditions allow abundant grass growth, fueling frequent low-severity fires during the typical summer drought.

Evidence of large, fire-related debris flows ca. 900 cal yr BP is found at site LO10 (Stop 4), and at the higher elevation GJ2 site (Stop 6). A ca. 900 cal yr BP forest fire also was dated at the Deadwood River archeological site (Stop 3) (Reid, 2001). These events occurred during the so called "Medieval Warm Period", or Medieval Climatic Anomaly 1,050–750 cal yr BP, a time of locally warmer temperatures and(or) episodes of severe drought in some regions (Bradley and others, 2003). Widespread and severe multi-decadal droughts occurred in the Western United States between 1,050–750 cal yr BP (Stine, 1994; Woodhouse and Overpeck, 1998; Benson and others, 2002). This also was a time of major fire-related debris-flow activity in Yellowstone (Meyer and others, 1995) (fig. 5) and of increased fire activity in a variety of northwestern United States conifer forests (Whitlock and others, 2003). These data suggest that in Idaho ponderosa forests, occasional large, stand-replacing fires may be typical during warmer and drier times.

Additional dating of fire-related sedimentation in the Payette River area is pending, and results will be presented on the field trip. We will use these data to test the hypotheses of relations between climate, fire, and sedimentation presented above. This understanding will allow better predictions of the impact of probable future climate warming on fire regimes in ponderosa pine forests.

Acknowledgments

This work was supported by National Science Foundation grants EAR 0096344 (awarded to Grant Meyer), in support of dating at the NSF-Arizona AMS Laboratory, and by grants from the UNM Department of Earth and Planetary Sciences and the University of New Mexico (awarded to Jennifer Pierce). We wish to thank Spencer Wood, Tim Lite, Lydia Rockwell, Sara Caldwell, Catharine North, Ken Pierce, and Wallace Andersen for field assistance, and Kari Grover-Wier of the U.S. Forest Service—Lowman Ranger District, and Spencer and Layle Wood for cooperation and logistical assistance.

Figure 6. Large boulders and matrix material from Staircase rapids debris flow, September 2001. Debris from channel on north side of South Fork Payette crossed road (note cars on left side of photo) and flowed into main stem Payette River out of photo to right (photo credit: Spencer Wood, Boise State University).

ROAD LOG—DAY 1

Mileage Cum.	Inc.	
		Depart from Boise, Idaho, and take State Highway 55 approximately 45 miles to the town of Banks, Idaho.
0.0	0.0	(lat 44°05'9"N., long 116°06'53"W.) Town of Banks. Turn right onto the Banks-Lowman Road and reset your odometer.
0.7	0.7	(lat 44°05'0"N., long 116°06'7"W.) 1997 debris flows from tributaries on the north side of the South Fork Payette raised local base levels in this area, drowning trees upstream of "Slalom Rapids," and significantly changing main-stem channel morphology. Stratigraphy of the small tributary junction alluvial fan exposed by the 1997 event shows a series of Holocene sheetflood and fire-related debris-flow deposits.
2.8	2.1	(lat 44°06'6"N., long 116°04'46"W.) "Staircase Rapids" debris flow. Debris flows from the tributary on the north side of the South Fork Payette blocked the road and partially dammed the mainstem river in September 2001 and again in May 2002 (fig. 6). Large boulders (>2 m) from this event have significantly altered channel habitat (and kayaking runs) in this reach, and provide another example of how tributary debris-flow events exert longer-term effects on mainstem channel morphology. Conversely, other recent debris flows from tributary drainages on the South Fork Payette (Jughead creek, Hopkins Creek) have provided significant (>15,000 m^3) amounts of sediment to mainstem channels (Meyer and others, 2001), but have limited effect on local channel morphology because they lack boulder-sized clasts.
10.1	7.3	(lat 44°05'53"N., long 115°57'48"W.) Pull into the parking lot of the Garden Valley St. Jules Catholic Church on north side of road and park. View of the Boise Ridge fault across Garden Valley to the southwest.

Stop 1-1. Garden Valley: Late Cenozoic Faulting on the Boise Ridge Fault, Idaho

By Spencer Wood

From the settlement of Banks, the highway parallels a steep reach of the South Fork Payette River with many rapids. The river is confined to a deep granite gorge for 6 mi and then breaks out into the expansive Garden Valley with low hills and alluvial flats. This dramatic change in scenery is a result of late Cenozoic movement on the Boise Ridge fault. The Quaternary geology and geomorphology of this valley and the fault deserve a detailed study. The rich placer gold deposits of Boise Basin to the south and the proximity of a seemingly active fault near urban Boise are topics that invite further investigation. What follows is a summary of related earlier work and some casual roadside observations.

The Boise Ridge fault is a down-to-east, normal fault, north-striking (006º), 900-m-high physiographic escarpment (figs. 7 and 8). The escarpment can be traced for a distance of 45 km. At the southern end, near the North Fork of Robie Creek, the fault appears to terminate against the Kelly Gulch fault (fig. 9). The surface traces become indistinct and are lost in an area of dense timber, brush cover, and thick grus (Kiilsgaard and others, 1997). The northern end has not been mapped, but appears he Boise Ridge fault is one of several north-south trending faults that occur in a belt along the west side of the Idaho batholith (Hamilton, 1962). These faults typi-

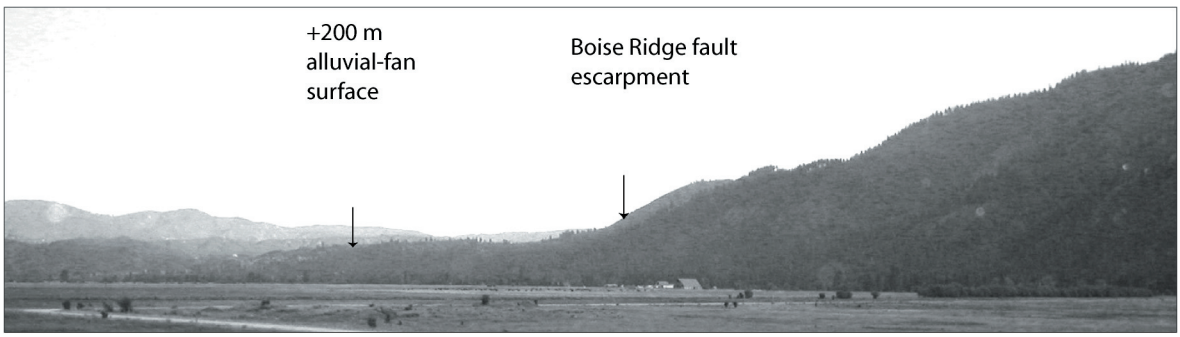

Figure 7. The Boise Ridge fault escarpment and the 1,130-m (3,700-ft) elevation alluvial-fan surface. The fan surface is 200 m above the alluvial flats of Garden Valley. Top of the ridge on the upthrown block of the fault is at 1,980-m (6,500-ft) elevation. View is to the south from the highway at Garden Valley.

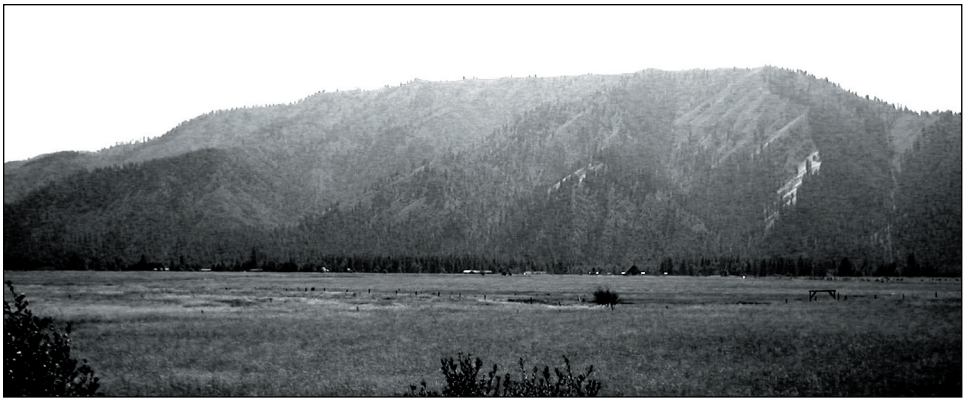

Figure 8. Faceted spurs along the southwest side of Garden Valley. View is to the southwest from the highway.

cally are spaced 10 to 20 km apart, and all have down-to-east displacement and west dipping fault blocks (fig. 10).

The footwall is the fault block to the west. The top of the ridge to the west is a much dissected old surface of granitic rock, pervasive over the Idaho batholith mountains, at about an elevation of 2,500 m (8,000 ft) (Anderson, 1935). Movement on the fault interrupted stream drainages and created the intermontane basin of Garden Valley and the gold placers of Boise Basin to the south. The gold-rich alluvium in Boise Basin was studied by Lindgren (1898), and although he recognized the fault origins of these basins, he did not show the fault on a map. Alfred Anderson in 1934 described geomorphic features and recognized the faceted ridges along the fault (fig. 8). In his 1947 study, he mapped the fault and discussed the offset of Columbia River Basalt and associated sediments in the basins. I quote here from his 1934 paper:

> *"Where the scarp bounds the west side of Garden Valley it is even more striking, for it involves a relief difference of from 3,000 to 3,500 feet. The faulting temporarily blocked the Payette River and caused deposition of gravels in the basin on the upstream side. But as in the case of the Deadwood fault, the river has carved a profound canyon across the tilted block range across its path."*

Kiilsgaard and others (1997) mapped the fault south of Garden Valley and document 580 m of displacement on the Columbia River Basalt of Hawley Mountain (fig. 9). On the downthrown eastern block are discontinuous patches of lacustrine and coarse fluvial sediment some of which is interbedded with basalt; however, much of the sediment clearly overlies the basalt in the Boise Basin (Forester and others, 2002). No basalt is known from the Garden Valley basin-sediment section. The sediment is deformed, and various steep dips occur near the fault. The sediment section overlying the granite probably does not exceed 100 m in thickness. On account of the association of the sediment with

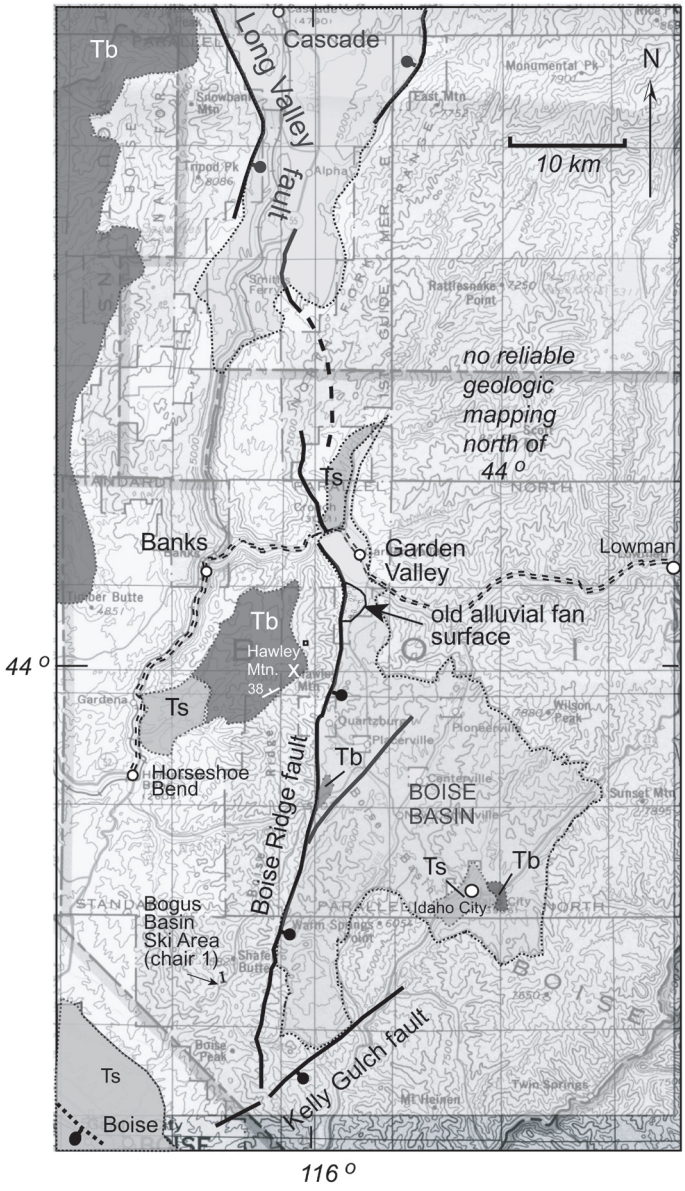

Figure 9. Geologic map of the Boise Ridge fault. The Boise Basin and Garden Valley basin areas are outlined and shaded. Tb, Columbia River Basalt and Ts, Miocene sediments of intermontane basins including what previous workers have called the Payette Formation. Most of the area is Mesozoic granitic rocks of the Idaho batholith and shallow intrusive rocks of Eocene age (partly from Kiilsgaard and others, 2001).

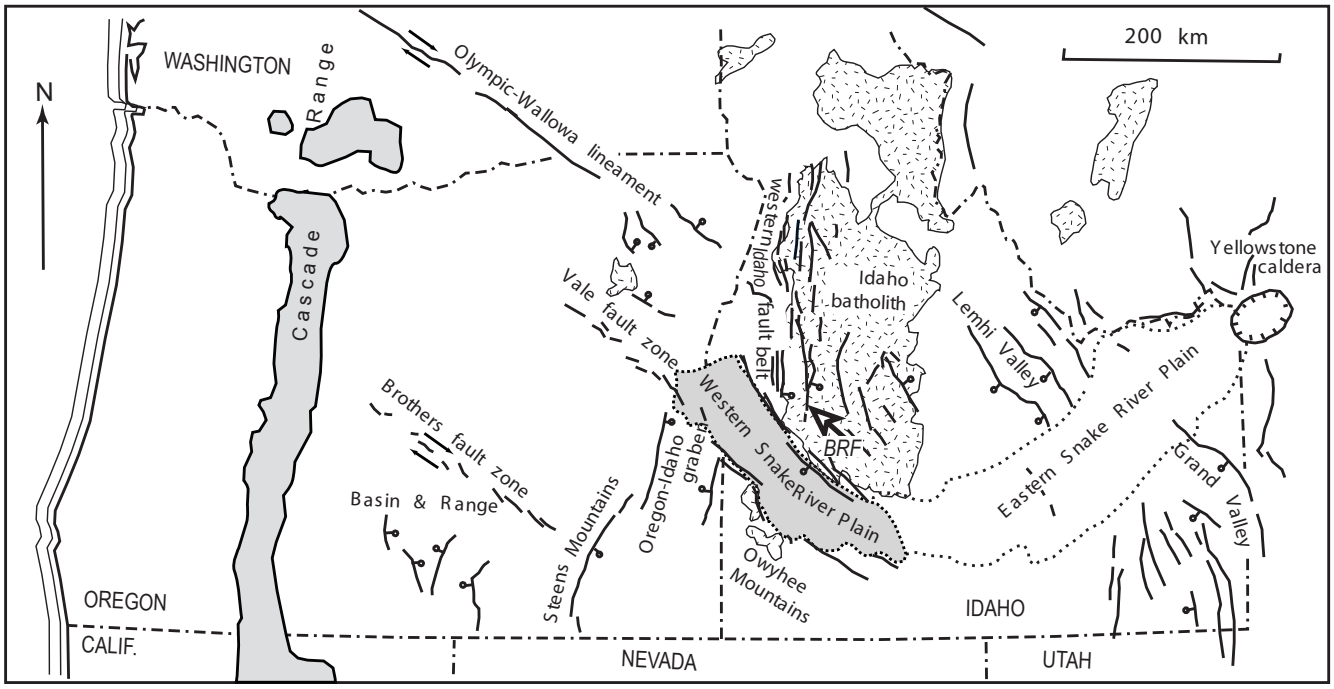

Figure 10. Location of the Boise Ridge fault (BRF) within the north-south trending western-Idaho fault belt. Late Cenozoic faults within the belt, and also the batholith mountains including the Sawtooth fault, are mostly east-facing escarpments with west-dipping footwall blocks. This contrasts with most faults east of the batholith, which have west-facing escarpments, east-dipping footwall blocks, and a more northwesterly trend (adapted from Wood and Clemens, 2002).

the Columbia River basalt in the Boise Basin, this sediment in Garden Valley has been called the Payette Formation (Fisher and others, 1992; Gibbons, 1995; Kiilsgaard and others, 1997, 2001). Kirkham (1931) originally defined the Payette Formation by its association with the basalt, but it is unlikely it was ever a continuous blanket over the area. More likely, these are just intermontane basin sediments, probably of different ages, confined to fault basins and subsequently preserved on down-dropped blocks. Miocene flora described by Smith (1941) and volcanic ash correlations by Forester and others (2002) indicate an age of 11.3 Ma for similar sediments overlying basalt in Boise Basin.

On the north side of the highway, just west of the bridge over the Middle Fork, sediments are dipping 15-20º to the southwest and are faulted by planes striking 315º and dipping 40º northeast consistent with the trend of the Boise Ridge fault.

An impressive section of alluvial-fan sediments stands as a terrace surface at the south end of the valley, west of the Alder Creek Road (fig. 9). The upper surface of the deposits is at elevation 1,130 m (3,700 ft), 180 m above the valley floor. In recent road cuts associated with the Crosstimber Ranch development, biotite-bearing granitic boulders of the deposit have disintegrated and can be cut with a spade. Weathering rinds on aphanitic basalt cobbles are 3 mm or more. Such thick rinds on basalt indicate an age of at least middle Pleistocene or older (Coleman and Pierce, 1986). This section of fan sediments appears to lap upon, and very likely is faulted against granite of the Boise Ridge block to the west. This depositional surface has been partly excavated away by the South Fork. The granite-strath surface beneath the fan deposits (which has not been mapped in detail) appears to be at elevation 975 m (3,200 ft), about 50 m above the bed of the South Fork Payette River. Clearly these deposits warrant further study if one is to understand the history of movement on the fault.

The classic faceted spurs along the fault and the steep mountain front attest to the youthful nature of the fault escarpment. Late Quaternary (the last 125,000 years) movement likely has occurred on the fault, but little is known of the slip rate. A minimum vertical slip rate is obtained by dividing the offset of Miocene basalt and sediment (14–11 Ma) by the 900 m of physiographic offset or the 600 m stratigraphic offset, giving 0.04 to 0.08 mm/yr. This minimum slip rate approaches the 0.1 mm/yr of better-documented active normal faults (dePolo and Anderson, 2000) of the Great Basin and Basin and Range.

Mileage Cum.	Inc.	
18.5	8.4	(lat 44°02'56"N., long 115°15'18"W.) Carefully pull off along the south side of road opposite the abandoned house and buildings to the north. At Stop 2, we will examine

sheetflood deposits from the 1997 New Year's Day storm event, as well as older dated fan stratigraphy exposed along the Hopkins Creek channel. If time permits, we will walk down the fan on the south side of the road, over the 1997 deposits, to the terrace gravels, placer workings, and modern bedrock strath of the South Fork Payette.

Stop 1-2. Hopkins Creek

By Jennifer Pierce, Grant Meyer, Spencer Wood

Overview

In the January 1, 1997, storm, the 0.58 km^2 Hopkins Creek basin experienced intense rain on melting snow that triggered colluvial failures, floods, and debris flows (Meyer and others, 2001). In this unburned south-facing grassland basin, failure of 15 individual colluvial hollows and erosion of material stored in channel and alluvial-fan sediments yielded 16,100 m^3 of erosion, equivalent to about 42,000 Mg/km^2 (Meyer and others, 2001). Sheetflooding over the Hopkins Creek fan partly buried many buildings of this homestead. The elderly woman residing here at first refused to be evacuated but later was rescued by neighbors. Small tributary fans such as this one have been popular sites for ranch and summer home development throughout central Idaho, but are subject to major flood and debris-flow hazards, especially after fire. The Hopkins Creek fan extends over a 24-m-high terrace tread that is deeply buried by fan sediments. Below, an 18-m-high bedrock strath covered with 2 m of alluvial material has been disturbed by placer mining. The Hopkins Creek fan probably also buries and obscures older terraces of the South Fork Payette River in this area.

Holocene fire and sedimentation record at Hopkins Creek

The 1997 event also exposed a record of Holocene fires and sedimentation in the stratigraphy of the upper Hopkins Creek alluvial fan (fig. 11). The lower part of the exposed sequence shows an approximately 1-m-thick dark, cohesive, clast-poor deposit with dates of 1,772±43, 1,722±43, and 1,651±41 ^{14}C yr BP. A change from a more clay-rich sandy loam texture at about 170 cm, and an increase in the percentage of clasts suggests a possible depositional boundary between the 1,722±43 and 1,651±41 ^{14}C yr BP ages, but also could be indicative of a facies change within the same depositional event. An oxidized sheetflood unit with a concentration of charcoal at the base of the unit, dated at 1,100±43 ^{14}C yr BP, overlies the lower unit(s). The overlying clast-rich debris flow deposit provides a very distinct depositional change; this charcoal-poor unit is dated at 411±31 ^{14}C yr BP. This in turn is overlain by thin sheetflood deposits dated at 197±43 ^{14}C yr BP, and the 1997 sheetflood and debris flow deposits at the top of the unit.

Mileage Cum.	Inc.	
30.5	12	(lat 44°04'45"N., long 115°39'28"W.) Intersection with Deadwood Road. Turn left onto

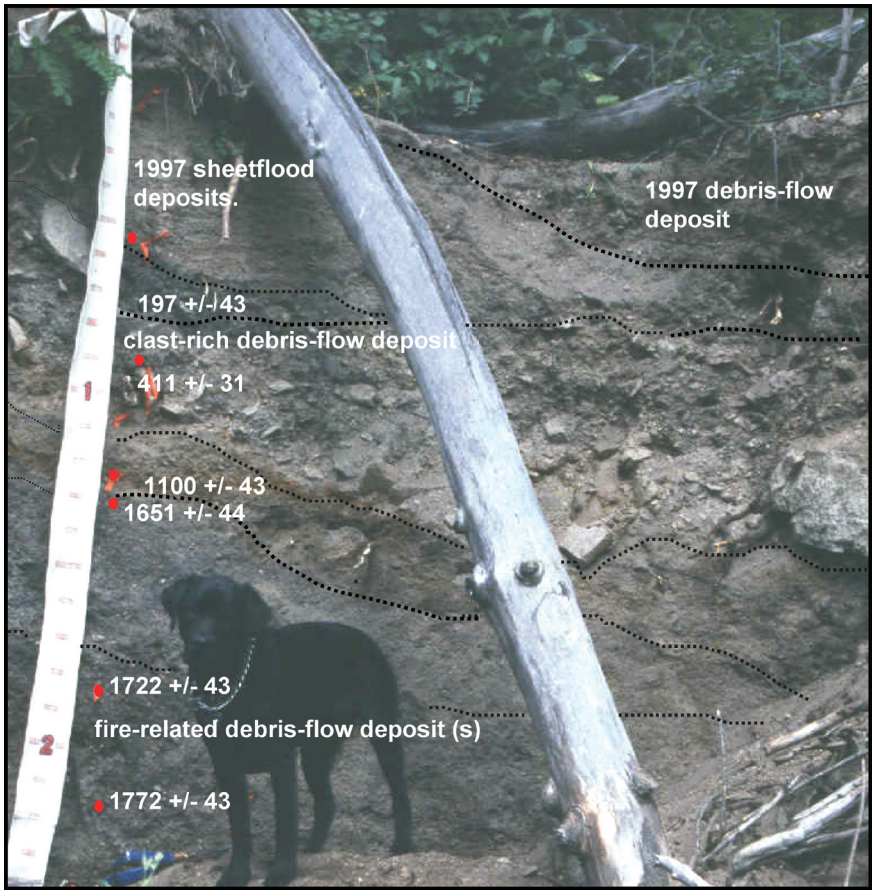

Figure 11. Alluvial-fan stratigraphy exposed at Hopkins Creek. Dates on figure are in radiocarbon years BP. Deposit characteristics are described in the text. This section generally is more charcoal poor than upvalley sections, likely due in part to the fewer trees in the basin. Charcoal macrofossils identified from this section were almost all from hardwood (riparian) species, although ponderosa pine needles were found near the base of the deposit.

Figure 12. Deadwood River with debris from August 22, 2003, storm event. Debris flows from tributary streams Slaughterhouse Creek and Slim Creek temporarily dammed the Deadwood (note mud and debris above channel on far side of Deadwood River) and trapped a family camping in the area.

the Deadwood Road and drive up gravel road approximately 2.7 km (1.7 miles) to Slaughterhouse Creek on the left (west) side of the road. Park on the side of road. Slim Creek is approximately 500 m upstream, also on the west side of the road.

Stop 1-3. Recent Debris Flows Along the Deadwood River

By Jennifer Pierce and Grant Meyer

On the afternoon of August 22, 2003, the Lowman area received approximately 1.25 inches of rain, likely more at this location. The adjacent basins of Slim Creek (6.0 km^2), Slaughterhouse Creek (~3.6 km^2), and Deadwood Jim Creek (2.0 km^2) all produced major debris-flow events, which appear to have originated at the very tops of the watersheds as rilling from overland flow on locally steep (~40°) slopes accumulated sediment and converged in tributary channels to produce debris flows (fig. 12). The debris flow temporarily dammed the Deadwood River and backed up water and debris

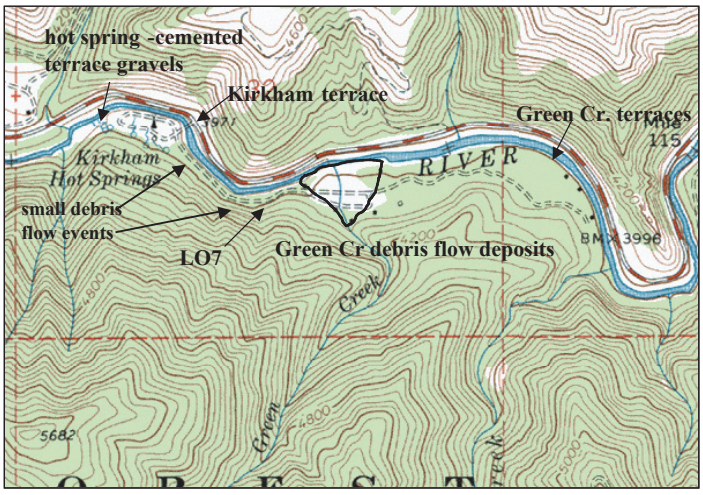

Figure 13. Map showing locations of site LO7, Green Creek, and cemented terrace gravels at Kirkham Hot Springs. Estimated area of deposition of 1997 debris flow at Green Creek is shown by triangle-shaped feature on figure.

at Slim Creek about 1.5 km upstream to Pigeon Flats (Kari Grover-Wier, August 2003, personal comm.).

Archeological sites on low terraces in Deadwood Campground area contain abundant charred ponderosa pine wood, which provides evidence for a ca. 900 cal yr BP forest fire (Reid, 2001). The timing of this event coincides with evidence of other major fire-related debris flows at a variety of elevations in the Payette area ca. 900 cal yr BP.

Mileage Cum.	Inc.	
33	2.5	Return to junction of the Deadwood Road and the Banks-Lowman Road and turn left.
36.5	3.5	(lat 44°4'57"N., long 115°36'44"W.) At intersection of Banks-Lowman road and Highway 21, turn left on to Highway 21 towards Lowman Ranger Station.
37.5	1.0	(lat 44°4'34"N., long 115°35'48"W.) Lowman Ranger Station on right. Terrace sequence below station with tread heights of about 1.5 m, 3.0 m, 6.3 m and 10.5 m above the current channel bankfull level. On the 1.5-m terrace are large (meter-scale) subangular boulders in a cigar-shaped bar deposit, which could either have been deposited during a major flood on the main stem Payette or could be deposits from a major debris-flow event originating from the tributary (LO25) on the opposite side of the river from the terrace. Alluvial-fan site LO25 contains a series of fire-related sheetflood and debris-flow deposits with dates on selected units of 3,479±30, 2,796±44 and 2,072±36 ^{14}C yr BP. The highway is on the 10.5-m terrace tread, with an approximately 25-degree slope up to the 20-m terrace (USFS residential area).
39.5	2.0	(lat 44°4'26"N., long 115°33'44"W.) We now are driving through the area that was extensively burned in the 1989 Lowman fire. Terraces on south side of river, across from "Burnt Pines" store, have terrace-tread heights of 5.3 m, 8.2 m, 13.5 m, and 16.5 m. Variable bedrock strath heights of 4.5–5.5 m are present in this reach, upstream past Kirkham Campground. In this study, bedrock strath terraces are differentiated from other terraces by either exhumed bare bedrock strath, or bedrock strath covered by less than 2 m of gravel and cobble fill.
40.5	1.0	(lat 44°4'23"N., long 115°32'42"W.) Kirkham Hot Springs on south side of river. Cobble- and boulder-rich alluvial fill terraces above the hot springs are partially cemented by hot-spring deposits (fig. 13).
41.5	1.0	(lat 44°4'21"N., long 115°31'38"W.) During the 1996-1997 storm event, failures of colluvial hollows produced debris flows in the Green Creek and nearby small steep tributary drainages of the South Fork Payette (fig. 13). Debris-flow deposits of grussy material from a large debris flow in Green Creek itself extend onto the 18- and 10-m terraces, filling the road with sediment, and transporting a large water tank. The Green Creek fan progrades out onto

Figure 14. Alluvial-fan stratigraphy at site LO7. Dashed lines show depositional breaks. Ages are in radiocarbon years BP, shovel for scale, approximate depth of section is 3 m.

a series of gravel and cobble-rich fill (?) or fill-cut (?) terraces.

At site LO7 (fig. 13), Holocene alluvial-fan deposits are exposed by incision of the fan during the 1997 events. The LO7 fan contains a series of multiple debris-flow deposits, most of which date between about 2,700–2,900 ^{14}C yr BP, with the exception of the lowest date of about 6,050 ^{14}C yr BP (fig. 14). The 2,911±99 and the approximately 6,049±55 ^{14}C yr BP events are considered 'major events' based on criteria previously described. The upper unit(s) contain multiple layers of charcoal concentrations that form prominent dark layers in the stratigraphy. These may represent lower energy deposits between pulses of a single event (note lower date of 2,788±57 ^{14}C yr BP).

45.5 4.0 (lat 44°4'24"N., long 115°30'41"W.) East of Archie Creek Road, (near milepost marker 79), turn right into the informal campsite area and park. At this site, we will examine deposits from the 1997 event at Jughead creek and discuss how estimated sediment yields from this event and the event at Hopkins Creek compare with other estimates of sediment yields in this area. We also will examine early Holocene alluvial-fan stratigraphy exposed in perched fan of Jughead creek and the alluvial-fan stratigraphy at site LO10 on the north side of the highway.

Figure 15. This large colluvial failure at Jughead creek produced about 40 percent of the total eroded volume of the 1997 debris flow event (Meyer and others, 2001). Spencer Wood (circled) in bottom left for scale.

Stop 1-4. Jughead Creek and Site L010: Recent Debris-Flow Events and Holocene Alluvial-Fan Stratigraphy

By Jennifer Pierce, Grant Meyer, and Spencer Wood

During the New Year's Day 1997 storm, a massive slab of colluvium slid from a broad hollow in the Jughead creek basin, (fig. 15), which was burned in the 1989 Lowman fire. A rather boulder-poor debris flow resulted, with maximum velocity at the basin mouth estimated at between 12 and 25 m/s (Meyer and others, 2001). This extremely rapid debris flow crossed the Payette River, and despite strongly divergent flow, climbed terraces on the north side up to nearly 7 m above the river's bankfull level. Many ponderosa pines on the terraces were removed by the flow, and a few "bayonet trees" knocked partly over are still visible. The flow deposited a broad lobe of material that was ringed by logs concentrated at the flow front (Meyer and others, 2001), although woodcutters have removed some of the original logjam. The sediment yield from the Jughead creek basin (0.50 km^2) is estimated at 14,600 m^3 (Meyer and others, 2001). Erosion in Hopkins Creek (~42,000 Mg/km^2) and Jughead creek (~44,000 Mg/km^2) was similar, suggesting burned forested areas respond similarly to unburned rangelands after tree root strength in burned forested areas decreases.

Early Holocene alluvial-fan stratigraphy, and comparisons of sediment yields at different time scales

An early Holocene alluvial-fan stratigraphic section at Jughead creek contains between 10 and 24 thin, charcoal-rich sheetflood deposits and burned soil surfaces that were formed between 7,400 and 6,600 cal yr BP (Meyer and others, 2001). The recurrence interval for the fire-related events is estimated

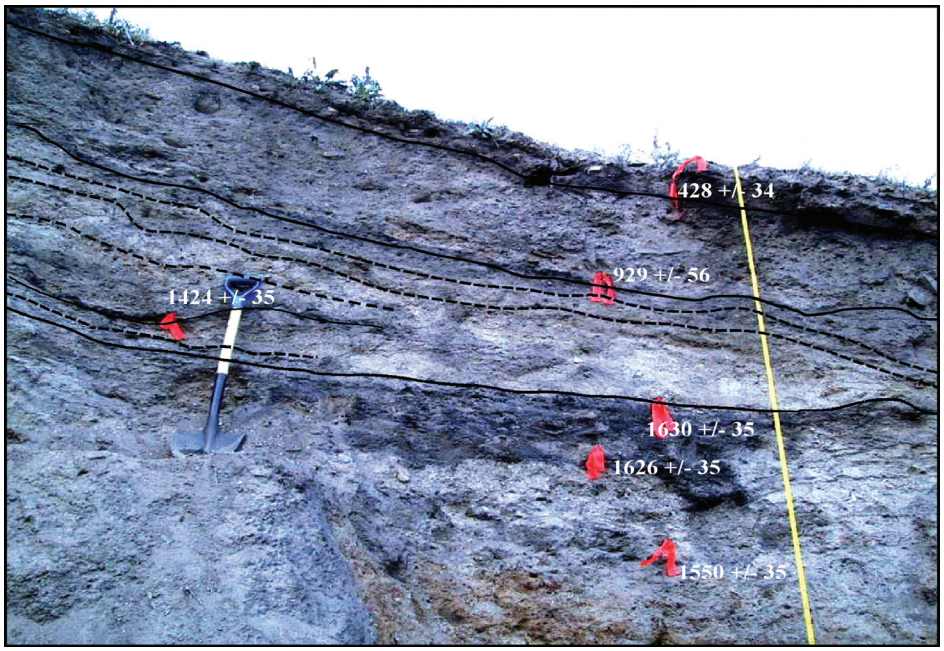

Figure 16. Incised alluvial fan at site LO10, exposing Holocene burned soil surfaces (solid lines) and deposit boundaries (dashed lines). Ages on figure are given in radiocarbon years BP. The debris-flow deposit above the burned surface dated at 929±56 ^{14}C yr BP is a single, large, debris-flow deposit; while the sequence is characterized by multiple sheetflood deposits between 1,630±35 ^{14}C yr BP and 929±56 ^{14}C yr BP. The lowest debris-flow deposit with a mottled dark appearance also is likely a single event, where the age of 1,550±35 ^{14}C yr BP represents the most accurate date (least inbuilt age) for the deposit.

to be 33–80 years, depending on how many events are interpreted as stemming from fires. Since not all fire-related events are recognizable in the stratigraphic record, and since low-severity surface fires may not produce sedimentation events, this represents a minimum recurrence interval for fires. These small fire-induced sheetfloods occurred with a much higher frequency than observed for fire-induced events at any site in Yellowstone (Meyer and others, 1995), and imply frequent, low-severity fires.

The stratigraphic section in the early Holocene fan shows a conformable sequence of roughly parallel contacts between sheetflood deposits and burned soil surfaces with no erosional breaks or inset channel deposits (Meyer and others, 2001). We assume, therefore, that this fan section accurately records the volume of sediment deposited during this time period. Assuming a typical cone-shaped fan morphology, the sediment yield during the time period between 7,400 and 6,600 cal yr BP was calculated to be approximately 16 Mg/km^2/yr (Meyer and others, 2001). This evidence of frequent, small, fire-related events is consistent with the regime of frequent, low-intensity fires thought to be characteristic of Idaho ponderosa pine forests (Steele and others, 1986). The estimated sediment yield is similar to short-term sediment-yield estimates in Idaho batholith watersheds of 2.7-30 Mg/km^2/yr (Clayton and Megahan, 1986). The sediment yields from the 1997 erosion events, however, are orders of magnitude greater than the early Holocene record, and are equivalent to several thousands of years of background sediment yield. In order to account for the 10,000-yr average Idaho batholith sediment yields of approximately 112 T/km^2/yr (Kirchner and others, 2001), events as large as the 1997 events could only occur about once every 400 years. Compared to the Holocene average, erosion rates during the 7.4- to 6.6-ka interval were unusually low, suggesting fluctuating sediment yields.

Fluvial terraces

Terrace-tread heights at the Jughead debris-flow site are approximately 3.2 m, 5.4 m, and 7.0 m above bankfull level. All terraces appear to be fill-cut terraces; no bedrock straths are seen outcropping at this location. Less than 500 m downstream, however, bedrock is exposed at bankfull, covered with 4.8 m of sandy alluvial gravels, and bedrock can be seen in the current channel in the Jughead creek area. This indicates that the current stream is close to bedrock in this reach, or that the

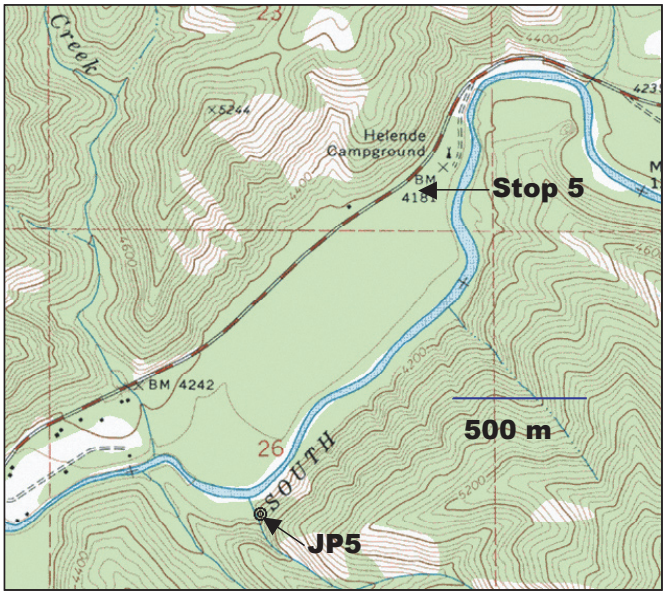

Figure 17. Location of Stop 5 at Helende Campground and the JP5 alluvial-fan site.

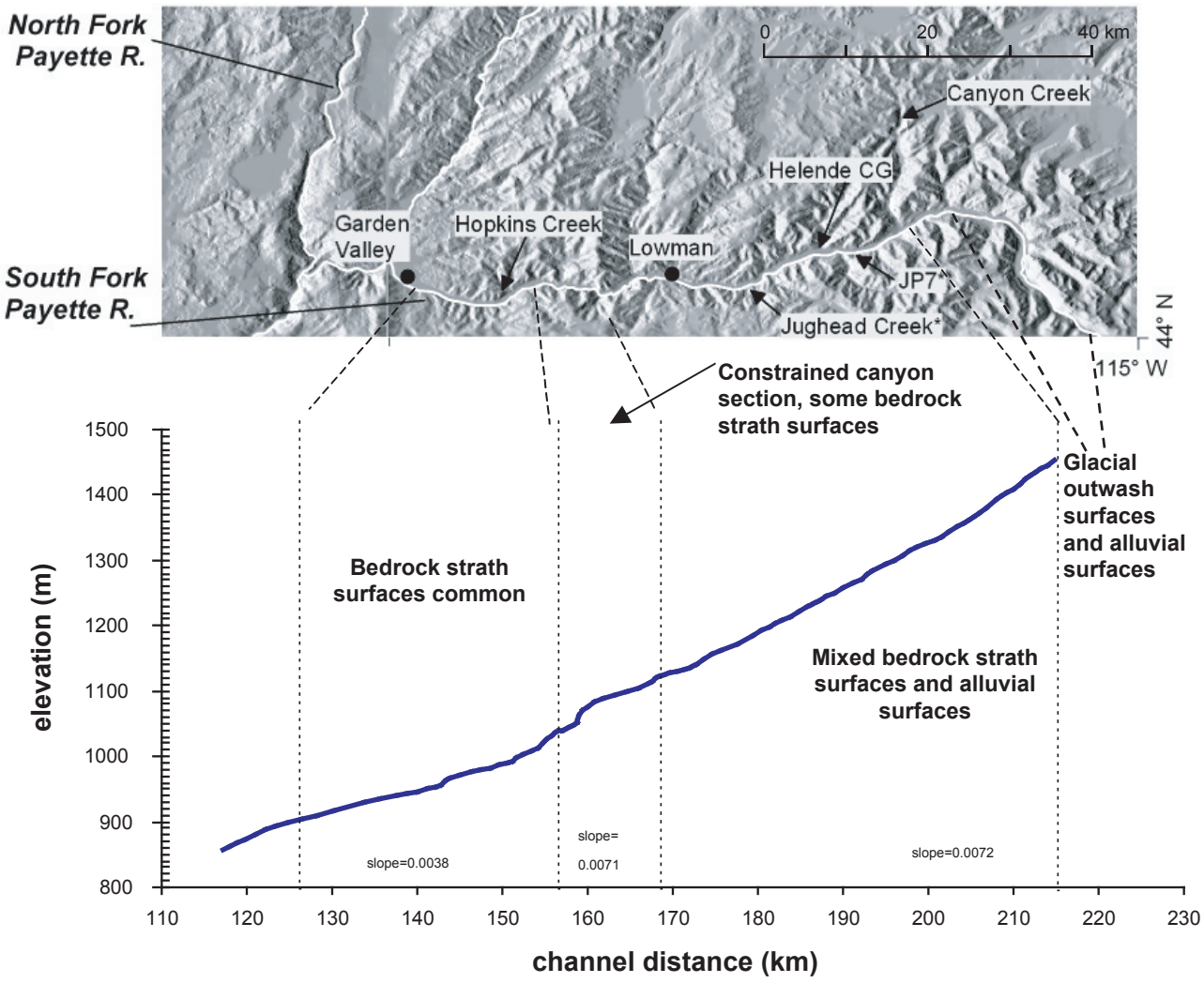

Figure 18. Locations of terrace study areas referred to in text. Asterisks (*) denote locations of radiocarbon-dated terraces.

bedrock channel may be covered with only a few meters of alluvium. Alluvial-fan sediments from the early Holocene fan at Jughead creek were deposited on the 5.4-m terrace tread. A basal date from the fan sediments of 6,495±60 ^{14}C yr BP (~7,425 cal yr BP) provides a minimum age for the 5.4-m terrace gravels underlying the alluvial-fan deposits (Meyer and Pierce, 2003).

Site LO10

Radiocarbon dates from the LO10 site, a south-facing drainage across the South Fork Payette River from Jughead creek provide a later Holocene (ca. 1,500 cal yr BP through present) record of fire-related sedimentation events (fig. 16). In this fan sequence, the 1989 burned soil surface is covered with only a few centimeters of washed debris-flow deposit from 1997. During the 1997 event, the proximal fan became deeply incised, and most of the volume of the debris-flow was deposited on the medial to distal end of the fan, creating a new fan lobe. This fan contains distinct burned soil surfaces at 428±34 ^{14}C yr BP and 929±56 ^{14}C yr BP, underlain by multiple deposits dating between approximately 1,550±35 ^{14}C yr BP, and 929±56 ^{14}C yr BP (fig. 16). The 929±56 ^{14}C yr BP (ca. 907 cal yr BP) burned soil surface is distinct, continuous, and exhibits little sign of bioturbation or post-fire disturbance. A relatively thick, continuous, charcoal-rich debris-flow deposit overlies the burned soil surface; all these characteristics indicate this likely is a fire-related debris flow. Evidence of a ca. 907 cal yr BP fire also is found at the GJ2 site, over 30 km upstream. This corresponds to the

Medieval Warm Period (1,050–750 cal yr BP) and also was a time of major fire-related debris-flow activity in Yellowstone (Meyer and others, 1995). The time period between 1,308–1,529 cal yr BP seems to represent a period of more frequent small sedimentation events, as seen at the Hopkins Creek site, at sites downstream near Banks, Idaho, and at nearby sites PL, LO13, LO33, and LO30. This record of frequent small fires corresponds with a time of little fire-related fan deposition in Yellowstone (Meyer and others, 1995), and the coldest phase of the approximately 1,400 yr cycle of ice-rafted debris in the North Atlantic (Bond and others, 1997).

Mileage Cum.	Inc.	
48.6	3.1	(lat 44°04'45"N., long 115°39'28"W.) Stop 5: A preliminary characterization of Holocene terraces of the South Fork Payette River and JP5 fan site. Turn right into Helende Campground area and follow paved road into campground and park in campsite parking. Restrooms available. At this stop, we will discuss preliminary work on Holocene terraces of the South Fork Payette River, then we will continue down a dirt road to examine alluvial-

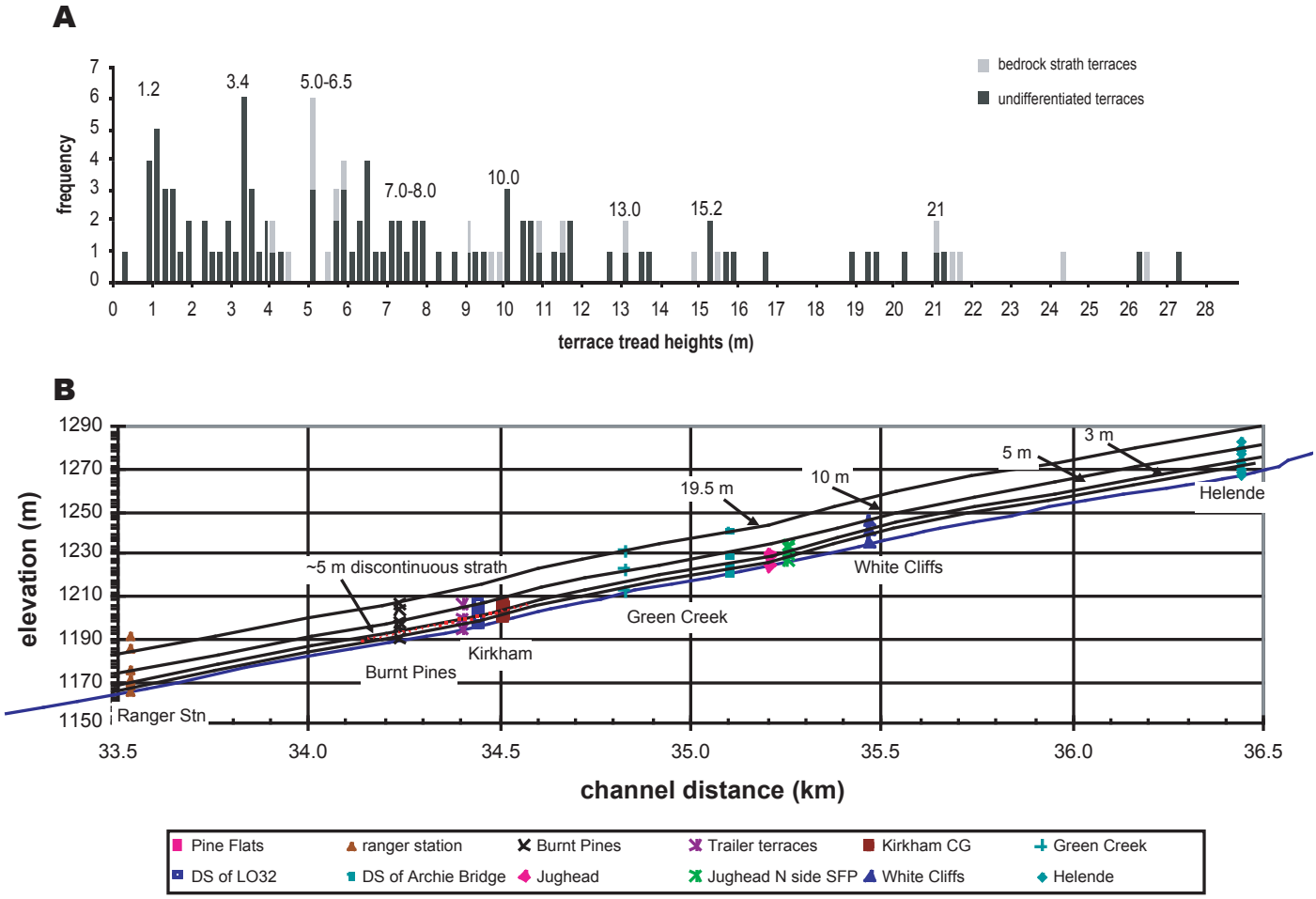

Figure 19. (A) Histogram of South Fork Payette terrace-tread heights above bankfull. For the purpose of this figure, bedrock straths have been defined as tread surfaces with less than 2 m of fill on bedrock. Some undifferentiated terraces are fill-cut into glacial terrace material. Numbers above histograms indicate preliminary groupings of major modes of terrace heights in meters. (B) Longitudinal profile of the South Fork Payette River between the Lowman Ranger Station and Helende Campground. Locations of measured terrace-tread heights above bankfull are denoted with symbols. Lines show tentative correlations assuming constant terrace-tread height, which are unsupported at present.

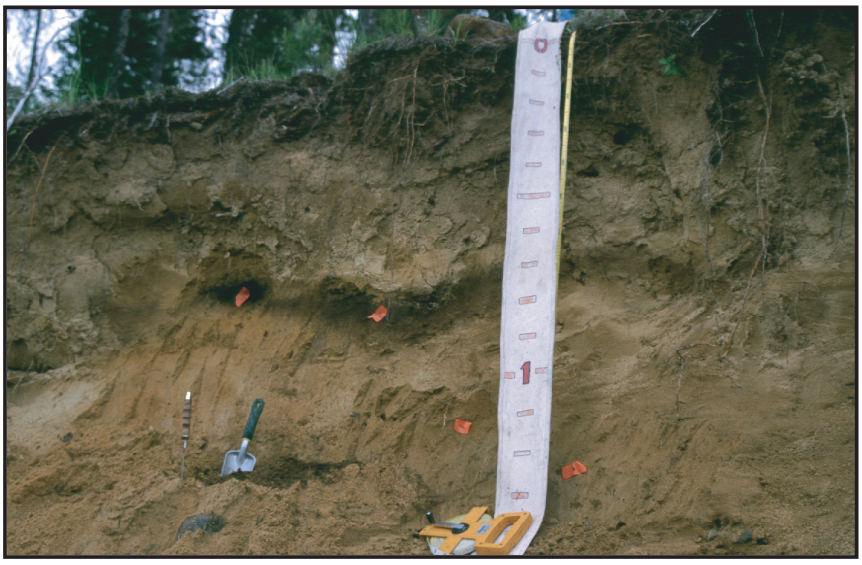

Figure 20. Site JP7, 3.2-m terrace tread, with radiocarbon samples from fine-grained channel-fill deposit at 0.8 m depth.

fan stratigraphy at a location across the South Fork Payette River (fig. 17).

Stop 1-5. A Preliminary Characterization of Holocene Terraces of the South Fork Payette River and JP5 Fan Site

By Jennifer Pierce and Grant Meyer

The South Fork Payette River valley features a well-formed sequence of fluvial terraces, especially between the last-glacial ice margin near Grandjean and Lowman (fig. 18). Although fluvial gravels can be found at heights of 180 m above the current channel, this study focuses on the terraces with treads of less than 15 m in height that likely are late glacial or postglacial in age (Stanford, 1982). The following is a preliminary description of terrace characteristics, terrace-tread heights above bankfull level, and when possible, radiocarbon ages of material collected from fine-grained overbank or slackwater deposits.

Description of South Fork Payette River terraces

The gravel and cobble-rich terraces with terrace-tread heights of about 20 m likely are glacial fill terraces, containing an estimated 10 m thickness of fill material. In the South Fork Payette area above Lowman, terrace exposures near the Lowman Ranger Station, Green Creek, and Helende Campground contain gravel- and cobble-fill material. Locally, in reaches of more resistant bedrock or bedrock "fins" extending down to the channel, bedrock straths underlie the 20-m terraces. In the lower South Fork Payette below the canyon section, bare bedrock straths at about 20 m, or bedrock at about 18 m covered by approximately 2–3 m of fill are common (fig. 18). In general, bedrock strath terraces typify the section of the valley below the canyon section, with terrace-tread heights of about 20 m, about 15 m, 11-13 m, and 9-10 m above local bankfull levels. The upper section of the drainage has a combination of bedrock strath terraces in higher gradient reaches or reaches of locally more

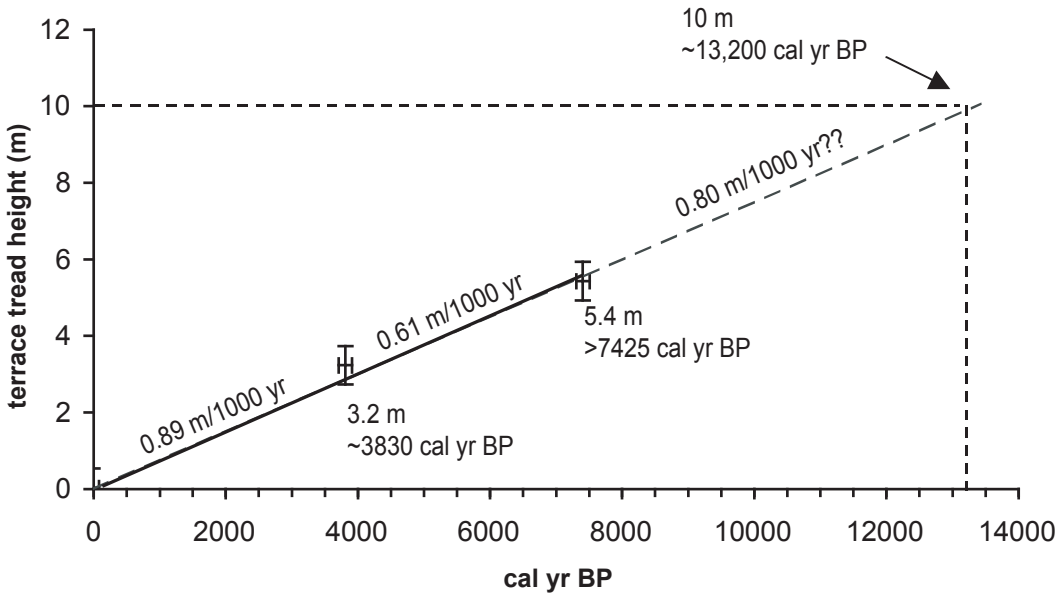

Figure 21. Estimated incision rates from radiocarbon ages of terrace treads given in calibrated years BP. Two sigma variation in ages given by x-axis error bars; 0.5 m variation in terrace height given by y-axis error bars. Estimates of incision rates calculated between individual points using calibrated radiocarbon ages, and change in terrace-tread height. Assuming constant incision rates, a rough age estimate for 10-m terrace of ~13,200 cal yr BP was calculated by extending the linear trendline fitted to dated terrace heights.

resistant bedrock (*i.e.*, at Kirkham Campground), and glacial fill (?) terraces and late-glacial and post-glacial fill-cut (?) terraces in wider valley sections. In some wider reaches (*i.e.*, at Jughead creek area, Lowman Ranger Station, Helende Campground) terraces are preserved on the north side of the valley, and the active, bedrock-bottomed channel of the South Fork Payette River is confined against hillslopes and small terrace remnants on the southern side.

Terrace-tread heights

Hand-level surveying of terrace tread heights in the South Fork Payette valley from the Warm Springs Creek down to Garden Valley shows that terrace heights form several apparent groups (fig. 19). The major modes in terrace-tread heights center around 1.2 m, 3.4 m, 5.0-6.5 m, and 10.0 m above current bankfull (fig. 19A). The range of tread heights between about 5.4 m and 6.8 m makes this grouping more ambiguous. Some of this variation is due to a variety of bedrock strath heights around 5.5 m, although there is a fairly consistent fill-cut terrace height at 6.6 m. Figure 19B shows the locations of surveyed terrace heights between Lowman Ranger Station and Helende Campground and correspondence of terrace-tread heights within the reach. The terrace heights surveyed in this relatively short valley distance provide information on possible terrace-tread correlations within this specific area; more data on other sections of the South Fork Payette are needed to make further inferences about general terrace-tread heights within the upper basin.

Figure 22. Cluster of large boulders, perhaps from a large flood event, on the 11-m terrace-tread surface at Helende Campground. The boulder surfaces are extensively pitted (~5 cm deep), but the high weathering rates of the batholith granitic rock make calibration of weathering characteristics difficult.

Dating of terrace deposits and estimated postglacial incision rates

At site JP7, upstream from Helende campground an age of 3,535±45 ^{14}C yr BP (~3,830 cal yr BP) was obtained from a large charcoal fragment collected from fine-grained channel fill deposits 0.8 m below the top of a 3.2-m terrace-tread surface (fig. 20). Similar fine-grained deposits are not uncommon in the approximately 3-m terrace from the Jughead creek area to site JP7. A basal radiocarbon age of 6,495±60 ^{14}C yr BP (~7,425 cal yr BP) from the inset alluvial fan of Jughead creek also provides a minimum age for the 5.4-m terrace gravels underlying the alluvial-fan surface (Meyer and Pierce, 2003). Although the approximately 10-m terrace surface has not been dated, an age of approximately 13,200 yr was hypothesized, assuming incision rates have been constant over Holocene time scales. These data provide an average Holocene incision rate of about 0.076 m/k.y. for approximately13,000 yr (fig. 21). More data are needed from the South Fork Payette terraces to consider relations between fan sedimentation and terrace formation. Meyer and others (1995) found that most tributary sedi-

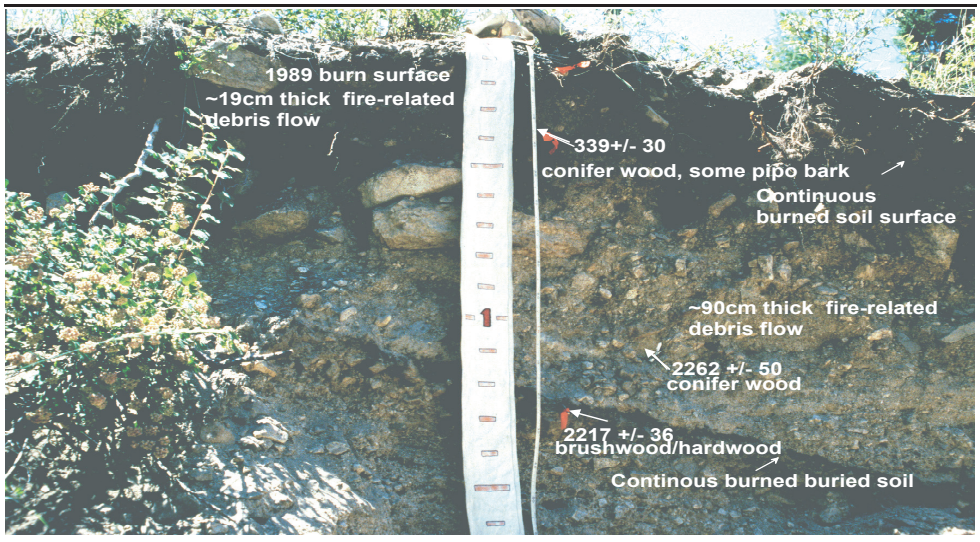

Figure 23. Fan stratigraphy exposed at site JP5. Dates are in ^{14}C yr BP, with major features of the deposit noted on the photo.

ments in glacial trough valleys of Yellowstone remain stored in fans for long periods and are worked downstream during periods of increased flow in the mainstem streams. Since the tributary fans of the South Fork Payette drainage are more proximal to the mainstem river than fans in the wider glacial valleys of Yellowstone, sediment supply in the Payette River may be more closely tied to hillslope erosion and deposition on fans.

In the Helende Campground area, a series of terraces with tread heights of 1.3 m, 3.3 m, 7.3 m, 6.1 m, 10.0 m, 11.5 m, 12.5 m, and 15.5 m are preserved on the north side of the South Fork Payette River. Higher terrace surfaces are also present, but were not mapped or measured in this area; the terraces less than 10 m in height are likely fill-cut terraces, while the higher terraces of glacial age are likely fill terraces. An additional feature of note is the cluster of large (~4-m-tall) boulders on the 11.5-m terrace, near the campground (fig. 22). Other large (>1 m b-axis) boulder deposits are found on a 10.4-m terrace about 1.5 km upstream from Helende Campground (site JP12). The boulders at the campsite likely were deposited during a large flood event.

The ca. 2,280 cal yr BP debris-flow event is overlain by another distinct continuous burned soil surface at 30-33 cm depth, dated at 339±30 ^{14}C yr BP. Fire-related sedimentation events are common in the Payette study area during this time period, which coincides with low fire activity in Yellowstone. This event is in abrupt contact with an approximately 19-cm-thick charcoal-rich debris-flow deposit, which appears to be an event associated with the underlying burned surface.

Mileage Cum.	Inc.	
0.0	0.0	Reset odometers when exiting Helende Campground. Turn right onto Highway 21.
6.8	6.8	(lat 44°07'24"N., long 115°20'35"W.) Terraces at Warm Springs station, across from MacDonald Creek. Alluvial terrace-tread heights above bankfull level of 0.8 m, 2.1 m, 2.6 m, 8.9 m characterize surfaces upstream of a major valley constriction. Bedrock strath

Alluvial-fan stratigraphy at site JP5

The tributary stream at site JP5 is located on the south side of the South Fork Payette, downstream of the campground, and just downstream of the steep granite cliff opposite the Helende terrace surfaces (fig. 23). The storm event of 1997 deposited material on top of the perched fan, crossed the South Fork Payette River depositing material on the other side, and then deeply incised the tributary channel exposing fan material, channel deposits, and weathered bedrock in the channel wall.

This section contains a very prominent, continuous burned buried soil surface (115 cm below the top of the section), with a weak A horizon extending for approximately 10 cm below a burned O horizon. The burned surface, which contains abundant fine charred material, is in abrupt contact with an overlying 90-cm-thick fire-related debris flow (fig. 23). Based on these characteristics, the debris flow is interpreted as being a sedimentation event related to the fire that burned the underlying surface. The debris-flow deposit is clast rich (~40 percent), and the lack of variation in color, sorting, or texture indicates this is a single event. The radiocarbon ages of 2,217±36 ^{14}C yr BP for the burned surface, and 2,262±50 ^{14}C yr BP for the deposit are statistically indistinguishable, and well within the range of possible "inbuilt age" and analytical error. The timing of this event (~2,280 cal yr BP) falls within a time of increased fire-related sedimentation in Yellowstone (Meyer and others, 1995), and high fire frequency in mountain hemlock forests of British Columbia (Hallett and others, 2003).

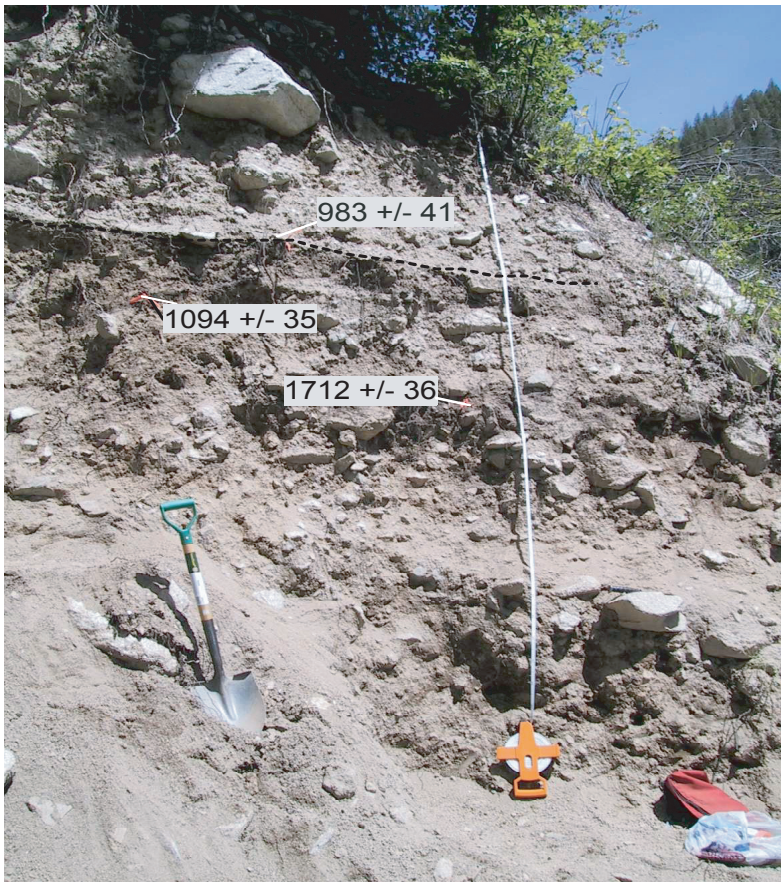

Figure 24. Alluvial-fan stratigraphy of site GJ2, showing multiple clast-rich debris-flow deposits. This site, and other high elevation (over ~1600 m) mixed conifer sites lack high-frequency fire-related debris-flow deposits. Site GJ2 contains a prominent burned soil surface and fire-related debris flow dated at about 930 cal yr BP (983±41 ^{14}C yr BP).

terraces with tread heights of 5.6 m, and 6.6 m, and alluvial terraces with tread heights of 11.1 m and 21.0 m characterize the downstream, constricted section.

8.7 1.9 (lat 44°04'45"N., long 115°39'28"W.) Abundant clast-rich debris-flow deposits of Chapman Creek can be seen in main channel to right.

12.8 4.1 (lat 44°10'32"N., long 115°14'48"W.) Emile Grandjean historic sign and view of the glacial landscapes of the western Sawtooth Mountains. Deposits from three glaciations can be found in the upper South Fork Payette River valley, informally named by Stanford (1982) the Penrod Creek (pre-Bull Lake?), Camp Creek (Bull Lake?), and Grandjean (Pinedale?) glaciations.

~14 ~1.2 The area burned in the August 14–20, 2003, Canyon Creek Fire can be seen for the next several miles. Keep a lookout for fire-related debris-flow activity in tributaries of Canyon Creek and post-fire erosion on hillslopes.

16.6 2.6 (lat 44°13'13"N., long 115°13'56"W.) Pull off along right side of the road and walk along to the fans exposed near the west side of the road.

Stop 1-6. High-Elevation Alluvial-Fan Stratigraphy

By Jennifer Pierce and Grant Meyer

Alluvial-fan sites GJ2 and GJ1, in the high elevation (~1700 m) mixed conifer forest, provide a record of fire-related debris-flow events. Unlike lower elevation fan sites in the study area, deposits at these sites do not contain fine-grained sheetflood or hyperconcentrated flow deposits, but instead are dominated by boulder rich, massive debris-flow deposits (fig. 24). Both GJ1 and GJ2 contain a fire-related debris flow event ca. 907 cal yr BP (928 ^{14}C yr BP at site GJ1 and 983±41 ^{14}C yr BP). These events are very similar in age to the fire-related debris-flow event at site LO10, also dated at ca. 907 cal yr BP, and the approximately 900 cal yr BP burned ponderosa pine found at the archeological site along the Deadwood River (Reid, 2001).

Mileage
Cum. Inc.

~23 ~8.4 (lat 44° 18'22"N., long 115°13'51"W.) Banner Summit.

~47 ~24 (lat 44° 12'41"N., long 114°56'42"W.) Stanley, Idaho.

End Day 1

References

Anderson, A.L., 1934, A preliminary report on recent block faulting in Idaho: Northwest Science, v. 8, no. 2, p. 17–28.

Anderson, A.L., 1935, The valley of Grimes Creek in the Payette Canyon, Idaho: Journal of Geology, v. 43, p. 618–629.

Anderson, A.L., 1947, Geology and ore deposits of Boise Basin, Idaho: U.S. Geological Survey Bulletin 944-C, 319 p.

Armstrong, R.L., 1974, Geochronometry of the Eocene volcanic-plutonic episode in Idaho: Northwest Geology, v. 3, p. 1–15.

Arno, S.F., Harrington, M.G., Fiedler, C.E., and Carlson, C.E., 1995, Restoring fire-dependent ponderosa pine forests in western Montana: Restoration Management Notes, v. 13, p. 32–36.

Barrett, S.W., 1988, Fire suppression's effects on forest succession within a central Idaho wilderness: Western Journal of Applied Forestry, v. 3, p. 760.

Barrett, S.W., Arno, S.F., and Menakis, J.P., 1997, Fire episodes in the inland Northwest (1540–1940) based on fire history data: Odgen, Utah, USDA-Forest Service, Intermountain Research Station, General Technical Report INT-GTR-370, 17 p.

Benda, L., Dunne, T., 1997, Stochastic forcing of sediment supply to channel networks from landsliding and debris flow: Water Resources Research, v. 33, p. 2849–2863.

Benson, L., Kashgarian, M., Rye, R., Lund, S., Paillet, F., Smoot, J., Kester, C., Mensing, S., Meko, D., Lindstrom, S., 2002, Holocene multidecadal and multicentennial droughts affecting northern California and Nevada: Quaternary Science Reviews, v. 21, p. 659–682.

Blair, T.C., McPherson, J.G., 1994, Alluvial fan processes and forms, *in* Abrahams, A.D., and Parsons, A.J., eds., Geomorphology of desert environments: London, Chapman and Hall, p. 344–402.

Bond, G., Showers, W., Cheseby, M., Lotti, R., Almasi, P., deMenocal, P., Priore, P., Cullen, H., Hajdas, I., and Bonani, G., 1997, A pervasive millennial-scale cycle in North Atlantic Holocene and glacial climates: Science, v. 278, p. 1257–1266.

Bradley, R.S., Hughes, M.K., and Diaz, H.F., 2003, Climate in medieval time: Science, v. 302, p. 404–405.

Cannon, S.H., Gartner, J.E., Parrett, C., and Parise, M., 2003, Wildfire-related debris-flow generation through episodic progressive sediment-bulking processes, Western USA, *in* Rickenmann, D., and Chen-lung, C., eds., Debris-flow hazards mitigation—Mechanics, prediction, and assessment: Rotterdam, Milllpress, p. 71–82.

Cannon, S.H., Powers, P.S., and Savage, W.Z., 1998, Fire-related hyperconcentrated and debris flows on Storm King Mountain, Glenwood Springs, Colorado, USA: Environmental Geology, v. 35, no. 2–3, p. 210–218.

Cannon, S.H., and Reneau, S.L., 2000, Conditions for generation of fire-related debris flows, Capulin Canyon, New Mexico: Earth Surface Processes and Landforms, v. 25, p. 1103–1121.

Clayton, J.L., 1979, Soil and bedrock properties—Weathering and alteration products and processes in the Idaho batholith: Odgen, Utah, USDA Forest Service Research Paper 237, 35 p.

Clayton, J.L., and Megahan, W.F., 1986, Erosional and chemical denudation rates in the southwestern Idaho batholith: Earth Surface Processes and Landforms, v. 11, p. 389–400.

Colman, S.M., and Pierce, K.L., 1986, Glacial sequence near McCall, Idaho—Weathering rinds, soil development, morphology, and other relative-age criteria: Quaternary Research, v. 25, p. 25–42.

Cooper, C.F., 1960, Changes in vegetation, structure, and growth of southwestern pine forest since white settlement: Ecological Monographs, v. 30, p. 129–164.

Costa, J.E., 1984, Physical geomorphology of debris flows, *in* Costa, J.E., and Fleisher, P.J., eds., Developments and applications of geomorphology: Berlin, Springer-Verlag, p. 268–317.

Costa, J.E., 1988, Rheologic, geomorphic, and sedimentologic differentiation of water floods, hyperconcentrated flows, and debris flows, *in* Baker, V.R., Kochel, R.C., and Patton, P.C., eds., Flood geomorphology: New York, John Wiley & Sons, p. 113–121.

Covington, W.W., and Moore, M.M, 1994, Southwestern ponderosa forest structure—Changes since Euro-American settlement: Journal of Forestry, v. 92, p. 39–47.

Criss, R.E., and Taylor, H.P., 1983, An $^{18}O/^{16}O$ and D/H study of Tertiary hydrothermal systems in the southern half of the Idaho batholith: Geological Society of America Bulletin, v. 94, p. 640–663.

dePolo, C.M., and Anderson, J.G., 2000, Estimating the slip rates of normal faults in the Great Basin, USA: Basin Research, v. 12, p. 227–240

Druschel, G.K., and Rosenberg, P.E., 2001, Non-magmatic fracture-controlled hydrothermal systems in the Idaho batholith—South Fork Payette geothermal system: Chemical Geology, v. 173, p. 271–291.

Esper, J., Cook, E.R., and Schweingruber, F.H., 2002, Low-frequency signals in long tree-ring chronologies for reconstructing past temperature variability: Science, v. 295, p. 2250–2253.

Fisher, F.S., McIntyre, D.S., and Johnson, K.M., 1992, Geologic map of the Challis 1° x 2° quadrangle, Idaho: U.S. Geological Survey Miscellaneous Investigations Map I-1819, scale 1:250,000.

Forester, C.S., Wood, S.H., and Nash, B.P., 2002, An 11.8±0.2 Ma silicic volcanic ash in the Miocene Payette Formation, Boise Basin, Idaho: Geological Society of America Abstracts with Programs (Rocky Mountain Section), v. 34, p. A-48.

Fule, P.Z., Covington, W.W., and Moore, M.M., 1997, Determining reference conditions for ecosystem management of southwestern ponderosa pine forests: Ecological Applications, v. 7, p. 895–908.

Gavin, D., 2001, Estimation of inbuilt age in radiocarbon ages of soil charcoal for fire history studies: Radiocarbon, v. 43, p. 27–44.

Gibbons, A.B., 1995, Tertiary sedimentary rocks of the Payette Formation (Miocene) and the lower part (Miocene and Pliocene) of the Idaho Group, Hailey 1º x 2º quadrangle and vicinity, west-central Idaho: U.S. Geological Survey Bulletin 2064-K, 9 p.

Grissino-Mayer, H.D., and Swetnam, T.W., 2000, Century-scale climate forcing of fire regimes in the American Southwest: The Holocene, v. 10, p. 213–220.

Grove, J.M., 1988, The Little Ice Age: New York, Methuen, 498 p.

Grove, J.M., 2001, The initiation of the “Little Ice Age” in regions round the North Atlantic: Climatic Change, v. 48, p. 53–82.

Hallett, D.J., Mathewes, R.W., and Walker, R.C., 2003, A 1000-year record of forest fire, drought and lake level change in southeastern British Columbia: The Holocene, v. 13, p. 773–783.

Hamilton, W.B., 1962, Late Cenozoic structure of west-central Idaho: Geological Society of America Bulletin, v. 73, p. 511–516.

Hyndman, D.W., 1983, The Idaho batholith and associated plutons—Idaho and western Montana, *in* Roddick, J.A., ed., Circum-Pacific plutonic terranes: Geological Society of America Memoir 159, p. 213–240.

Jones, P.D., New, M., Parker, D.E., Martin, S., and Rigor, I.G., 1999, Surface air temperature and its changes over the past 150 years: Reviews of Geophysics, v. 37, p. 173–199.

Kiilsgaard, T.H., Stanford, L.R., and Lewis, R.S., 2001, Geologic map of the Idaho City 30x60-minute quadrangle, Idaho: Idaho Geological Survey Map 29, scale 1:100,000.

Kiilsgaard, T.H., Scanlan, T.M., and Stewart, D.E., 1997, Geologic map of the Boise Basin vicinity, Boise, Ada and Elmore Counties, Idaho: Idaho Geological Survey Map M–7, scale 1:50,000.

Kipfmueller K.F., and Baker W.L., 2000, A fire history of a subalpine forest in south-eastern Wyoming, USA: Journal of Biogeography, v. 27, p. 71–85.

Kirchner, J.W., Finkel, R.C., Riebe, C.S., Granger, D.E., Clayton, J.L., King, J.G., and Megahan, W.F., 2001, Mountain erosion over 10 yr, 10 k.y., and 10 m.y. time scales: Geology, v. 29, p. 591–594.

Kirkham, V.R.D., 1931, Revision of the Payette and Idaho Formations: Journal of Geology, v. 39, p. 193–239.

Lavee, H., Kutiel, P., Segev, M., and Benyamini, Y., 1995, Effect of surface roughness on runoff and erosion in a Mediterranean ecosystem—The role of fire: Geomorphology, v. 11, p. 227–234.

Lindgren, W., 1898, The mining districts of the Idaho Basin and the Boise Ridge, Idaho: 18th Annual Report of the U.S. Geological Survey, pt. 3, p. 617–619.

Luckman, B.H., 2000, The Little Ice Age in the Canadian Rockies: Geomorphology, v. 32, p. 357–384.

Mann, M.E., Bradley, R.S., and Hughes, M.K., 1999, Northern hemisphere temperatures during the past millennium—Inferences, uncertainties, and limitations: Geophysical Research Letters, v. 26, p.759.

McCarthy, J.H., and Kiilsgaard, T.H., 2001, Soil gas studies along the trans-Challis fault system near Idaho City, Boise County, Idaho: U.S. Geological Survey Bulletin 2064, http://geology.cr.usgs.gov/pub/bulletins/b2064-11/.

McNabb, D.H., and Swanson, F.J., 1990, Effects of fire on soil erosion, *in* Walstad, F.D., Radosevich, S.R., and Sandberg, D.V., eds., Natural and prescribed fire in Pacific Northwest forests: Corvallis, Oregon State University Press, p. 159–173.

Megahan W.F., and Molitor, D.C., 1975, Erosional effects of wildfire and logging in Idaho, *in* Watershed Management Symposium: Logan, Utah, American Society of Civil Engineers, Irrigation and Drainage Division, p. 423–444.

Meyer, G.A., and Pierce, J.L., 2003, Climatic controls on fire-induced sediment pulses in Yellowstone National Park and central Idaho—A long-term perspective: Forest Ecology and Management, v. 178, p. 89–104.

Meyer, G.A., and Wells, S.G., 1997, Fire-related sedimentation events on alluvial fans, Yellowstone National Park, U.S.A.: Journal of Sedimentary Research, v. A67, p. 776–791.

Meyer, G.A., Pierce, J.L., Wood, S.H., and Jull, A.J.T., 2001, Fires, storms, and erosional events in the Idaho batholith: Hydrological Processes, v. 15, p. 3025–3038.

Meyer, G.A., Wells, S.G., and Jull, A.J.T., 1995, Fire and alluvial chronology in Yellowstone National Park—Climatic and intrinsic controls on Holocene geomorphic processes: Geological Society of America Bulletin, v. 107, p. 1211–1230.

National Interagency Fire Center, 2003, Wildland fire season overview, accessed 8/26/03 at *http://www.nifc.gov.*

Parrett, C., 1988, Fire-related debris flows in the Beaver Creek drainage, Lewis and Clark County, Montana: U.S. Geological Survey Water Supply Paper W-2330, p. 57–67.

Pierson, T.C., and Costa, J.E., 1987, A rheologic classification of subaerial sediment-water flows, *in* Costa, J.E., Wieczorek, G.F., eds., Debris flows/avalanches: Geological Society of America Reviews in Engineering Geology 7, p. 1–12.

Pollack, H.N., Huang, S., and Shen, P., 1998, Climate change record in subsurface temperatures—A global perspective: Science, v. 282, p. 279–281.

Reid, K.C., 2001, The prehistory of fire in the Idaho Rockies: Idaho Yesterdays, v. 45, no. 3, p. 3–13.

Robichaud, P.R., 2000, Fire effects on infiltration rates after prescribed fire in North Rocky Mountain forests, USA: Journal of Hydrology, v. 231–232, p. 220–229.

Schmidt, K.M., Roering, J.J., Stock, J.D., Dietrich, W.E., Montgomery, D.R., and Schaub, T., 2001, The variability of root cohesion as an influence on shallow landslide susceptibility in the Oregon Coast Range: Canadian Geotechnical Journal, v. 38, p. 995–1024.

Shaub, S., 2001, Landslides and wildfire—An example from the Boise National Forest: Boise, Idaho, Boise State University, unpublished M.S. thesis, 85 p.

Smith, H.V., 1941, A Miocene flora from Thorn Creek, Idaho: The American Midland Naturalist, v. 25, p. 473–523.

Stanford, L.R., 1982, Surficial geology of the upper South Fork Payette River area, south central Idaho: Idaho Geological Survey Technical Report 82-7.

Steele, R., Arno, S.F., and Geier-Hayes, K., 1986, Wildfire patterns change in central Idaho's ponderosa pine-Douglas-fir forest: Western Journal of Applied Forestry, v. 3, p. 76–80.

Stine, S., 1994, Extreme and persistent drought in California and Patagonia during medieval time: Nature, v. 369, p. 546–549.

Strom, B., Nutt, G., McConnaughey, D., and Lancaster N., 1998, Historic Large Fires in Boise National Forest (1900-1997), SW IDAHO ECO-GIS, Boise, Idaho, available online at *http://inside.uidaho.edu/data/bnf/bnf/utm/metadata/histfire_bnf_bnf.htm.*

Stuiver, M., Reimer, P.J., 1993, Extended ^{14}C data base and revised CALIB 3.0 ^{14}C age calibration program: Radiocarbon, v. 35, p. 215-230.

Swanson, F.J., 1981, Fire and geomorphic processes, *in* Mooney, H.A., Bonnicksen, T.M., Christensen, N.L., Loctan, J.E., and Reiners, W.A., eds., Fire regimes and ecosystem properties: Washington, D.C., USDA Forest Service General Technical Report WO-26.

Sweetkind, D.S., and Blackwell, D.D., 1989, Fission-track evidence of the Cenozoic thermal history of the Idaho batholith: Tectonophysics, v. 157, p. 241–250.

Swetnam, T.W., 1993, Fire history and climate change in giant sequoia groves: Science, v. 262, p. 885–889.

Swetnam, T.W., and Baisan, C.H., 1996, Historical fire regime patterns in the southwestern United States since AD 1700, *in* Allen, C.D., ed., Proceedings of the second La Mesa Fire Symposium, 29–30 March 1994, Los Alamos, New Mexico, USDA Forest Service General Technical Report, RM-GTR-286, p. 11–32.

Wells, W.G., II, 1987, The effect of fire on the generation of debris flows, *in* Costa, J.E., and Wieczorek, G.F., eds., Debris flows/avalanches: Geological Society of America Reviews in Engineering Geology 7, p. 105–114.

Whitlock, C., Shafer, S.L., Marlong, J., 2003, The role of climate and vegetation change in shaping past and future fire regimes in the northwestern US and the implications for ecosystem management: Forest Ecology and Management, v. 178, no. 1–2, p. 5–21.

Wood, S.H., 2004, Stop 1-1. Garden Valley—Late Cenozoic faulting on the Boise Ridge fault, Idaho: this volume.

Wood, S.H., and Clemens, D.M., 2002, Geologic and tectonic history of the western Snake River Plain, Idaho and Oregon, in Bonnichsen, B., White, C.M., and McCurry, M., eds., Tectonic and magmatic evolution of the Snake River Plain volcanic province: Idaho Geological Survey Bulletin 30, p. 69–103.

Woodhouse, C.A., Overpeck, J.T., 1998, 2000 years of drought variability in the central United States: American Meteorological Society, v. 79, p. 2693–2714.

Late-Pleistocene Equilibrium-Line Altitudes, Atmospheric Circulation, and Timing of Mountain Glacier Advances in the Interior Northwestern United States

By Grant A. Meyer[1], Peter J. Fawcett[1], and William W. Locke[2]

Abstract

We reconstructed equilibrium-line altitudes for late-Pleistocene glaciers in eastern Oregon, central and northern Idaho, and western Montana. Over 500 cirque to small valley glaciers were mapped where moraines and other evidence for ice margins could be confidently interpreted on digital topographic maps. Equilibrium-line altitudes (ELAs) were estimated using the accumulation-area ratio method. Spatial patterns of ELAs show a strong correspondence to present-day precipitation patterns. Modern dry regions have relatively high ELAs (*e.g.*, 2,600–2,900 m at about lat 44.5°N. in the Lost River and Lemhi Ranges south-central Idaho), whereas wetter regions at similar latitudes have considerably lower ELAs (*e.g.*, 2000–2200 m in mountains southwest of McCall, Idaho). Steep eastward increases in ELAs across larger massifs such as the Wallowa, Sawtooth, and central Bitterroot Mountains reflect orographic effects on westerly flow. The Columbia River basin of eastern Washington and Oregon provided a lowland corridor for moist, eastward-moving Pacific air-masses, producing anomalously low ELAs in bordering ranges (*e.g.*, <1,800 m around lat 46.5°N. in the Clearwater River drainage of northern Idaho currently the wettest region of the study area). Smaller-scale features such as the Salmon and Payette River canyons also appear to have acted as conduits for atmospheric moisture. Overall, the ELA data point strongly toward a moisture source in the north Pacific Ocean. General circulation climate model results indicate that at the last continental glacial maximum, an anticyclone centered over the continental ice sheets and southward deflection of the jet stream should produce dry conditions in the interior northwestern United States. Our results suggest that the anticyclone is weaker than in some previous simulations, and easterly winds are not clearly indicated across the study region. By 15 ka, northward retreat and decline in continental ice-sheet elevation caused contraction of the anticyclone, and winter westerlies from the north Pacific continued to strengthen across the study area until 12 ka. An associated increase in snowfall may have allowed more precipitation-sensitive mountain glaciers to remain near their maxima or expand during the post-late glacial maximum period, before the dramatic warming into the early Holocene. Similar positions and topography of continental ice sheets during buildup prior to the late glacial maximum also might promote glacial advances by focusing strong westerly flow on mountain ranges of the interior northwest. Further dating of mountain glacier advances is necessary to test these hypotheses.

Introduction

We mapped perimeters and reconstructed equilibrium-line altitudes (ELAs) for small late Pleistocene alpine glaciers in the interior northwestern United States east of the Coast and Cascades Ranges and south of the continental glacial limit (fig. 1 and 2). This region has a high density and continuity of glaciated mountains, especially in central Idaho. Last-glacial moraines (*i.e.*, those usually attributed to the "Pinedale glaciation" of the Rocky Mountains, *e.g.*, Porter and others, 1983) are commonly well displayed in the field and on topographic maps.

Climatic Significance of Regional ELAs

Equilibrium-line altitudes of alpine glaciers are a function of a suite of local and regional climatic and topographic

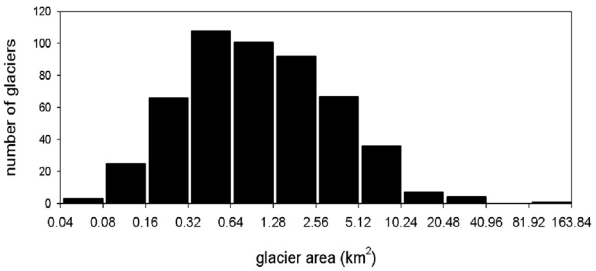

Figure 1. Distribution of total surface area of reconstructed glaciers (log_2 scale).

[1]Department of Earth & Planetary Sciences, University of New Mexico, Albuquerque, NM 87131, gmeyer@unm.edu

[2]Department of Earth Sciences, Montana State University, Bozeman, MT 59717

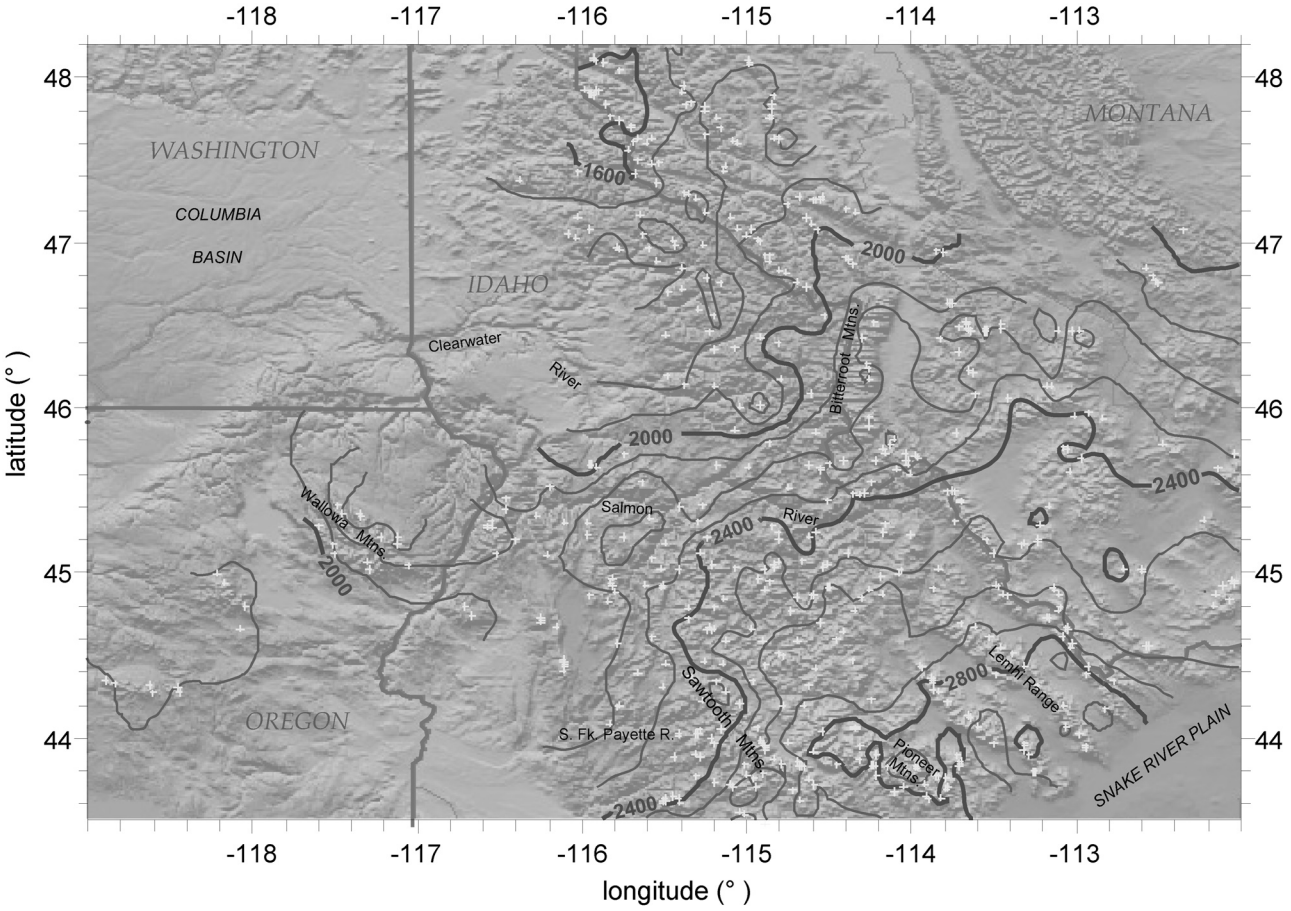

Figure 2. Contour map of last-glacial ELAs for glaciers of all aspects (but mostly northwest through east aspects) produced using a kriging routine; data points shown by white crosses. Contour interval 50 m.

factors that affect mass balance including air temperature, precipitation, patterns of wind erosion and deposition of snow, and insolation. In general, glacier mass balances are most strongly controlled by winter precipitation in coastal regions and by summer temperatures in continental interiors (*e.g.*, Hostetler and Clark, 1997). The regional pattern of ELAs, however, is influenced by proximity to moisture sources and prevailing wind directions, as well as by latitudinal changes in insolation and temperature (*e.g.*, Porter and others, 1983; Leonard, 1984; Locke, 1990).

Previous Work

A small-scale contour map of cirque-floor elevations for the entire Western United States was compiled by Porter and others (1983), which shows a similar overall pattern to our results, but considerably less detail. Locke (1990) reconstructed ELAs for western Montana using a variety of methods and discussed their relative accuracy. We consider data to be most reliable where obtained by the AAR method from relatively small glaciers reconstructed where ice-affected areas are clear, and include those data here, along with some newly generated ELA data for western Montana.

Methods

We used commercial software with digital raster USGS topographic maps to map late-Pleistocene glaciers and measure areas and elevations. We estimated ELAs by applying the observation that the accumulation area of small modern alpine glaciers is approximately 65 percent of the total surface area (Meierding, 1982; Locke, 1990), in other words, the AAR method. Because ELAs produced by this method will generally have smaller uncertainties for small glaciers, we concentrated mostly on reconstruction of cirque to small valley glaciers with total area of 0.1 to 10 km^2 (fig. 1). The margins of ice-affected areas were identified in part through erosional features, including the tops of cirque headwalls and oversteepened trough valley walls, and the lower limits of U-shaped valley profiles. Mapped lower ice margins were marked at least in part by lateral and terminal moraines. Glaciated

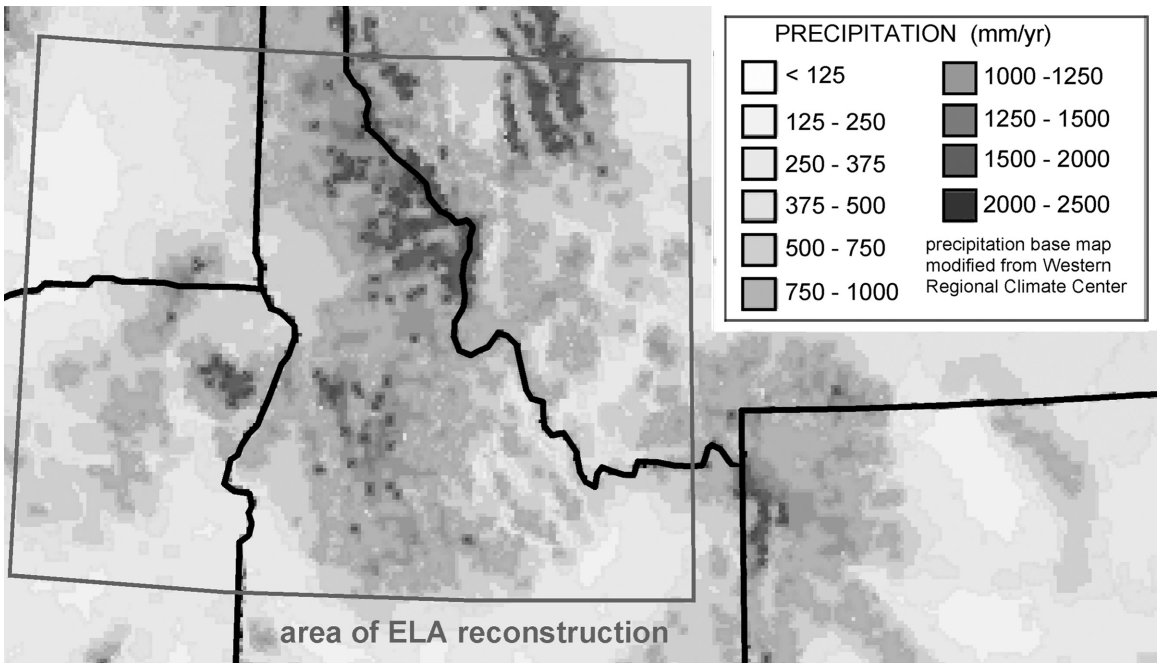

Figure 3. Map of mean annual precipitation in the interior northwestern United States; compare to figure 2.

cirques and valleys without clear evidence of ice margins were rejected. Where nested moraine sequences were identified, we assumed that the innermost large, well defined, sharp-crested, and relatively continuous moraine set represented the last local glacial maximum (typically termed "Pinedale" glaciation; Porter and others, 1983). Narrow, lower, and discontinuous moraine ridges were sometimes identified in larger glacial valleys, typically well upvalley from major moraines. These were considered recessional moraines and were not used in ELA reconstruction. We obtained a total of 510 ELAs for the study area.

To consider atmospheric circulation patterns and their possible effects on moisture delivery to glaciers in the study area, we used the GENESIS (v. 2) atmospheric general circulation model (GCM) to simulate winds over North America at 21 ka (late glacial maximum, LGM), 15 ka, 12 ka, and the present. The major boundary conditions that were systematically changed include ice-sheet extents and elevations (from Peltier, 1994), and orbital configurations. Simulation results reported here include near-surface (993 mb) and lower-troposphere (866 mb) wind vectors to describe the response of the lower atmosphere to the imposed boundary conditions.

Results

Late-Pleistocene ELA Reconstructions

Equilibrium-line altitudes range from about 1600 m in the northern study region near Lookout Pass along the Montana-Idaho border to about 3000 m in the Basin and Range mountains north of the eastern Snake River Plain (fig. 2). The overall pattern of ELAs generally mimics the present-day pattern of precipitation, where low ELAs correspond to high annual precipitation (figs. 2 and 3). There is a general eastward rise in summit elevations and a trend to colder winter climates from west to east across central Idaho, but late Pleistocene ELAs nonetheless rise steeply toward the east, including along the route of this field trip. For example, the average gradient from the West Mountains southwest of McCall, Idaho, to the Beaverhead Mountains at similar latitude on the Montana border is about 2.5 m/km. Locally, large eastward increases in ELA are present across the Wallowa Mountains in eastern Oregon and the Sawtooth Mountains of Idaho, suggesting that these prominent highlands caused significant precipitation shadows in a dominant westerly flow of moisture. The eastward rise in ELAs is as steep as 6.6 m/km from the western Sawtooth Mountains to the central Pioneer Mountains. Anomalously high ELAs in the high-altitude core of the Pioneer Mountains are consistent with diversion of low-level moist airflow around this relatively large massif, as observed elsewhere by Meierding (1982), Porter and others (1983), Leonard (1984), and Locke (1990). These relations indicate a strong precipitation control on ELAs.

A zone of relatively low ELAs extends eastward across northern Idaho and into northwestern Montana, probably from penetration of moist Pacific air masses across the Columbia Basin lowlands and up the Salmon and Clearwater River canyons. The highest ELAs were found in Idaho in the central Pioneer Mountains and the southern Lost River and Lemhi Ranges and the Beaverhead Mountains, where a combination of precipitation shadows and moist airmass diversion up the eastern Snake River Plain result in a dry climate (similar to the

results of Porter and others, 1983). Local heating of the low, arid Snake River Plain also may create warmer conditions in adjacent mountains. Not surprisingly, glaciers on west through southeast aspects have higher ELAs than the local average. East-facing glaciers are abundant regardless of mountain ridge orientation and other large-scale topographic controls, and approximately equal numbers of east, northeast, and north-facing glaciers are included in the dataset. Less than 10 percent of the data are derived from glaciers of other aspects, and west-facing cirques are notably uncommon over much of the study region, especially in the dry Lost River and Lemhi Ranges, and the Beaverhead Mountains. These observations are consistent with wind erosion of snow on west slopes and wind loading on the lee side of mountain ridges by westerly winds.

Locke (1990) found that late-Pleistocene ELAs in western Montana lie about 450 m lower than modern glaciers, which lie in topographically favorable sites for snow accumulation and preservation. Porter and others (1983), however, cite literature indicating that late-Pleistocene ELAs were generally about 1,000 m lower than present across the Western United States. No true glaciers are known in Idaho. Flint (1971) notes that elsewhere in the Rocky Mountains, the lower limit of perennial snowfields corresponds approximately to the ELA of small cirque glaciers in the same area. A few perennial snowfields are mapped on USGS 1:24,000 quadrangles, mainly in the Sawtooth Mountains. However, the mapped lower limits of these snowfields range widely in elevation, and the absence of modern glaciers even on suitable slopes rising up to 300 m above these limits show that they are a poor indicator of modern "ELAs." The lack of modern glaciation in cirques at the head of late-Pleistocene glaciated valleys in the Sawtooths implies a minimum last-glacial ELA depression of about 500 m relative to the present.

GCM Simulations

General circulation model results for January at the LGM (21 ka) show a glacial anticyclone (high-pressure system and clockwise circulation) centered over the continental ice sheet northwest of the study region (fig. 4). The main effect of the anticyclone, however, was to weaken the westerlies across this region, rather than to create persistent easterly flow. Easterly near-surface winds are modeled near the ice-sheet margin in the Central United States, but do not extend into the study region. Lower tropospheric flow over the study region was predominantly westerly, with persistent ridging creating northward deflection of winds and drier conditions (see 866 mb results). With weakening and contraction of the anticyclone by 15 ka, moisture supply in the interior northwest was probably enhanced by stronger westerly flow carrying Pacific airmasses into the interior. Although global ice volume was diminishing, increased snowfall may have sustained or caused advances of more precipitation-sensitive mountain glaciers in the study region. Higher-level ridging was reduced, and temperatures likely were somewhat increased, promoting greater winter precipitation. By 12 ka, the extent of the continental ice sheets was considerably reduced, and the western glacial anticyclone was absent. Greater transport of moisture into the interior northwest by strong near-surface and lower-troposphere westerly flow possibly could maintain some mountain glaciers until terminal Pleistocene warming raised ELAs to unsustainable levels.

Relation to Glacial Chronology

Numerical and calibrated ages for glacial advances are relatively rare in this region and are reported below in calendar years. Minimum limiting ^{14}C ages of 14 ka for Sawtooth Mountains advances in Idaho (Thackray and others, 2004) may provide evidence that increased precipitation maintained these mountain glaciers well after the LGM. Cosmogenic surface-exposure dating using ^{10}Be reveals major advances at both 21 ka and 17 ka in the Wallowa Mountains, however, suggesting that precipitation at the LGM was not limiting for ice accumulation in that area (Licciardi and others, 2000). Between these two ranges, near McCall, Idaho, Colman and Pierce (1986) used calibrated weathering-rind ages to estimate moraine formation at 14 ka, 20 ka, and 60 ka. These moraines were formed by an outlet glacier of an ice cap on the highlands between the North Fork Payette River and South Fork Salmon River, an area of relatively high modern precipitation in central Idaho (fig. 3). Although approximate, the McCall data indicate that near-maximum advances of this piedmont lobe occurred both well before and well after the LGM. Combined ^{3}He and ^{10}Be ages indicate a relatively late maximum advance of the northern Yellowstone outlet glacier at about 16.5 ka (Licciardi and others, 2001), which may have stemmed from an increased flow of moist airmasses up the Snake River Plain following the LGM. Licciardi and others (2003) also suggest that the late culmination of the Yellowstone glacial system may reflect the protracted interval of buildup and longer response time of the plateau ice cap (Pierce, 1979).

Conclusions

Overall, the ELA data imply that patterns of precipitation and wind flow generally similar to present existed during the time of maximum advances of these alpine glaciers, and that moisture originating in the Pacific was depleted by orographic effects as air masses moved eastward. Some paleoclimatic reconstructions indicate that the northwestern United States was significantly drier overall around the last continental glacial maximum (LGM) (*e.g.*, Whitlock and Bartlein, 1997; Locke, 1990). Easterly winds generated by the glacial anticyclone over the continental ice sheets have been implicated in this reduction of precipitation (*e.g.*, COHMAP, 1988; Bartlein and others, 1998). Nonetheless, our data show that the primary moisture source for alpine glaciers in the northwestern United

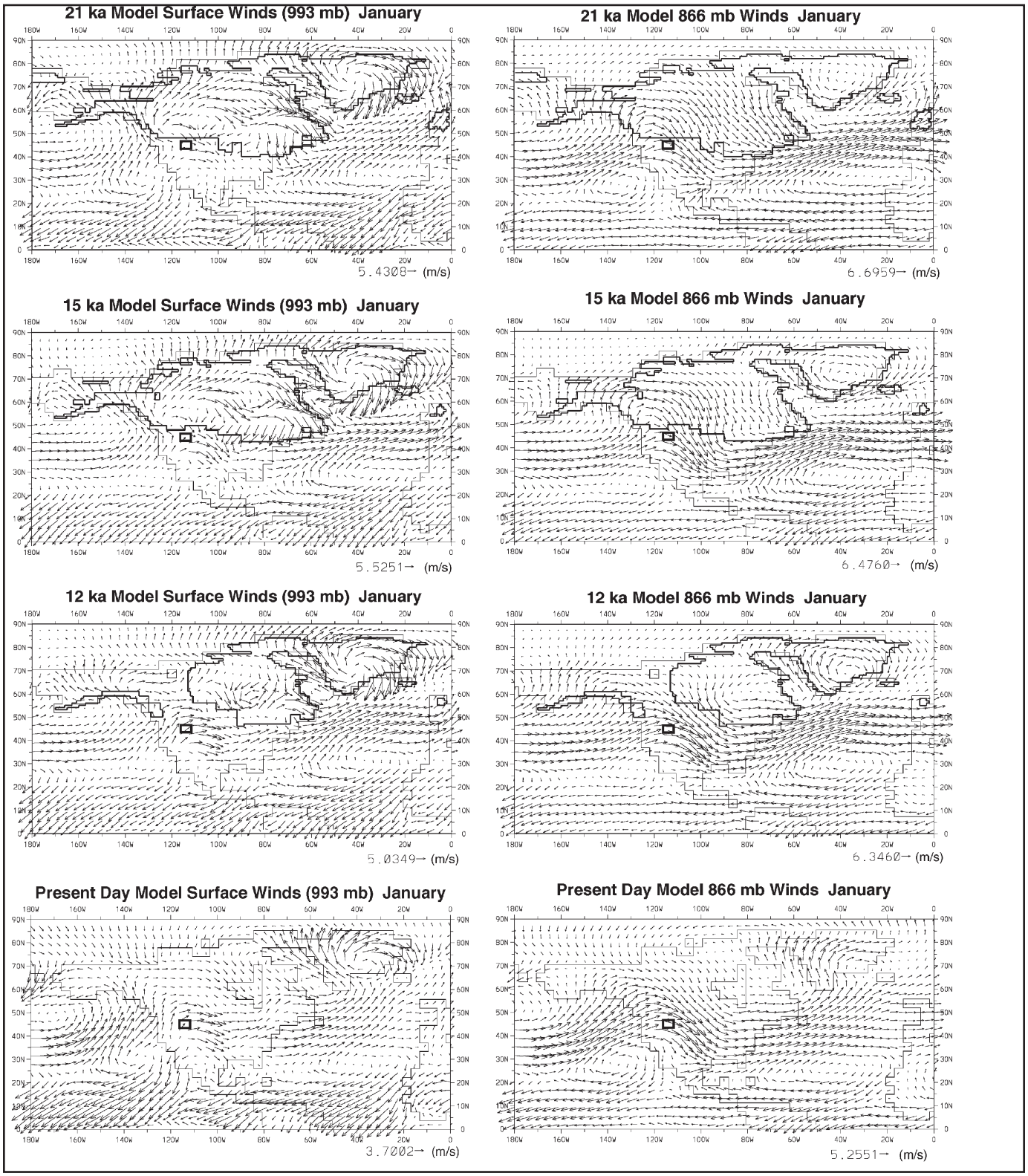

Figure 4. Modeled wind speed and direction over North America for 4-time periods from the LGM (21 ka) to present, for near surface (993 mb) and higher-elevation but still lower troposphere (866 mb) winds. Ice-sheet extent is shown by a heavy line; the small box outlines the central Idaho region (lat 43.5–45.5°N., long 113–117°W.).

States was clearly the North Pacific. The net effect of the glacial anticyclone was probably weakening of westerly flow during the LGM. Locke (1990) inferred that convergence of westerlies with katabatic easterly flow at the southern margin of the continental ice sheets caused lifting and enhanced precipitation, resulting in lower ELAs along the east flank of the Rocky Mountains in Montana.

Further understanding of glacial chronology in the interior northwest is necessary to test inferred changes in paleoclimatic conditions over the last glaciation, including decreased precipitation during the LGM, and later strengthening of westerlies and presumably increased precipitation. Rapid temperature changes in the latest Pleistocene probably also had a relatively large impact on small cirque and valley glaciers. In addition, the contrasting dynamics and response times of small mountain glaciers, mountain ice caps as in Yellowstone, and continental ice sheets are likely involved in asynchronous advances among these glaciers of vastly different spatial scales (*e.g.*, Gillespie and Molnar, 1995).

Acknowledgments

Grant Meyer and Bill Locke are grateful to students in a number of past geomorphology and glacial geology classes at Middlebury College, University of New Mexico, and Montana State University for assistance in ELA reconstructions. Peter Castiglia helped with GCM simulations at UNM. We thank Ken Pierce and Les McFadden for helpful reviews and discussions.

References

Bartlein, P.J., Anderson, K.H., Anderson, P.M., Edwards, M.E., Mock, C.J., Thompson, R.S., Webb, R.S., Webb, T., III, and Whitlock, C., 1998, Paleoclimate simulations for North America over the past 21,000 years—Features of the simulated climate and comparisons with paleoenvironmental data: Quaternary Science Reviews, v. 17, p. 549–585.

COHMAP Project Members, 1988, Climatic changes of the last 18,000 years—Observations and model simulations: Science, v. 241, p. 1043–1052.

Colman, S.M., and Pierce, K.L., 1986, Glacial sequence near McCall, Idaho—Weathering rinds, soil development, morphology, and other relative age criteria: Quaternary Research, v. 25, p. 25–42.

Flint, R.F., 1971, Glacial and Quaternary geology: New York, John Wiley, 892 p.

Gillespie, A., and Molnar, P., 1995, Asynchronous advances of mountain and continental glaciers: Reviews of Geophysics, v. 33, p. 311–364.

Hostetler, S.W., and Clark, P.U., 1997, Climatic controls of Western U.S. glaciers at the last glacial maximum: Quaternary Science Reviews, v. 16, p. 505–511.

Leonard, E.M., 1984, Late Pleistocene equilibrium-line altitudes and modern snow accumulation patterns, San Juan Mountains, Colorado, U.S.A.: Arctic and Alpine Research, v. 16, p. 65–76.

Licciardi, J.M., Clark, P.U., Brook, E.J., Elmore, D., and Sharma, P., 2000, Cosmogenic Be-10 chronology of late-Pleistocene glaciation in the Wallowa Mountains, Oregon, USA: EOS, Transactions, American Geophysical Union, v. 81, no. 48, Fall Meeting Supplement, Abstract U21A-14.

Licciardi, J.M., Clark, P.U., Brook, E.J., Pierce, K.L., Kurz, M.D., Elmore, D., and Sharma, P., 2001, Cosmogenic He-3 and Be-10 chronologies of the late Pinedale northern Yellowstone ice cap, Montana, USA: Geology, v. 29, p. 1095–1098.

Licciardi, J.M., Pierce, K.L., and Kurz, M.D., 2003, Ongoing investigation of the late Pleistocene Yellowstone and Grand Teton ice cap histories, Montana and Wyoming, USA: Geological Society of America Abstracts with Programs, v. 34, no. 7, p. 541.

Locke, W.W., 1990, Late Pleistocene glaciers and the climate of western Montana, U.S.A.: Arctic and Alpine Research, v. 22, p. 1–13.

Meierding, T.C., 1982, Late Pleistocene glacial equilibrium-line altitudes in the Colorado Front Range—A comparison of methods: Quaternary Research, v. 18, p. 289–310.

Peltier, R., 1994, Ice age paleotopography: Science, v. 265, p. 195–201.

Pierce, K.L., 1979, History and dynamics of glaciation in the northern Yellowstone National Park area: U.S. Geological Survey Professional Paper 729-F, 90 p.

Porter, S.C., Pierce, K.L., and Hamilton, T.D., 1983, Late Wisconsin mountain glaciation in the Western United States, *in* Porter, S.C., ed., Late Quaternary environments of the United States, v. 1, The late Pleistocene: Minneapolis, University of Minnesota Press, p. 71–111.

Thackray, G.D., Lundeen, K.A., and Borgert, J.A., 2004, Late Pleistocene alpine glacier advances in the Sawtooth Mountains, Idaho—Reflections of midlatitude moisture transport at the close of the last glaciation: Geology, v. 32, p. 225–228.

Whitlock, C., and Bartlein, P.J., 1997, Vegetation and climate change in northwest America during the past 125 kyr: Nature, v. 388, p. 59–61.

Late Pleistocene Alpine Glaciation in the Southeastern Sawtooth Mountains, Idaho: Moraine Characteristics, Sediment Coring, and Paleoclimatic Inferences

By Glenn D. Thackray[1], Kari A. Lundeen[2], and Jennifer A. Borgert[3]

Introduction

Glaciers descended the eastern flanks of the Sawtooth Mountains repeatedly during late Pleistocene time, constructing an extensive moraine belt at the range front in the Sawtooth Valley. The glacial sequence and the numerous lakes it hosts preserve a detailed record of those fluctuations, themselves a reflection of complex climatic processes during the last glaciation. In particular, we infer that the chronology derived to date reflects strong influences of Pacific moisture delivery on the alpine glacial system.

The last glaciation involved dramatic reorganization of oceanic, atmospheric, and cryospheric systems. The complexity of glaciation is particularly stark in western North America, where the growth and subsequent shrinkage of the Laurentide/Cordilleran ice-sheet system strongly influenced atmospheric patterns and, thus, precipitation-delivery patterns. Coupled with the diverse orography of the cordillera, those precipitation patterns exerted complex influences on mountain glacier systems during middle Wisconsin time (ca. 50,000 to 25,000 yr), late Wisconsin full-glacial time (ca. 21,000 to 17,000 cal yr BP) and late-glacial time (ca. 17,000 to 11,000 cal yr BP). Consequently, the timing of maximum alpine glacier advances shows considerable variation across the region (*e.g.*, Chadwick and others, 1997; Thackray, 1999 and 2001; Licciardi and others, 2001) as does the more detailed timing of late-glacial advances, particularly pre-Younger Dryas (*e.g.*, Clark and Gillespie, 1997) versus syn-Younger Dryas advances (*e.g.*, Gosse and others, 1995).

Extensive mountain glacier fluctuations left an extensive moraine and lake system on the eastern flank of the Sawtooth Mountains constructed during late full-glacial time (ca. 16,00–17,000 cal yr BP) and early late-glacial time (ca. 13,000–14,000 cal yr BP). Herein, we describe these features and a sequence of older moraines, yet undated but inferred to have originated during early or middle Wisconsin time, and an apparent lack of moraines correlative with the ice-sheet maximum. We infer that the advances required reinvigoration of moisture transport into the northwestern interior of the United States.

[1]Department of Geosciences, Idaho State University, Pocatello, ID 83209, thacglen@isu.edu

[2]Connecticut Department of Environmental Protection, Hartford, CT 06106, kari.lundeen@po.state.ct.us

[3]Retec, Inc., St. Paul, MN, JBorgert@retec.com

Setting and Context

The Sawtooth Mountains comprise one of the highest ranges in central Idaho. The range trends roughly north-south and rises to about 3,300 m, exposing Cretaceous granitic rocks and Paleozoic metasedimentary wall rocks of the Idaho batholith as well as Eocene granites of the Sawtooth batholith. Most importantly, the Sawtooth Mountains represent the first high orographic barrier encountered by moist Pacific air masses east of the Cascade Range. Indeed, the Sawtooth Mountains today receive the bulk of their precipitation from winter and spring Pacific storms and mark the transition between the wetter forested ranges of western Idaho and drier, largely unforested ranges to the east. The latter are dominated by summer monsoonal precipitation (see fig. 4 of Whitlock and Bartlein, 1993). Inferred late-Pleistocene equilibrium line altitudes (ELAs) rise steeply across the range (Stanford, 1982; Borgert, 1999; Lundeen, 2001), indicating similar influence of prevailing, moist westerly winds.

Major valleys marking the eastern and western flanks of the Sawtooth Mountains hosted large valley glaciers (>10 km length) during late-Pleistocene glacial episodes. On the eastern flank, glaciers constructed a broad moraine belt in the adjoining extensional basin. Late Pleistocene moraines dominate the moraine belt in the southeastern portion of the range (Williams, 1961; Breckenridge and others, 1988; Borgert and others, 1999), the focus of this study.

Methods

We employed surficial geologic mapping, relative weathering assessment of glacial landforms, analysis of sediment cores, and radiocarbon dating. Surficial geologic mapping, utilizing air photo and topographic map interpretation, digital terrain analysis, and field observation, identified 7 to 9 equilibrium moraines in each of four valleys. In order to determine

Table 1. Radiocarbon ages for core samples described in this report. Additional radiocarbon dates are reported in Borgert (1999) and Lundeen (2001).

Location name	Sample name	CAMS	^{14}C age	± (1 σ)	Material submitted	Calibrated age*	± (1 σ)
McDonald Lake	Mac 2-126	60638	10,590	50	wood	12,780	60
McDonald Lake	Mac 3-132	60639	11,640	50	gyttja	13,570	100
McDonald Lake	Mac 3-140	60637	11,920	90	gyttja	13,960	140
Pettit Lake	P1-94	73098	10,010	50	conifer needle	11,390	60
Pettit Lake	P2-63	73099	11,930	40	charcoal	13,940	150
Lost Boots Marsh	LBM1	41458	9,960	40	plant fragments	11,300	40
Lost Boots Marsh	LBM2	41457	10,300	40	gyttja	12,010	60
Lost Boots Marsh	LBM3	41459	11,990	60	gyttja	13,980	120
Lost Boots Marsh	LBM4	41460	13,660	70	plant fragments	16,400	240
Lost Boots Marsh	LBM5b	51315	14,060	300	plant fragments	16,860	410
Lost Boots Marsh	LBM5a**	41461	11,030	120	plant fragments		

* Calibrated per Stuiver and others (1998). Age ranges with the highest probability are reported.

** Sample 5a produced the initial date on this horizon, derived from a very small amount of carbon; therefore, this date is disregarded. Two additional cores subsequently were obtained from the site and the horizon resampled to obtain sample LBM5b.

relative-age moraine groups, we collected soil and morphometric data from the moraine sequences and performed simple statistical analysis on those data. We then collected sediment cores from 10 sites, including lakes, marshes, and fens, in order to analyze glacial and post-glacial sediment patterns. We collected several types of data from the cores, including visual description, magnetic susceptibility, total organic carbon, and grain-size distribution. Our methods are described fully in Borgert (1999) and Lundeen (2001). Finally, we submitted 19 samples to the Center for Accelerator Mass Spectrometry at Lawrence Livermore National Laboratory for radiocarbon dating (table 1). Where possible, macrofossils were submitted, but bulk gyttja samples were submitted in several cases, as noted in table 1.

Results

Relative Age Assessment

As noted, 7–9 end moraines were delineated in each of four valleys (fig. 1). All moraines we describe here are distinctly better defined, more steeply sloping, and more sharply crested than are middle Pleistocene moraines in drainages within 20 km to the north. Therefore, we consider all moraines in this study to be of late Pleistocene age. This broad age determination is consistent with that of Williams (1961) and Breckenridge and others (1988), who mapped the outermost moraines in these four valleys as late Pleistocene in age.

Our analysis of soil and moraine morphometry data from the late Pleistocene moraine sequence delineated two relative age groups (Lundeen, 2001; Borgert, 1999). Moraine crest angularity and depth to B horizon proved to be the most consistent relative age indices (fig. 2). The downvalley group of voluminous, broad-crested, multiple-ridged moraines (Busterback Ranch moraine group) is statistically distinct from the upvalley group of smaller, sharp-crested moraines (Perkins Lake moraine group; Lundeen, 2001). Because of the distinct differences between the moraine groups, we infer that the Busterback Ranch group is at least 10,000 yr older than the Perkins Lake group and that the age difference probably is considerably larger. The difference between inferred equilibrium-line elevations (ELAs) of the two moraine groups is small; while the moraines are widely separated spatially, their elevational separation is relatively small. Paleo-ELA estimates lie between 2,400 and 2,700 m, with an ELA difference of less than 200 m in each valley. The moraine groupings are shown in figures 1 and 2.

Sediment Cores and Radiocarbon-Age Constraints

Cores from 3 of 10 locations provide reliable constraints on the timing of glacier fluctuations. At Lost Boots Marsh, which lies within 0.5 km upvalley of the oldest moraine in the Perkins Lake moraine group in the Alturas valley (fig. 1), we collected three cores with similar stratigraphy (fig. 3A). The most notable feature of these cores is the radiocarbon date of 16,860±410 cal yr BP, which was obtained from an organic-bearing silt layer about 15 cm above ice-proximal sandy gravel. We consider this date a close minimum limiting date for the moraine lying 0.5 km downvalley. Overlying laminated

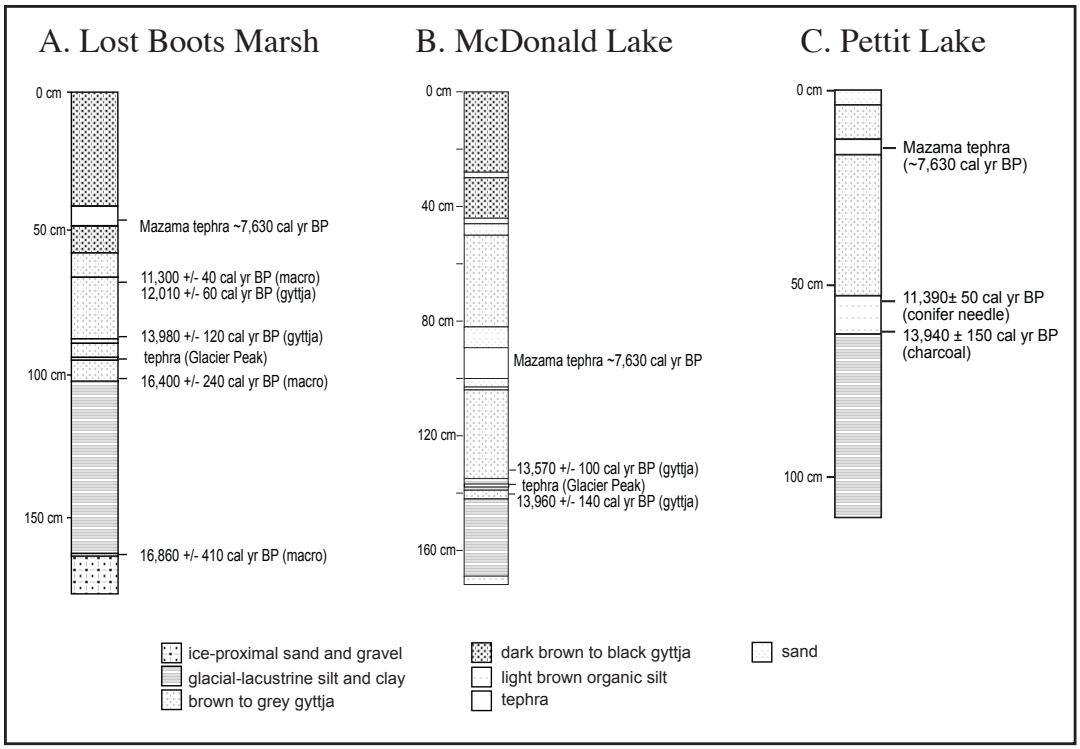

Figure 1. Map of moraines in the southeastern Sawtooth Mountains, showing moraine groups, core sites, and field-trip stops. Moraine groups are delineated by relative weathering criteria. We infer that the two moraine groups are separated in age by at least 10,000 yr.

silt and clay, with high magnetic susceptibility and low total organic carbon, represent glacial-lacustrine sedimentation, most likely a larger lake than those of today, dammed by the moraine downvalley of the core site. Glacial-lacustrine sedimentation terminated and organic-rich sedimentation began ca. 16,400 cal yr BP. The transition to organic-rich sedimentation at that time represents either the retreat of glaciers from the lake margin, coupled with the invigoration of organic production, or the partial drainage of the inferred, large lake and consequent isolation of the marsh from the adjacent, smaller lakes. Also of note is an anomalous, 3-cm-thick, light-brown layer within the organic-rich section. This layer did not produce distinct total organic carbon, magnetic susceptibility, or grain-size values; however, its anomalous color and minimum limiting date of 13,980±120 cal yr BP, which correlates with dates in the two cores described below, suggest that it pertains to a glacial readvance upvalley or to a distinct climatic episode that reduced organic production or increased inorganic sedimentation in the Alturas Lake drainage.

The McDonald Lake 3 core (fig. 3B), one of three taken from this small (9 ha) lake in the Yellowbelly drainage, constrains a later portion of the glacial record. McDonald Lake is dammed by the youngest moraine in the Busterback Ranch group, and three moraines of the Perkins Lake group lie within 2 km upvalley. Our core did not reach ice-proximal sediment.

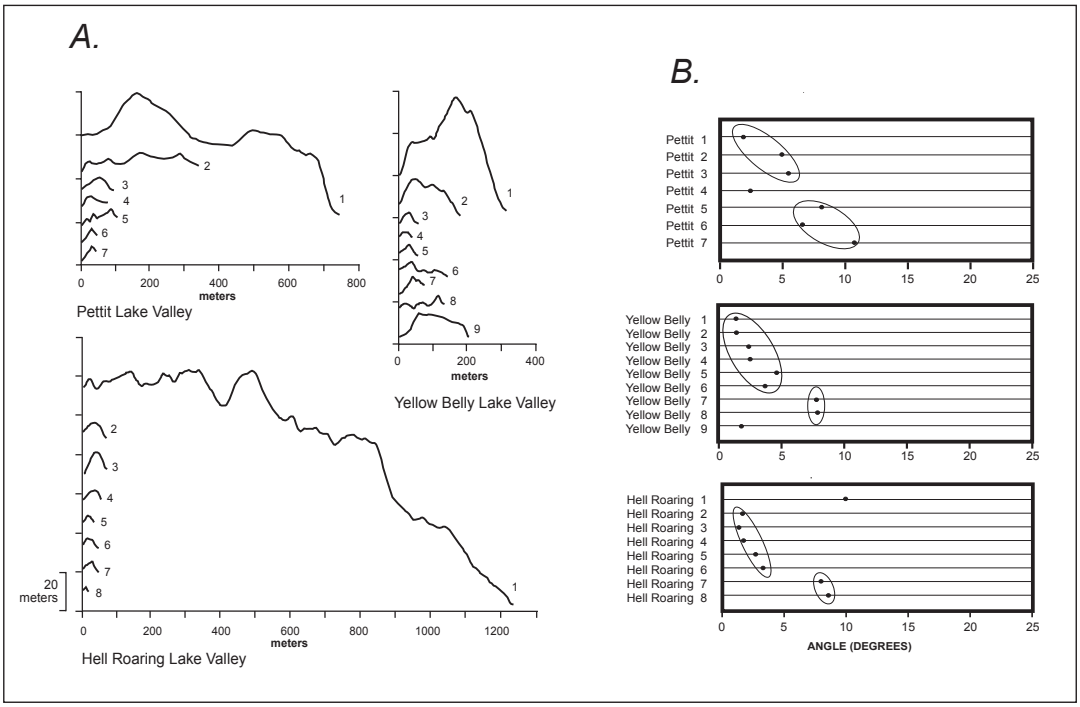

Figure 2. Moraine profiles (A) and morphometry data (B) for eastern Sawtooth valleys. Relative-age groupings, which consider the statistical variability of the moraine profiles, are circled.

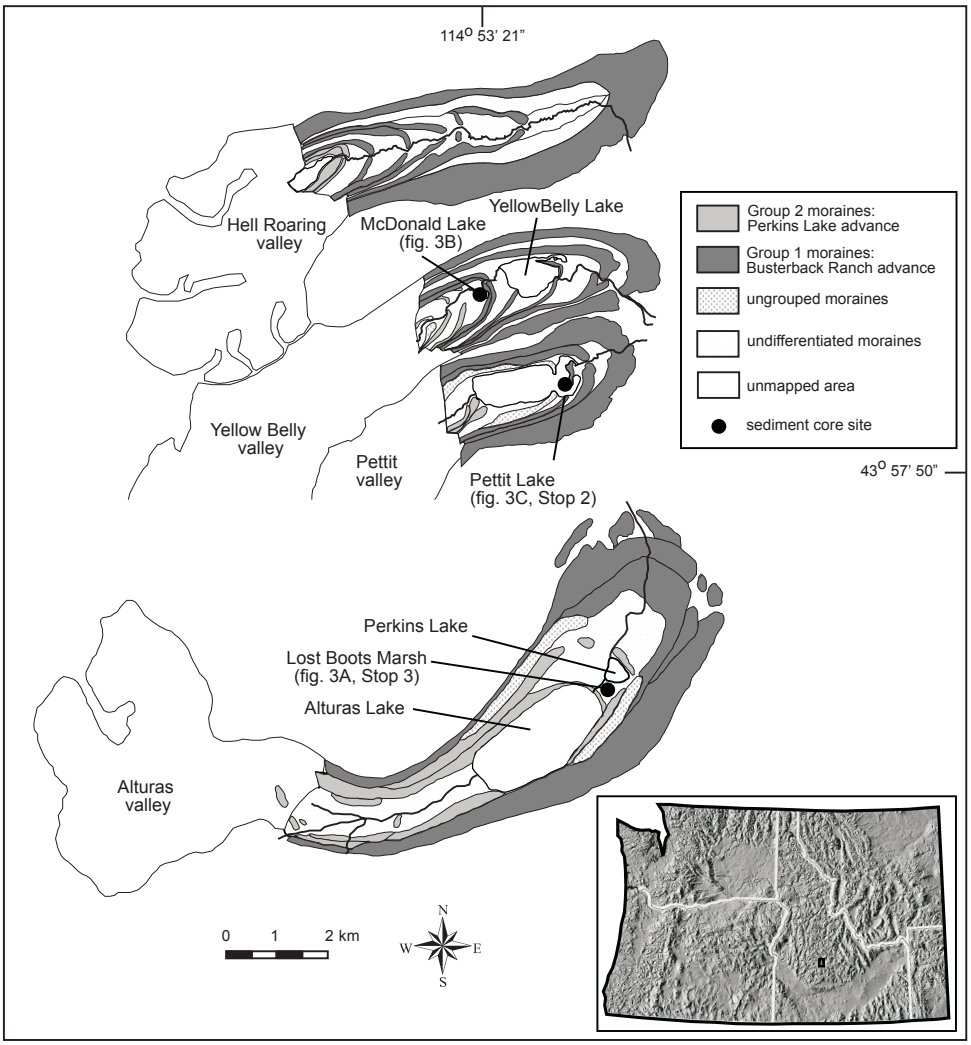

Figure 3. Data from three cores that provide reliable age constraint for the younger moraine group. (A) Lost Boots Marsh, Alturas valley. (B) McDonald Lake 3, Yellowbelly valley. (C) Pettit Lake (composite of two cores), Pettit valley.

However, the core does contain about 30 cm of glacial-lacustrine sediment at its base. The sediment has characteristics of a high glacier activity index (sensu Souch, 1994). Because two sediment-trapping lakes lie upvalley of the youngest Perkins Lake moraines, we infer that the glacial-lacustrine sediment in the core was deposited during the time the glacier constructed those moraines. Thus, the minimum-limiting date of 13,960±140 cal yr BP for the glacial-lacustrine sediment constrains, indirectly, the age of the moraines upvalley of the lake.

The Pettit Lake core (fig. 3C), one of three obtained from the downvalley end of the lake, contains a similar sedimentary sequence, and we make a similar inference regarding the relation of cored glacial-lacustrine sediment with upvalley moraines. A minimum limiting date of 13,940±150 cal yr BP was obtained from a horizon immediately above the glacial-lacustrine sediment.

In summary, these three cores provide close minimum limiting ages for two glacier advances and/or significant recessional stillstands, both associated with the Perkins Lake moraine group. The near-basal date of 16,860 cal yr BP from Lost Boots Marsh provides a minimum limiting age for the oldest moraine in the Perkins Lake group. Closely correlative dates from the McDonald Lake and Pettit Lake cores provide a minimum limiting date of ca. 13,950 cal yr BP for younger moraines of that group. A third date of 13,980 cal yr BP, at the top of the anomalous, light-colored horizon in the Lost Boots Marsh core, lends support to those dates.

The Busterback Ranch moraine group was likely constructed during marine oxygen isotope stage (OIS) 3 or 4. As discussed above, relative weathering data indicate that the Busterback Ranch moraine group is at least 10,000 yr older than the Perkins Lake group. With a minimum limiting age of 16,900 cal yr BP for the oldest moraine in the Perkins Lake group, we estimate that the Busterback Ranch group was constructed prior to around 27,000 yr BP.

Regional Correlations and Paleoclimatic Inferences

Two aspects of this glacial record are noteworthy. First, the close minimum limiting date of ca. 16,900 cal yr BP pertains to the maximum ice advance during marine oxygen isotope stage 2 (OIS 2) in these valleys; the maximum OIS 2 advance thus postdates the peak of the ice-sheet last glacial maximum (ca. 21,000 cal yr BP) by ca. 4,000 cal yr BP. Second, the dates of ca. 14,000 cal yr BP, pertaining to the youngest moraines in this sequence, imply that extensive ice volume—with paleo ELAs less than 200 m above those of the outermost moraines—was maintained into or reestablished in early late-glacial time.

We infer from the local chronology and from correlations with similar records in the Puget Lowland, Wallowa Mountains, and Yellowstone Plateau, that the Sawtooth glaciers responded strongly to fluctuations in precipitation. The glacier extent was apparently diminished by weakened westerly flow (and consequent diminished moisture transport). Westerly flow was apparently diminished by two factors: by the inferred Laurentide ice sheet anticyclone, and by a minimum

in orbitally modulated seasonality (*e.g.*, Kutzbach and others, 1993). These inferences are more thoroughly discussed in Thackray and others (2004).

Finally, we suggest that other "moisture dependent" glacial systems—those typically exposed to moist westerly flow and with mass balance characteristics adjusted to abundant precipitation—likely responded similarly. Improved glacial chronologies across the Western United States should further constrain temporal and spatial patterns of Pacific moisture delivery.

Field Guide

The field guide that follows focuses on the moraine sequences and relevant sediment cores in five major valleys on the eastern flank of the Sawtooth Mountains. The guide is derived from information in Breckenridge and others (1988), Borgert and others (1999), Borgert (1999), Lundeen (2001), and Thackray and others (2004).

Acknowledgments

Radiocarbon dating was performed by John Southon of the Center for Mass Spectrometry at Lawrence Livermore National Laboratory. Doug Clark provided invaluable practical and scientific input at various stages of the project. We were assisted in the field by Will Glasgow, David Bates, Doug Whitmire, Zachary Lundeen, Emma Thackray, Diane Wheeler, and Butch Wheeler. Funding was provided by Idaho Board of Education Specific Research Grant S98-071 to GDT, by Geological Society of America student research grants and Idaho State University Graduate Student Research Committee grants to KAL and JAB, and by a Sigma Xi student research grant to KAL.

Mileage Cum.	Inc.	
0.0	0.0	At Stanley, turn right (south) on Idaho Highway 75. Reset odometer. Upper Stanley sits on high terraces described by Breckenridge and others (1988) as Bull Lake outwash terraces. South of Stanley, Highway 75 passes close to the risers of these terraces.
4.5	4.5	Turn right to enter Redfish Lake area. Road passes through moraines of Pinedale age (Williams, 1961; Breckenridge and others, 1988) within 0.5 mi of turnoff.
6.3	1.8	Turn left toward visitor center and North Beach picnic area (not toward lodge).
6.7	0.4	Turn right into North Shore picnic area.

Stop 1. Redfish Lake Area Glacial Geomorphology Overview and Lunch

Redfish Lake lies on a platform of Pleistocene glacial sediment, rimmed by Pinedale-age moraines and flanked to northwest and southeast by Bull Lake-age moraines and outwash terraces (Williams, 1961; Breckenridge and others, 1988). The prominent morainal ridges high above the lake to the northwest and southeast are similar to the large, outermost moraines marking major drainages farther south on the Sawtooth front, likely constructed during early or middle Wisconsin time (Borgert, 1999; Lundeen, 2001; Thackray and others, 2004). Due west of this location are similar moraines, merging with the large Redfish moraines but constructed by glaciers descending the Fishhook Creek drainage. Smaller, younger moraines mark the shores of Redfish Lake and areas upvalley, but, surprisingly, remain unstudied.

Mileage Cum.	Inc.	
		Return to Highway 75.
8.9	2.2	Turn right (south). The highway is cut through Pinedale moraines just south of the junction.
9.5	0.6	Breckenridge and others (1988) described a road cut section near the bridge, since reclaimed. The exposure revealed Bull Lake-age outwash, overlain by glacial-lacustrine sediments and till, interpreted as evidence for damming of the Salmon River during Bull Lake time by Redfish Lake moraines.
13.5	4.0	Bull Lake-age moraines are visible as low-relief hills to right (west) of the road. The long, wooded ridge ahead and to the right (2:00 to 12:00) is a lateral moraine on the north edge of Hell Roaring Creek constructed early in the last glaciation.
15.7	2.2	Sessions Lodge, store and gas station.
18.9	3.2	Landslides to left on Sawtooth Springs Ranch (formerly Thousand Springs Ranch). Breckenridge and others (1988) describe deltaic glacial-lacustrine sediments in the landslide head scarp and suggested that they represent a long-lived glacier-dammed lake. The sediments remain undated and their relation with similar sediments near Redfish Lake is unclear.

19.1	0.2	Cross 4th of July Creek. Williams (1961) and Breckenridge and others (1988) mapped glacial landforms and sediments in this drainage within several kilometers of the highway. They inferred Pinedale ages for two distinct drift units and a Bull Lake age for the third.
21.1	2.0	Moraines of the Yellow Belly drainage lie to right of highway. The visible moraines are the voluminous, outermost moraines that mark the major drainages on the eastern side of the Sawtooths. These moraines will be discussed at the Pettit Lake stop.
21.4	0.3	Cross Salmon River.
22.3	0.9	Moraines of the Pettit drainage lie to right.
22.6	0.3	Turn right (west) on marked gravel road, toward Pettit Lake. After crossing Alturas Lake Creek, the road passes through the two outermost moraines, of seven in the lower part of this drainage. Note the very steep distal edge of the outermost moraine.
24.2	1.6	Turn right (north) at road junction.
24.3	0.1	Just past Pettit Lake Creek, turn right (northeast) again. Road crosses second moraine in sequence.
24.5	0.2	Parking for the next stop can be found in pullouts on either side of the road, over the next 0.3 mi. We first will walk downvalley from here, then upvalley, so the specific parking location does not matter. After parking, continue downvalley (east) on foot until the road rises to cross the outermost moraine. Turn left (north) to climb to top of moraine.

Stop 2. Pettit Lake Moraines: Moraine Morphometry and Lake Coring

The Pettit Lake moraine sequence is an easily accessible example of the moraines marking the major drainages on the eastern flank of the Sawtooth Mountains. As noted in the text, we have used moraine morphometry data, derived from measured moraine profiles, to distinguish two moraine groups: the older Busterback Ranch Group and the younger Perkins Lake group. The start of this moraine walk is the crest of the outermost moraine in the Busterback Ranch group. The moraine crest is approximately 70 m above the Sawtooth Valley floor, reflecting the large volumes of sediment moved by glaciers in the initial late Pleistocene advance. The considerable height and volume of this moraine are typical of the outermost moraines in each drainage, and likely are a result of erosion of sediment accumulated in the valley during the last interglaciation. Note the rounded crest and slightly muted topography of this moraine. Walking upvalley toward Pettit Lake, one crosses the second moraine of the Busterback Ranch group, smaller than the first but also with a rounded crest. Pettit Lake is impounded, in part, by this moraine. The third moraine in the Busterback Ranch group forms a small peninsula that includes the day-use parking area. The younger Perkins Lake group includes three moraines, none of which are easily accessible. They are located in the wooded hills at the upvalley end of Pettit Lake. The Perkins Lake moraines are characterized by smaller volume, sharper crests, and steeper slopes in comparison to the Busterback Ranch moraines. An additional, intermediate-age moraine forms the paired, cabin-laden peninsulas and associated shoal (<2-m deep!) that separate the small, relatively shallow (6 m) lower lake basin from the large, deep (>100 m) upper basin. This moraine did not fall into either morphometric moraine group (fig. 2), probably because cabin construction has altered its form.

We collected sediment cores from the lower basin of Pettit Lake and from McDonald Lake in the adjacent Yellow Belly drainage. Both coring sites lie in the same position with respect to the moraine sequence (*i.e.*, between the youngest Busterback Ranch moraine and the oldest Perkins Lake moraine). None of the cores penetrated to coarse-grained, ice-proximal glacial sediment, so the age of the Busterback Ranch moraines cannot be constrained by the cores. However, the cores partially penetrate thick sequences of glacial-lacustrine sediment with a high glacier activity index (sensu Souch, 1994), indicating that the glacier terminus was located a short distance upvalley. We infer that those glacial-lacustrine sediments were deposited while the glacier terminus lay at or near the positions of the younger moraines in the Perkins Lake group. Radiocarbon dates at the top of the glacial-lacustrine sediments are very similar: 13,940±150 cal yr BP in the lower basin of Pettit Lake and 13,960±140 cal yr BP at McDonald Lake. Thus, we infer that the glacier termini in the two valleys remained at or near the positions of the upper Perkins Lake moraines until ca. 14,000 cal yr BP. Contrasts in equilibrium line altitudes for the entire moraine sequence are minimal (<150 m), so near full-glacial ELAs were maintained until that time.

Mileage Cum.	Inc.	
24.5	0.0	Return to cars and drive back to Highway 75.
26.4	1.9	At Highway 75, turn right (south) toward the Alturas drainage.
27.8	1.4	Turn right (west) onto gravel road. Road crosses outwash terrace for about 0.9 mi.
28.7	0.9	Bear left (southwest) at first road junction since the highway.

29.0	0.3	Fork in road. Follow the left (southern) fork and continue around the outermost Alturas valley moraine.
29.6	0.6	Crest of second moraine in the Busterback Ranch moraine group.
30.1	0.5	Crest of third moraine, also in the Busterback Ranch group. Note the character of the moraines in this area. While they have broad crests like the outermost Pettit moraines, these moraines are of lower relief and contain abundant dry kettle depressions. The low relief and hummocky topography indicate substantial burial of dead ice during construction. The stranding of this ice likely was caused by overextension of the Alturas valley glacier into its low-gradient lower valley, where a small rise in ELA would cause rapid retreat of the terminus.
31.6	1.5	Junction with paved road near northwestern shore of Alturas Lake. Turn left (east-southeast).
32.2	0.6	After crossing Alturas Lake Creek at the lower end of Alturas Lake, turn right into gravel road turnoff. Park and walk across road for Stop 3.

Stop 3. Lost Boots Marsh: Age Constraint on the Younger Moraine Group

Lost Boots Marsh lies between two moraines of the Perkins Lake group, and cores from this site provide further constraint for the moraine group. The moraine that retains Perkins Lake lies 500 m downvalley of this site, while the moraine that retains Alturas Lake lies approximately 300 m upvalley. The former is the oldest moraine in the Perkins Lake group in the Alturas valley.

Three sediment cores from this site reveal a succession of depositional environments and provide radiocarbon constraint on basinal changes (fig. 3A). The most notable feature of these cores is the radiocarbon date of 16,860±410 cal yr BP, which was obtained from an organic-bearing silt layer approximately 15 cm above ice-proximal sandy gravel. We consider this date to be a close minimum limiting date for the Perkins Lake moraine. Overlying laminated silt and clay, with high magnetic susceptibility and low total organic carbon, represent glacial-lacustrine sedimentation, most likely in a larger lake than those of today, dammed by the Perkins Lake moraine. Glacial-lacustrine sedimentation terminated and organic-rich sedimentation began ca. 16,400 cal yr BP. The transition to organic-rich sedimentation at that time represents either the retreat of glaciers from the lake margin, coupled with the invigoration of organic production, or the partial drainage of the inferred, large lake and consequent isolation of the marsh. Also of note is an anomalous, 3-cm-thick, light-brown layer within the organic-rich section. This layer did not produce distinct total organic carbon, magnetic susceptibility, or grain-size values; however, its anomalous color and minimum limiting date of 13,980±120 cal yr BP, which correlates with minimum dates on glacial lacustrine sediments in Pettit Lake and McDonald Lake cores (figs. 3B and 3C) , suggest that it pertains to a glacial readvance upvalley or to a distinct climatic episode that reduced organic production or increased inorganic sedimentation in the Alturas Lake drainage.

Mileage Cum.	Inc.	
32.8	0.6	Perkins Lake moraine is on left (northwest) side of road. Wooded hills to right (southeast) are lateral moraines of the Busterback Ranch group.
35.0	2.2	Road passes through moraines of the Busterback Ranch group.
35.2	0.2	Intersection with Highway 75. Turn right (south) toward Galena Summit and Sun Valley.
35.6	0.4	Distal edge of Busterback Ranch moraine (Alturas Valley) at right.
37.8	2.2	Enter Sawtooth City, home of Smiley Creek Lodge (good food and milkshakes, as well as gas and a small convenience store). Note moraines at right, constructed by glaciers descending the Smiley Creek drainage.
38.5	0.7	Terminal moraines at the mouth of Pole Creek, a major drainage in the Boulder-White Clouds Mountains to the east. These moraines and a sediment core obtained from a kettle pond within the moraine sequence are described by Breckenridge and others (1988).
40.9	2.4	Cross the mighty Salmon River. Formerly glaciated headwaters lie to the right (south).
41.6	0.7	Road cuts at left, extending the next 0.6 mi, expose till in lateral moraine of the Pole Creek drainage.
44.8	3.2	Turn right into viewpoint parking lot for Stop 4. Parking here will be tight, and the traffic sometimes is a bit hazardous, so please use caution.

Stop 4. Galena Summit Viewpoint

This viewpoint provides a final overview of the Sawtooth Mountains and Sawtooth Valley. The Sawtooth Mountains include abundant high elevation area that served as accumulation zones for the large Pleistocene glaciers. The wooded hills at the foot of the range are the moraines constructed by glaciers descending the major Sawtooth drainages, while the sagebrush-covered valley floor is largely outwash fill. To the right (east) are moraines of the Pole Creek drainage, while directly below the viewpoint are moraines of the Salmon River headwaters drainage.

Mileage Cum.	Inc.	
45.8	1.0	Continue south on Highway 75 to Galena Summit.
55.4	9.6	Prairie Creek area lies to the right (west). Glaciers descending this drainage from the crest of the Smoky Mountains constructed moraines that represent the type locality of the Bull Lake-age Prairie Creek advance (Pearce and others, 1988).
61.4	6.0	Boulder Creek area lies to the left (north). Moraines in this drainage, constructed by glaciers descending from the crest of the Boulder Mountains, represent the type locality of the Pinedale-age Boulder Creek advance of Pearce and others (1988).
75.2	13.8	Enter Ketchum.

References

Borgert, J.A., 1999, Extent and chronology of alpine glaciation in the Alturas Valley, Sawtooth Mountains, Idaho: Pocatello, Idaho State University, unpublished M.S. thesis, 100 p.

Borgert, J.A., Lundeen, K.A., and Thackray, G.D., 1999, Glaciation of the southeastern Sawtooth Mountains, central Idaho, *in* Hughes, S.S., and Thackray, G.D., eds., Guidebook to the geology of eastern Idaho: Special Publication of the Idaho Museum of Natural History, p. 205–217.

Breckenridge, R.M., Stanford, L.R., Cotter, J.F.P., Bloomfield, J.M., and Evenson, E.B., 1988. Glacial geology of the Stanley Basin, *in* Link, P.K., and Hackett, W.R., eds., Guidebook to the geology of central and southern Idaho: Idaho Geological Survey Bulletin 27, p. 209–221.

Chadwick, O.A., Hall, R.D., and Phillips, F.M., 1997, Chronology of Pleistocene glacial advances in the central Rocky Mountains: Geological Society of America Bulletin, v. 109, p. 1443–1452.

Clark, D.H., and Gillespie, A.R., 1997, Timing and significance of late-glacial and Holocene cirque glaciation in the Sierra Nevada, California: Quaternary International, v. 38/39, p. 21–38.

Gosse, J.C., Evenson, E.B., Klein, J., Lawn, B., and Middleton, R., 1995, Precise cosmogenic ^{10}Be measurements in western North America—Support for a global Younger Dryas cooling event: Geology, v. 23, p. 877–880.

Kutzbach, J.E., Guetter, P.J., Behling, P.J., and Selin, R., 1993, Simulated climatic changes—Results of the COHMAP climate-model experiments, *in* Wright, H.E., Kutzbach, J.E., Webb, T., III, Ruddiman, W.F., Street-Perrott, F.A., and Bartlein, P.J., eds., Global climates since the last glacial maximum: Minneapolis, University of Minnesota Press, p. 24–93.

Licciardi, J.M., Clark, P.U., Brook, E.J., Pierce, K.L., Kurz, M.D., Elmore, D., and Sharma, P., 2001, Cosmogenic ^{3}He and ^{10}Be chronologies of the late Pinedale northern Yellowstone ice cap, Montana, USA: Geology, v. 29, p. 1095–1098.

Lundeen, K.A., 2001, Refined late Pleistocene glacial chronology for the eastern Sawtooth Mountains, central Idaho: Pocatello, Idaho State University, unpublished M.S. thesis, 117 p.

Pearce, S., Schlieder, G., and Evenson, E.B., 1988, Glacial deposits of the Big Wood River valley, *in* Link, P.K., and Hackett, W.R., eds., Guidebook to the geology of central and southern Idaho: Idaho Geological Survey Bulletin 27, p. 203–207.

Souch, C., 1994, A methodology to interpret downvalley lake sediments as records of Neoglacial activity, Coast Mountains, British Colombia, Canada: Geografiska Annaler, v. 76A, p. 169–185.

Stanford, L.R., 1982, Glacial geology of the upper South Fork Payette River, south-central Idaho: Moscow, University of Idaho, unpublished M.S. thesis, 83 p.

Stuiver, M., Reimer, P.J., Bard, E., Beck, J.W., Burr, G.S., Hughen, K.A., Kromer, B., McCormac, G., Van der Plicht, J., and Spurk, M., 1998, INTCAL98 radiocarbon age calibration, 24000-cal BP: Radiocarbon, v. 40, p. 1041–1084.

Thackray, G.D., 1999, Pacific moisture delivery and the variability of alpine glacier chronologies in western North America: Geological Society of America Abstracts with Programs, v. 31, no. 4, p. 58.

Thackray, G.D., 2001, Extensive early and middle Wisconsin glaciation on the western Olympic Peninsula, Washington, and the variability of Pacific moisture delivery to the Pacific Northwest: Quaternary Research, v. 55, p. 257–270.

Thackray, G.D., Lundeen, K.A., and Borgert, J.A., 2004, latest Pleistocene alpine glacier advances in the Sawtooth Mountains, Idaho, USA—Reflections of mid-latitude moisture transport at the close of the last glaciation: Geology, v. 32, p. 225–228.

Whitlock, C., and Bartlein, P.J., 1993, Spatial variations of Holocene climatic change in the Yellowstone region: Quaternary Research: v. 39, p. 231–238.

Williams, P.L., 1961, Glacial geology of the Stanley Basin: Moscow, Idaho Bureau of Mines and Geology Pamphlet 123, 29 p.

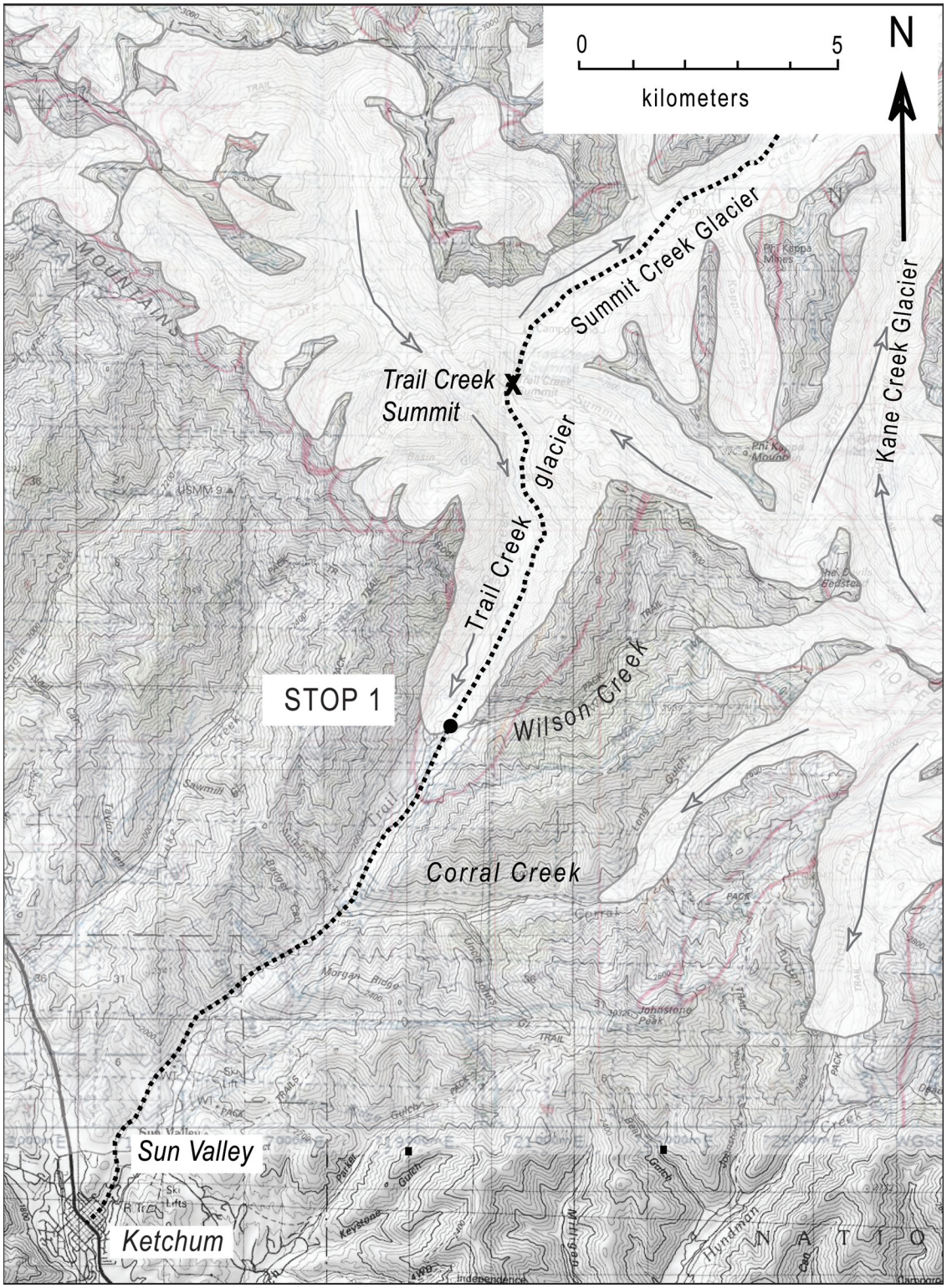

Figure 1. Location of Stop 1, 8 mi northeast of Ketchum. Map shows estimated positions of alpine glaciers in the southern Boulder and western Pioneer Mountains. Reconstruction of glaciers is based upon cirque walls, terminal moraines and canyon topography observed on 1:24,000 maps and not on field mapping.

Terminal Moraine Remnants of the Trail Creek Glacier Northeast of Sun Valley, Idaho

By Eric L. Rothwell and Spencer H. Wood

Introduction

This optional excursion is 8 miles on paved road from the center of Ketchum (Main Street and Sun Valley Road traffic light), northeast through Sun Valley along the Trail Creek Road (fig. 1). A short walk of 10 minutes takes you to the crests of two moraines of very different ages. Here we view and discuss calcareous soils developed into the deposits, the pretty weathering-rinds developed on the sandstone cobbles, and ages of Pinedale and Bull Lake advances.

During the Quaternary, an extensive system of mountain glaciers accumulated in the Pioneer and Boulder Mountains and flowed down valleys emanating from the ranges (Evenson and others, 1982, Pearce and others, 1988). An ice field several miles across accumulated in the Trail Creek Summit area and contributed ice to both the northeast-flowing Summit Creek glacier and to south-flowing Trail Creek glacier (fig. 2). Despite barroom talk in Sun Valley and Ketchum, we find no evidence that the resort towns or the Mt. Baldy ski hill were glaciated during the last ice ages. Rather, the glacier of closest approach was the Trail Creek glacier that advanced down valley to about elevation 1,950 m (6,400 ft), where Wilson Creek flows into Trail Creek, about 10 km (6 mi) northeast of the Sun Valley Inn.

The remnants of the two terminal moraines are best seen on the spur at the confluence of Wilson Creek and Trail Creek (fig. 3). From the road, facing northeast, the moraines appear as low ridges sloping 12° from the walls of Trail Creek Canyon down to Wilson Creek Canyon. Crest of the upper moraine stands 55 m higher than the lower moraine. The 12° crestal slope down into Wilson Creek, and low position in the valley indicate that this was the terminus of the two glacial advances. Furthermore, only outwash sand and gravel terraces occur below this area; no till or erratics are observed on the canyon walls down valley.

Figure 2. Photo looking northeast up Trail Creek from the Trail Creek Road. Moraine remnants are on the spur where Wilson Creek enters from the right. Shadowed terrace in the center of the picture is one of several Pinedale-aged outwash terraces in Trail Creek Canyon.

Department of Geosciences, Boise State University, Boise, ID 83725,
EricRothwell@mail.boisestate.edu

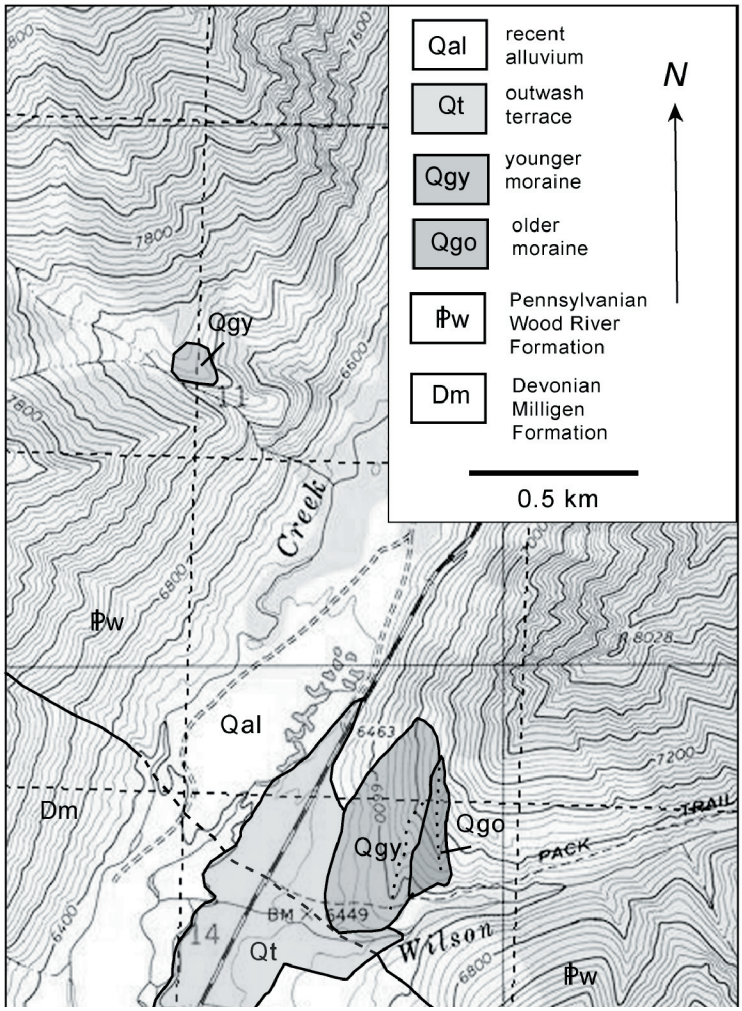

Figure 3. Map showing moraine deposits at the confluence of Wilson Creek and Trail Creek. Mapping based partly on Dover (1983).

Geologic Setting

Bedrocks units in Trail Creek Canyon are equivalents of the Paleozoic Antler orogenic belt sequences extending north from central Nevada (Link and others, 1988). From Sun Valley to Wilson Creek rocks on both sides of the canyon are black argillite or slate and quartzite of the Devonian Milligen Formation. At Wilson Creek, the Wood River thrust fault puts the Pennsylvania-Permian Wood River Formation over the Milligen Formation. Outcrops in the canyon above this point are Wood River Formation, and higher up on the pass are graptolite-bearing black shales of Ordovician and Silurian age (Dover, 1983). The Wood River Formation is chiefly calcareous sandstone, limestone, and dolomite. The area is structurally fascinating with rocks folded and deformed by Mesozoic thrust planes, which in themselves have been folded. Some low-angle thrusts are now interpreted as more recent detachments from the Pioneer Mountains core complex (Wust and Link, 1988).

Background

We originally were drawn to these deposits because the grey calcareous-sandstone clasts of the Wood River Formation within the till develop impressive (cm-scale) brown weathering rinds (fig. 4). Upon digging soil pits on the moraine crests to sample the clasts we also find a significant difference in soil development. All data presented here are field observations; we have no detailed laboratory data.

Soils Developed on Moraine Deposits

The till has abundant carbonate-rock clasts in a sandy silt matrix, which probably also has high initial carbonate-grain content. Soil development in the lower-moraine deposit goes no deeper than 0.8 m, identified by a brown-colored B horizon over unaltered grayish brown till (fig. 5). A 0.15-m-thick calcic horizon (Stage I) of lighter color has begun to form 0.5 m deep within the B horizon, characterized by thin irregular patches of carbonate on the bottoms of stones. Nomenclature for the various stages of calcic horizon development is from Machette (1985) and Birkeland and others (1991). Soil development in the upper-moraine deposit is much deeper. In fact, we have not yet gotten to the bottom of the hard calcic horizon in a 1.3-m-deep soil pit. The calcic horizon is more than 1-m thick, and all grains are carbonate coated. Thickness

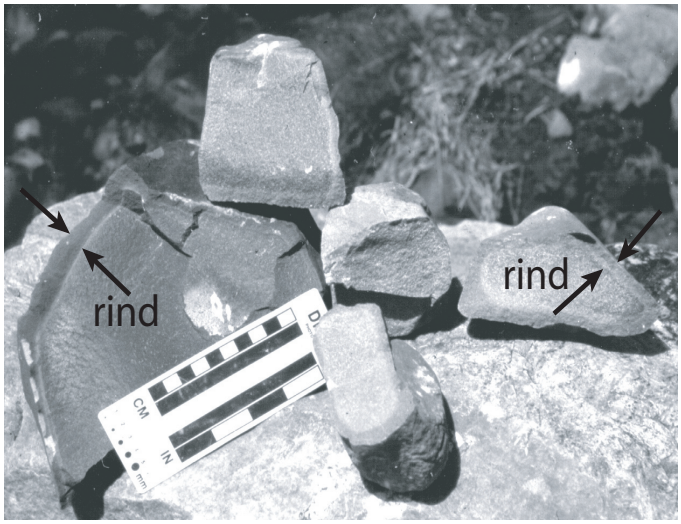

Figure 4. Weathering rinds developed upon calcareous-sandstone cobbles of the Wood River Formation. Thin-section examination shows that calcite has been leached from rind and that iron oxidation has stained the sand grains to give them a yellowish-brown color.

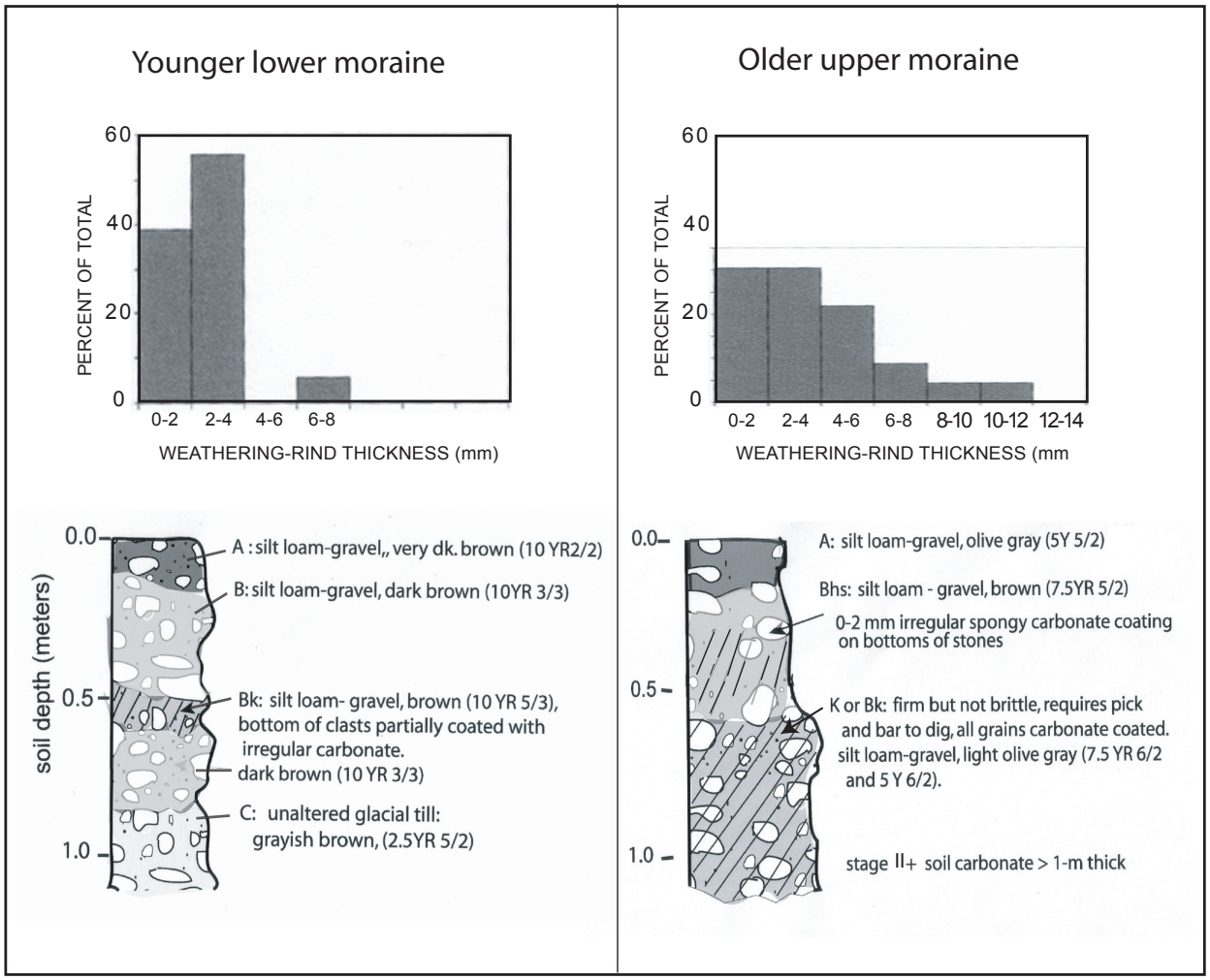

Figure 5. Soil-pit data from crests of moraines: histograms and soil profile descriptions. Weathering rinds are on about 25 stones from 0.15- to 0.3-m deep in the moraine deposits. Thickest rinds on tops of stones are reported. Lower moraine has Stage I calcic soil development. Upper moraine has Stage II+ development.

and high carbonate content indicate it is Stage II calcic soil development (fig. 5).

Weathering Rinds on Calcareous Sandstone Clasts

Cobbles of gray, calcareous, fine sandstone of the Wood River Formation have conspicuous pale yellow (2.5Y 7/4-6/2) weathering rinds (fig. 4). Rinds were measured on cobbles from the upper 0.3 m of soil pits at the crests of the two left-lateral moraines. Rinds on the top surface of cobbles are 2–5 times thicker than those on the bottom surface. We report only the thick top rinds of about 25 stones from each of the moraine crests.

The thickest 20 percent fraction of the lower-moraine rinds is 2 to 4 mm, whereas the thickest 20 percent of the upper-moraine rinds is 8 to 12 mm. Both have a similar mode of 2 to 4 mm, but are clearly distinguished by considering the thickest 20 percent.

Interpretation of the histograms in figure 5 is problematic. Most lower-moraine rinds do not exceed 4 mm. In the older, upper moraine, many rinds are of similar thickness (4 mm), but there are clearly many thicker rinds up to 12 mm. Arguably, one could make a good case for choosing the more abundant 4 to 8 mm. It is difficult to explain why we do not have a clear mode of thicker rinds in the upper moraine and why similar thin (2–4 mm) rinds predominate on both histograms. Minor lithology differences or the orientations of the upper stone surface upon which the thicker rinds develop may contribute to scatter in the data. Some older clasts with preexisting rinds may account for a few anomalous thick rinds.

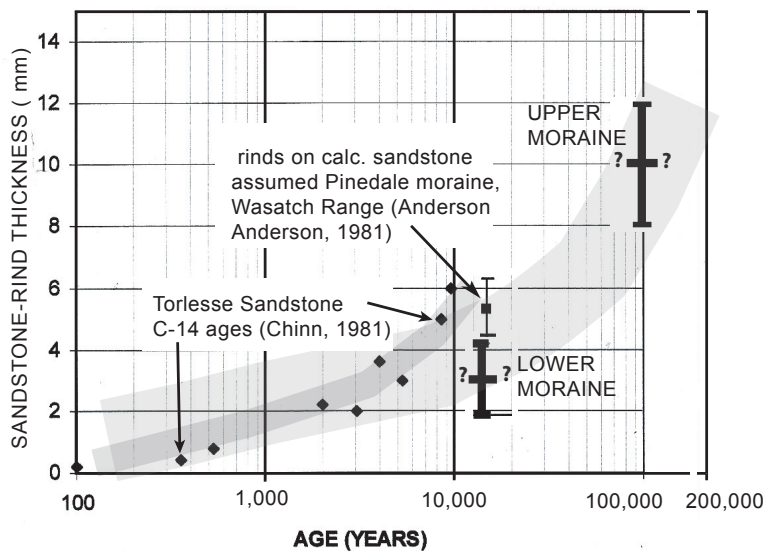

Figure 6. Calcareous-sandstone rind thickness versus estimated age. Symbol showing rinds for lower moraine (Qgy) spans estimated time of the latest Pinedale glaciation and is used as an approximate calibration to extrapolate trend for age of the upper moraine (Qgo). Shown also are the radiocarbon calibrated points for the New Zealand Torlesse sandstone from Chinn (1981) and the estimated age of moraines with clasts of Oquirrh Formation calcareous sandstone with rinds from the Wasatch Range reported by Anderson and Anderson (1981).

We have chosen the thickest 20 percent (*i.e.*, the tail of the histogram, 8–12 mm) as representative of the oldest and thickest rinds and show those thicknesses on the graph of figure 6.

Discussion

Rind and soil data indicate a significant age difference between these two terminal moraines. If the lower moraine is late Pinedale in age (16–23 ka, according to Chadwick and others, 1997) with 2 to 4 mm rinds, a log-log-plot extrapolation of 8–12-mm rinds suggests an age older than 100 ka. Other workers in the area have identified multiple advances of Pinedale age glaciation and a few separate advances of Bull Lake age (Borgert and others, 1999; Evenson and others, 1982, and Brugger, 1996, and Pearce and others, 1988). We believe most workers would agree that the lower moraine is a Pinedale age advance.

The older upper moraine is interesting because the calcic horizon is thicker than those in the Pioneer Mountains described by Wigley and others (1978) for advances they suggested were Bull Lake age. We have seen similar soils with calcic horizons thicker than 1 m on fan deposits over river terraces mapped by Schmidt (1961) as probable Bull Lake outwash. These terraces are 35 m (120 ft) above the present bed of the Wood River at Ohio Gulch near Hailey.

The thick calcic horizon and the thick weathering rinds suggest the age of this upper moraine may be 100,000 yr or more. We would like to know whether this upper moraine was formed during an advance of Stage 6 before the last interglacial (Isotope Stage 5e, 122–128 ka), or if it is an advance since the last interglacial. Mountain glacier advances are dated in the Sierra Nevada between 70 to 100 ka, and at Yellowstone 90 to 102 ka (fig. 7). Although it is tempting to match these mountain glacier deposits to the marine isotope stages, we are cautioned by Gillespie and Molnar (1995) that mountain glaciers may reach their maximum extent before the maximum ice volume of continental ice sheets. It is this continental ice volume that dominates the marine isotope record. They show that the maximum extent of mountain glaciers may

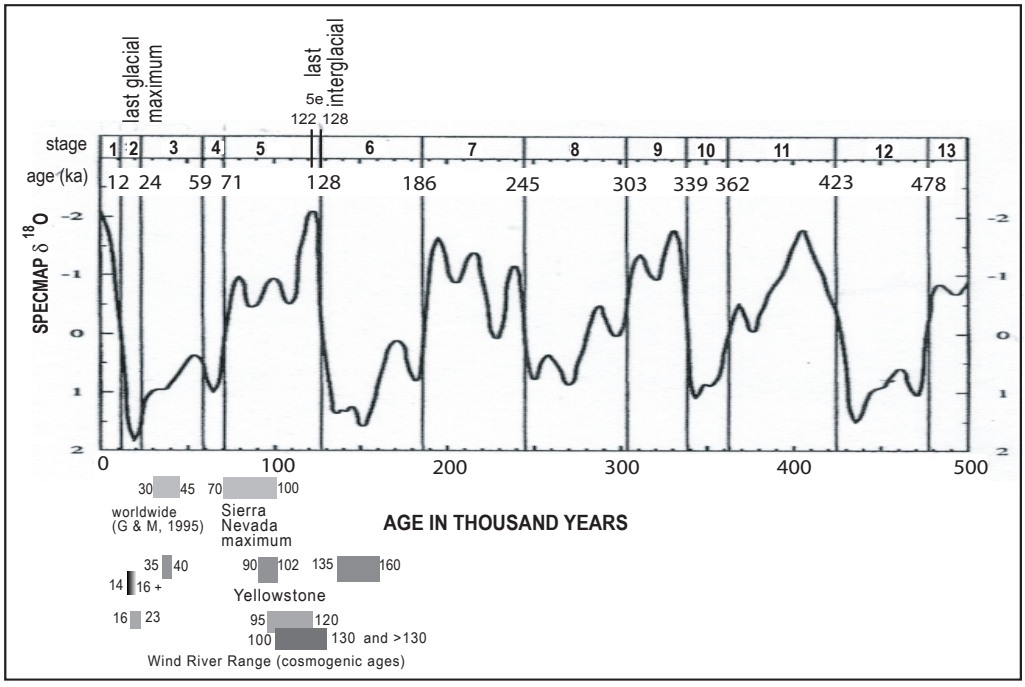

Figure 7. Marine oxygen isotope stages from Wright (2000) after Imbrie and others (1984), ages of mountain glaciation compiled by Gillespie and Molnar (1995), and cosmogenic ages on glacial deposits in the Wind River Range, Wyoming, from Chadwick and others (1997). Cosmogenic age on late-Pinedale northern-Yellowstone ice cap (14 to 16+ ka) from Licciardi and others (2001).

precede the continental ice maximum volume by 15,000 to 20,000 yr.

Ages of Bull Lake advances continue to be a problem in the study of Rocky Mountain glacial deposits. It is our hope that someone will refine the soil and weathering-rind data introduced here to correlate the extensive outwash terrace system in the Wood River Valley mapped by Schmidt (1961). Some of these terrace deposits interfinger with Snake River Plain basalt that can potentially be dated by argon-argon methods.

References

Anderson, L.W., and Anderson, D.S., 1981, Weathering rinds on quartzite arenite clasts as a relative-age indicator and the glacial chronology of Mount Timpanogos, Wasatch Range, Utah: Arctic and Alpine Research, v. 13, p. 25–31.

Birkeland, P.W., Machette, M.N., and Haller, K.M., 1991, Soils as a tool for applied Quaternary geology: Utah Geological and Mineral Survey Miscellaneous Publication 91-3, 63 p.

Borgert, J.A., Lundeen, K.A., and Thackray, G.D., 1999, Glacial geology of the southeastern Sawtooth Mountains, *in* Hughes, S.S., and Thackray, G.D., eds., Guidebook to the geology of eastern Idaho: Pocatello, Idaho Museum of Natural History, p. 205–217.

Brugger, K.A., 1996, Implications of till-provenance studies for glaciological reconstructions of the paleoglaciers of Wildhorse Canyon: Annals of Glaciology, v. 22, 9 p.

Chadwick, O.A., Hall, R.D., and Phillips, F.M., 1997, Chronology of Pleistocene glacial advances in the central Rocky Mountains: Geological Society of America Bulletin, v. 109, p. 1443–1452.

Chinn, T.J.H., 1981, Use of rock weathering-rind thickness for Holocene absolute age-dating in New Zealand: Arctic and Alpine Research, v. 13, p. 33–45.

Dover, J.H., 1983, Geologic map and sections of the central Pioneer Mountains, Blaine and Custer Counties, central Idaho: U.S. Geological Survey Miscellaneous Investigations Series Map I-1319, scale 1:48,000.

Evenson, E.B., Cotter, J.F.P., and Clinch, J.M., 1982, Glaciation of the Pioneer Mountains—A Proposed model for Idaho: *in* Bonnichsen, B., and Breckenridge, R.M., eds., Cenozoic geology of Idaho: Idaho Geological Survey Bulletin 26, p. 653–665.

Gillespie, A.R., and Molnar, P., 1995, Asynchronous maximum advances of mountain and continental glaciers: Reviews of Geophysics, v. 33, p. 311–364.

Imbrie, J., Hays, J.D., Martinson, D.G., McIntyre, A., Mix, A.C., and others, 1984, The orbital theory of Pleistocene climate—Support from a revised chronology of the marine $\delta^{18}O$ record, *in* Berger, A.L., Imbrie, J., Hays, J.D., Kukla, G., and Saltzman, B., eds., Milankovich and climate (Pt. 1) : Dordrecht, Reidel, p. 269–305.

Licciardi, J.M., Clark, P.U., Brook, E.J., and Pierce, K.L., 2001, Cosmogenic ^{3}He and ^{10}Be chronologies of the late Pinedale northern Yellowstone ice cap, Montana, U.S.A.: Geology, v. 29, p. 1095–1098.

Link, P.K., Skipp, B., Hait, M.H., Jr., Janecke, S., and Burton, B.R., 1988, Structural and stratigraphic transect of south-central Idaho—A field guide to the Lost River, White Knob, Pioneer, Boulder, and Smoky Mountains, *in* Link, P.K., and Hackett, W.R., eds., Guidebook to the geology of central and southern Idaho: Idaho Geological Survey Bulletin 27, p. 5–42.

Machette, M.N., 1985, Calcic soils of the southwestern United States: Geological Society of America Special Paper 203, p. 1–21.

Pearce, S., Schlieder, G., and Evenson, E.B., 1988, Glacial deposits of the Big Wood River valley, *in* Link, P.K., and Hackett, W.R., eds., Guidebook to the geology of central and southern Idaho: Idaho Geological Survey Bulletin 27, p. 203–207.

Schmidt, D.L., 1961, Quaternary geology of the Bellevue area in Blaine and Camas Counties, Idaho: Seattle, University of Washington, unpublished Ph.D. thesis, 135 p.

Wigley, W.C., Pasquini, T.P., and Evenson, E.B., 1978, Glacial history of the Copper Basin, Idaho—A pedologic, provenance, and morphologic approach, *in* Mahaney, W.C., ed., Quaternary soils: Norwich, England, Geological Abstracts, p. 265–307.

Wright, J.D., 2000, Global climate change in the marine stable isotope records, *in* Noller, J.S., Sowers, J.M., and Lettis, W.R., eds., Quaternary geochronology—Methods and applications: Washington, D.C., American Geophysical Union Reference Shelf 4, p. 427–433.

Wust, S.L., and Link, P.K., 1988, Field guide to the Pioneer Mountains core complex, south-central Idaho, *in* Link, P.K., and Hackett, W.R., eds., Guidebook to the geology of central and southern Idaho: Idaho Geological Survey Bulletin 27, p. 43–54.

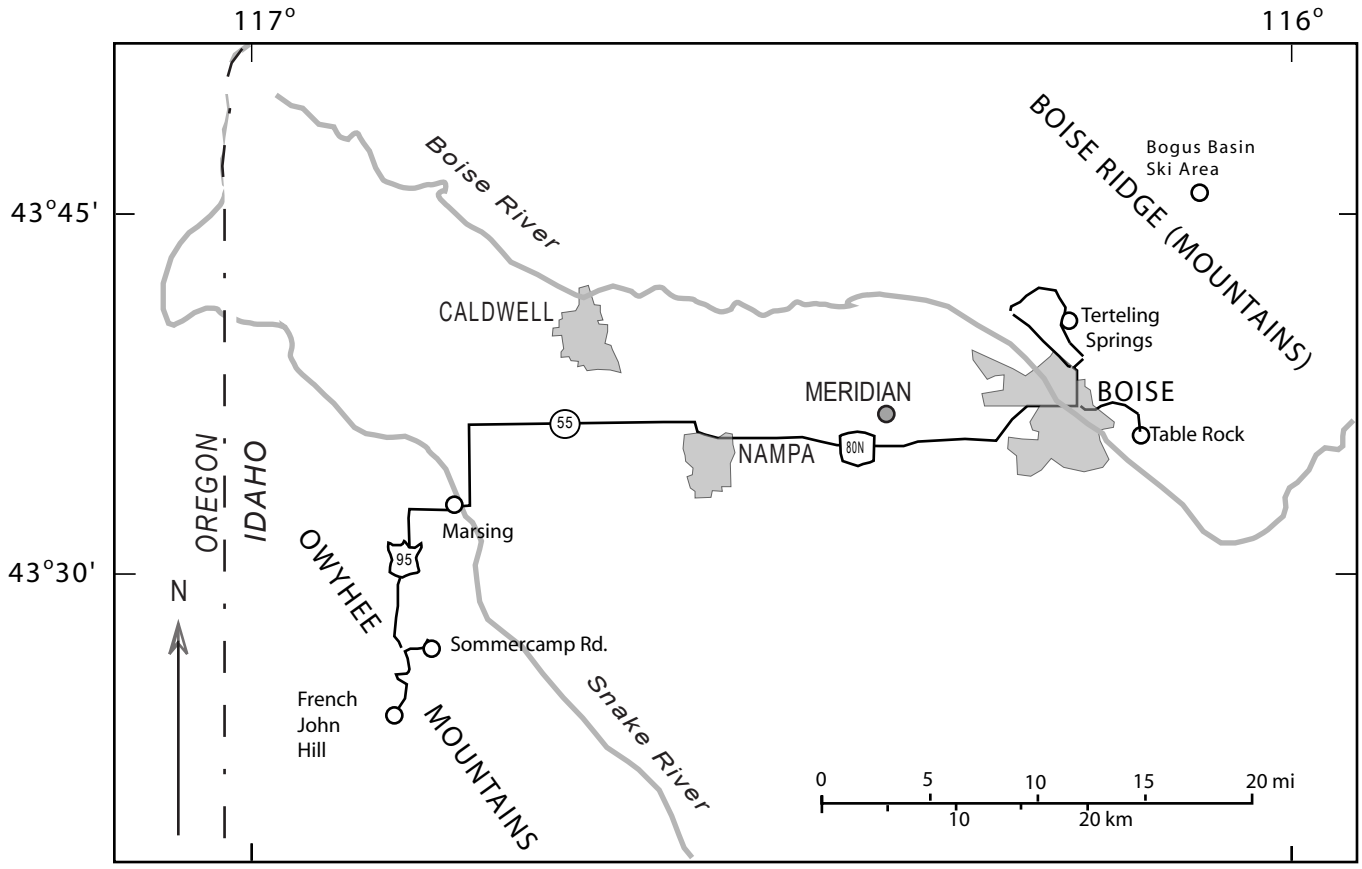

Figure 1. Field-trip route from Boise to the Owyhee Mountains and back to points of interest in the Boise foothills.

Geology Across and Under the Western Snake River Plain, Idaho: Owyhee Mountains to the Boise Foothills

By Spencer H. Wood

Introduction

This 1-day field trip is a transect across the western Snake River Plain (fig. 1). The western plain is a continental-rift structure, 300 km long and 70 km wide. It is bounded and internally faulted by northwest-trending normal faults. The western Snake River Plain has a different orientation and structure than the eastern plain. The eastern plain is a curious downwarp related to magmatism and extension along the track of the Yellowstone hot spot (fig. 2). The faulted basin of the western plain began forming about 12 m.y. ago, and much of the relief was completed by 9 Ma. This timing corresponds with the passage of the hot spot located to the south about 11 Ma. Wood and Clemens (2002) suggest that softening of the lithosphere by the passing hot spot triggered extension and basin formation. The hot spot passage was accompanied by voluminous rhyolite volcanism to the south and by eruptions of rhyolite at or near the margins of the western plain (Bonnichsen and others, 2004; Perkins and Nash, 2002; Pierce and Morgan, 1992). Northwest of the western plain and in southeastern Oregon voluminous eruptions of the Columbia River and Steens Mountains flood basalts occurred between 16.1 and 15.0 Ma (Hooper and others, 2002a, 2002b; Camp and others, 2003). Earliest Columbia River basalts are as old as 17.5 Ma (Baksi, 2004)

Understanding of the sedimentary record builds upon earlier work in the central and southern part of the western plain by Malde and Powers (1962) who defined many of the stratigraphic units. Work of Squires (1992) improved our knowledge of the subsurface near Boise. The sediments record

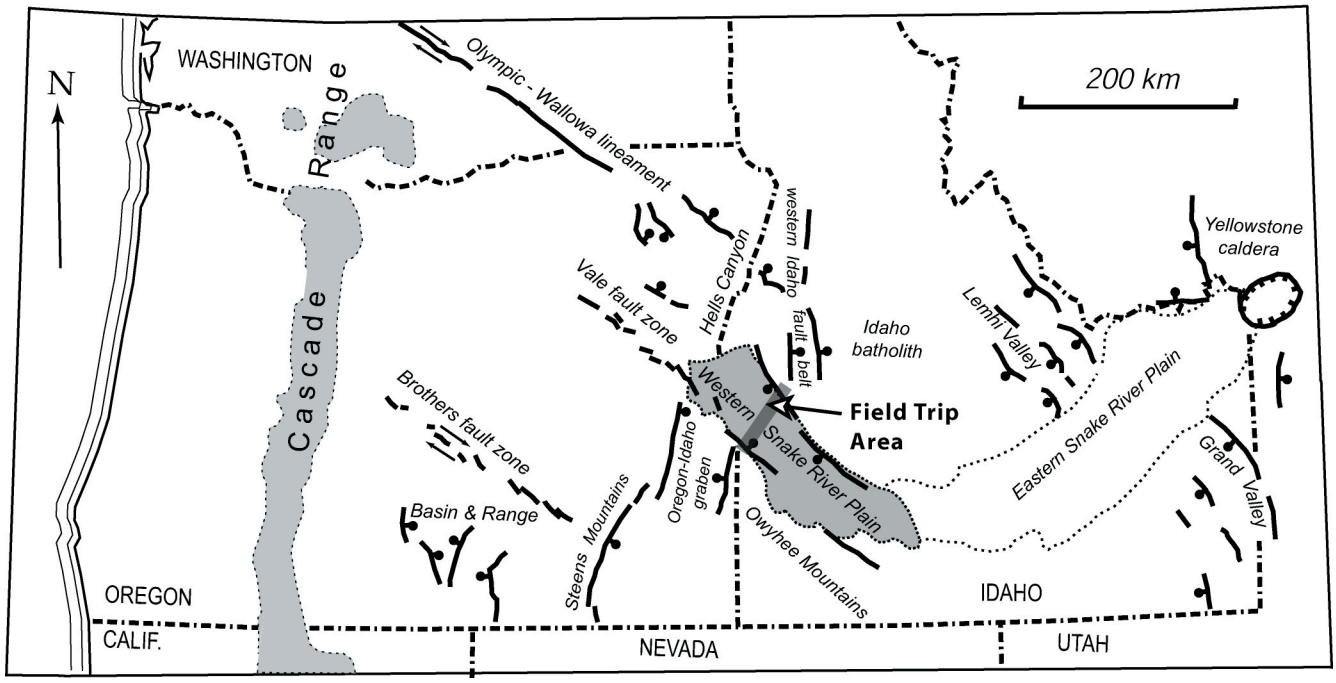

Figure 2. Western and eastern Snake River Plain and late Cenozoic geologic features of the northwestern United States. The western plain was a lake basin in the late Miocene to late Pliocene, usually referred to as "Lake Idaho" (after Wood and Clemens, 2002).

Department of Geosciences, Boise State University, Boise, Idaho 83725,
swood@boisestate.edu

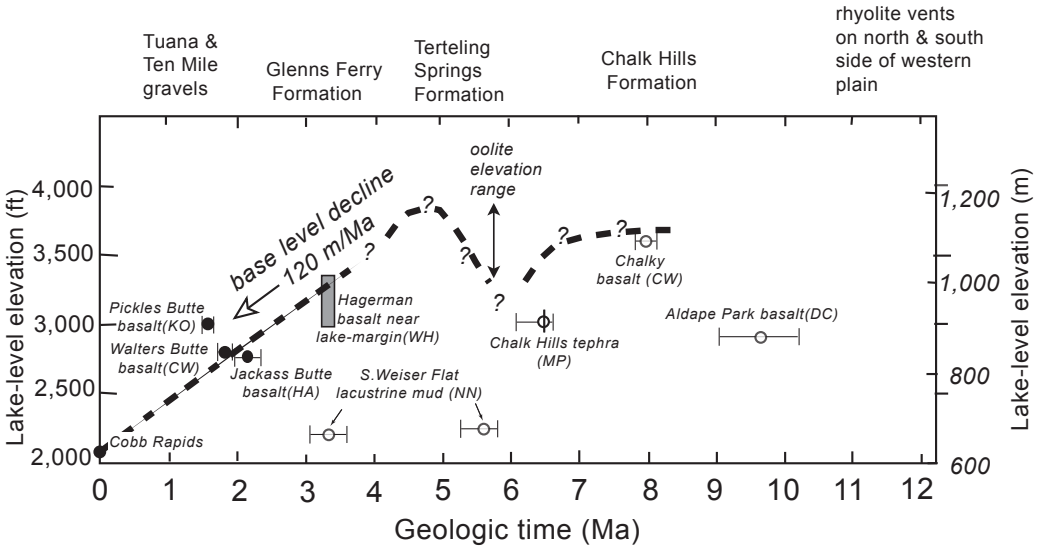

Figure 3. Plot of elevation of the lake deposits versus time. This plot does not take into account tectonic deformation that may have altered the elevation of lake deposits. Most localities are on the margin of the plain, which has not been so much affected by tectonic movement or compaction subsidence (Wood, 1994). Points on the graph are dates on lacustrine sediment, or basalt associated with or overlying the lacustrine section: K-Ar dates on basalt are: DC (Clemens and Wood, 1993), HA (Amini and others, 1984), Zircon fission-track ages on silicic ash are NN (Nancy Naeser, published in Thompson, 1991); $^{40}Ar/^{39}Ar$ ages on basalt are: CW (White and others, 2004), and KO (Othberg and others, 1995), WH (Hart and others, 1999), and tephrochronology from MP (Perkins and others, 1998).

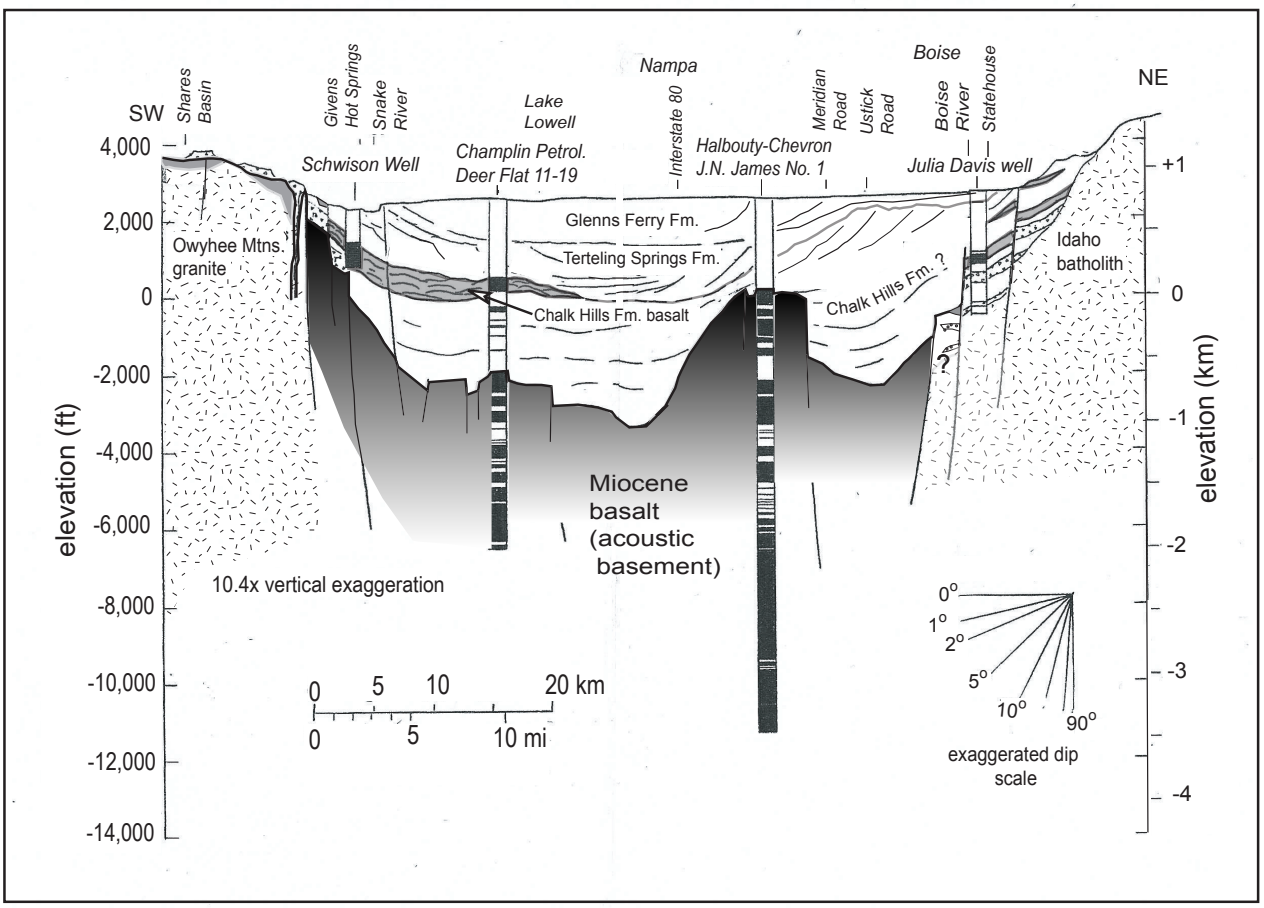

Figure 4. Section across the western plain showing major stratigraphic units, based upon seismic-reflection and well data. Dark patterns on well columns are basalt intervals: dotted pattern is rhyolite: no pattern is sediment.

two major episodes of large lakes that filled the basin (figs. 3 and 4). The Chalk Hills Formation records the first deposition of sand, lacustrine muds, and intercalated volcanics. Subsequently the level of the "Chalk Hills lake" declined, or perhaps the lake completely drained. Sediments and volcanics of the Chalk Hills Formation are deformed by tilting and faulting. The lake system then refilled and transgressed over eroded Chalk Hills Formation. The transgressive lake sediments grade upward and shoreward to calcareous muds and oolites; this sequence is called the Glenns Ferry Formation on the south side of the plain, and the Terteling Springs Formation on the north side (figs. 3 and 4). This last lake system is popularly known as "Lake Idaho". The calcareous sediments indicate increased alkalinity of a lake within a closed basin. The lake then overtopped its spill point into ancestral Hells Canyon and, as it lowered, the drained basin filled with mostly sandy delta-plain units that are important aquifers.

The field trip starts in a rhyolite field in the Owyhee Mountains: the 11-Ma Jump Creek Rhyolite (fig. 5). We then look at the high gravels overlying the rhyolite at elevation 1,100 m. Descending onto the plain, we will examine the basal lacustrine sediments along Sommercamp Road, mapped as the Chalk Hills Formation. The lower Chalk Hills Formation contains numerous volcanic ash beds and an unusual pumice-block layer. Several basalt fields occur in the subsurface and in exposures along the margins. Along the Owyhee Mountains front, the transgressive sequence overlying the deformed and eroded Chalk Hills Formation is readily identified by an angular unconformity with a locally occurring ledge of nearly horizontal, brown, coarse, pebbly sandstone laying upon the

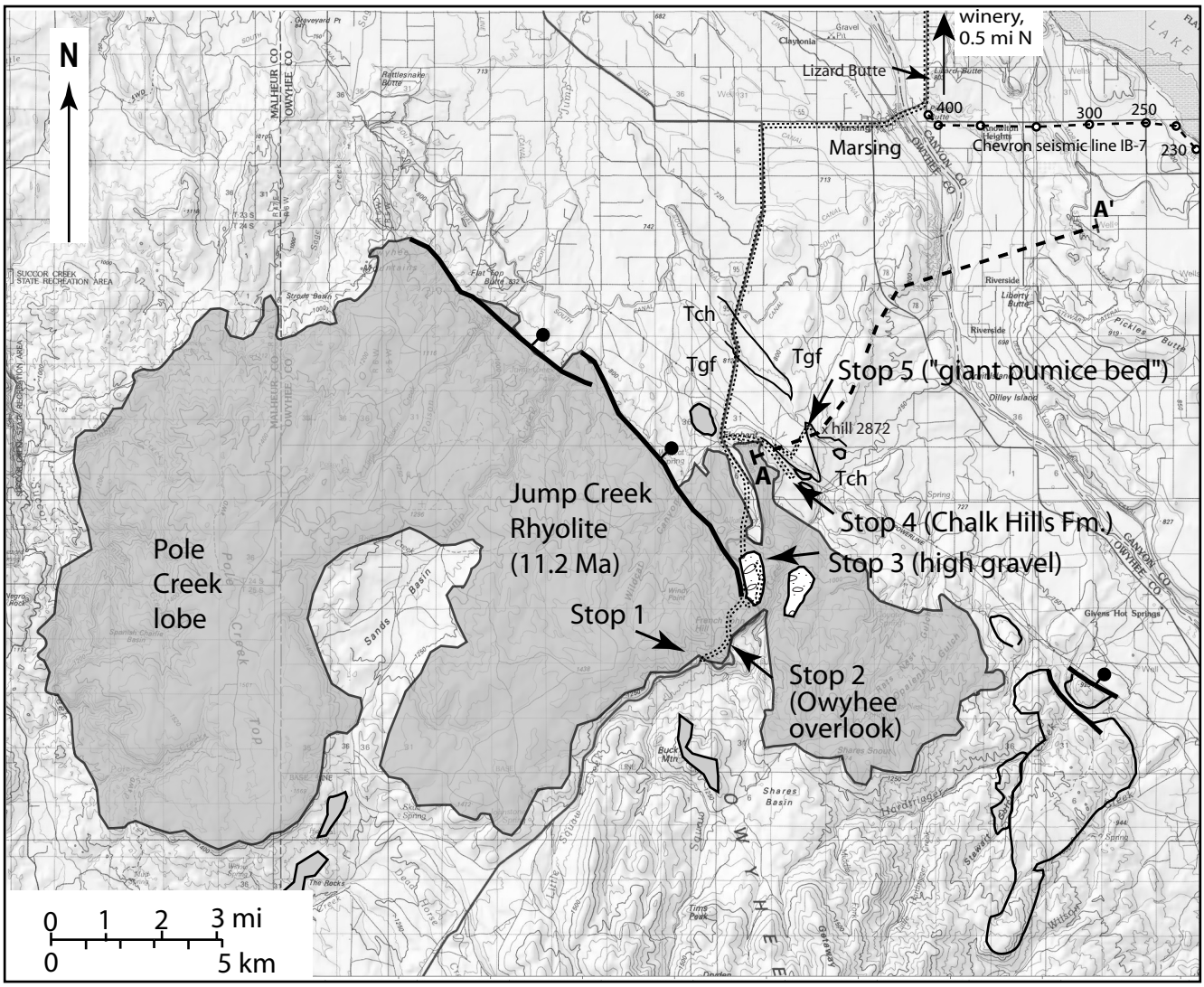

Figure 5. Map showing field-trip route along the Owyhee Mountains front near Marsing, Idaho, distribution of the 11-Ma Jump Creek Rhyolite, and associated geologic features along the edge of the western Snake River Plain. Location of cross-section A-A' (fig. 16), seismic line (fig. 12), field-trip route (shaded line), and Stops 1-5 are shown.

tilted mudstone. This sandstone ledge is overlain by mudstone of the Glenns Ferry Formation.

Over most of the plain, we rely on seismic data and deep wells for information on the subsurface. From Marsing, we will drive across the plain through the towns of Nampa and Meridian to Boise. Squires and others (2003) describe a 15-km-long seismic line from Meridian to Boise from which we can interpret the episodes of lake filling and sedimentation as seen on the plain margins.

The angular unconformity between the Chalk Hills Formation and the Glenns Ferry Formation is not exposed along the Boise foothills; however, a section containing oolite bars is interpreted as the upper part of the transgressive sequence named the Terteling Springs Formation. Overlying the transgressive sequence is a massive Gilbert-style delta sequence of coarse sand that is interpreted as the response to regression of the lake after the lake overtopped the spill point at Hells Canyon. Downcutting of the outlet resulted in a slowly declining lake level and delta progradation over the basin. The basin filled and rivers flowed across the plain. Along the field-trip route, we observe valleys of the Snake and Boise Rivers that are incised about 150 m into the lake sediments.

FIELD-TRIP ROAD LOG

*Mileages for this first leg of the trip are based upon the **green milepost signs,** posted every mile on the northbound side of the highway.*

Milepost	Inc.	
13.8	0.0	We travel north on U.S Highway 95 toward Boise. Starting point for mileage is at the south end of a large road cut at the crest of the highway at French John Hill, 14 mi south of Marsing, Idaho. Parking area is on the north side of highway, or continue south about 0.1 mi to large pullout on south side, where one can make a U-turn with good visibility.

Stop 1. Road Cut with Deformed Sediments and Pyroclastics at the Base of the Jump Creek Rhyolite, French John Hill, Owyhee Mountains

Road cuts here expose a jumble of rhyolite vitrophyre breccia and older sediments beneath the flow-banded and sheeted stoney rhyolite flows on the skyline (fig. 6). The Jump Creek Rhyolite covers 275 km^2 and is one of the younger rhyolites erupted along the margin of the western Snake River Plain (fig. 5). Neill (1975) obtained a K-Ar age of 11.2±0.2 Ma on sanidine. The rhyolite has many lobate flows, one upon another, and in this area is up to 250-m thick. Volume is estimated at 70 km^3. Bonnichsen and others (2004) consider this a rhyolite field made up of many segments. They report ^{40}Ar/^{39}Ar and K-Ar ages ranging from 10.6 to 11.7 Ma.

Rocks of the Jump Creek Rhyolite are identified by abundant (12–23 percent), conspicuous (up to 4 mm) phenocrysts of plagioclase. Sanidine and quartz vary in abundance up to 4 percent and are up to 2 mm in size. Microphenocrysts of ferrohypersthene and clinopyroxene are present (Ekren and others, 1981, 1982). A single analysis of this rock, on a water-free basis, shows 71 percent silica making it truly a rhyolite (analysis published in Ekren and others, 1984).

In the valley southeast of U.S. Highway 95, Squaw Creek has cut through the rhyolite into a 130-m-thick section of ashy stratified sediments mapped by Ekren and others (1981) as the Sucker Creek Formation. In the lower part of this section is an 8-m-thick, ledge-forming ash-flow tuff. The section rests upon 500 m of older Miocene basalt.

Directly beneath the rhyolite flow rock is about 20 m of dismembered silicic-ash beds and mud and ashy sediments, basalt breccia, beds of rounded stream gravels, and rhyolite

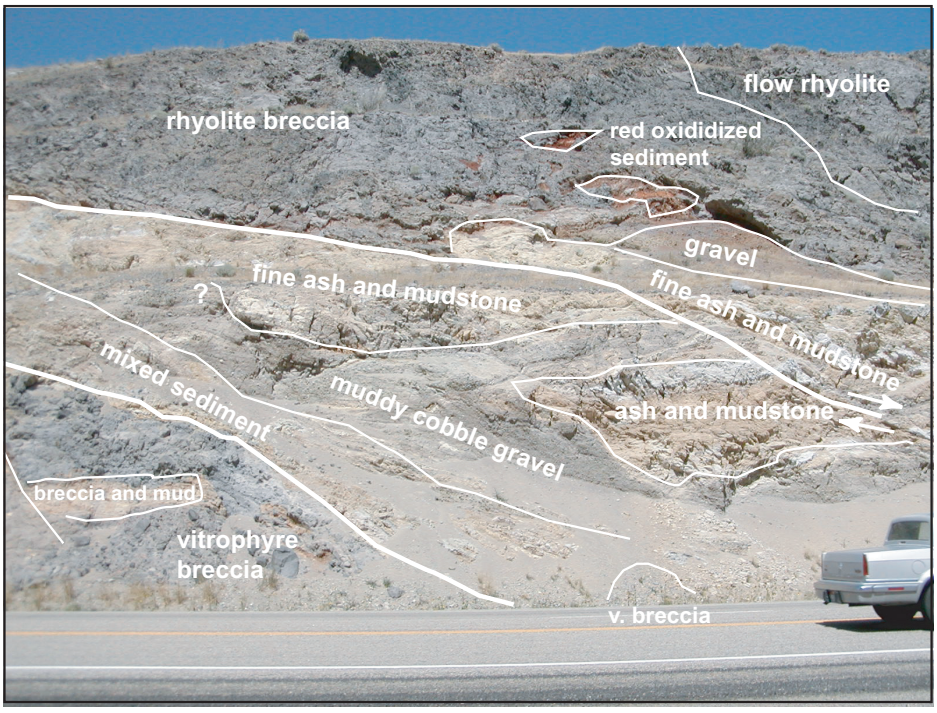

Figure 6. Deformed sediment and rhyolite at the base of the Jump Creek Rhyolite, Stop 1, west side of road cut on U.S Highway 95 (milepost 13.8).

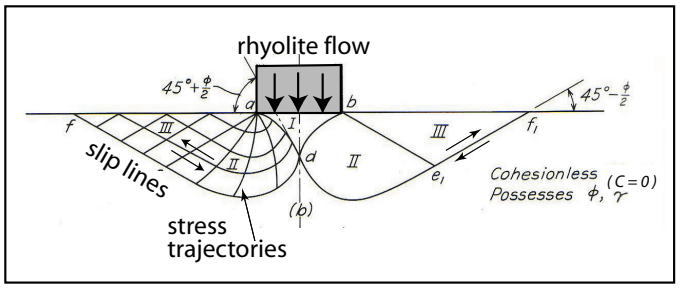

Figure 7. Diagram showing model of bearing-failure slip lines for fairly dense or stiff soil with frictional strength and no cohesion. This type of failure, with low-angle slip lines may have occurred as the thick flows of the Jump Creek Rhyolite piled up over wet sediments of the underlying Sucker Creek Formation (drawing after Terzaghi and Peck, 1967).

breccia. Such structural complexity originally suggested to me that this is a near-vent area of the rhyolite. Low-angle faulting cuts through the section exposed in the road cut which suggested sliding of near-vent volcanic topography (fig. 6). However, the low-angle faults are more likely analogous to bearing failures produced by loading the area with the thick rhyolite flows (fig. 7). The complex structures here are similar to larger scale features in the Absaroka volcanics described by Decker (1990) and which he attributed to liquefaction of saturated epiclastic and pyroclastic rocks in response to loading by lava flows. In this area, the overlying rhyolite lava was up to 200-m thick and imposition of such a great load over a short period of time (perhaps days to decades) could well have liquefied and deformed these materials.

Ekren and others (1984) suggested the Jump Creek Rhyolite may have been a rheomorphic tuff, but Bonnichsen and Kauffman (1987) have shown that thick breccias and features seen here are typical of large rhyolite flows. This area warrants a detailed description and study as few areas of the large hot-spot related rhyolite flows are so well exposed as here in Squaw Creek Canyon.

The older Miocene volcanic rocks of the Owyhee Range host major silver-gold deposits (*e.g.*, the Delamar Mine), about 30 mi due south of here (Halsor and others, 1988). The volcanic rocks rest upon Cretaceous (62 to 70 Ma) granitic rocks exposed at several places in the mountains southeast of here, which Taubeneck (1971) called the southern extension of the Idaho batholith.

Mile-post	Inc.	
		Walk north 0.5 km through the road cut to see the deformed sediments and rhyolite. Continue walking north, and the vans will be moved to the Owyhee Mountains Viewpoint, to pick you up.
14.1	0.3	Park for Stop 2.

Stop 2. Owyhee Country Viewpoint

Large parking area on the east side of road. The sign explains that the origin of the name "Owyhee" is not an Indian name as it would seem. It is an antiquated spelling of Hawaii, as used by Captain Cook. In 1819, Donald MacKenzie of the Canadian Northwest Company sent a group of trappers into these mountains. Among the party were several native Hawaiians who were never seen again, and so the mountains are named for those lost "Owyheeans".

The hill to the west of here is called French John Hill, named for "French" John Carrey who built a road in the early 1870s parallel to the present U.S. Highway 95 (Boone, 1988). From the view point, one looks across the deep rhyolite gorge of Squaw Creek and the north flank of the Owyhee Mountains to the western Snake River Plain. Across the plain are the Idaho batholith mountains north of Boise. Rimrock basalt along the north side of the Snake River Canyon overlies gravels, which are underlain by lake beds of the Pliocene Glenns Ferry Formation. Pickles Butte is a basalt vent area $^{40}Ar/^{39}Ar$ dated by Othberg (1994) at 1.58±0.085 Ma, which is the minimum age usually quoted for the complete withdrawal of Lake Idaho from this area. Basalts in this area, including Lizard Butte, are the westernmost extent of young basalt that overlies lakebeds.

About 14,500 yr ago, floodwaters of the Bonneville flood roared 60-m (200–ft) deep through the Snake River canyon below, but were confined to the canyon below 755-m (2,480-ft) elevation (O'Conner, 1993).

Mile-post	Inc.	
15.0	0.9	Turn east at milepost 15 on a paved road, that turns to gravel within 0.1 mi. Proceed for 0.3 mi, and continue straight at the Y to the old Highway 95 grade, and follow the abandoned highway north for a total of 1.1 mi from the turnoff at milepost 15. The road cuts are in the high gravel deposit of Stop 3.

Stop 3. High Gravels of the Owyhee Mountains and an Overlook of the Chalk Hills Formation-Glenns Ferry Formation Contact

From this abandoned grade of U.S. Highway 95, there is a good view over the western plain and the area of the next stop, Stop 4 (fig. 8). The road cuts are in an alluvial-fan gravel perched high in the Owyhee Mountains. Ekren and others (1981) mapped these high gravels (figs. 5 and 9) but did not comment on their significance. The gravels clearly overlie the Jump Creek Rhyolite, but their relationship to the lake deposits is unclear. The elevation here is 1,100 m (3,600 ft), which is the highest elevation of most lake deposits around the plain margin. It is likely this is an old alluvial fan sequence

Figure 8. Overlook of the western Snake River Plain, looking north from Stop 3.

that graded to Lake Idaho, but we do not know the age of the gravels or the amount of vertical faulting that displaced the gravel downward to the north. We will see a thinner, but very similar, gravel overlying the top of the Chalk Hills Formation in the Sommercamp Road cut at the next stop (see fig. 10).

The road is blocked at a distance of 1.3 mi, so turn around, park, examine the gravels and the view (fig. 8), and then return by the same route back to the new U.S. Highway 95.

Mile-post	Inc.	
15.0	1.1	Turn north toward Boise on U.S Highway 95 and proceed down the grade.
16.8	1.8	Road cut to the west side of the road exposes the contact between vitrophyre and overlying stoney rock of the Jump Creek Rhyolite. The vitrophyre contains abundant spherulites and stretched lithophysae. These features in the glassy part of the flow are attributed to pockets of higher vapor content that cause crystallization and devitrification emanating from the vapor-filled voids. These stoney-rhyolite spherulites form in the hot glass (Lofgren, 1971; Cas and Wright, 1988).
16.9	0.1	Road cut on west side of road exposes a northwest-trending fault, with a 1.5-m-thick fault breccia. Bentonitic claystone of the lower Chalk Hills Formation is faulted down to the northeast against the Jump Creek Rhyolite.
18.4	1.5	Turn east from Highway 95, just past the weigh station, on to Sommercamp Road. Travel east on Sommercamp Road for 0.9 mi to the top of the grade and road cut.

Figure 9. High gravels at Stop 3 (see fig. 5 for location). Mudstone overlain and interbedded with cross-bedded coarse sand and subangular gravel. Rock pick handle is 30 cm, for scale.

Stop 4. Chalk Hills Formation Along Sommercamp Road

We will walk down the grade and examine the road cut of deltaic sediments and then return to vans at the top of the grade on Sommercamp Road.

The Chalk Hills Formation represents sediments of the earliest large lake in the western Snake River Plain rift. The age of the formation is poorly constrained. In their review of radiometric ages on the formation, Wood and Clemens (2002) place its age between 10 and 6 Ma. The road cut along Sommercamp Road exposes a section of foreset and topset beds of a delta (fig. 10). These sediments are near the base of the formation and rest upon a section of clay-altered vitrophyre of the Jump Creek Rhyolite (fig. 11).

The delta sediments in the road cut are unconformably overlain by a gently-west-dipping, grey cobble gravel, similar to that seen at Stop 3. The gravel is faulted at the west end of

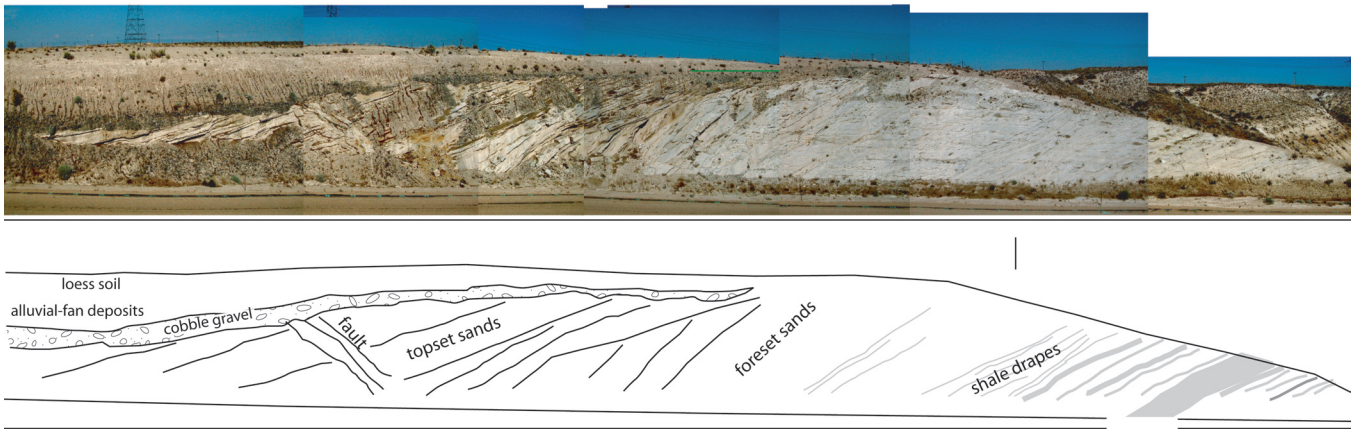

Figure 10. Delta foreset and topset beds of the Chalk Hills Formation along road cut of Sommercamp Road at Stop 4. The basalt ash marker bed in figure 11 is about 50 m west of photo along road cut.

the road cut and is overlain by unfaulted alluvial fan deposits and a loess soil. The Glenns Ferry Formation is missing in this road-cut exposure. One kilometer north of this road-cut exposure, 10 m of lacustrine sediment of the Glenns Ferry Formation unconformably overlies the Chalk Hills Formation with an angular discordance of about 8°.

The Chalk Hills Formation is about 110 m thick in this area (fig. 11). We will be looking at the sediment and volcanic features at two outcrop areas, here along Sommercamp Road, and another in a gulch 1.6 km (1.0 mi) northeast of here. The formation here is mostly claystone with an arkosic sandstone bed near the base, abundant intercalated silicic-ash layers, and delta sands that are mostly coarse silicic ash. Topset beds have well-preserved ripple marks. The foreset beds are mostly coarse sand ash with mud drapes, typically 0.1–0.5 m thick. Mud drapes form on the foreset sand beds in the time intervals between sand avalanche and deposition on the foreset slopes, or when a particular depositional delta lobe is temporarily abandoned by a distributary.

Exposed along Snake River Plain margins and also detected on seismic sections and wells beneath the plain, 10 km (6 mi) north of here (figs. 12 and 5) are intercalated local basalt fields within the Chalk Hills Formation. Many of these basalt fields erupted into water (Bonnichsen and others, 1997). At this locality, basalt occurs as one or two layers of scoriaceous ash and lapilli beds about 0.5-m thick at the west end of the road cut and indicated in the upper part of the stratigraphic section (fig. 11).

At the top of the Sommercamp Road grade, take the dirt road to the north through the barbed-wire gate and follow the track that parallels the power transmission line to the southeast. Travel 0.3 mi to a road that turns left (north) and follows the wooden-pole power line to the northeast. Travel 0.7 mi to the edge of the mesa and park.

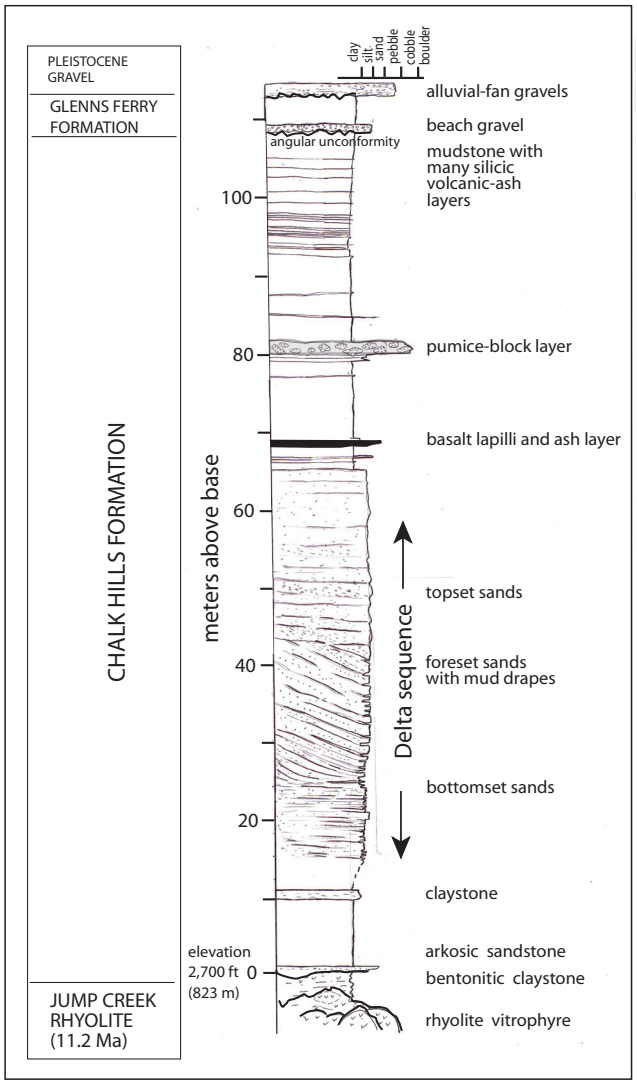

Figure 11. Graphic stratigraphic column of the Chalk Hills Formation at Stops 4 and 5.

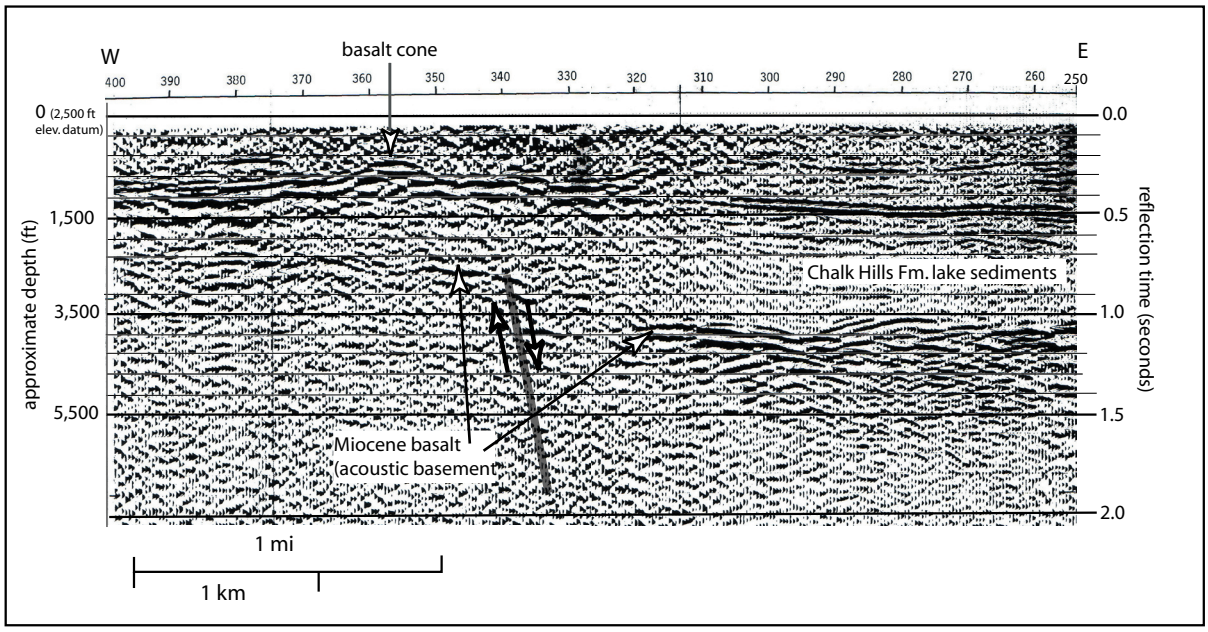

Figure 12. Seismic-reflection section showing a subsurface basalt field in the Chalk Hills Formation, between Marsing and Lake Lowell Reservoir (shotpoint locations shown on fig. 5, Chevron Seismic Line IB-7, shot points 250–400). The basalt field is 305–460 m (1,000–1,500 ft) below the surface. The top of the basalt appears as high-amplitude reflections from the sediment-basalt interface. The basalt field has relief due to cones with slopes of 23°. On the west end of the section, at a depth of 670 m (2,200 ft), is the surface of the older Miocene basalt beneath the Chalk Hills Formation. This older basalt surface is faulted down to the northeast to a depth of 1,070 m (3,500 ft,) or a displacement of 400 m (1,300 ft). Faulting of the basalt field within Chalk Hills Formation appears to be less than 90 m (300 ft).

Stop 5. Giant-Pumice Bed of a Sublacustrine Rhyolite-Dome Eruption Within the Chalk Hills Formation Sediments

There is a rough road over the rim and down to the valley below, on which we will walk 300 m northeast to exposures of the "giant-pumice bed".

A remarkable layer of large (up to 1 m) pumice blocks, about 1.5-m thick, is exposed in a gulch in the SW quarter of section 32, T. 2 N., R. 5 E. The pumice blocks are radially fractured, but the broken pieces are intact, indicating they were deposited before they fractured (fig. 13). Post-deposition fractures indicate the blocks were still hot when emplaced and then cracked upon cooling. This unusual type of deposit also has been described at La Primavera Volcano, Mexico, by Clough and others (1982) and Cas and Wright (1988). The blocks are interpreted as pieces of the pumiceous carapace of a rhyolite dome that erupted beneath a lake and then floated and shoaled while still hot and intact (fig. 14). Also in this gulch, is the continuation of the section above the basalt ash seen in the road cut of Stop 4. Here the section contains many silicic volcanic ash layers within claystone, and is locally overlain by

Figure 13. Large fractured pumice block in pumice-block layer within the upper Chalk Hills Formation at Stop 5.

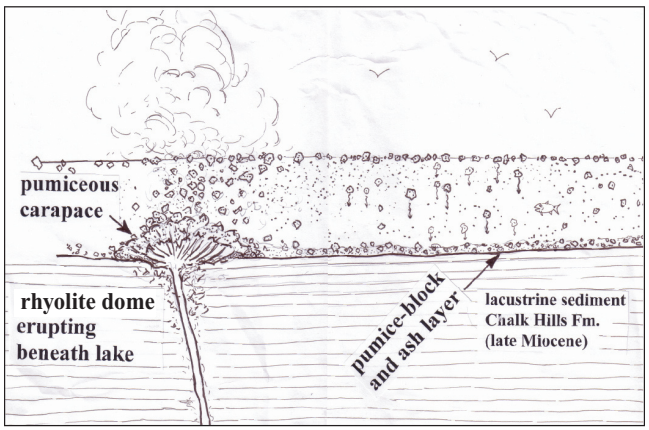

Figure 14. Sketch of a pumice dome eruption beneath the lake. It seems unlikely the large blocks waterlogged and sank, because they must have been hot and intact when emplaced. More than likely, the large blocks were steaming hot and still intact and then fractured in place upon further cooling.

a 1-m-thick horizontal ledge of pebbly sandstone and 10 m of massive lacustrine mudstone of the Glenns Ferry Formation (figs. 15 and 11).

The Glenns Ferry Formation dips a few degrees to the north, and the section is much thicker north of here (fig. 16). About 0.5 km (0.3 mi) south of this valley along the dirt road that climbs the north mesa is a sequence of silicic volcanic ashes, one of which is about 1-m thick and can be traced for several miles to the north (fig. 16). The lowest part of the Glenns Ferry Formation contains veins of selenite gypsum suggesting local lagoons along the lake shore that dried intermittently. However, none of the formation here is calcareous. It does become very calcareous in its upper part, about 3 km north of here (fig. 16). Much of the lacustrine mud in a 670-m (2,200-ft) deep well beneath Caldwell, 22 km north of here, is also calcareous (Wood, 1994).

Optional 0.25-mi walk is a 180 ft climb to the mesa to the east (hill 2872), for a good view and photo of the angular unconformity. In this valley, at the bottom of the mesa to the north is the contact of the Glenns Ferry Formation over the Chalk Hills Formation; however, the prominent rusty-colored sandy gravel visible on the south side of the valley is missing here. The lower 7 m of the Glenns Ferry Formation contains selenite gypsum veins (satin spar), and the 70-m-thick section here is a monotonous mudstone with several volcanic-ash beds.

Mile-post	Inc.	
		Return to vans at top of the south mesa and retrace the route back west to U.S. Highway 95.
18.4		Turn right (north) on to the new U.S. Highway 95.
19.8	1.4	The angular unconformity is in the road cut on the west side of the highway. A horizontal ledge of brownish-orange pebbly sandstone of the basal Glenns Ferry Formation overlies the slightly tilted claystone and ash layers of the Chalk Hills Formation.
24.0	4.2	Junction of U.S. Highway 95 and State Route 55. Turn right (east) on to State Route 55 toward Marsing.

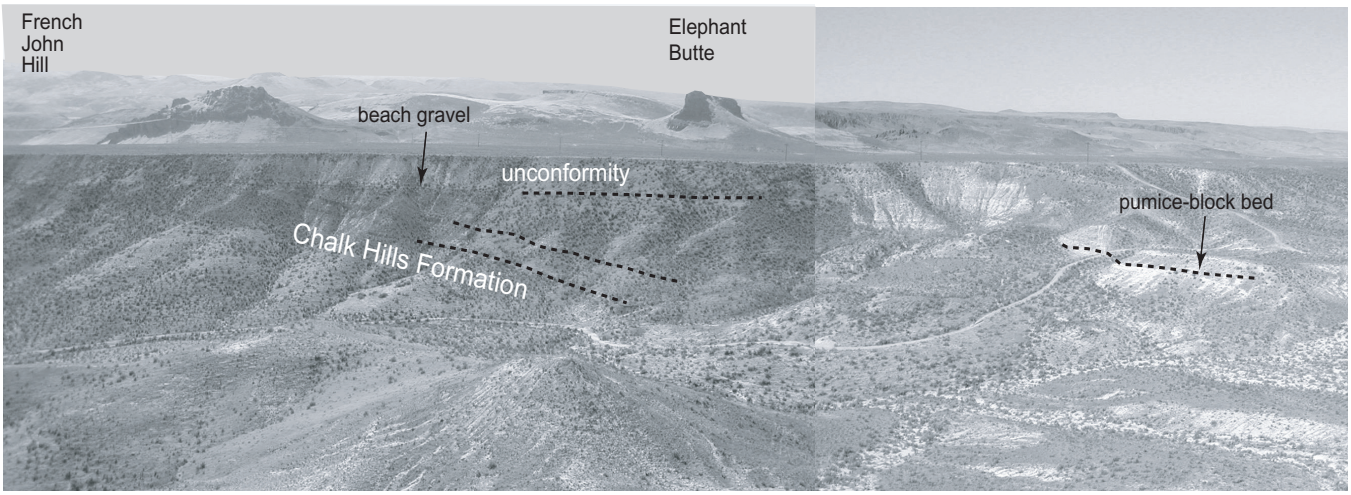

Figure 15. Angular unconformity between the tilted Chalk Hills Formation and the Glenns Ferry Formation. Base of the Glenns Ferry Formation is an 1-m-thick discontinuous sandstone, interpreted as a beach sand. Overlying the sandstone is 10 m of mudstone. Mudstone thickens to the north as shown in figure 19. View is looking south from mesa north of Stop 5.

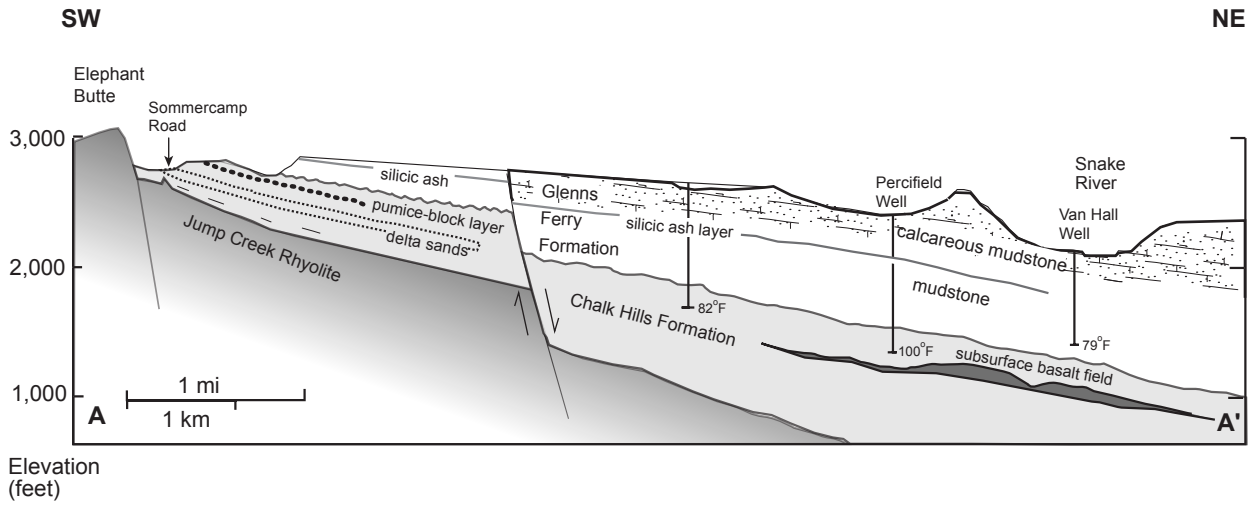

Figure 16. Stratigraphic cross section showing the position of calcareous mudstones of the upper Glenns Ferry Formation. Section is from Sommercamp Road area to the Marsing Hills. Location of section line A-A′ is shown on figure 5.

Mileposts on State Route 55 start at 0.0 at this junction

Mile-post	Inc.	
0.0	0.0	Junction U.S. Highway 95 and State Route 55, traveling east on State Route 55.
1.7	1.7	Marsing
2.7	1.0	Snake River bridge at Marsing. The river at Marsing flows in a natural low-gradient reach. The valley of the river is about 120 m (400 ft) below the surrounding plain. When the Bonneville flood roared through here 14,500 yr ago, the raging river was about 60-m (200-ft) deep over Marsing (O'Conner, 1993). Today, the average flows are about 240 m^3/s (8,500 cfs), but this reach accommodates spring flood flows greater than 1,420 m^3/s (50,000 cfs). A steady flow from springs of about 127 m^3/s (4,500 cfs) enters the river in the Thousand Springs-Hagerman reach, about 250 km (155 mi) away. This reach between the backwaters of Brownlee Dam in Hells Canyon and Swan Falls Dam, 56 km (35 mi) upstream has an average gradient of 0.00025 m/km (1.32 ft/mi), making this a long natural reach of the river without hydroelectric dams. The ecology and physical characteristics of the riverbank have been studied recently to provide information for legal proceedings between the U.S. Department of Fish and Wildlife and the State of Idaho over claims for Federal water rights to protect wildlife refuges on the islands (Ostercamp and others, 2001; Ostercamp, 1998; and Dixon and Johnson, 1999).
3.4	0.7	Lizard Butte east of the highway is the eroded remnant of a complex basalt volcano having many features of hydrovolcanism. The volcano erupted through the wet lacustrine sediment of the Glenns Ferry Formation. The deposits include deformed stream gravels, steeply dipping bomb-and-lapilli beds of scoria and surge deposits. The cap rock is a hard basalt agglutinate with chunks of white sediment, which is interpreted as a welded basalt spatter (Craig White, personal communication, 2003). Although the cap rock displays columnar jointing, it is welded spatter and not a lava flow as one would surmise from the highway view. Age is estimated to be late Pliocene or early Pleistocene.
3.9	0.5	Several light-colored hills forming the north rim of the Snake River valley are at about 10:00. These also are called the Chalk Hills, but they are not the Chalk Hills of the type locality of the Miocene Chalk Hills Formation. These "Chalk Hills" are sand and calcareous mudstone of the upper Glenns Ferry Formation and are of the floodplain and marsh facies (Reppening and others, 1994). They contain an important vertebrate fauna of early Pleistocene age (latest Blancan-earliest Irvingtonian), known as the Froman Ferry fauna. Important fossils, collected by local resident George R. Scott, are microtine rodents, early Pleistocene horse, puma, and an archaic

rabbit. Sediments are of reversed magnetic polarity (Van Domelen and Rieck, 1992), and estimated age is 1.5-1.7 Ma (Reppening and others, 1994).

4.8 0.9 **STOP FOR PICNIC LUNCH.** Ste. Chappelle Winery is the first post-prohibition winery in Idaho. Experimental vineyards were first planted in 1972, and the winery established in 1976 by the Symms Fruit Ranch. Well-drained loess soils, the microclimate of south-facing slopes of the Snake River valley, and the late growing season combine to produce Riesling, Chardonnay, Merlot, and other varietal grapes. There are now eight wineries in this area of which Ste. Chappell is the largest, shipping 200,000 cases per year. Figure 17 is a view from the winery.

6.8 2.0 Going north and then due east on State Route 55, we leave the Snake River valley and travel across the broad western plain.

9.2 3.6 Between Huston and the Lake Lowell turnoff is the "Lower Deer Flat channel", a 3-km-wide, northwest-trending, gravel-mantled, middle-Pleistocene channel incised about 30 m into an upland surface of Glenns Ferry Formation capped by the Tenmile Gravel (Othberg, 1994). This probably is an old channel of the Snake River that was blocked to the southeast by the basalt fields of Kuna Butte and other large shield volcanoes. Eruptions of these lavas forced the river south to its present course on the south side of the plain.

16.2 7.0 Continue straight east through the stoplight at the intersection of State Route 55 and Caldwell Boulevard. This easterly continuation is named Karcher Boulevard, and there are no more mileposts. You will cross over the railroad tracks and the Interstate heading toward the Amalgamated Sugar Refinery.

18.0 1.8 Just past the sugar beet refinery, turn right (south) on Northside Boulevard and then left (east) to enter Interstate 84, heading east to Boise.

Mileages are now based upon mileposts of Interstate 84.

Milepost	Inc.	
38.0	3.0	Just before Exit 38, the Interstate Highway descends over a basalt-mantled surface (one of the Amity or Deer Flat surfaces). This lava can be traced to Caldwell where it was $^{40}Ar/^{39}Ar$ dated by Othberg (1994) at 0.799±0.095 Ma and has a reversed magnetic polarity. From here east, the Interstate is on the Sunrise Terrace surface.
46.0	8.0	From Exit 46 (Eagle Road) the Interstate heads east, along a route for which we have a high-resolution seismic line all the way to Boise (about 8 mi east). Because of urbanization and traffic in this area, we used a route along the Union Pacific Railroad right-of-way, one mile south of the Interstate.
49.0	3.0	Take signs to CITY CENTER, as you negotiate the "Flying Y" complex of freeway overpasses.
49.5	3.5	About 0.5 mi beyond the Interstate "Flying Y" intersections, the highway descends to the Whitney Terrace surface.
51.8	2.3	Four lanes descend from the Whitney terrace onto the modern flood plain of the Boise River and downtown Boise. The Interstate Connector merges with city streets at Front Street. Continue east on Front Street.

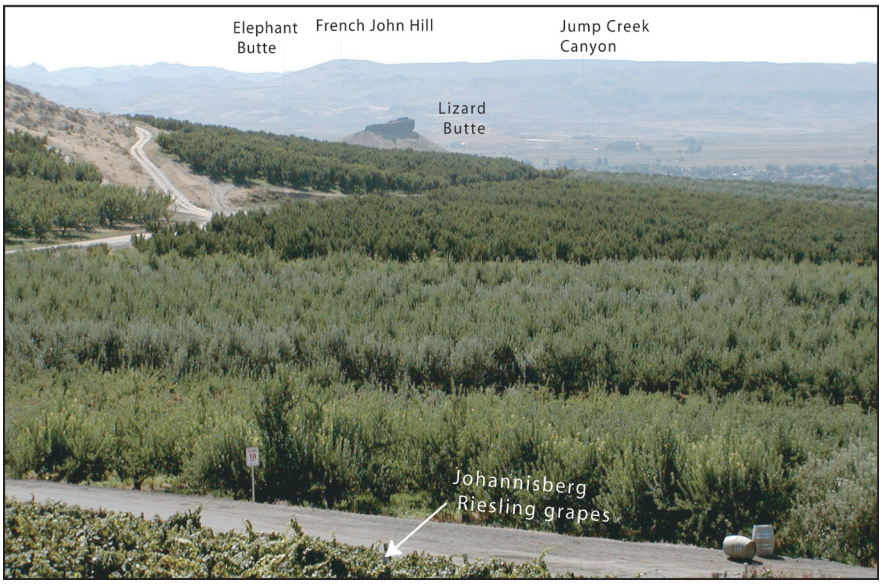

Figure 17. View to the south across the Snake River valley to the Owyhee Mountains from the Ste. Chappelle vineyards (Lunch Stop).

53.5	1.7	At the Capitol Boulevard stoplight, turn left (north-northeast), and the State Capitol Building should be in sight about 5 city blocks ahead.
53.8	0.3	At the Idaho State Capitol Building, turn left one half block in front of the capitol, and then right on 8th Street to the northwest corner of the State Capitol. The 1920 State Capitol building is constructed of Miocene Boise Sandstone from the Table Rock Quarries (Stop 9).

Reset mileages at the 8th Street and State Street intersection.

WESTERN BOISE FOOTHILLS LEG OF FIELD TRIP

Mileage Cum.	Inc.	
0.0	0.0	This leg of the field trip starts at 8th and State Street, the northwest corner of the State Capitol grounds (fig. 18). Continue 3 blocks northeast on 8th Street and turn left (northwest) on Hays Street.
0.0	0.2	Hays Street and 8th Street. Travel 0.6 mi northwest on Hays Street.

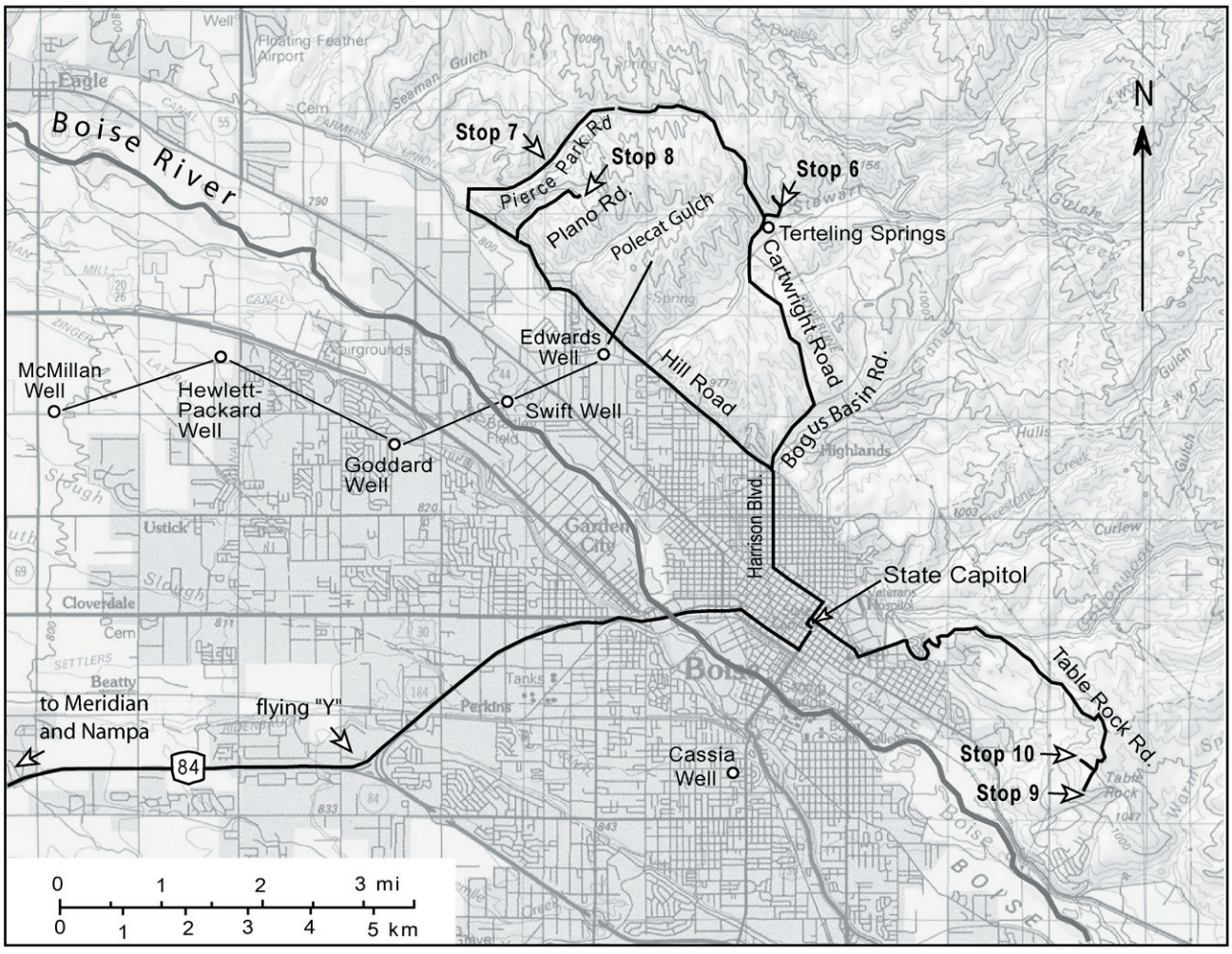

Figure 18. Map showing route of trip through the Boise foothills.

0.8 0.6 Bear right (north) and merge with Harrison Boulevard. Continue straight ahead (north) to the Hill Road intersection.

1.8 1.0 Hill Road stoplight. Continue straight ahead. Harrison Boulevard turns into Bogus Basin Road.

2.1 1.0 In the road cuts behind the buildings, on the left (west), is fine- and medium-grained sand with hummocky cross stratification (HCS) (Gallegos and others, 1987). HCS is produced by currents near the wave base, induced by storm waves. This type of cross stratification indicates near shore sedimentation, and under oceanic conditions within a 10–20-m depth (Walker and Plint, 1992).

2.6 0.5 Turn left (northwest) onto Cartwright Road. This turn is beneath the green-lawn-covered hill of the J.R. Simplot Mansion. Sediment along the road is mostly nearshore muds and sand of the Terteling Springs Formation.

3.3 0.7 Crest of hill. Ahead are hills with the conspicuous contact between mudstone of the Terteling Springs Formation and the overlying coarse Gilbert-style delta sands of the Pierce Gulch Sand (fig. 19). The mudstone is grass covered because of good moisture retention of the fine soil, whereas the Pierce Gulch Sand has only dark bitterbrush clumps with roots that reach deeper into the ground for moisture on dry sandy slopes. This vegetation contrast is seen on most south-facing slopes of these lithologies. North-facing slopes in the foothills have a substantial mantle of loess soil, 1–4-m thick, which supports bitterbrush and sage thickets.

4.6 1.3 Sediments dipping 28° W. in the road cut are inferred to be the Chalk Hills Formation. Sediments of the overlying Terteling Springs Formation, at the gate to the Owyhee Motorcycle Club, 0.2 mi to the northeast, are dipping only 12°. Generally, it is inferred that an unexposed angular unconformity exists between these units. This is the only place where existence of an angular unconformity can be demonstrated within the lacustrine sequence in the foothills. Possibly, it compares with the unconformity at Stop 5 along the Owyhee Mountains front.

4.8 0.2 Park for Stop 6.

Stop 6. Oolites and Fossil Clams of Lake Idaho, Owyhee Motorcyle Club in Stewart Gulch

Park at the entrance to the Owyhee Motorcycle Club. View the foreset beds at the gate, go through the gate, and walk around the hill to the northeast, observe the sediments in the excavated cut at the bleachers on the racetrack, and then proceed about 200 m up the gulch to the oolites. Coarse sand foreset beds of a Gilbert-style delta are overlain by Terteling Springs Formation mudstone at the entrance gate of the motorcycle club (figs. 20 and 21). This contact is interpreted as a "flooding surface" caused by a rise in lake level. Alternatively, one might argue it is the result of lobe switching of delta distributaries, but mass-failure deposits into deep water seen around the hill to the east suggest deepening of waters. The foreset-bedded sand unit at the entrance gate crops out again as cemented sandstone in the canyon of Dry Creek, about 1 mi north of here. In Dry Creek valley, this sand is one layer of foreset-bedded sandstone about 25-m (80-ft) thick. It is believed that Terteling Springs, just below the road here, is

Figure 19. Contact of the Pierce Gulch Sand overlying mudstone and oolite bars of the Terteling Springs Formation. View is to the northwest from the Cartwright Road across Stewart Gulch. Greenhouses in the foreground are heated by geothermal water.

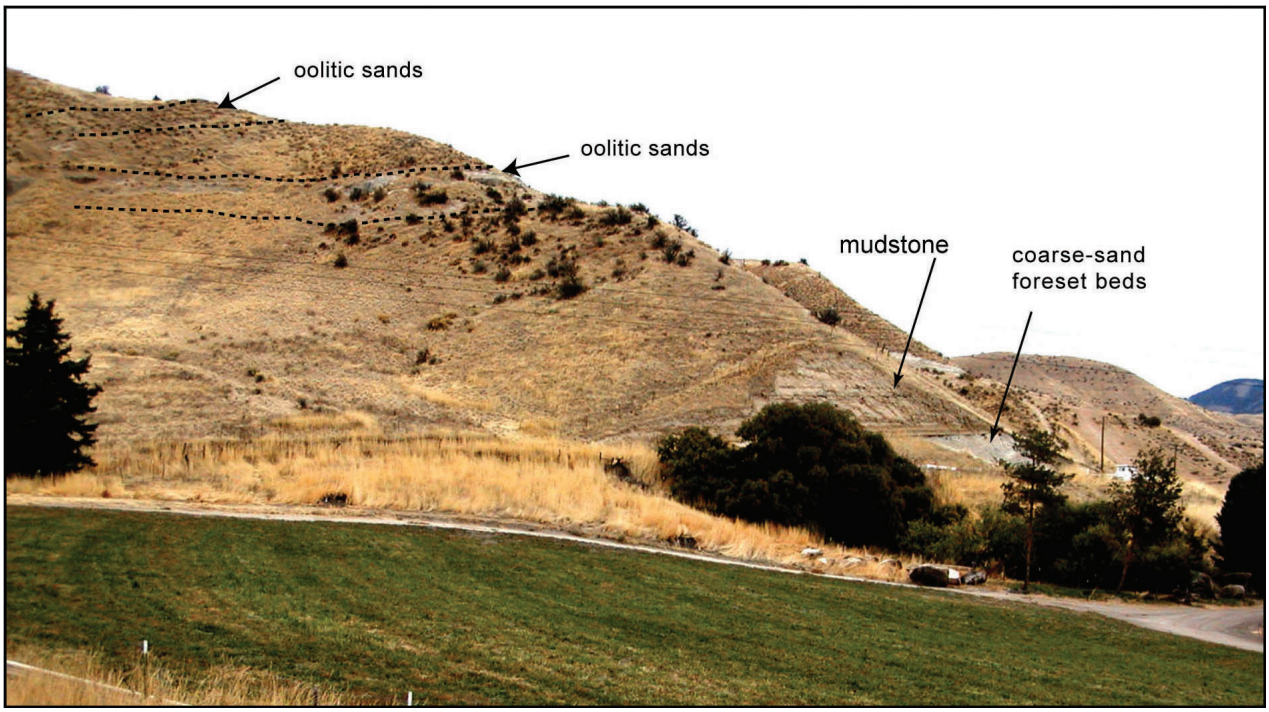

Figure 20. Coarse sand of a Gilbert delta overlain by mudstone and the oolite bars at Terteling Springs in Stewart Gulch. View is to the northeast from Cartwright Road.

discharge from this permeable sand unit intercalated within mudstones of the Terteling Springs Formation.

Walk through the gates and continue left around the hill about 200 m past the bleachers to the beer and pop stand. In the excavated cut behind the stand is a bed of coarse orange sand, over 3-m thick, and fine beds contorted by soft sediment deformation. The sand contains abundant white shells of gastropods and clams chaotically oriented in the sand (fig. 22A). I interpret the sand as a mass-failure into deep water, derived from failure of a shoal or beach associated with a delta. The sand was deposited rapidly on the lake bottom causing soft sediment deformation of the fine beds.

Continue walking up the gulch about 100 m beyond the racetrack and through an unmaintained fence to a smooth rock ledge at the foot of the hills. This rock ledge is made up of carbonate-coated sand grains, commonly called "oolites" (fig. 22B). Formation of lacustrine oolites occurs in wave-agitated waters of beaches and shoals. Origin of ooids is still debated, but precipitation of concentric microlayers from carbonate-saturated waters onto grains of fine sand seems clear here. Davaud and Giradclos (2001) show that biofilms act as a catalyst or substrate for submicron-sized calcite crystals forming on oolites in temperate, freshwater Lake Geneva (Switzerland), at depths of 1–5 m.

Several lenses of oolitic sand occur here over a stratigraphic interval of 120 m (fig. 23). On the south side of the western plain, these oolite occurrences have been interpreted as a transgressive unit at the base of the Glenns Ferry Formation (Malde and Powers, 1962; Swirydczuk and others, 1979, 1980a, 1980b, Reppening and others, 1994). Wood and Clemens (2002) agree they are a transgressive unit, and propose that the oolites are an indication that Lake Idaho was a closed-lake basin of increasing alkalinity. The closed-basin environment is confirmed by a ^{13}C isotopic analysis of del^{13}C

Figure 21. Closeup of foreset-bedded coarse sand overlain by mudstone of the Terteling Springs Formation.

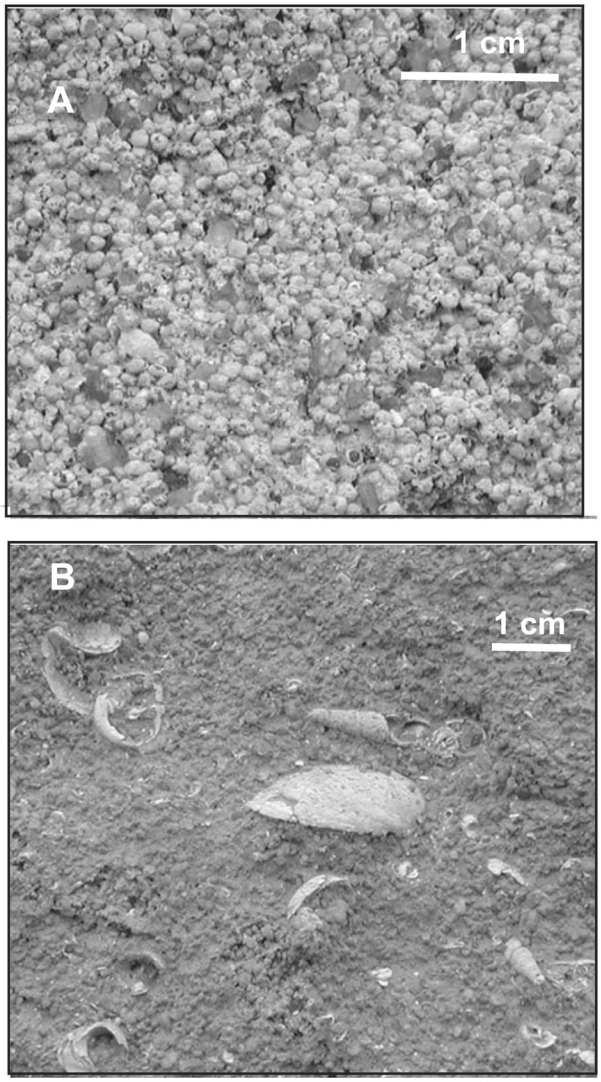

Figure 22. (A) Carbonate-coated grains (oolites), mostly about 0.8 mm in size from the outcrop at the Owyhee Motorcycle Club. (B) Fossil clams and snails in a coarse sand at the Owyhee Motorcycle Club. Shells are scattered without orientation indicating this may be a mass-wasting deposit collapsed from a delta front and not a beach deposit.

= +2.0 for carbonate in oolites collected from drill cuttings from a depth of 40 m in the Cassia Street water well in central Boise (fig. 18), about 8 km (5 mi) south of here (Cavanagh, 2000). Worldwide, the del^{13}C of closed-lake carbonates range from -2 to +5, whereas open-lake carbonate ranges from -5 to -15 (Talbot, 1990).

Mileage Cum.	Inc.	
		Walk back to the vans parked at the entrance to the motorcycle club. Continue driving northwest on Cartwright Road.
5.8	1.0	Crest of the hill. The road traverses the contact of the Pierce Gulch Sand over the Terteling Springs Formation.
6.3	0.5	Pierce Park Road. Bear left (southwest) on Pierce Park Road.
6.7	0.5	Many springs occur at the contact of the base of the permeable Pierce Gulch Sand upon mudstone along this road, as indicated by the abundant black locust, cottonwood, and willow trees and blackberry thickets.
7.6	0.9	Mudstone of the Terteling Springs Formation with a 2-cm-thick white silicic volcanic ash. Near here, visible when the grader cleans the road cut, is a white sand hummock within the mudstone, probably storm-wave reworked sands that avalanched from a delta edge.
7.9	0.3	Pull off on the right side of road and park at the entrance to the sand quarry in the Pierce Gulch Sand. Walk down the road (south) to the road cut in Terteling Springs Formation.

Stop 7. Pierce Park Road: Pierce Gulch Sand Over Mudstone of the Terteling Spring Formation

The quarry exposes 20-m-thick foreset beds of the Pierce Gulch Sand. The sand is a Gilbert–style delta of coarse sand. Walk down the road (about 150 m) just past the high road cut in Terteling Springs Formation mudstone, on the west side of road, to see the 20-cm-thick, white silicic volcanic ash near the top of the mudstone unit. The coarsest grains at the base

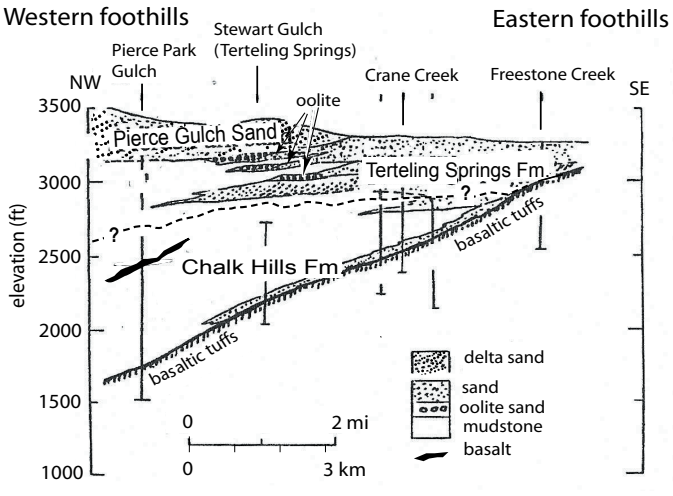

Figure 23. Stratigraphic diagram showing relation of the Chalk Hills Formation with the overlying Terteling Springs Formation and the Pierce Gulch Sand (from Wood and Clemens, 2002).

of this ash layer consist of 0.15- to 0.2-mm shards of white pumice and very light-gray glass. This size suggests it came from a volcanic source within several hundred kilometers. This relatively thick ash occurs in many places in the western foothills and is a good marker near the top of the Terteling Springs mudstone.

Mileage Cum.	Inc.	
		After this stop, return to vans and continue down Pierce Park Road.
9.1	1.2	Pierce Park Road and Hill Road. Turn left (east) onto Hill Road.
9.7	0.6	North Plano Road and Hill Road. Turn left (north) on North Plano Road, and continue northeast. We will travel 1.4 mi up this road.
	0.1	End of pavement. Continue on North Plano Road. It is uncertain whether this is still a private road, despite the abundance of "no-trespassing notices" on the side of the road. The road serves several residences at the top of the hill. I think it now is a public county road.
	0.8	Turn around and park at the switchback, which is a posted entrance to private sand quarries. Walk back about 150 m to the road cut on the south side of the road.

Stop 8. North Plano Road: Base of the Pierce Gulch Sand

The road cut on this dirt road into the foothills is the only good exposure of the base of the Pierce Gulch Sand over mudstone of the Terteling Springs Formation. The contact is so easily mapped on air photos by contrast in vegetation and soil that one might believe it is an unconformity. However, at this locality the deposition appears continuous, and the boundary between these two different lithologic units is simply that of a coarse-sand delta prograding and downlapping over prodelta mudstone. On a large scale, when viewed from a distance, the lower sand crossbeds shallow downward in slope and appear tangential to the contact.

Geophysical logs of water wells west of here show a major delta unit in the upper section (fig. 24). At the McMillan Well, 10 km (6 mi) west of here, the delta sand thickens to 210 m (700 ft). The delta unit is built out into a deeper lake basin and is thicker there because of "greater accommodation depth".

In this road cut, a 1.5-m-thick bed of coarse sand overlies mudstone, and the sand is overlain by yet another mudstone. The main thick body of coarse sand lies just a few meters above the road cut (fig. 25). Mudstone fingers and lenses penetrate the sand, suggesting the muds were semisoft when overlain by the sand. Small sand dikes also wedge upward about 0.3 m into the overlying mudstone. The boundaries are quite sharp and appear conformable, suggesting that sand prograded rapidly over the mud bottom of the lake.

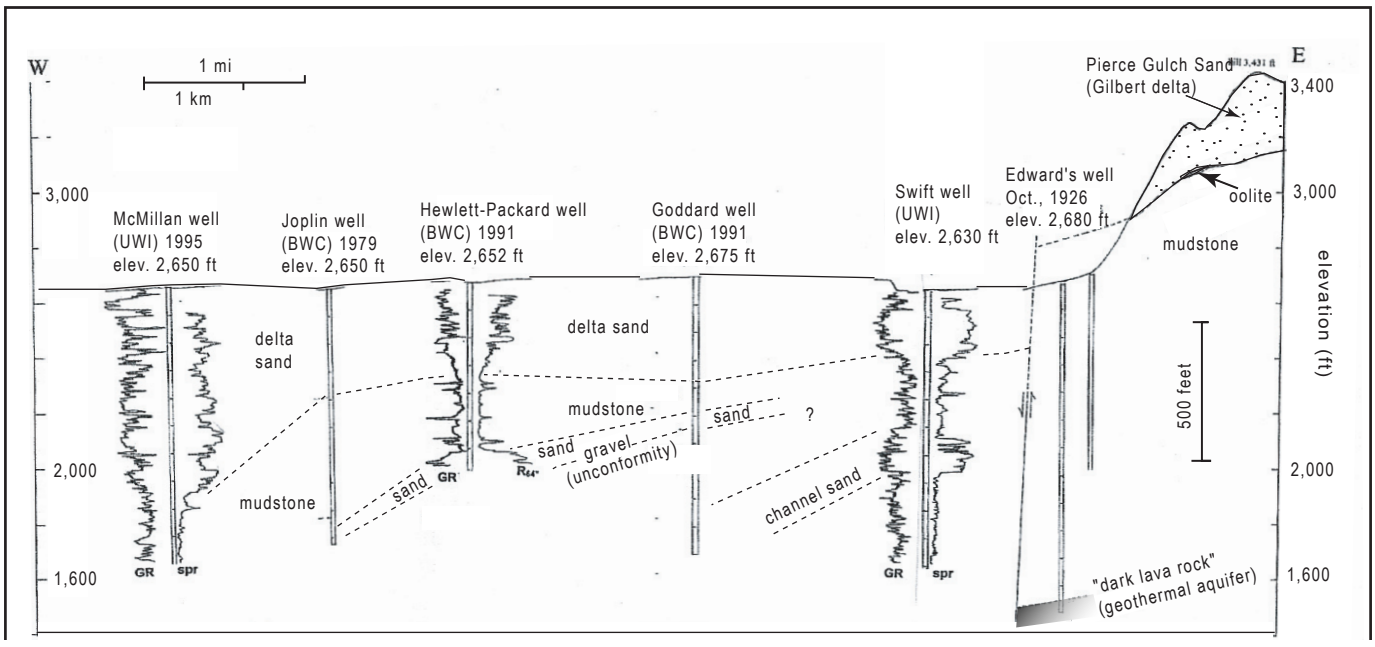

Figure 24. Stratigraphic section and well logs from Polecat Gulch in the foothills to west Boise, showing the Pierce Gulch Sand and equivalent delta facies in the subsurface. Well locations shown in figure 18. GR, natural gamma log; spr, single-point resistance log; and R_{64}, 64-inch normal-resistivity log. Well logs courtesy of United Water Idaho, Inc. (UWI), and its predecessor, Boise Water Company (BWC).

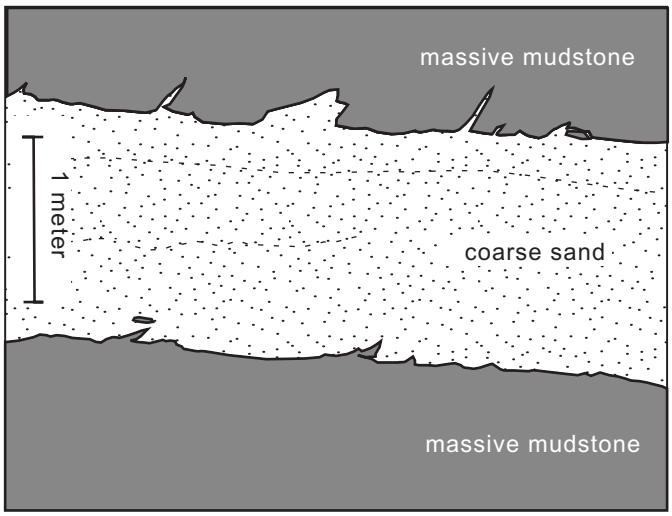

Figure 25. Tracing of photo showing an bed of coarse sand interbedded within mudstone, just beneath the base of the massive Gilbert-style delta of the Pierce Gulch Sand at North Plano Road. The sand bed is interpreted to be a sublacustrine avalanche out on to the muddy lake bottom, formed as the main foreset sand body was advancing basinward.

Mileage Cum.	Inc.	
		After viewing this stop, drive 1.4 mi back to Hill Road.
9.7	1.4	Return to the intersection of Hill Road and North Plano Road and turn left (east) on Hill Road.
11.1	1.4	Hill road makes a 90º turn to the left (east).
11.9	0.8	To the right (south) is the road to Edward's Greenhouse, a highly successful geothermally-heated greenhouse operation raising garden plants and decorative flower baskets of all sorts for the Boise market. Location of the Edward's well is shown in figure 18. The geothermal system here is of historical importance in Idaho groundwater law, because in 1931, the Idaho Supreme Court issued a landmark decree (Silkey v. Tiegs) on the doctrine of "the illegality of mining of an aquifer". The court interpreted the declining pressure and artesian-well flows of hot water to be the result of discharge exceeding recharge of an aquifer. In those situations, the rights of the junior appropriators (those owners of the later wells) to produce water are curtailed. The wells are about 350-m (1,150-ft) deep, into a "dark volcanic rock", probably a rhyolite, and produce 47° C (117° F) water (Young and others, 1988).
12.4	0.53	6th Street and Hill Road stoplight, continue southeast on Hill Road.
13.8	1.4	Bogus Basin Road and Hill Road and Bogus Basin Road (Harrison Boulevard) intersection. Turn right (south) on Harrison Boulevard, and travel 1.0 mi to where Harrison merges with the east-bound lane of Hays Street, follow east on Hays Street for 0.8 mi to 9th Street.
15.6	1.8	9th Street and Hays Street. Turn right (south) on 9th Street.
15.8	0.2	State Street and 9th Street. Turn left (east) on State Street.
15.9	0.1	Idaho State Capitol Building, 8th and State Street.

Reset mileages at the 8th Street and State Street intersection.

EASTERN BOISE FOOTHILLS LEG OF FIELD TRIP

Mileage Cum.	Inc.	
0.0	0.0	This leg of the trip starts at the intersection of 8th Street and State Street, the northwest corner of the State Capitol Building grounds. Travel east on State Street.
0.1	0.1	Intersection of Fort Street and State Street. Bear right (east) onto Fort Street.
0.4	0.3	Turn left (north) on Reserve Street.
0.6	0.2	Intersection of Mountain Cove Road and Reserve Street, continue north on Reserve Street. The dike on the northwest (left) side of the street was built in 1998 to increase the volume of the sediment retention reservoir where Cottonwood Creek flows from the foothills. The September 1996 foothills fire focused awareness on potential debris flows out of the foothills gulches, particularly after major fires in the watersheds.
0.9	0.3	Main road bears right and uphill (east) and changes name to Shaw Mountain Road at this intersection with San Felipe Way. Three hundred feet northwest along a gated gravel

road is the Boise Geothermal, Inc. Well No. 1, drilled to a depth of 634 m (2,080 ft). Idaho batholith granite is at a depth of 512 m (1,680 ft) in this well (Burnham and Wood, 1983).

1.0 0.1 The basalt of Aldape Heights crops out along Shaw Mountain Road to about this intersection with Santa Paula Place. This basalt is intercalated with sands of the Chalk Hills Formation. Clemens and Wood (1993) obtained a whole-rock K-Ar age of 9.5±0.6 Ma. They

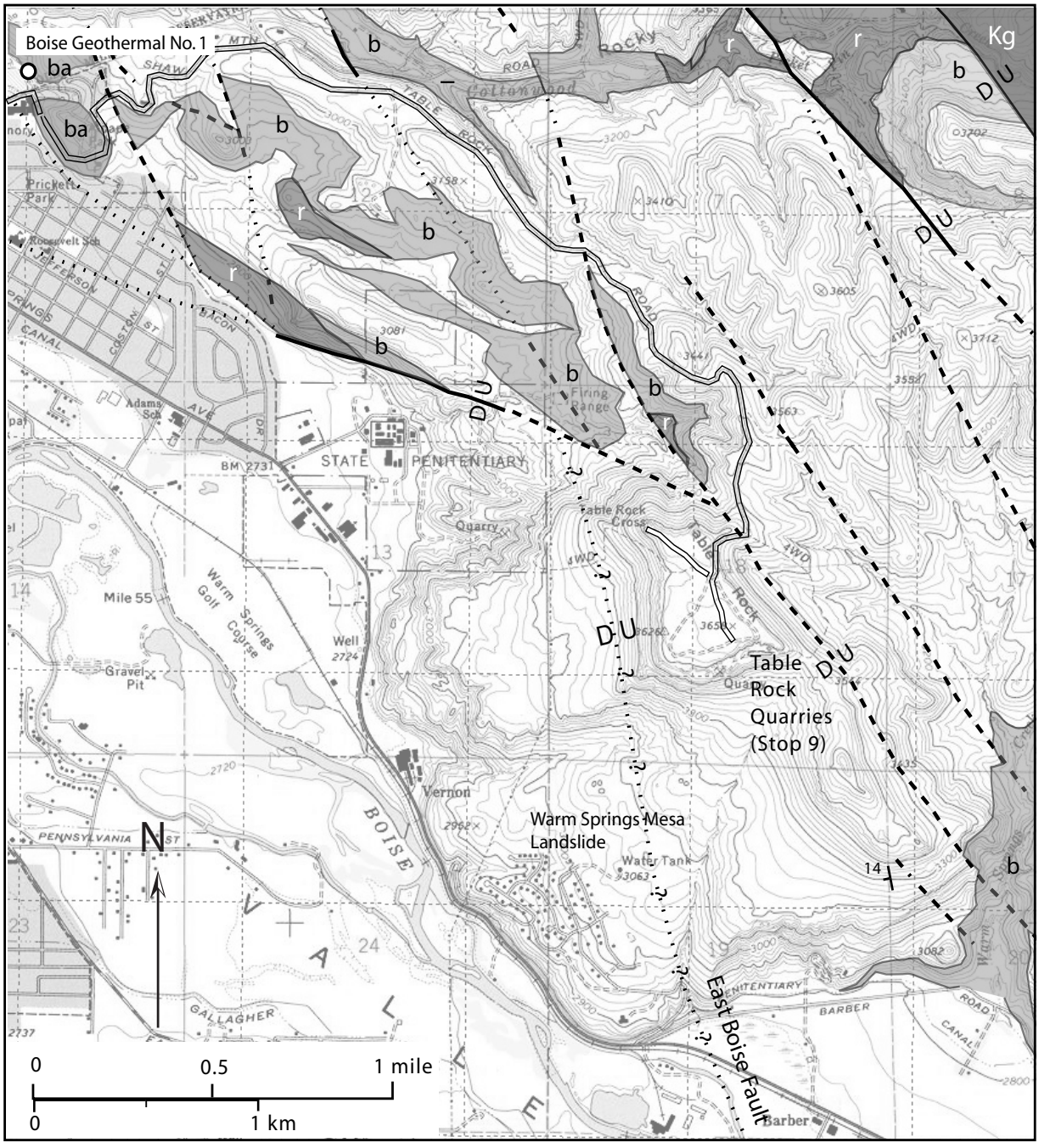

Figure 26. Geologic map showing the route to Table Rock. The Table Rock area is a downfaulted block, with respect to the foothills on the north. Because it is structurally lower, it contains one of the more complete stratigraphic sections in the foothills of 210 m (700 ft) of fluvial and lacustrine sediment over the Miocene rhyolite and basalt. Symbols on map: Kg, granodiorite of the Idaho batholith; r, Quarry View Park and Cottonwood Creek rhyolite (11.8±0.6 and 11.3±0.3 Ma, respectively); b, basalt and basaltic tuffs; ba, basalt of Aldape Park; and unshaded areas are fluvial and lacustrine sediment (after Clemens and Wood, 1993).

		show that this rock petrochemically matches basalt that occurs in the Capitol Mall Geothermal wells by the Statehouse, at a depth of about 223 m (730 ft), indicating vertical separation due to dip of beds and offset along faults is about 260 m (850 ft) between the outcrop and the wells by the Statehouse.
2.0	1.0	Turn right (east) on Table Rock Road at this intersection of Shaw Mountain Road and Table Rock Road.
4.0	2.0	Bear right (south) on Table Rock Road at this intersection with E. Wildhorse Lane (private lane).
4.2	0.2	Gate unlocked between 1 hour before sunrise and 1 hour after sunset. This point is in a saddle between hills and is the location of the normal fault (fig. 26) that down drops the Table Rock section of sediments to the southeast relative to the foothills to the north.
4.5	0.3	Park for Stop 9.

Stop 9. Table Rock Quarries

Park here and procede 0.25 mi to the southeast along a deeply-rutted road to the rim of the mesa and the quarries for the "Boise Sandstone".

Table Rock is a mesa capped by silica-cemented sandstone, forming a prominent landmark above east Boise. The mesa is comprised of younger lake and stream sediments faulted down relative to the northern foothills, about 300 m (1,000 ft), thus preserving a 200-m (700-ft) section of sedimentary strata (Wood and Burnham, 1987; Clemens and Wood, 1993) (fig. 26). The 15-m-thick sandstone layer at the top (fig. 27) has been quarried for over 100 yr and widely marketed as a dimension stone. It is the stone of which the Idaho State Capitol Building was constructed in 1920. This "Boise Sandstone" also is a standard for many rock mechanics and petroleum reservoir experiments (Wong and others, 1997). Porosity of 0.27 and a permeability of 910 mD (9.6 x 10^{-4} cm/s, hydraulic conductivity) are reported by Kovscek and others (1995).

The massive character of this sandstone makes it a good stone for sculptors and for dimension stone. I have puzzled over how a 15-m-thick layer of sand, of such uniform grain size (D_{10} = 0.2, D_{50} = 0.35, D_{95} = 0.7 mm), was deposited. Gallegos and others (1987) suggested it was a gravity-driven mass flow beneath the lake based on the character of its basal scour surface. Above the massive sandstone is 5 m of bedded sandstone with 0.5 mm coated grains (ooids) and rip-up slabs of coarse sandstone mixed with ooids (fig. 27 and 28). Above the bedded sand is thin-bedded mudstone and uncemented sand and sandy gravel.

Silica cementation of the sand occurred as silica-saturated geothermal waters percolated through permeable beds and cooled allowing the dissolved silica to precipitate. Silica-cemented sandstone around the western plain commonly occurs within several kilometers of fault systems. The faults were conduits for upward flow of silica-bearing hot water from depths of a few kilometers.

From the quarries is the best view of the Pleistocene terrace sequence of the Boise River Valley (fig. 29). Othberg (1994) established a chronology for the four terraces observed

Figure 27. Massive medium-grained sandstone at the Table Rock Quarries. This 15-m-thick layer is the "Boise Sandstone" sold throughout the United States as a dimension stone during the early 20th Century. The layer can be traced laterally for at least 800 m. Sedimentary architecture of this sand has not been studied, and its origin remains uncertain. It is overlain by bedded sands that contain up to 30 percent coated grains, that look very much like carbonate coated oolites, but do not effervesce. The sands also contain rip-up clasts of oolite-bearing coarse sand (fig. 28). The upper bedded sands display low-angle, tangential cross stratification. Above the sandstone is mudstone and pebbly sands.

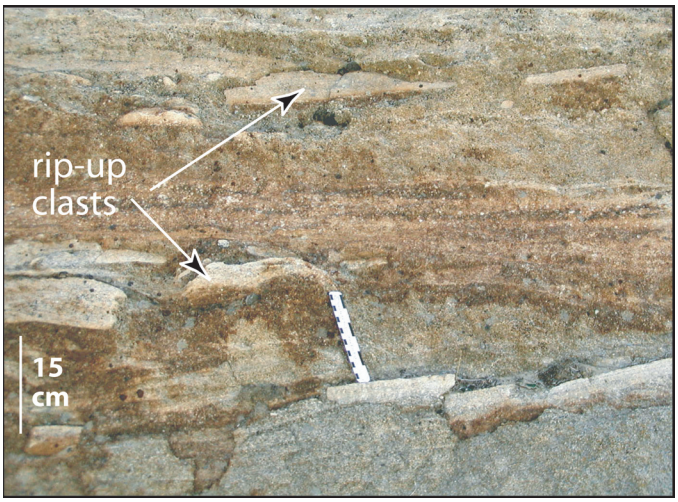

Figure 28. Rip-up clasts (light colored) of cemented coarse sand with 0.5 mm coated grains within bedded coarse and small-pebble sandstone. Locality shown in figure 27 at the Table Rock Quarries.

here by dating the basalt layers that lay upon the terrace surfaces. He also recognized the much older (but undated) Bonneville gravels on the southeastern skyline of figure 29. The terraces are typically overlain by 15 to 30 m of gravel on a strath surface of eroded lacustrine sand or mudstone (Squires, 1992). Downward erosion of the Boise Valley leaving this sequence of abandoned flood plains was in response to lowering of base level and related downcutting by the Snake River. During the late Pliocene and the Quaternary, the Snake River was downcutting the entrance to upper Hells Canyon as shown by the "base-level decline" of figure 3. This is a good place to address the question of why rivers incise episodically leaving broad terrace remnants. Othberg (1994) indicated that climate fluctuation in the Quaternary likely was the cause that triggered incision. However, questions remain about whether it was related to a change in sediment load or discharge characteristics associated with glaciation in the headwaters of the Boise River or related to overall climate change. Pazzaglia and Brandon (2001) present a model for coastal streams where they associate fill and flood plain deposition with the increased load accompanying deglaciation. In this model, strath incision occurs during periods of alpine glacial advance. Their study of coastal streams, however, also is complicated by sea-level fluctuation. At this time, the factors tht controlled or triggered downcutting and terrace formation in this region are unknown.

Mileage Cum.	Inc.	
		After viewing the quarries return to the parked vans and proceed west toward the group of radio towers and continue on to the parking area at the large white cross.
4.7	0.2	Park for Stop 10.

Stop 10. Table Rock Cross Viewpoint: View to the West Over Boise and the Western Plain

This final stop of the trip looks west over the city of Boise (fig. 30). Directly below us are the grounds of the 1860 Idaho Territorial Penitentiary and the Boise Warm Springs geothermal area. The prison buildings were constructed by prisoners from sandstone quarried from the hill below. The area now is a public park and houses the Idaho Museum of Mining and Geology. From this area, one can embark on short hikes on well-marked trails into the foothills. City bus service along Warm Springs Avenue leaves every 30 minutes from downtown at 8th and Idaho Street and takes you to within

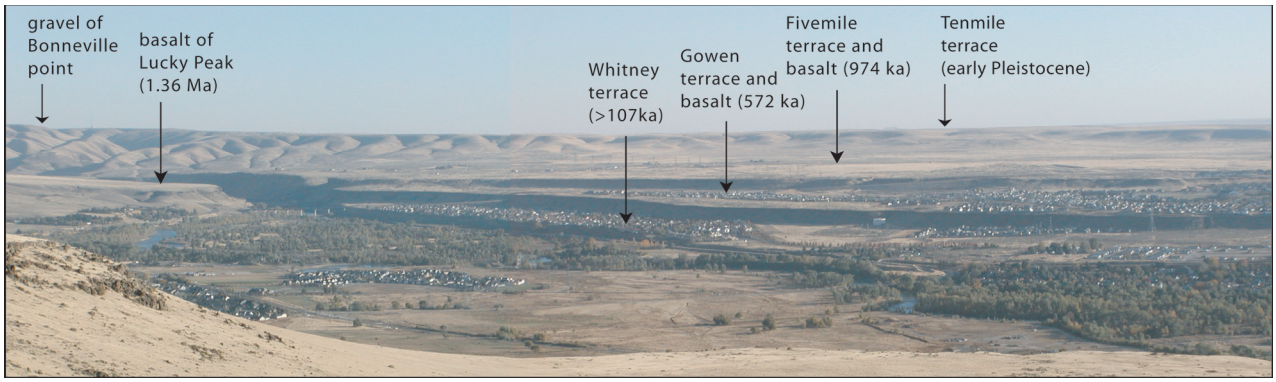

Figure 29. View to the southeast from the Table Rock Quarries. Othberg (1994) obtained Pleistocene ages on the several basalt units that flowed over the successively lower braided floodplains of the Boise River. The early Pleistocene Tenmile terrace surface forms the skyline. This surface is 150 m (500 ft) above the modern Boise River.

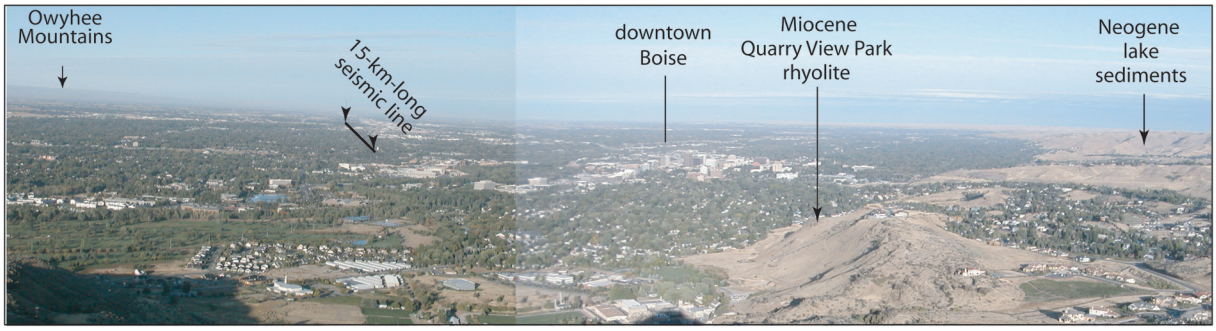

Figure 30. View to the west over the Boise Valley and the western Snake River Plain. Building area at the bottom of the hill, beneath this viewpoint, are the grounds of the 1860 Idaho Territorial Penitentiary and the Boise Warm Springs area.

300 m (0.2 mi) of the park on weekdays; however, there is currently no weekend service.

The outcrop of the Quarry View Park rhyolite is described by Wood and Burnham (1987) and shown by the arrow in fig. 30. Clemens and Wood (1993) report a K-Ar age of the rhyolite of 11.8±0.6 Ma on andesine plagioclase separates. The rhyolite is overlain by basalt, which is in turn overlain by a ledge of cemented conglomeritic sandstone. The overlying lacustrine and fluvial sediments dip generally west-southwest 4–10º. Several northwest-trending normal faults trace through the foothills and beneath downtown Boise (Liberty, 1998). Despite our high elevation at the Table Rock viewpoint, 1,108 m (3,636 ft), we are on a down-thrown block relative to the hill below containing the Miocene rhyolite (figs. 26 and 30). Throw on the fault between the rhyolite and the flat area below is about 210 m (700 ft)(Wood and Burnham, 1987).

All of the state office buildings, many commercial buildings in downtown Boise, and many of the older homes in northeast Boise are heated by hot water from wells. The original two hot water wells were drilled 123-m (404-ft) deep in the warm springs area by the Penitentiary in the early 1900s. They initially had an artesian flow of 351 l/s (550 gallons/minute) of 77° C (170° F) water, but pressure has declined, and the wells must be pumped. The Warm Springs Water District is the oldest geothermal heating district in the United States. The State of Idaho, the U.S. Veterans Hospital, and the city of Boise since the 1980s, produce water from wells 600–920-m (2,000–3,000-ft) deep beneath downtown Boise and along the edge of the foothills. A reinjection well was drilled in 1994 near the State Historical Museum, 5 blocks south of the Convention Center to a depth of 975 m (3,200 ft). Location was based on a seismic reflection survey by Liberty (1998) that imaged the faulted basalt above the rhyolite. Flow from the rhyolite aquifers below 670 m (2,200 ft) was about 57 l/s (900 gallons per minute) of 77° C (170° F) water, and these aquifers have a shutin artesian hot-water-column head of 13 m (43 ft) above ground level. It is the most successful production well, but due to its location at the tail end of the building-heat-circulation system, it is used as a reinjection well. The geothermal aquifer system is in the same fractured rhyolite rock exposed on the upthrown fault block in the foothills below. Production is just now increasing for the city of Boise system to serve new buildings, but it is uncertain whether aquifer pressure and temperature will sustain continued exploitation in this downtown area. The area south of the Boise River has never been explored by deep wells. It is likely the downfaulted aquifer is deeper and hotter immediately to the south.

This is the end of the trip, and vans will return back to the Convention center.

References

Amini, H., Hehnert, H.H., and Obradovich, J.D., 1984, K-Ar ages of late Cenozoic basalts from the western Snake River Plain, Idaho: Isochron/West, v. 41, p. 7–11.

Baksi, A.K., 2004, Discussion and reply: Ages of the Steens and Columbia River flood basalts and their relationship to extension related calc-alkalic volcanism in eastern Oregon: Geological Society of America Bulletin, v. 116, p. 247–250.

Bonnichsen, B., McCurry, M., and Godchaux, M.M., 2004, Miocene Snake River Plain rhyolites of the Owyhee front, Owyhee County, Idaho: this volume.

Bonnichsen, B., White, C.M., and Godchaux, M.M., 1997, Basaltic volcanism, western Snake River Plain, *in* Link, P.K., and Kowallis, B.J., eds., Proterozoic to recent stratigraphy, tectonics and volcanism in Utah, Nevada, southern Idaho and central Mexico: Brigham Young University Geology Studies, v. 42, Part 1, p. 399–422.

Bonnichsen, B., and Kauffman, D.F., 1987, Physical features of rhyolite lava flows in the Snake River Plain volcanic province, southwestern Idaho, *in* Fink, J.H., ed., The emplacement of silicic domes and lava flows: Geological Society of America Special Paper 212, p. 119–145.

Burnham, W.L., and Wood, S.H., 1983, Field Trip Guide, Boise Front Geothermal Area: 12th Annual Rocky Mountain Groundwater Conference, Boise, Idaho, 36 p.

Boone, L. 1988, Idaho place names—A geographical dictionary: Moscow, The University of Idaho Press, 413 p.

Camp, V.E., Ross, M.E., and Hanson, W.E., 2003, Genesis of flood basalts and Basin and Range volcanic rocks from Steens Mountain to the Malheur Gorge, Oregon: Geological Society of America Bulletin, v. 115, p. 105–128.

Cas, R.A.F., and Wright, J.V., 1988, Volcanic successions—Modern and ancient: London, England, Unwin and Hyman, 528 p.

Clemens, D.M., and Wood, S.H., 1993, Radiometric dating, volcanic stratigraphy, and sedimentation in the Boise foothills, northeastern margin of the western Snake River Plain, Ada County, Idaho: Isochron/West, v. 59, p. 3–10.

Clough, B.J., Wright, L.V., and Walker, G.P.L., 1982, An unusual bed of giant pumice in Mexico: Nature, v. 289, p. 49–50.

Cavanagh, B.C., 2000, Western Snake River Plain, Idaho—Fluvial-lacustrine sediments, exhumation estimates from mudstone compaction, unconformity identification by buried soil carbonate, hydraulic conductivity estimates from well cuttings: Boise, Idaho, Boise State University, unpublished M.S. thesis, 96 p.

Davaud, E., and Girardclos, S., 2001, Recent freshwater ooids and oncoids from western Lake Geneva (Switzerland)—Indications of a common organically mediated origin: Journal of Sedimentary Research, v. 71/3, p. 423–429.

Decker, P.L., 1990, Style and mechanics of liquefaction-related deformation, lower Absaroka Volcanic Supergroup (Eocene), Wyoming: Geological Society of America Special Paper 240, 71 p.

Dixon, M.D., and Johnson, W.C., 1999, Riparian vegetation along the middle Snake River, Idaho—Zonation, geographical trends and historical changes: Great Basin Naturalist, v. 59, p. 18–34.

Ekren, E.B., McIntyre, D.H., Bennett, E.H., and Marvin, R.F., 1982, Cenozoic stratigraphy of western Owyhee County, Idaho, *in* Bonnichsen, B., and Breckenridge, R.M., eds., Cenozoic geology of Idaho: Idaho Geological Survey Bulletin 26, p. 215–235.

Ekren, E.B., McIntyre, D.H., Bennett, E.H., and Malde, H.E. 1981, Geologic map of Owyhee County, Idaho, west of longitude 116º W: U.S. Geological Survey Map I-1256, scale 1:125,000.

Ekren, E.B., McIntyre, D.H., Bennett, E.H., 1984, High-temperature, large-volume, lava-like ash-flow tuffs without calderas: U.S. Geological Survey Professional Paper 1272, 76 p.

Gallegos, D., Johnson, P., Wood, S.H., and Snyder, W., 1987, Depositional facies along the Boise front: Northwest Geology, v. 16, p. 47–59.

Halsor, S.P., Bornhorst, T.J., Beebe, M., Richardson, K., and Strowd, W., 1988, Geology of the DeLamar Silver Mine, Idaho—A volcanic dome complex and genetically associated hydrothermal system: Economic Geology, v. 83, p. 1159–1169.

Hart, W.K., Brueseke, M.E., Renne, P.R. and McDonald, H.G., 1999, Chronostratigraphy of the Pliocene Glenns Ferry Formation, Hagerman Fossil Beds National Monument, Idaho: Geological Society of America Abstracts with Programs, v. 31, no. 4, p. A-15.

Hooper, P.R., Binger, G.B., and Lees, K.R., 2002a, Age of the Steens and Columbia River flood basalts and their relationship to extension-related calc-alkalic volcanism in eastern Oregon: Geological Society of America Bulletin, v. 114, p. 43–50.

_____, 2002b, Erratum—Ages of the Steens and Columbia River flood basalts and their relationship to extension-related calc-alkalic volcanism in eastern Oregon:Geological Society of America Bulletin, v. 114, p. 923-924.

Kovscek, A.R., Patzek, T.W., and Radke, C.J., 1995, A mechanistic population balance model for transient and steady-state foam flow in Boise sandstone: Chemical Engineering Science, v. 50, p. 3783–3799.

Liberty, L., 1998, Seismic reflection imaging of a geothermal aquifer in an urban setting: Geophysics, v. 63, p. 1285–1295.

Lofgren, G., 1971, Spherulitic textures in glassy and crystalline rocks: Journal of Geophysical Research, v. 76, p. 5635–5648.

Malde, H.E., and Powers, H.A., 1962, Upper Cenozoic stratigraphy of the western Snake River Plain, Idaho: Geological Society of America Bulletin, v. 73, p. 1197–1220.

Neill, W.M., 1975, Geology of the southeastern Owyhee Mountains and environs, Owyhee County, Idaho: Stanford, California, Stanford University, unpublished M.S. thesis, 59 p.

O'Conner, J.E., 1993, Hydrology, hydraulics, and geomorphology of the Bonneville flood: Geological Society of America Special Paper 274, 83 p.

Ostercamp, W.R., Johnson, W.C., and Dixon, M.D., 2001, Biophysical gradients related to channel islands, middle Snake River, Idaho, *in* Dorava, J.M., Montgomery, D.R., Palcsak, B.B., and Fitzpatrick, F.A., eds., Geomorphic processes and river habitat: American Geophysical Union, Water Science and Application Volume 4, p. 73–83.

Ostercamp, W.R., 1998, Processes of fluvial–island formation, with examples from Plum Creek, Colorado and Snake River, Idaho: Wetlands, v. 18, p. 530–535.

Othberg, K.L., 1994, Geology and geomorphology of the Boise Valley and adjoining areas, western Snake River Plain, Idaho: Idaho Geological Survey Bulletin 29, 54 p.

Othberg, K.L., Bonnichsen, B., Swisher, C.C., III, and Godchaux, M.M., 1995, Geochronology and geochemistry of Pleistocene basalts of the western Snake River Plain and Smith Prairie, Idaho: Isochron/West, v. 62, p. 16–29.

Pazzaglia, F.J., and Brandon, M.T., 2001, A fluvial record of long-term steady-state uplift and erosion across the Cascadia forearc high, western Washington State: American Journal of Science, v. 301, p. 385–431.

Perkins, M.E., Brown, F.H., Nash, W.P., McIntosh, W., and Williams, S.K., 1998, Sequence, age, and source of silicic fallout tuffs in middle to late Miocene basins of the Basin and Range province: Geological Society of America Bulletin, v. 110, p. 344–360.

Perkins, M.E., and Nash, B.P., 2002, Explosive silicic volcanism of the Yellowstone hotspot—The ash-fall tuff record: Geological Society of America Bulletin, v. 14, p. 367–381.

Pierce, K.L., and Morgan, L.A., 1992, The track of the Yellowstone hot spot—Volcanism, faulting, and uplift, *in* Link, P.K., Kuntz, M.A., and Platt, L.B., eds., Regional geology of eastern Idaho and western Wyoming: Geological Society of America Memoir 179, p. 1–53.

Repenning, C.A., Weasma, T.R., and Scott, G.R., 1994, The early Pleistocene (latest Blancan-earliest Irvingtonian) Froman Ferry fauna and history of the Glenns Ferry Formation, southwestern Idaho: U.S. Geological Survey Bulletin 2105, 86 p.

Squires, E., 1992, Hydrogeologic framework of the Boise aquifer system, Ada County, Idaho: Boise, Idaho, Boise State University, unpublished M.S. thesis, (also Research Technical Completion Report 14-08-0001-G1559-06, Idaho Water Resources Institute, Moscow, Idaho, University of Idaho), 114 p.

Squires, E., Liberty, L.M., and Wood, S.H., 2003, Hydrostratigraphic characterization and Quaternary/Neogene history of Boise and Meridian, Idaho using drill-cuttings analysis, borehole geophysical logs, and high resolution seismic images: Geological Society of America Abstracts with Programs, v. 35, no. 6, p. 571.

Swirydczuk, K., Wilkinson, B.H., and Smith, G.R., 1979, The Pliocene Glenns Ferry oolite—Lake-margin carbonate deposition in the southwestern Snake River Plain: Journal of Sedimentary Petrology, v. 49, p. 995–1004.

_____, 1980a, The Pliocene Glenns Ferry oolite—Lake-margin carbonate deposition in the southwestern Snake River Plain—Reply: Journal of Sedimentary Petrology, v. 50, p. 999–1001.

_____, 1980b, The Pliocene Glenns Ferry oolite-II—Sedimentology of oolitic lacustrine terrace deposits: Journal of Sedimentary Petrology, v. 50, p. 1237–1248.

Talbot, M.R., 1990, A review of the paleohydrological interpretation of carbon and oxygen isotopic ratios in primary lacustrine carbonates: Chemical Geology, v. 80, p. 261–279.

Taubeneck, W.H., 1971, Idaho batholith and its southern extension: Geological Society of America Bulletin, v. 82, p. 1899–1928.

Terzaghi, K., and Peck, R.B., 1967, Soil mechanics in engineering practice: New York, Wiley and Sons, 729 p.

Thompson, R.S., 1991, Pliocene environments and climates of the Western United States: Quaternary Science Reviews, v. 10, p. 115–132.

Van Domelen, D.J., and Rieck, H.J., 1992, Paleomagnetic polarity of some vertebrate fossil localities of the Glenns Ferry Formation in the Chalk Hills, near Froman Ferry, western Snake River Plain, southwest Idaho: U.S. Geological Survey Open-File Report 92-542, 6 p.

Young, H.W., Parliman, D.J., and Mariner, R.H., 1988, Chemical and hydrologic data for selected thermal-water wells and non-thermal springs in the Boise area, southwestern Idaho: U.S. Geological Survey Open-File Report 88-471, 35 p.

Walker, R.G., and Plint, A.G., 1992, Wave-and-storm-dominated shallow marine systems, *in* Walker, R.G., and James, N.P., eds., Facies models—Response to sea level changes: Geological Association of Canada, p. 219–238.

White, C.M., Hart, W.K., Bonnichsen, B., and Matthews, D., 2004, Geochemical and Sr-isotopic variations in western Snake River Plain basalts, Idaho, *in* Bonnichsen, B., White, C.M., and McCurry, M., eds., Tectonic and magmatic evolution of the Snake River Plain Volcanic Province: Idaho Geological Survey Bulletin 30, 14 p.

Wong, T.F., David, C., and Zhu, W., 1997, The transition from brittle faulting to cataclastic flow in porous sandstone—Mechanical deformation: Journal of Geophysical Research, v. 102, p. 3009–3025.

Wood, S.H., 1994, Seismic expression and geological significance of a lacustrine delta in Neogene deposits of the western Snake River Plain, Idaho: American Association of Petroleum Geolgists Bulletin, v. 78, p. 102–121.

Wood, S.H., and Clemens, D.L., 2002, Geologic and tectonic history of the western Snake River Plain, Idaho and Oregon, *in* Bonnichsen, B., White, C.M., and McCurry, M., eds., Tectonic and magmatic evolution of the Snake River Plain Volcanic Province: Idaho Geological Survey Bulletin 30, p. 69–103.

Wood, S.H., and Burnham, W.L., 1987, Geological framework of the Boise Warm Springs geothermal area, Idaho, *in* Buess, S.S., ed., Rocky Mountain Section of the Geological Society of America, Centennial Field Guide, v. 2, p. 117–122.

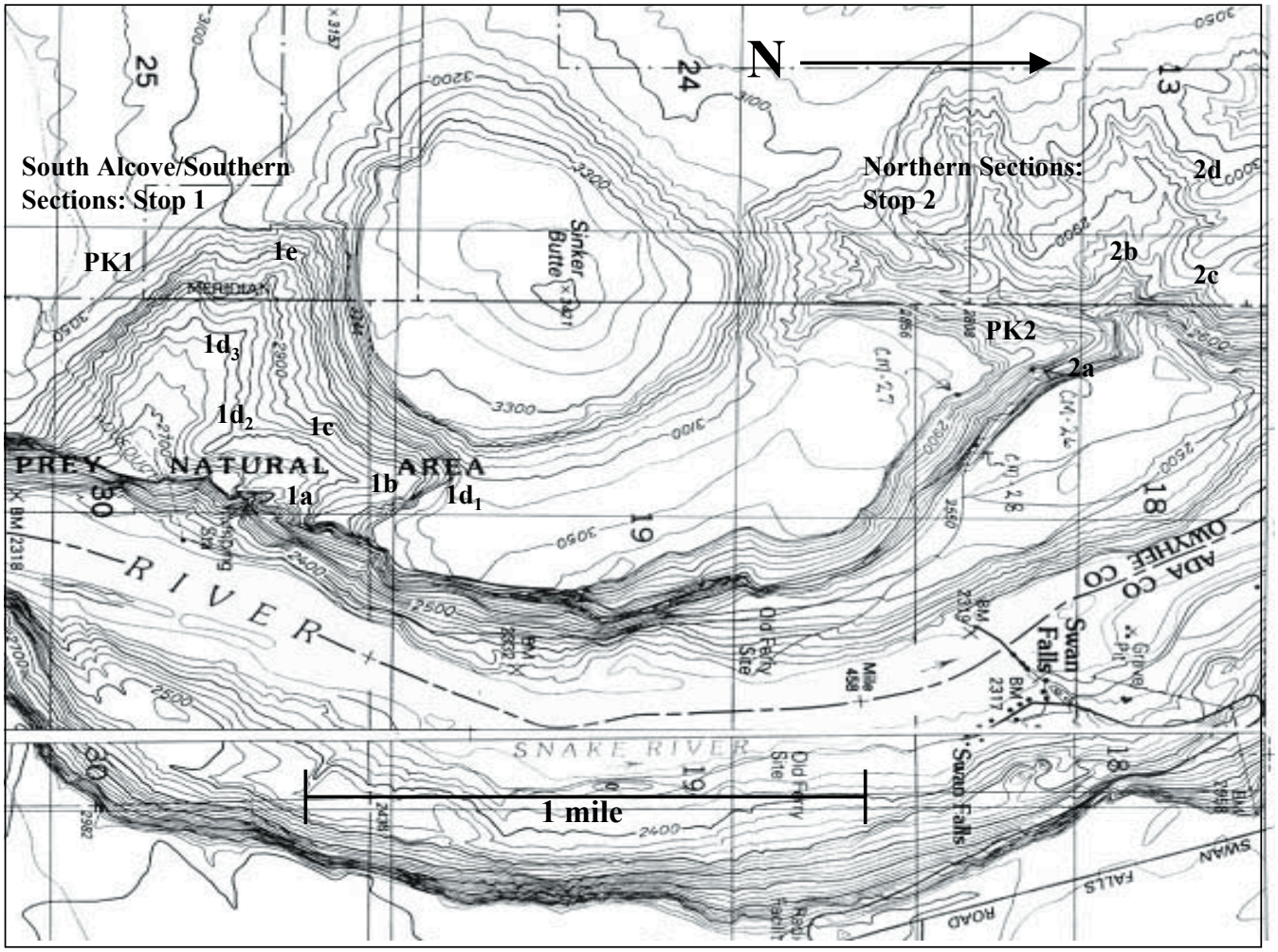

Figure 1. Topographic map of Sinker Butte showing the southern and northern sections with each stop (1a-1e, and 2a-2c) labeled.

Basalt Emergent Volcanoes and Maars, Sinker Butte - Snake River Canyon, Idaho

By Brittany Brand

Introduction

This field trip (fig. 1) offers the opportunity to explore the spectacular, well-exposed, hydrovolcanic tuff beds at Sinker Butte, a Pleistocene volcano that erupted underneath a freshwater lake in the western Snake River Plain (WSRP). The products of basaltic hydrovolcanism (maars, tuff rings, and tuff cones) are second only to scoria cones as the most abundant volcanic landforms on Earth (Cas and Wright, 1988); however, the mechanics of emplacement of these deposits remain poorly understood.

The volcanic stratigraphy at Sinker Butte has been subdivided into three main stages (fig. 2). The first stage of this eruption included deposition of a series of subaqueous tuff deposits as a volcanic-sedimentary platform grew toward the surface of the lake. Within these subaqueous deposits are many forms of cross stratification including channel scour and fill, dune bedding, trough cross bedding, and Bouma-turbidite sequences.

As the eruption progressed, the platform built above the water level, which represents the subaerial stage of the eruption (fig. 2). During this stage, the magma/water interaction was still significant, and caused a pulsatory type of eruption creating many thin interbedded-pyroclastic surge and fall deposits. Near the vent, large-scale, regressive, low-angle cross strata (wavelength 1–2 m) are found interbedded with thin planar beds. Regressive cross strata are analogous to antidunes, the crests of the strata migrate upstream with the coarser fragments deposited on the upstream side. The presence of accretionary and (or) armored lapilli, as well as vesicles due to trapped volatiles in wet ash, suggest emplacement by wet surges. Cross strata in deposits farther from the vent are generally thinly bedded and have gentler dip angles and shorter wavelengths. Other types of cross stratification found at Sinker Butte are wavy-planar beds, which are a mixture of fall and surge deposits, and deformed low-angle cross-stratified beds (0.5- to 1-m wavelength) containing abundant soft sediment deformation and sag structures. High in some sections are large-scale progressive cross strata (1- to 2-m wavelength) possibly deposited during a late-stage dry surge towards the end of eruption, just before the volcano isolated itself from all external water.

The low-angle cross stratification and irregular truncations reflect the highly pulsatory nature of surges during deposition. Cross-stratified bed thickness and average wavelengths decrease away from the vent. The fine cross stratification may be result of the same type of surges that formed the larger regressive cross strata, but may represent a loss in momentum,

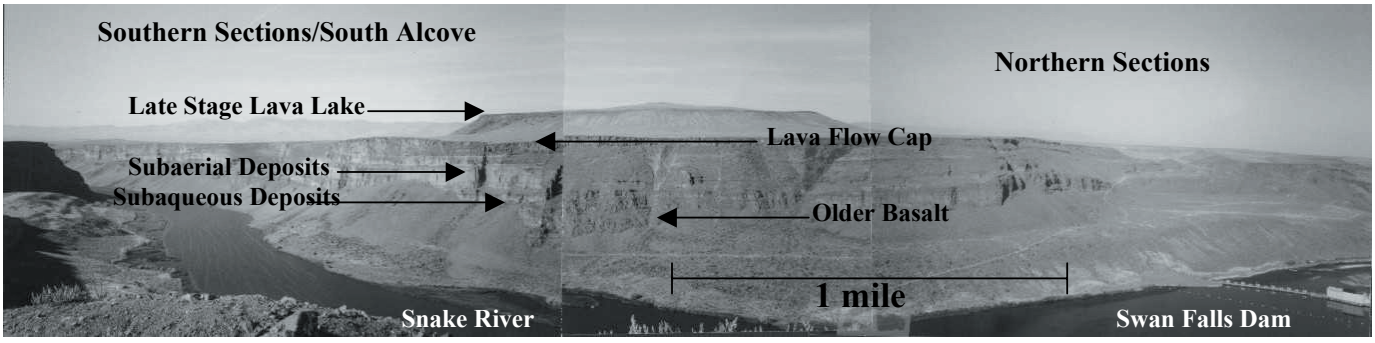

Figure 2. Sinker Butte as viewed from Swan Falls Road on the east side of the Snake River canyon. In this photo you can see the underlying older Swan Falls basalt deposits, the subaqueous deposits, the subaerial deposits, the lava flow cap, and the late-stage lava lake. Also identified are the southern and northern sections, as well as Swan Falls Dam.

Department of Geosciences, Boise State University, Boise, ID 83725,
BrittanyBrand@mail.boisestate.edu

sediment load, and heat as the surge travels farther from its source.

During the third and final stage of the eruption, the volcano effectively sealed itself off from external water and ended with a Strombolian lava flow that caps older deposits (fig. 2).

Geologic Setting of the Western Snake River Plain

The Snake River Plain extends across southern Idaho in a continuous arc. It is distinguished by its lower topography, and it contains several thousand feet of late Tertiary and Quaternary volcanics and sediments (Smith and Wilkinson, 1991). Mabey (1982) divided the plain into three parts: the northwest-trending western Snake River plain, the northeast-trending eastern Snake River Plain, and the central Snake River Plain between them. The eastern Snake River Plain (ESRP) is thought to have formed from the interplay of magmatism and extension associated with the Yellowstone hot spot (Parsons and others, 1998). The western Snake River Plain (WSRP) is a basin-and-range structure whose formation was triggered by the magmatism of the migrating Yellowstone hot spot (Clemens, 1993). Each of these parts of the plain has significant tectonic differences, but for the purposes of this study we will only focus on those in the western Snake River Plain.

The WSRP trends northwest and is the site of an extensive rift zone that widened perpendicular to the Yellowstone hot spot path. It is a depression with normal faults on both edges (Malde, 1965). The popular model for the formation of the WSRP is that a system of symmetrically-disposed half-grabens formed beyond the parabolic-shaped "wake" as the hot spot passed by (Anders and others, 1989; Pierce and Morgan, 1992). A problem with this model is there is no similar graben structure south of the path of the Yellowstone hot spot (Wood and Clemens, 2002).

Most of the northwestern portion of the WSRP is covered with Quaternary alluvium, whereas in the southeastern portion the dominant rocks are Tertiary and Quaternary lacustrine sediments and basalt flows. The plain is thought to have started extending around 11.6 to 10 m.y. ago (Bonnichsen and others, 1997), resulting in bimodal volcanism.

The volcanism in the WSRP region began with extrusion of rhyolitic lavas followed by the eruption of basalt and ash-flow tuffs. As the plain pulled apart and subsided, a lake, or succession of lakes, known as Lake Idaho formed (Godchaux and others, 1992). Volcanic activity occurring when the lake was present resulted in many spectacular examples of three major types of phreatomagmatic volcanoes: emergent, subaqueous, and subaerial. Emergent volcanoes, like Sinker Butte, began erupting under water and eventually build a volcanic edifice above the lake level. Subaqueous volcanoes erupt under water and never build above the lake level. Finally, subaerial volcanoes erupt through a buried aquifer system and produce classic maar volcanic features. All of these volcanic systems contain a significant amount of water, causing a high magma/water interaction. Emergent and subaqueous volcanoes usually form gently sloping tuff cones, whereas subaerial volcanoes form maars or tuff rings (Godchaux and others, 1992).

The WSRP is an excellent area to study phreatomagmatic eruptions and hydrovolcanism. Godchaux and others (1992) put it best when they stated, "This field has great potential for advancing our understanding of eruption mechanisms resulting from magma/water interactions across the entire magma/water-ratio spectrum."

ROAD LOG

Mileage Cum.	Inc.	
0.0	0.0	Trip starts from Bank of America Center on the corner of 9th and Front Streets.
1.68	1.53	Turn RIGHT onto W. FRONT STREET/US-20 W/ US-26 W. Continue to follow US-20 W/ US-26 W.
4.39	2.71	Stay straight to go onto I-184 W.
18.14	13.75	Merge onto I-84 W/ US-30 W via the exit- on the left.
18.41	0.27	Take the FRANKLIN BOULEVARD exit—exit number 36.
19.35	0.94	Turn LEFT onto FRANKLIN BOULEVARD.
20.16	0.81	Turn RIGHT onto 11TH AVENUE N/ I-84 BOULEVARD.
20.23	0.07	Turn LEFT onto E. 3RD STREET S/ ID-45 S.
38.0	17.77	Turn RIGHT onto 12TH AVE S/ ID-45. Continue to follow ID-45.
52.7	14.70	ID-45 becomes ID-78.
57.3	4.6	Turn left on first road past Murphy (road name is Murphy Flat Road, but there is no road sign).
60.3	3.0	Turn Left on Sinker Butte Road.
62.22	1.92	Turn Right on farm road just before barn (you will drive through the farm, between the agricultural fields). Continue straight through fence towards Butte. Park on south side of Butte.

Stop 1. South Alcove-Proximal Deposits

The South Alcove (fig. 2) contains the deposits nearest the vent. We will spend the first half of the day here, exploring and examining many of the exposed sections within the canyon walls. We will begin by observing deposits that mark the beginning of the eruptive sequence (fig. 1, Stop 1a). These are the units deposited subaqueously (fig. 3). Notice that the sequence begins with a massive, fine, white unit, which occurs around the entire volcanic edifice. This white unit is reworked lake sediment with incorporated juvenile and accidental fragments. The accidental fragments are pieces of older basalt or rip-up clasts of underlying siltstone and lake deposits. Above the white unit is a massive orange block lapilli tuff unit. Within this massive unit are many accidental blocks and clasts, as well as some juvenile clasts. In some areas, the deposits are massive, in other areas cross stratification and channel scours occur. The variations are indicative of a volcanic platform growing closer to the surface of the water causing turbidite sequences, channelization, and wave-base affects.

An extremely sharp contact occurs between the lower subaqueously deposited tuffs and the subaerial tuffs (fig. 3). The subaerial units are planar, fine-grained, well sorted, even thickness, laterally continuous, orange, palagonitic tuffs that contain a mixture of accidental and juvenile fragments. The accidental fragments are older basalts and siltstones. These are interpreted to be subaerial due to the presence of accretionary and armored lapilli, which indicates that there was enough condensing steam and heat to cause fine ash to adhesively clump together or plaster onto other grains. The presence of palagonite also indicates that there were significant amounts of heat and steam present. Vesiculated tuffs are present and form when volatiles get trapped within fine wet ash. Had these deposits been subaqueous, there would have been too much water and not enough heat to cause these depositional processes to occur.

We will walk up section examining these planar tuff beds. They continue for many tens of meters, and are interpreted to be a combination of fallout and low-density pyroclastic surge deposits. They vary slightly in thickness (4–10 cm) and grain size (alternating fine and coarse ash). These differences can be attributed to the pulsating nature of emergent volcanoes, each pulse of eruption being slightly different in force, sediment load, heat, water, and water vapor.

Stop 1b (fig. 1) is located just up section and west-southwest of the deposits we have observed. Here we see one of the most interesting things in the South Alcove: large, low-angle regressive cross strata (wavelength ~1–2 m, height ~1 m, fig. 4). These beds occur at several horizons throughout the subaerial tuffs and can be traced across the entire South Alcove. Wet pyroclastic surges are 3-phase flows that include gas, water, and particles (unlike dry surges which are 2-phase, containing gas and particles). The water causes the particles to plaster against the stoss side of the dune forms, causing the crests of regressive cross strata to migrate upstream and the coarser fragments to fall on the upstream side of the crest (Cas and Wright, 1988). These deposits also contain accretionary and armored lapilli, as well as vesicles in the fine ash, which supplies more evidence for a wet surge.

Stop 1c is farther northwestward in the alcove (fig. 1). High in this section is a light-colored unit that contains abundant cross stratification, block sags, and soft-sediment deformation (fig. 5). This unit is overlain by a planar/wavy bedded, orange, palagonitic tuff that also contains soft-sediment deformation. The abundant block sags and soft-sediment structures indicate that these tuffs were quite wet when deposited, suggesting a renewed source or influx of external water during the eruption.

As we make our way westward, toward the back of the South Alcove, we find many impressive radial dikes that cut the deposits (fig. 1, Stop 1d). The dikes broke out through the tuff cone during the later stages of the eruption and may have been the source of the lava flow that caps the deposits (fig. 6).

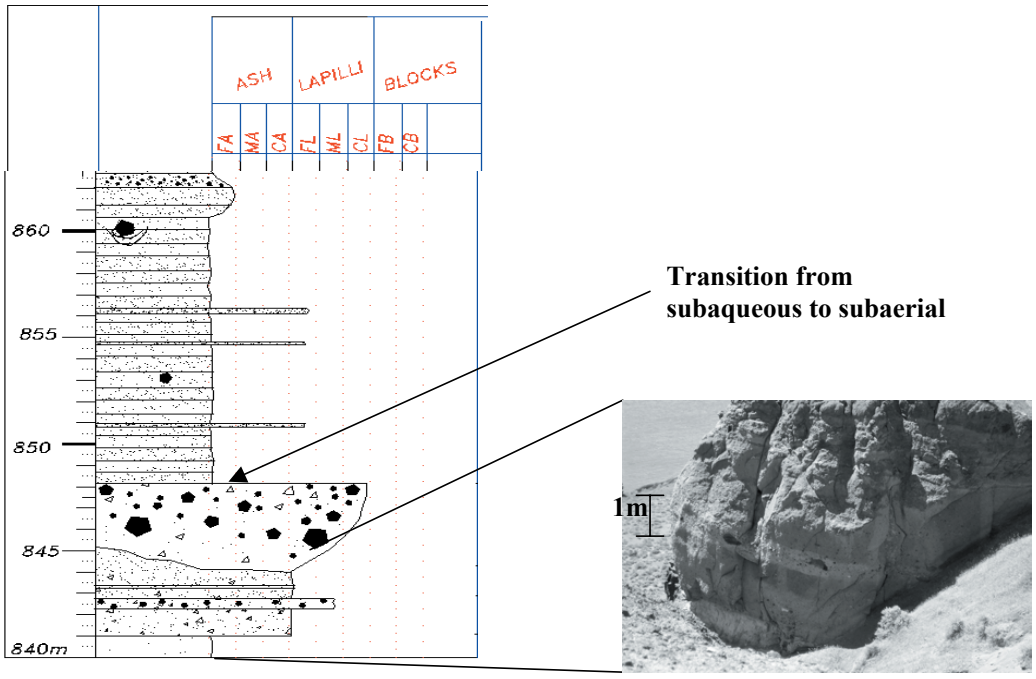

Figure 3. Stop 1a—Subaqueous deposits found within the canyon walls of the South Alcove.

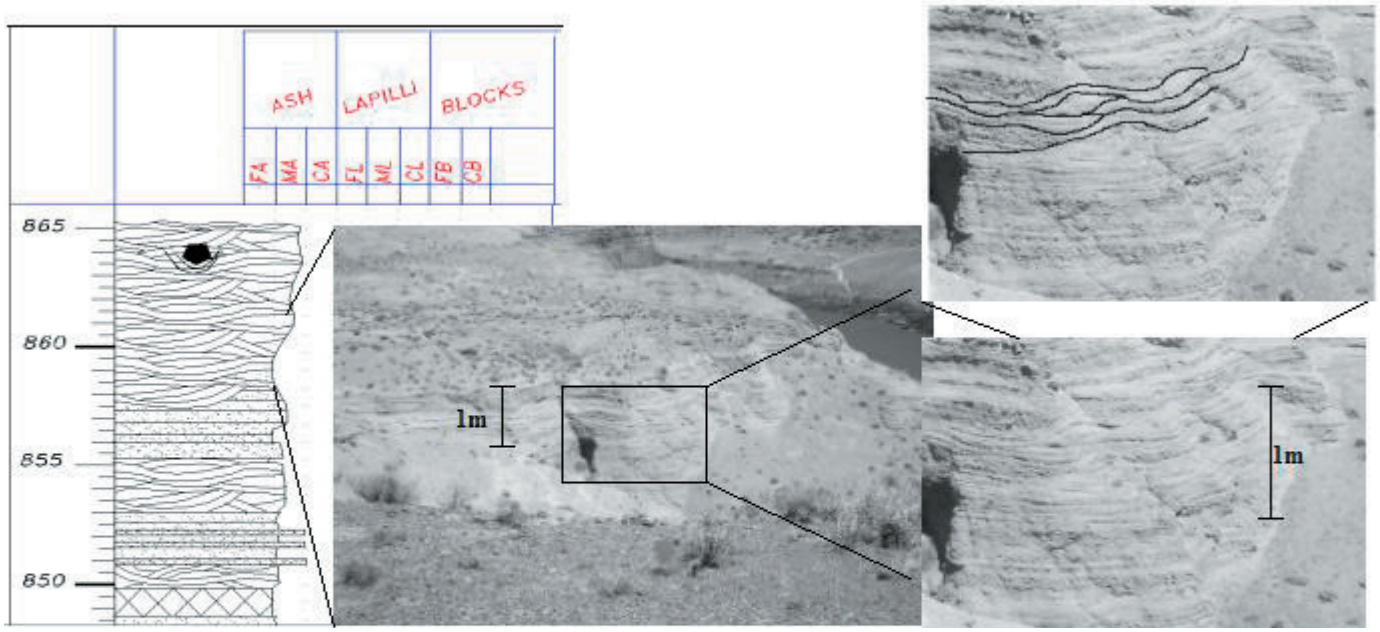

Figure 4. Stop 1b in South Alcove. These are the regressive dune beds found within the southern section. The sediment builds up on the stoss-side of the dune forming “anti-dunes”.

Finally we walk up towards the back of the South Alcove (fig. 1, Stop 1e), high in the eruptive sequence, to observe some brecciated tuff beds that are part of the inner and outer crater walls dipping away from the vent at 20° SE. and into the vent at 35° NW. (fig. 7). The beds that dip into the vent truncate each other at steep angles, indicating that some of the accumulated sediment had avalanched back into the vent.

Mileage Cum.	Inc.	
64.1	1.88	Drive to the north side of the Butte.

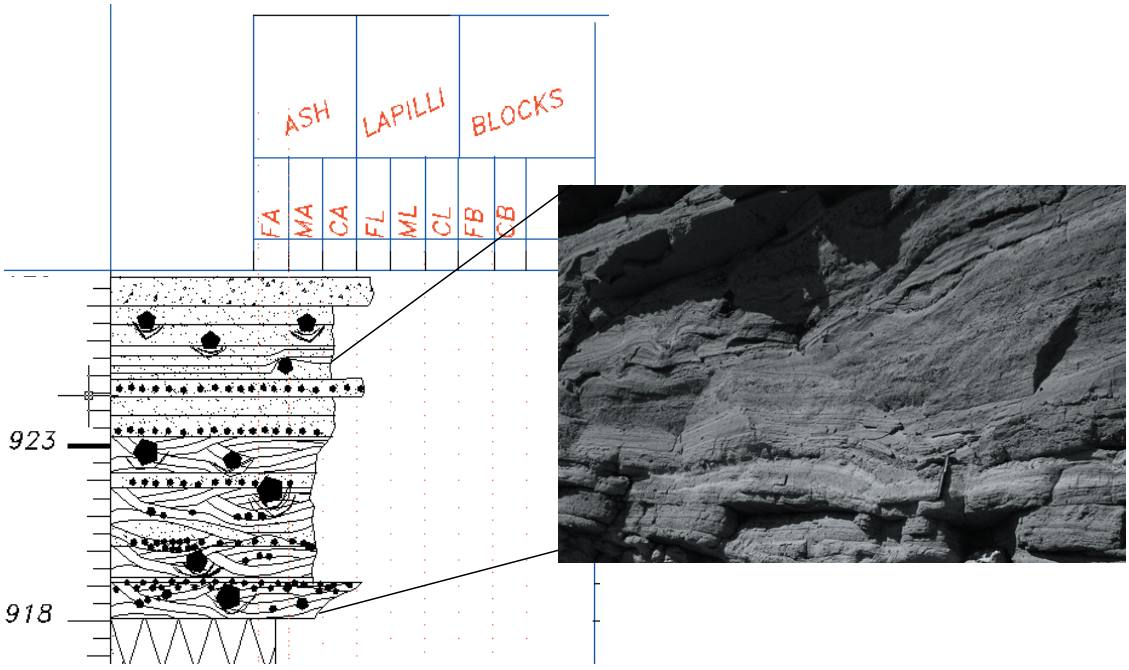

Figure 5. Stop 1c in South Alcove. This unit contains abundant bombs with bomb sags and soft-sediment deformation. These sediments show that during the eruption the water/magma ratio increased. Hammer for scale.

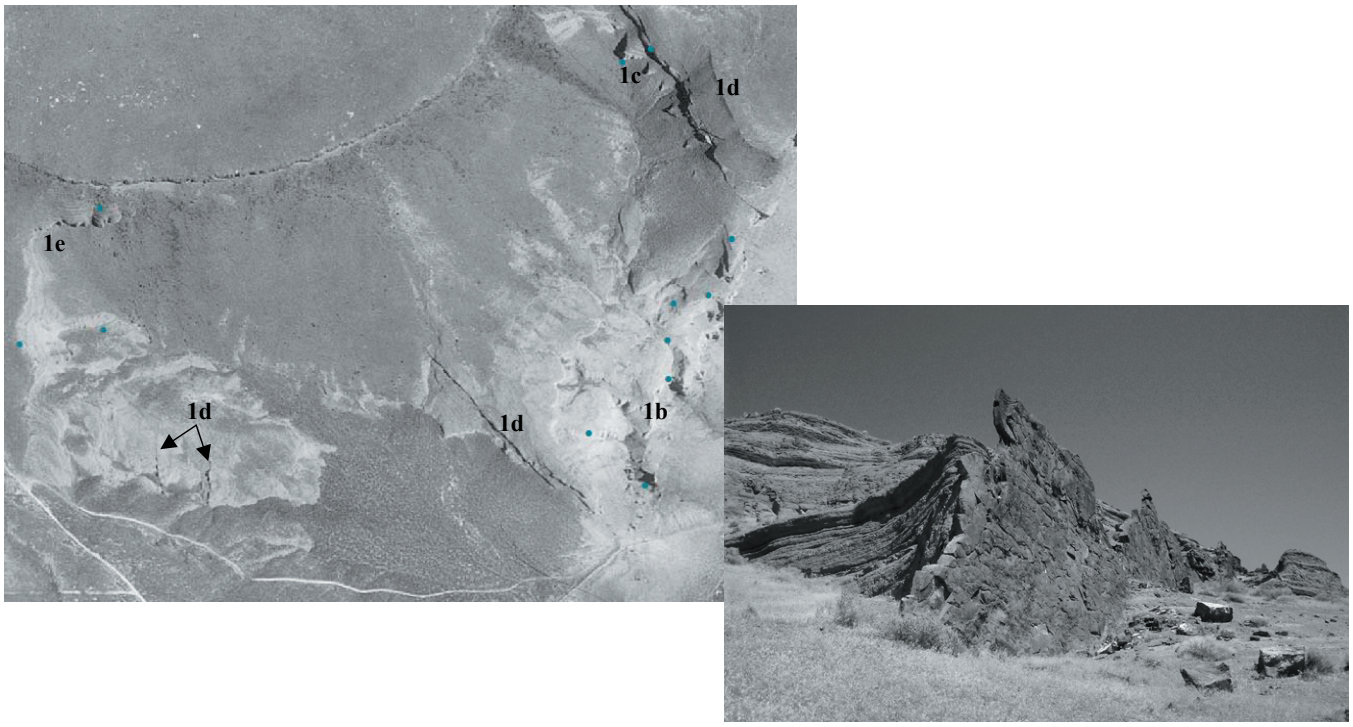

Figure 6. Ortho-photo quad (left) of the northwest corner of the southern alcove (Stop 1d). I also have identified some of the other stops. Notice the dark radial dikes that run through the deposits. Dike cutting through subaerial tuff deposits (right).

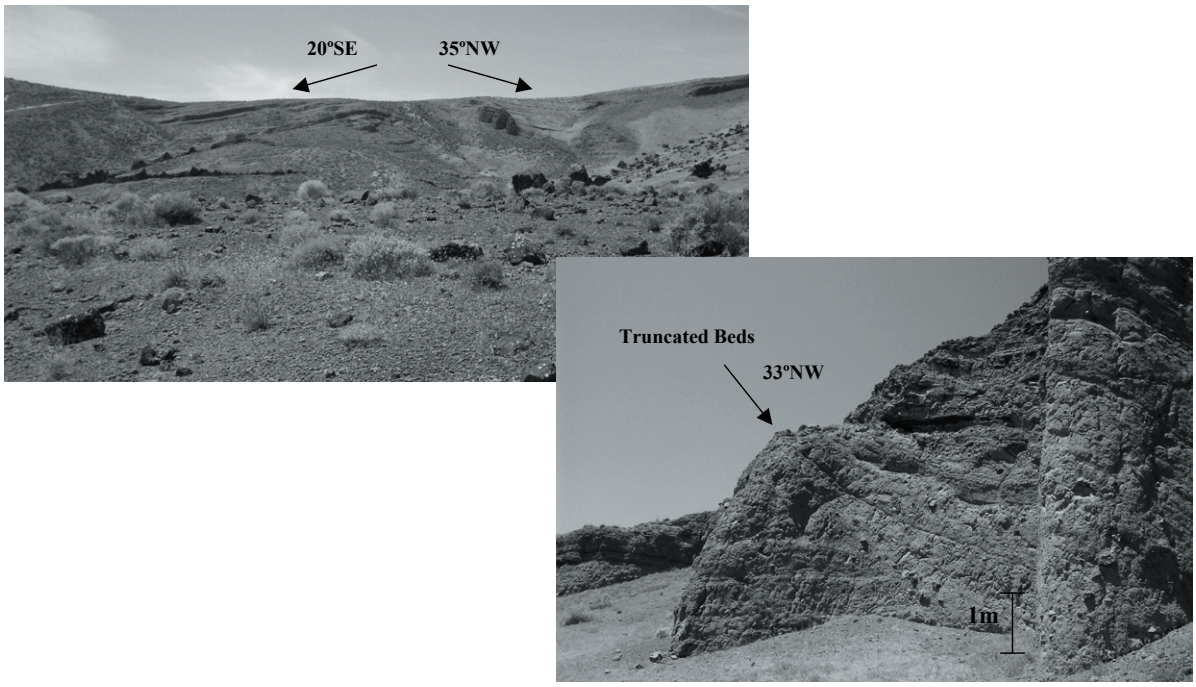

Figure 7. Final stop (Stop 1e) within the South Alcove. Here we are looking at the crater-wall deposits. View of the inner and outer crater walls (left). Note the opposing dip angles. Picture of the deposits that dip into the crater truncating one another. Truncation indicates avalanching into the crater after deposition.

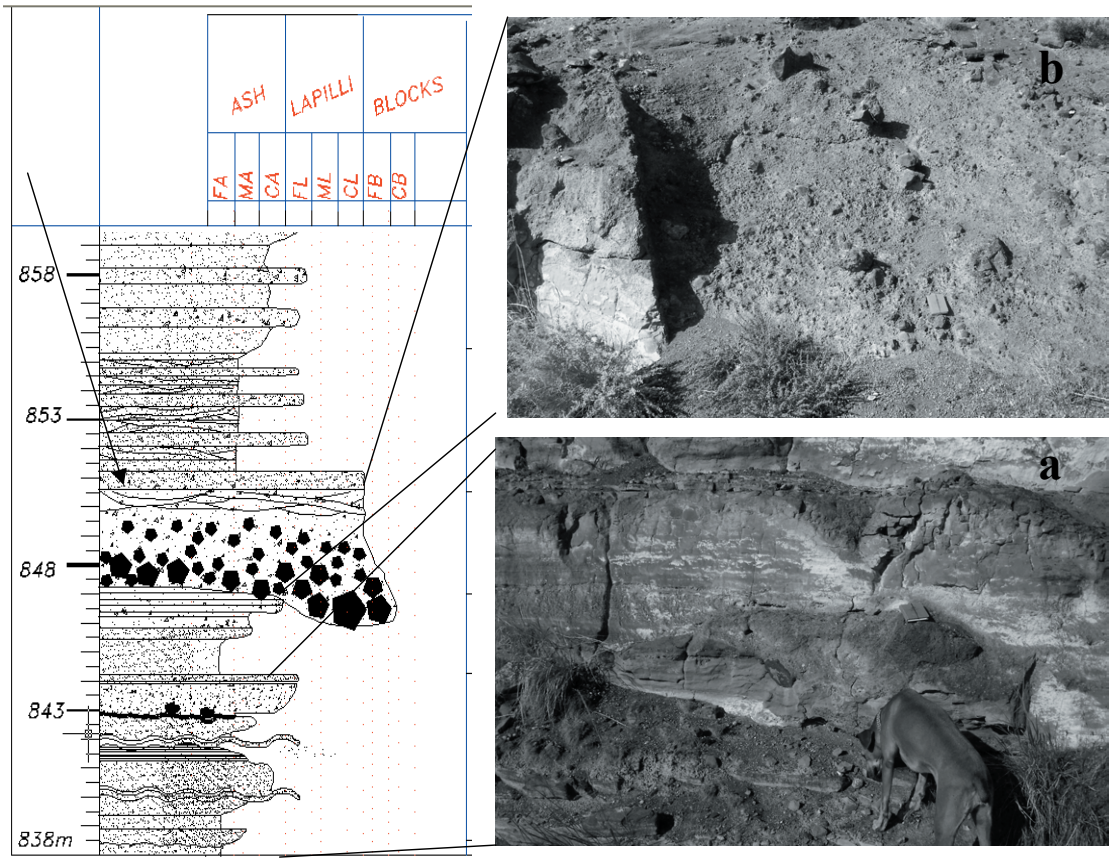

Figure 8. First stop in the northern sections (Stop 2a). We begin here by observing the subaqueous deposits up through to the transition into subaerial deposits. (a.) A Bouma sequence can be identified in the lower subaqueous deposits (dog for scale). (b.) This grades up into massive debris flow deposits (field book 19 x 12 cm for scale). The contact between the subaerial and subaqueus deposits is quite sharp. Notice the finely cross-stratified planar beds.

Stop 2. North Sections—Medial and Distal Deposits

Our second set of stops will be in the medial to distal portions of the deposits, which differ from those proximal to the vent. We will walk down the canyon along a gravel road examining the subaqueously deposited tuffs (fig. 1, Stop 2a) and then work our way up through the subaerial tuffs. The first unit in the sequence is much like the first one in the South Alcove. It consists of a fine-grained, massive, white tuff that is interpreted to be reworked lake sediment with accidental and juvenile clasts (similar to the white unit found in the south). Above this unit are cyclic beds that are analogous to a Bouma sequence (fig. 8a). Continuing up through the section, we encounter large erosive debris flows as well as large-scale cross stratification and channel scour and fills (fig. 9b). All of these units were deposited subaqueously and are a consequence of the volcanic platform growing progressively closer to the surface of the lake.

Above the subaqueous tuffs with again an extremely sharp contact are the subaerial tuff deposits (fig. 9a). These tuffs, like the proximal tuffs, contain accretionary and armored lapilli, as well as abundant amounts of palagonite. They differ from the proximal tuffs as follows: (1) beds alternate from planar to low-angle cross-stratified beds with an average wavelength of less than 10 cm (fig. 9b), (2) the tuffs alternate from fine ash to coarse ash, (3) contain a mix of accidental (older basalt and siltstone) and juvenile clasts, and (4) the overall wavelength of the cross stratification increases higher in the section. Cas and Wright (1988) interpreted such cross-stratified sedimentary features to be due to high velocity, current driven grain layers being sheared over an irregular, surface of low relief due to high bed-shear stress. The deposits at Sinker Butte suggest the same type of emplacement as turbulent, wet, low-density pyroclastic surges were codeposited with airfall deposits.

Coarse interbeds (up to 1-m thick) of ash- to lapilli-sized, juvenile, cinder-like layers are found within the orange tuffs. The beds increase in grain size, thickness, and abundance up section until they dominate the deposits. These juvenile beds become more abundant up section which suggests that the eruption was “drying out”, or the influx of external water was being depleted and no longer having as much effect on the magma.

The next unit upward consists of thick, massive, tuff breccias containing abundant accidental and some juvenile clasts within a medium- to coarse- ash matrix (fig. 10). These massive beds introduce new accidental clasts consisting of rounded river gravel and siltstone, which is evidence for downward coring of the volcano. This massive unit almost certainly indicates a new stage in the eruptive sequence involving more water. The rounded river gravels and the water-affected deposits suggest that as the volcano cored

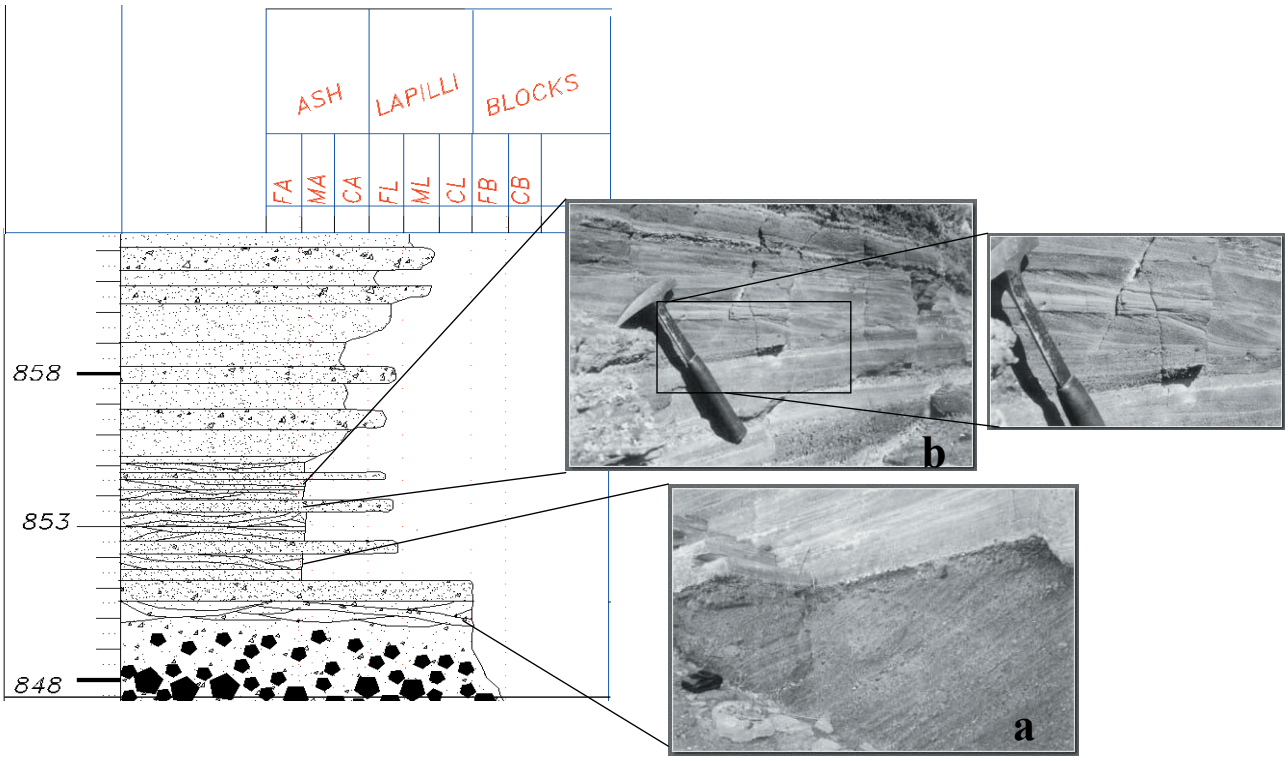

Figure 9. Column located high in the section at Stop 2a. (a.) The abrupt transition from the subaqueous deposits into the subaerial deposits. (b.) The fine cross-stratification in this section. (Camera case for scale in a; hammer for scale in b.)

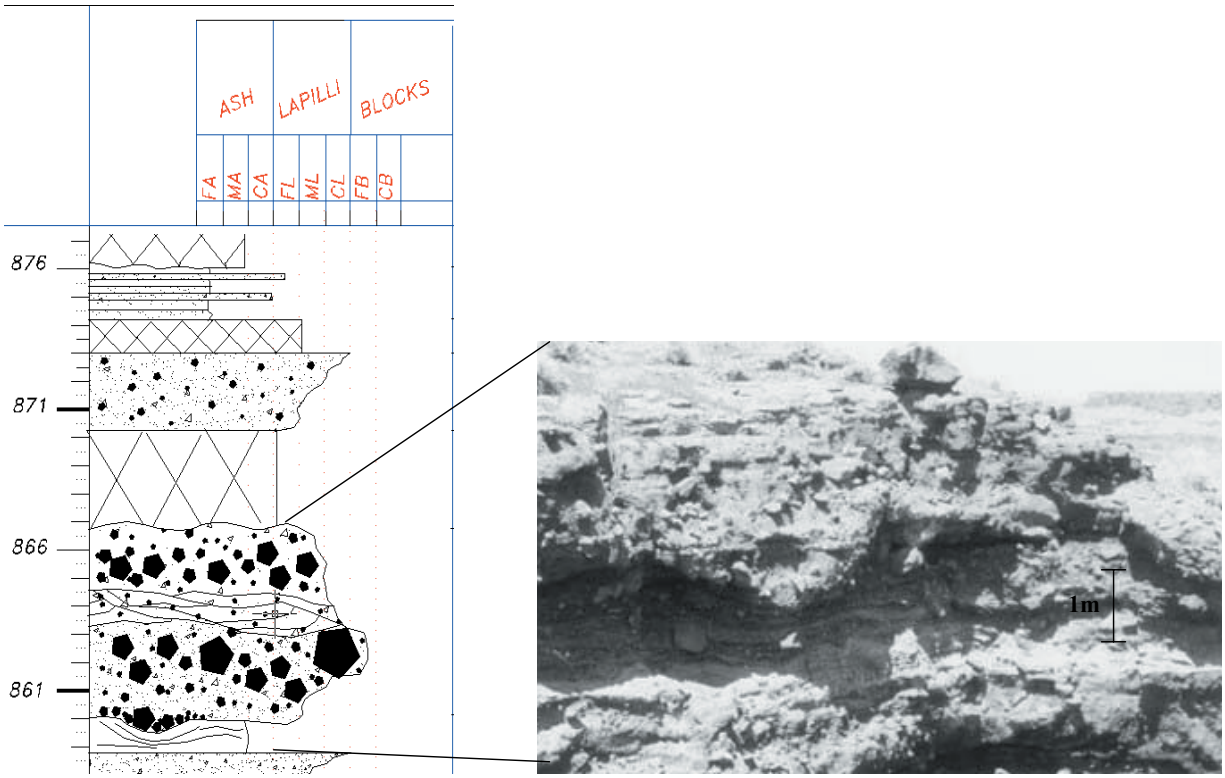

Figure 10. Deposit found just above the previous subaerial deposits (Stop 2a). These massive deposits represent an eruptive event involving additional water. Notice that the blocks have reverse grading.

Figure 11. Pictures of the more distal outcrops (Stops 2b, on left, and 2c, on right). Notice the wavy stratification, abundant sags under large clasts, and soft sediment deformation. This may indicate that more water was condensing as the pyroclastic flows cooled and slowed further from the vent, creating these "wetter" looking deposits (tired dog for scale in both, she is nearly 1 m).

downward into the underlying stratigraphy, it may have hit an aquifer exposing a new influx of water. Above these massive units are more orange, planar, and cross-stratified tuffs with interbeds of juvenile layers. These are followed by the lava flow capping the deposits, which indicates that the volcano effectively isolated itself from all external water and became Hawaiian or Strombolian in nature.

Next we will continue hiking northwest around different outcrops throughout the north section until we reach the most distal deposits in the area (fig. 1, Stop 2b and 2c). We will see the same sequence of planar and cross-stratified tuffs transitioning into massive tuff breccias (fig. 11). Notice that as we get more distal from the vent, the deposits tend to look "wetter". There is a lot of wavy bedding, block sags, and soft sediment deformation. This suggests one of two interpretations. The first is that these deposits either are flowing back down into or towards the body of the lake and being affected by water. The second is that as the surges cool, more water condenses and creates "wetter" deposits.

The last stop of the trip is high in the northern section (fig. 1, Stop 2d). Present here are large, low-angle, cross-stratified beds (fig. 12). Unlike the large regressive cross strata we observed in the Southern Alcove, these are progressive and analogous to normal sedimentary dune beds. The wavelength of the dunes is approximately 2–3 m, and the height is around 1 m. They are internally massive with the juvenile and accidental clasts supported within a fine-ash matrix. There are no apparent accretionary or armored lapilli, and the deposits are much finer grained than the other massive beds closer to the vent.

These cross-stratified beds suggest emplacement by a dry surge and represent a drying out of the eruption in the latest stages before the volcano was completely isolated from external water. The general lack of accretionary/armored lapilli, as well as the progressive cross strata, supports this interpretation.

Conclusions

On this trip we observe, discuss, and argue about the depositional environments, mechanics of emplacement, and the resulting deposits of an emergent hydrovolcano. Within the unique and diverse volcano-clastic deposits, we observe how the changes in the magma/water ratio affect the evolution of the volcano as the eruption progresses, as well as the many changes that occur from proximal to distal. I hope that this field excursion has peaked your interest, answered questions, and created new arguments and theories regarding these types of eruptions and their subsequent deposits.

References

Anders, M.H., Geissman, J.W., Piety, L.A., and Sullivan, J.T. 1989, Parabolic distribution of circumeastern Snake River Plain seismicity and latest Quaternary faulting—Migratory pattern and association with the Yellowstone hotspot: Journal of Geophysical Research, v. 94, p. 1589–1621.

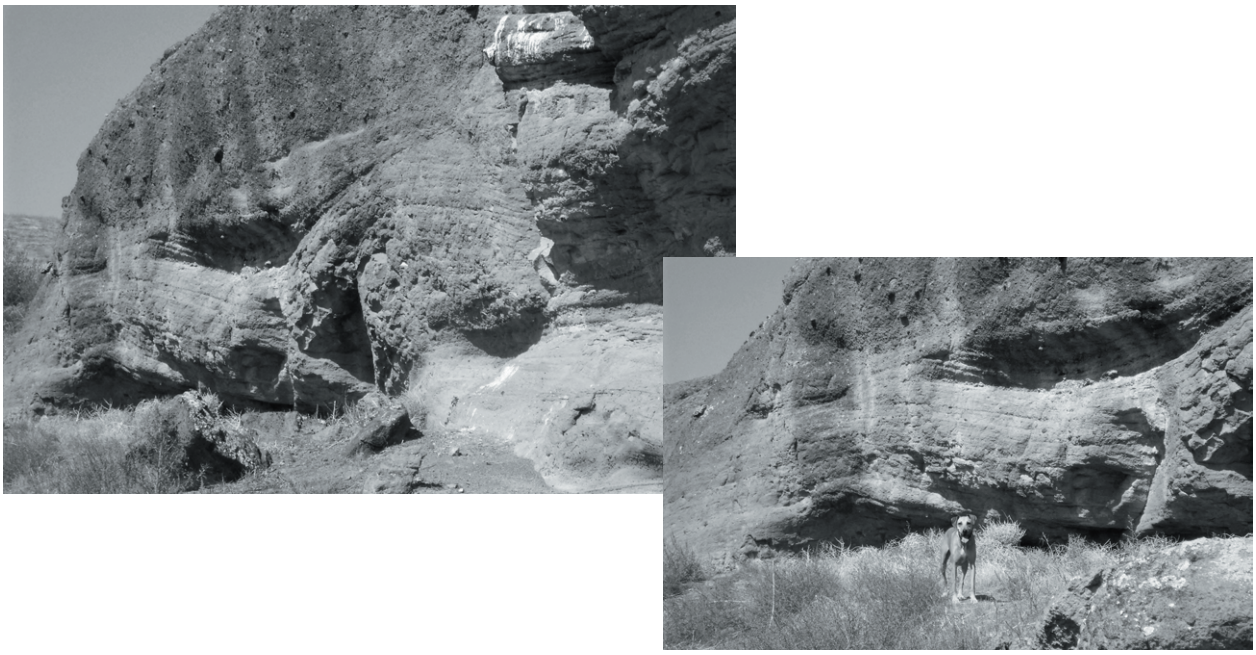

Figure 12. Large-scale cross-stratified progressive dune beds at Stop 2d, which is the last stop of the day. The progressive nature is characteristic of a dryer surge deposit, which suggests that the magma/water ratio during this later stage of the eruption was decreasing (tired dog for scale).

Bonnichsen, B., White, C.M., and Godchaux, M.M., 1997, Basaltic volcanism, western Snake River Plain, *in* Link, P.K., and Kowallis, B.J., eds., Proterozoic to recent stratigraphy, tectonics and volcanism in Utah, Nevada, southern Idaho and central Mexico: Brigham Young University Geology Studies, v. 42, Part 1, p. 399–422.

Cas, R.A.F. and Wright J.V., 1988, Volcanic successions—Modern and ancient*:* London, England, Unwin and Hyman, Ltd., 528 p.

Clemens, D.M., 1993, Tectonics and silicic volcanic stratigraphy of the western Snake River Plain, Idaho: Tempe, Arizona State University, unpublished M.S. thesis, 209 p.

Godchaux, M.M., Bonnichsen, B., and Jenks, M.D., 1992, Types of phreatomagmatic volcanoes in the western Snake River Plain, Idaho, USA: Journal of Volcanology and Geothermal Research, v. 52, p. 1–25.

Mabey, D.R., 1982, Geophysics and tectonics of the Snake River Plain, Idaho, *in* Bonnichsen, B., and Breckenridge, R.M., eds., Cenozoic geology of Idaho: Idaho Geological Survey Bulletin 26, p. 139–154.

Malde, H.E., 1965, Snake River Plain, *in* Wright, H.E., Jr., and Frey, D.G., eds., The Quaternary of the United States: Princeton University Press, p. 255–263.

Parsons, T., Thompson, G.A., and Smith, R.P., 1998, More than one way to stretch—A tectonic model for extension along the plume track of the Yellowstone hotspot and adjacent Basin and Range Province: Tectonics, v. 17, p. 221–234.

Pierce, K.L., and. Morgan, L.A, 1992, The track of the Yellowstone hot spot—Volcanism, faulting, and uplift, *in* Link, P.K., Kuntz, M.A., and Platt, L.B., eds., Regional geology of eastern Idaho and western Wyoming: Geological Society of America Memoir 179, p. 1–53.

Smith, G.R., and Wilkinson, B.H., 1991, Rift geology and sedimentology of the western Snake River Plain Arco field trip: Field Trip Guide.

Wood, S.H., and Clemens, D.M., 2002, Tectonic and magmatic evolution of the Snake River Plain volcanic province, *in* Bonnichsen, B., McCurry, M., and White, C., eds., Tectonic and magmatic evolution of the Snake River Plain volcanic province: Idaho Geological Survey Bulletin 30, p. 69–103.

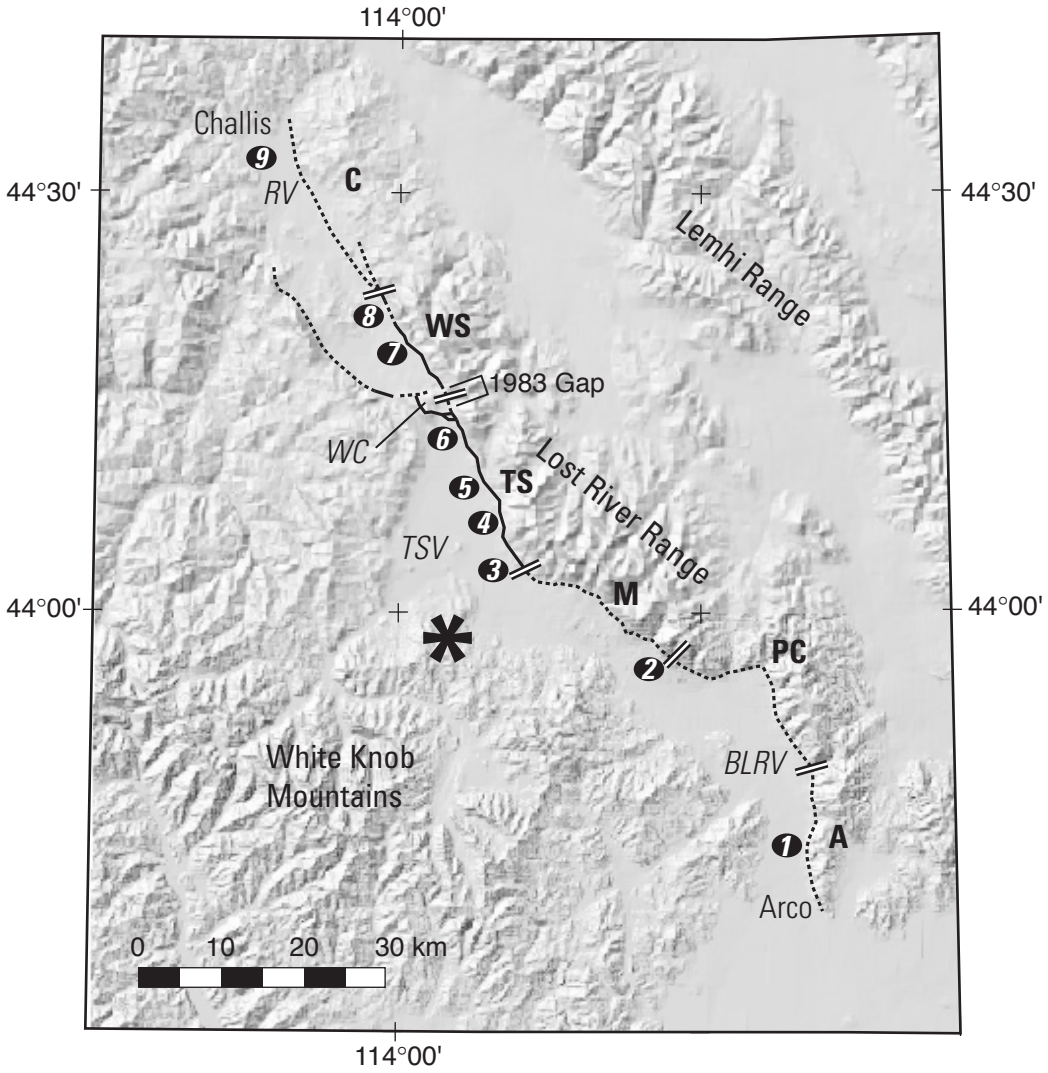

Figure 1. Map of Lost River fault and location of the Borah Peak earthquake (M 7.3, star) in east-central Idaho. Solid line shows the 1983 surface rupture on the Lost River fault; dotted line shows unruptured parts of the fault. Field-trip stops are shown by numbered circles. Selected locations are Big Lost River Valley (BLRV), Round Valley (RV), Thousand Springs Valley (TSV), and Willow Creek hills (WC). Segments, from south to north, of the Lost River fault are bounded by double black line: Arco (A), Pass Creek (PC), Mackay (M), Thousand Springs (TS), Warm Spring (WS), and Challis (C).

Twenty Years After the Borah Peak Earthquake—Field Guide to Surface-Faulting Earthquakes Along the Lost River Fault, Idaho

By Kathleen M. Haller and Anthony J. Crone

Introduction

The spectacular range front on the southwestern side of the Lost River Range has caught the attention of many geologists in the past century. Anderson (1934) and Livingston (1934) were the first to document that faulting was, in part, responsible for the abrupt range front; however, other investigators speculated that erosion was the causative agent (*e.g.*, Ross, 1937, 1947) or that the abrupt range front was caused by thrust faulting (*e.g.*, Kirkham, 1927). Thereafter, Baldwin (1943, 1951) clearly documented the Basin-and-Range style of faulting in this area, as well as the recency of movement and large amounts of throw across the Lost River fault and nearby faults. His 1951 article is one of earliest to use the name Lost River fault for this structure, which defines the 140-km-long southwest flank of Lost River Range (fig. 1). In the late 1960s and early 1970s, the seismic potential of this fault was confirmed in trenching studies by Malde (1971). On October 28, 1983, the Borah Peak (M 7.3) earthquake (fig. 2) ruptured 34 km of the central part of the Lost River fault. Following the earthquake, preliminary results from a multitude of geophysical, hydrologic, geologic, and seismologic studies were summarized in a special volume on the earthquake (Stein and Bucknam, 1985). These studies made the Borah Peak earthquake one of the most comprehensively documented historical ruptures at the time. Only six major, historical normal, surface-rupturing earthquakes have occurred in the intermountain west, thus every one is important and contributes new insight into our understanding of the coseismic failure of major range-front normal faults in extensional tectonic settings.

The Basin-and-Range region of Idaho north of the Snake River Plain, including the Lost River Range and ranges to the east (fig. 3), has a long and complex orogenic history. The mountain blocks are structurally and geomorphically similar to those elsewhere in the Basin and Range province (Reynolds, 1979) in that they are the result of extension on range-front normal faults; however, bedrock in these ranges records episodes of tectonic deformation that occurred in earlier stress regimes. The mountain blocks are composed of allochthonous Precambrain and Paleozoic rocks that were folded and thrust northeastward starting in the Cretaceous and continuing into Eocene time. This earlier deformation produced spectacular folds, some of which are beautifully exposed on many of the high peaks, including Borah Peak. About 4–7 m.y. ago, regional extension began to form the present topography. Borah Peak, which is composed of Proterzoic to Early Penn-

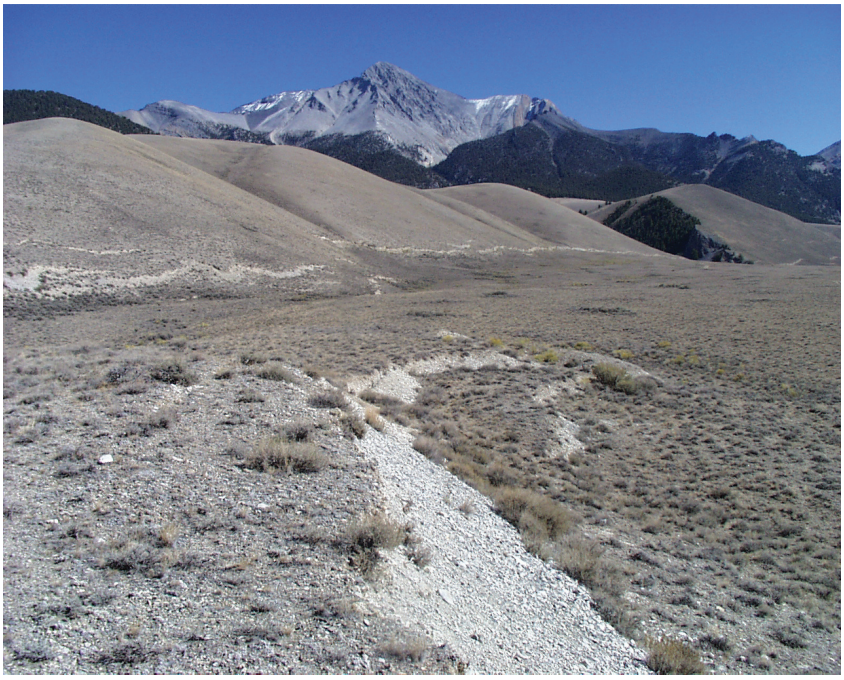

Figure 2. Echelon surface rupture (foreground and middleground) northwest of Borah Peak (in background). View is to the southeast.

U.S. Geological Survey, Denver, CO 80225, haller@usgs.gov, crone@usgs.gov

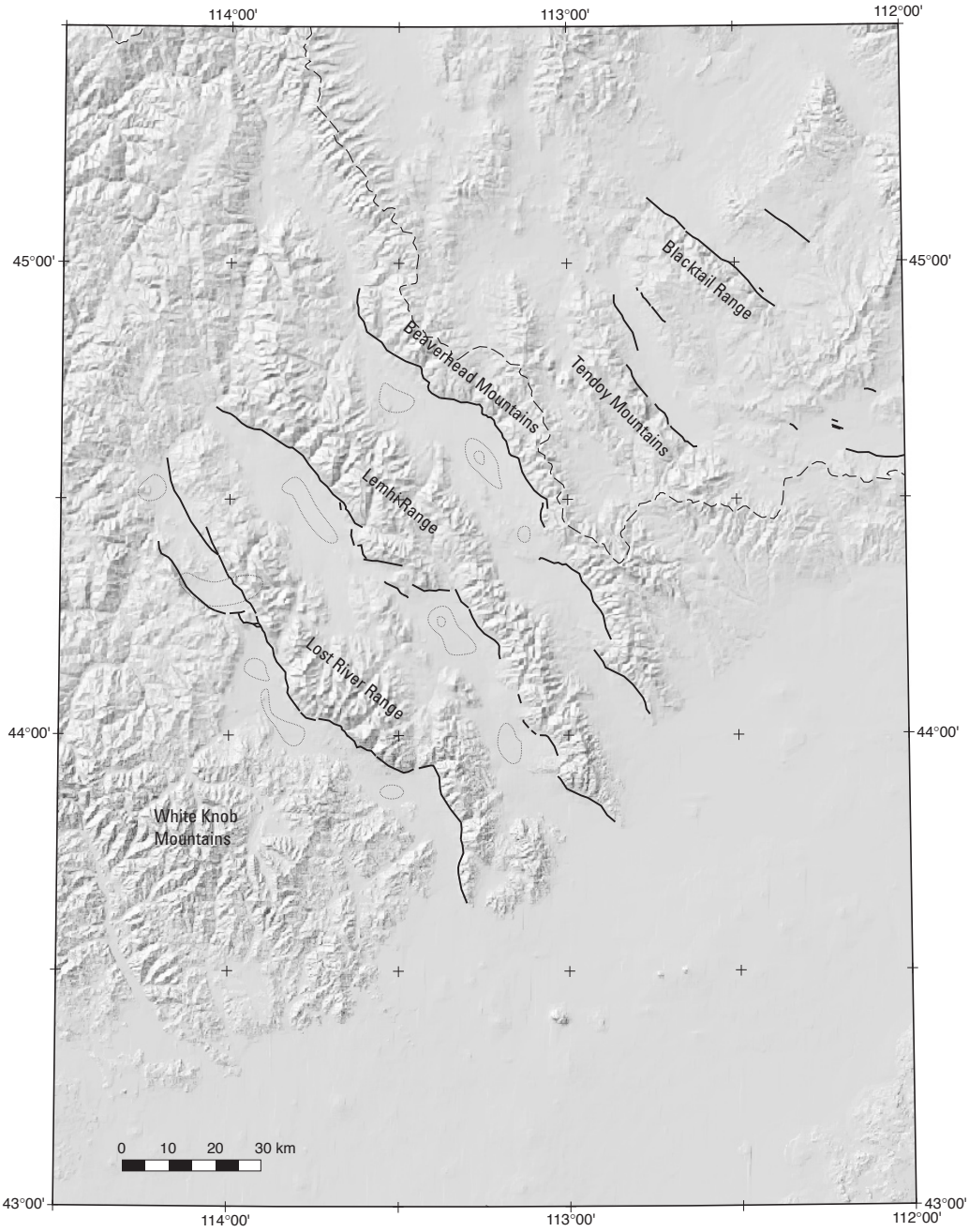

Figure 3. Generalized map of Quaternary range-front normal faults in east-central Idaho and adjacent parts of southwestern Montana. Closed gravity lows in adjacent basins are shown by dotted (gray) lines (from Bankey and others, 1985).

sylvanian rocks of the Lost River thrust plate, is the highest point in Idaho at 3,859 m; many peaks in the central parts of Lost River Range are higher than 3,700 m. In contrast, peaks at the ends of the range, commonly have elevations around 2,500 m. The adjacent valley floors range in elevation from 1,600 m, in the southern Big Lost River Valley near Arco, to 2,500 m adjacent to the central part of the range near the Willow Creek hills, and back down to 1,500 m in northern Round Valley, near Challis.

The two largest historical normal-faulting earthquakes in the United States (Barrientos and others, 1987) are the 1983 Borah Peak earthquake and the 1959 Hebgen Lake earthquake (M 7.5); they occurred 24 years and about 200 km apart. Both are in the Centennial Tectonic Belt (Stickney and Bartholomew, 1987), an east-trending band of seismicity that extends from the Borah Peak aftershock zone to Yellowstone National Park. Interestingly prior to the Borah Peak earthquake, the Centennial Tectonic Belt was poorly defined

west of the Idaho-Montana state line because the region surrounding the Lost River Range had a low rate of historical seismicity (Smith and others, 1985). No foreshocks preceded the Borah Peak main shock and, in fact, only two small earthquakes were recorded within 35 km of the Borah Peak main shock in the 4 years prior to the 1983 earthquake (King and others, 1987). In the months following the Borah Peak earthquake, thousands of aftershocks were recorded, mainly northwest of the epicenter on the Thousand Springs and Warm Spring segments. One of the largest aftershocks, the M 5.8 Devil Canyon event, occurred on August 23, 1984, nearly 10 months after the main shock (Jackson, 1994).

Regional Faults

Similar to the Lost River Range, range-front normal faults bound mountain ranges to the northeast, including the Lemhi Range and Beaverhead Mountains in Idaho, and the Tendoy Mountains and Blacktail Range in Montana. The presence of well-preserved fault scarps on Quaternary alluvium along large parts of these range-front faults is clear evidence of ongoing Quaternary tectonism throughout the region. Although the details of each fault's Quaternary behavior remain unresolved, these faults have been studied sufficiently to characterize the age(s) of the most recent event(s) and to show that single earthquakes do not rupture the entire length of any of these faults. From a regional perspective, the prominent range fronts, the heights of mountain blocks, and the lengths of faults tend to decrease toward the northeast, which might imply that the rate of fault activity also would decrease to the northeast. However, the most active, central parts of the faults shown in figure 3 all appear to have recurrent surface-faulting events every several to about ten thousand years, so there does not appear to be any obvious correlation between the length of the fault, the prominence of the range front, or the recurrence time for surface ruptures on the fault's most active segments. The long-term, late Cenozoic activity of these range-front faults has produced 1.5–2 km of topographic relief and as much as 6 km of structural relief (Skipp and Hait, 1977).

The range-front faults that bound the southwestern side of the Lost River and Lemhi Ranges and Beaverhead Mountains in Idaho are subparallel and have similar lengths and two-dimensional shapes. Prominent embayments and salients in the fronts of these ranges roughly align in a north-south direction (fig. 3), which hints at some deep structural control. Typically, each of the faults have either several-kilometer-long gaps in scarps or major echelon steps in the fault trace, which are interpreted to mark discontinuities that define the ends of independent surface ruptures (Crone and Haller, 1991).

Segmentation

Historical observations demonstrate that the entire length of long normal faults (>50–60 km) generally do not rupture during single large earthquakes. The tendency for only part of such long faults to fail coseismically is called segmentation, and in its strictest sense, the term defines parts of a fault that have a distinctly different rupture history than neighboring parts. In the model of a well-behaved segmented fault, surface ruptures are confined to a single segment through several to many seismic cycles. In this part of the intermountain west, surface-rupturing earthquakes are infrequent, thus the change in morphology of fault scarps along strike of the fault may suggest the presence of a segment boundary. Scott and others (1985) divided the 140-km-long Lost River fault into six segments generally based on morphology and continuity of Quaternary fault scarps and the inferred age of faulted deposits. Although the number of segments has not changed in the nearly 20 years since their study was published, the location of some boundaries have been refined and generally now coincide with geologic structures that may be effective barriers to rupture propagation. On this trip, we will travel from south to north along the Lost River fault and look at the geomorphic and structural similarities and differences between the Arco, Pass Creek, Mackay, Thousand Springs, Warm Spring, and Challis segments (fig. 1). The segments average 23 km in length, and all but the Challis segment have evidence of at least one surface-rupturing earthquake in the past 20–30 k.y.

Schwartz and Coppersmith (1984) proposed a model for characteristic earthquakes in which a fault or fault segment tends to repeatedly generate approximately the same maximum-size earthquake. Since the publication of their paper, a great deal of work has been conducted to determine if faults repeatedly rupture in earthquakes having a relatively narrow range of magnitudes near some maximum value for that part of the fault. Thus, when we speak of a part of a fault as behaving characteristically, we infer that the amount of displacement and the part of the fault that ruptures are similar over several seismic cycles. We will see on this trip that some segments of the Lost River fault appear to behave characteristically whereas others do not.

The segmentation model and characteristic behavior are closely linked. If a fault displays segmented behavior and earthquakes are largely confined to a specific segment, then the magnitude of the successive earthquakes should be similar. Since 1983, the refined location of the segment boundaries of the Lost River fault, as well as other nearby faults, have identified several types of structural barriers that seem to effect the propagation of ruptures and, thereby, reinforce the geomorphically based segmentation model that was developed prior to the Borah Peak earthquake (Scott and others, 1985). Most segment boundaries on the Lost River fault are marked by the absence of scarps on alluvium and occur near major changes in the fault's strike. It has been apparent for years that several boundaries coincide with areas of densely faulted bedrock, but

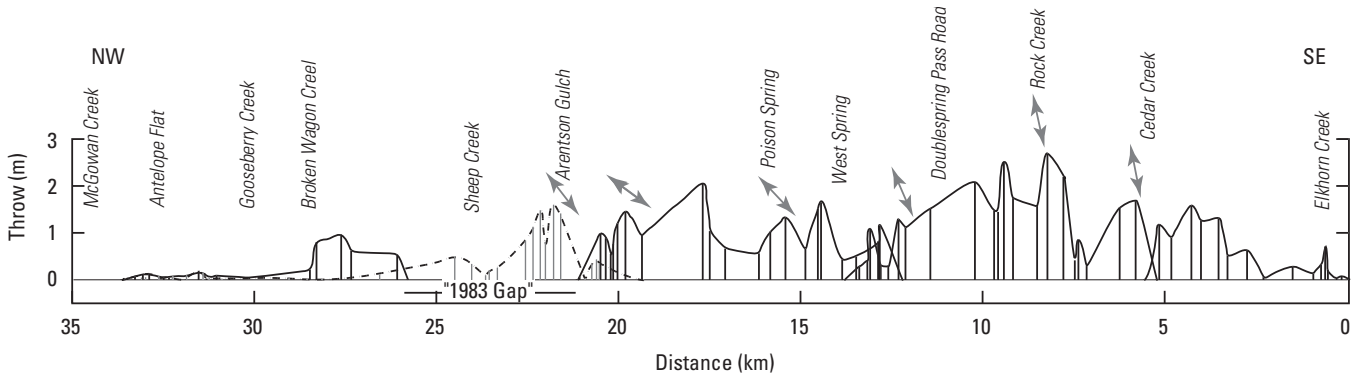

Figure 4. Plot showing the vertical throw resulting from the 1983 Borah Peak earthquake. Maximum net vertical throw was 2.7 m (near Rock Creek at the base of Borah Peak); although, individual scarps are almost twice as high (5 m). Average vertical throw was 0.8 m for the entire rupture, and 1.1 m along the Thousand Springs segment (from Arentson Gulch to Elkhorn Creek). The highest scarps are on the Thousand Springs segment. Scarps along the Willow Creek hills part of the rupture are shown by the dashed line. Offsets northwest of the "1983 Gap" are on the Warm Springs segment. The earthquake epicenter was located southeast of Elkhorn Creek.

the three-dimensional interaction of the faults in the footwall at a segment boundary was only recently addressed (Janecke, 1993). Janecke's (1993) structural interpretations have tremendous potential for providing yet another line of evidence to successfully define segment boundaries. Despite the notion that a segment boundary will usually halt a propagating rupture, it is clear that at times, surface rupture must propagate through the boundary otherwise the present range-crest morphologies would not exist (Crone and Haller, 1991).

Our paleoseismic record of the Lost River and other similar range-front normal faults is too short and incomplete to confirm the persistence of segment boundaries through multiple seismic cycles, however, gravity data provide some insight into the overall persistence of segment boundaries through time. In alluvium-filled valleys adjacent to these faults, gravity data show the general configuration of the bedrock beneath the valley fill. During individual coseismic ruptures, the amount of vertical slip usually is highest in the middle of the rupture and decreases towards the ends (see fig. 4). If this pattern is repeated many times, the central part of segments should coincide with closed gravity lows where the bedrock is deepest, and the ends of the rupture should coincide with gravity highs (Haller, 1988). This model holds true for the Warm Springs segment of the Lost River fault, which has a well-defined, centrally located gravity low (fig. 3). But elsewhere gravity lows do not necessarily coincide with central parts of segments (fig. 3). In many cases, bedrock highs (gravity highs) in the valley floor do, however, project to segment boundaries in range-front faults, and we will cross several of these on this trip.

The Borah Peak Earthquake

The Borah Peak earthquake occurred on at 8:06 a.m. (local time) October 28, 1983, and was the largest earthquake in the intermountain west in nearly 25 years. It was felt over an area of 670,000 km^2, in part or all of seven adjacent states. The felt area is elongated in the north-south direction and extended from the Canadian border to Salt Lake City (Stover, 1985). The earthquake produced 34 km of surface rupture with a maximum vertical displacement (throw) of 2.7 m, individual scarps nearly 5-m high, and a component of left-lateral movement as much as 17 percent (Crone and others, 1987). In the weeks following the earthquake, field mapping defined a Y-shaped surface rupture (fig. 1); continuous ruptures formed along the entire 20.8-km-long Thousand Springs segment and discontinuous scarps formed to the north along the Warm Spring segment (14.2 km) and to the northwest across the Willow Creek hills (7.9 km) joining the west-dipping Lost River fault and the east-dipping Lone Pine fault (Crone and others, 1987). Characteristics of the scarps are markedly different on the three parts of the ruptures. The largest scarps (fig. 4) are along the Thousand Springs segment where scarps greater than 1-m high exist along more than one-half of the segment. Considerably smaller scarps are present to the north and northwest, where the 1983 ruptures rarely exceed 1 m in height.

The earthquake hypocenter was at a depth of about 16 km and about 15 km southwest of the southern end of the surface rupture. The fault rupture propagated upward, first reaching the surface near Elkhorn Creek and progressed unilaterally to the northwest, producing normal slip with a small amount of left-lateral slip at the surface. The location of the main shock with respect to the surface rupture (Doser and Smith, 1985), the 3-dimensional location of aftershocks (Richins and others, 1987), and geodetic modeling suggest that the fault generally is planar in the upper crust (not listric), and it dips about 40–50° SW. to seismogenic depths (Barrientos and others, 1987). This modeled dip is consistent with the depth, location, and focal mechanisms of the main shock.

Paleoseismology of the Lost River Fault

Paleoseismological studies of the Lost River fault have a long and interesting history. Studies of the fault's seismic potential began in 1969 to address seismic hazards at the National Reactor Testing Station, now Idaho National Engineering Environmental Laboratory (INEEL), 25 km southeast of Arco, Idaho. These studies included some of the first trenching efforts in the intermountain west; one trench was excavated on the southern part of the Lemhi fault, and a stream exposure was cleaned to expose the southern part of the Lost River fault. (We will visit the latter of the two sites on this trip.) In the 1970s, two additional trenching studies were conducted farther north on the Lost River fault: one trench was excavated at Lower Cedar Creek near Mackay, Idaho, and a second, noteworthy trench was excavated near Doublespring Pass road. The 1983 rupture occurred on this part of the fault and exposed a cross section of the filled trench in the fresh fault scarp. This remarkable circumstance provided an opportunity unlike any other to characterize fault behavior and earthquake cycles.

Following the Borah Peak earthquake, trenches on various parts of the fault were excavated to develop a better understanding of the entire fault's rupture history. The exhumed trench at Doublespring Pass road was reopened and remapped shortly after the earthquake. Other sites also were studied including some near those originally excavated in the 1970s. In the 1990s, the issue of seismic hazards at INEEL once again stimulated additional studies, including studies at two new sites on the southern part of the fault and reevaluation of the 1969 site. These site-specific investigations, additional geomorphic studies, and more recent bedrock mapping have enhanced our understanding of this fault.

FIELD-TRIP ROAD LOG

Mileage Inc.	Cum.	
0	0	Intersection of U.S. Highways 20/26 and 93 in Arco, Idaho. Proceed north out of town on U.S. Highway 93.
2.5	2.5	Turn right (east) on to 2700 N. Directly ahead is a typical example of the Arco scarp of Malde (1971, 1985, 1987). As we drive northward along scarps of the Arco segment, note that they are fairly continuous, large (generally about 8-m high) and prominent with slope angles of 18– 27° (Malde, 1985). Road turns northward 0.7 mi from intersection and becomes King Mountain Road.
0.6	3.1	The scar across the scarp to the right is the Arco Peak trench (Olig and others, 1995) excavated in 1994.
3.3	6.4	Turn right on side road for Stop 1 (lat 43.73595°N., long 113.32624°W.).

Stop 1. Trench Site on Arco Segment

The Arco segment is characterized by faceted bedrock spurs (Malde, 1971) and high, dominantly west-facing scarps on alluvium along much of range front. Scarps range from 2 to 25 m in height (Pierce, 1985) but most are about 12 m (Malde, 1985; 1987). High scarps are on deposits thought to be less than 600 ka, whereas 2- to 3-m-high scarps are on late Pleistocene deposits (Pierce, 1985). The youngest unfaulted deposits probably are latest Pleistocene and Holocene in age (Pierce, 1985; Scott and others, 1985). Olig and others (1995) estimate that single-event displacements are 1.2–1.5 m based on 6 m of total offset thought to represent 4 or 5 surface-faulting events.

This site was originally excavated in April 1969 by Malde (1971) and called Site A-2. This specific location (shown as a borrow pit on the 1972 version of the Arco North 7.5 minute topographic map) was selected, in part, because it is near the middle of the part of the fault that Malde defined as the Arco scarp, and he expected the site to yield a faulting history that was representative of the rest of the Arco scarp. In addition, excavation at the site simply required freshening a natural exposure, which was expedient. However, the natural exposure is not normal to the strike of the scarp, which complicates some stratigraphic relations (Olig and others, 1995). It is worth noting here and at the other sites we visit that displacement during these large-magnitude events is typically accommodated in a narrow zone. All of the fault planes in Malde's (1971, 1985, 1987) trench map span a horizontal distance of only a few meters.

The objective of Malde's work, which he clearly proved, was to document that large-magnitude earthquakes occurred here sometime in the past. The stratigraphy exposed in this 15-m-high scarp was interpreted to represent two or more events (Malde, 1971). The earliest event (about 5–6.5 m displacement) occurred when the fan was still active (160 ka) based on the absence of soil on the buried-fan surface. The time of the most recent faulting event was thought to be between 15 and 30 ka (Malde, 1985), based on uranium-series dating of carbonate coats on clasts, which estimates the soil age (23–30 ka) of fan gravels that are displaced by a 3-m-high scarp (Pierce, 1985).

Olig and others (1995) reevaluated the faulting history at this site in 1994 and found evidence of seven surface-faulting earthquakes since deposition of the fan gravels. The age of those gravels was not reevaluated in the 1994 study, so they based their chronology on the 160-ka age for the fan cited by Malde. The composite history of the Arco segment developed by Olig and others (1995) from this site and the

Figure 5. View of southern part of Pass Creek segment from near Darlington. Note the high old scarps above center fence post. Other scarps are apparent as shaded slopes. The range crest is substantially higher along this part of the fault than to the south.

one that we drove by earlier suggests that surface rupturing has been episodic with several closely spaced events followed by longer periods of quiescence. Following an initial faulting event, a period of quiescence occurred between 100–130 and 60 ka, followed by two or three faulting events near 58 ka, then another period of quiescence until about 21 ka, when two more closely spaced events occurred. The evidence for these four or five events is in the upper colluvial package mapped by Malde (1971). The time of the two youngest events is constrained by two nearly identical thermoluminescence ages of 20±4 ka and 21±4 ka from deposits stratigraphically above the most recent event and below the penultimate event, respectively. Interestingly, even though the intervening periods between the events are highly variable, Olig and others (1995) conclude that the displacement per event is fairly uniform.

Mileage Inc.	Cum.	
		Return to cars and proceed north on Hill Road
0.5	6.9	Turn left on 3150 N.
1.6	8.5	Turn right on to U.S. Highway 93.
0.5	9.0	Town of Moore.
5.9	14.9	Darlington, Idaho. The canyon directly east of town is Ramshorn Creek, where the boundary between the Arco and Pass Creek segment is located (Crone and Haller, 1991; Janecke, 1993; Olig and others, 1995). This segment boundary coincides with a down-to-the-north normal fault in the footwall of the Lost River fault (Wilson and Skipp, 1994). Note the significant change in the geomorphic expression of the range. Northward from near Ramshorn Canyon, the range is high, and the mountain front is impressive (fig. 5). In contrast, the Arco Hills to the south are considerably lower and less precipitous. Scarps on alluvium on the Pass Creek segment are short, poorly preserved, and much less continuous than those to the south. However, many of the scarps on the Pass Creek segment are over 20-m high (Olig and others, 1995).

To the northeast, there is a prominent embayment in the range front; the fault changes trend by about 70–80° at Elbow Canyon. Although no studies have attempted to evaluate the times of faulting on either side of this prominent change in strike, no one has suggested that this bend might be a segment boundary. In fact, Janecke (1993) states that the cross fault in the footwall that extends up Elbow Canyon has too shallow of a dip to effect rupture propagation.

4.6	19.5	Leslie, Idaho. Jaggles Canyon trench site is located at the range front directly east of Leslie. Olig and others (1995) report evidence for 7–9 surface faulting events at this site; the oldest event is >140-220 ka and 4–5 events are younger than 21 ka based on thermoluminescence ages. Three of these events occurred between 17 and 18 ka; this implies that surface-faulting events occurred on the average every few hundred years during this short time period, as compared to the shortest interval on the Arco segment of about 20 k.y. This highly active period is not evident in the landscape,

which Olig and others (1995) suggest is because the fault is at the bedrock-alluvium contact. In contrast to interpretations at the Arco Peak site, faulting here is interpreted to have variable recurrence and variable amounts of displacement per event.

8.1	27.6	Mackay, Idaho. Turn right (east) on Bar Road (the main business street) (lat 43.91485°N., long 113.61261°W.). Bear right 0.4 mi. The town of Mackay, Idaho, is approximately 5 km southwest of the Pass Creek-Mackay segment boundary. Janecke (1993) characterized the boundary in the footwall of the Lost River fault as a 2.5-km-long, 1-km-wide zone of as many as four faults. At this boundary, the range-front fault changes strike by about 25°. The controlling structure here might be the near-vertical, northeast-striking Paleogene Swauger Gulch fault.
1.3	28.9	Entrance to Mackay town dump (lat 43.91384°N., long 113.59161°W.). Turn right at the southern fence line of the dump. Follow the right fork (not the road along the fence line) to the northeast.
0.9	29.8	At the irrigation ditch, turn due north. Stay on the best road, but make sure you stay on top of the fan. Do not drive into Lower Cedar Creek canyon. There are two ditch crossings farther up the fan. The first is relatively easy to cross; the second (at about 2.5 mi) can be narrow and deep depending on what road you are on. If you do not think you can make the crossing, turn to the southeast along the ditch until you find a suitable crossing (lat 43.95493°N., long 113.58303°W.).
~2.9	32.7	Location of Lower Cedar Creek trenches. South trench (lat 43.96548°N., long 113.58168°W.), north trench (lat 43.96560°N., long 113.58173°W.).

Stop 2. Trench Site on Mackay Segment

One notable characteristic of the Mackay segment (fig. 6) is the high-fan surfaces along this part of the range front. Scott (1982) shows that alluvial deposits on the hanging wall here are older than the majority of valley fill to the south along the Pass Creek segment. The road that we followed to this stop is on middle to lower (?) Pleistocene alluvium; to the north of the road, a higher deposit is identified as being possibly as old as Pliocene. Lower Cedar Creek is entrenched into the fan surface about 10 m below the trench site.

The morphology of the scarps clearly suggests a young (Holocene) age, in contrast to our previous stop, and the size of the scarps suggests multiple-faulting events. Trenches excavated in the 1980s extended across the prominent graben at this site. An earlier trench, excavated by M.T. Hait at this location, showed evidence of at least one surface rupture that postdates Glacier Peak ash (11.3 ka in Schwartz and Crone, 1988). To the north, near Lone Cedar Creek, two faulting events were

Figure 6. View of Mackay segment looking northwest from U.S. Highway 93. Right edge of photo is at the approximate location of the Pass Creek-Mackay segment boundary. The next drainage northward is Lower Cedar Creek (Stop 2). The farthest high peak is Leatherman Peak (elev. 3,737 m).

recognized, one that predates and one that postdates Mazama ash (6.7 ka) (Schwartz and Crone, 1988).

Mileage Inc.	Cum.	
5.1	0.0	Return to intersection of Bar Road and U.S. Highway 93 in Mackay. Turn right (north) on U.S. Highway 93. RESET TRIP ODOMETER.
3.0	3.0	Bedrock in valley and old high fan (lat 43°56.662'N., long 113°39.163'W.).
1.6	4.6	Entrance to Mackay Reservoir (picnic area and restrooms).
3.4	8.0	Gravel pit on west side of the highway offers a good view of the northern Mackay segment. Leatherman Peak (elev. 3,727 m), on the skyline (fig. 6), is the second highest peak in the Lost River Range. Below it is Lone Cedar Creek, the location of the trenching study briefly discussed at the last stop. The large alluvial fan at the mouth of Lone Cedar Creek canyon is upper Pleistocene in age according to Scott (1982), and based on the poor degree of soil development and relation to moraines and outwash, it probably has an age that is equivalent to Pinedale (about 15 ka). We cross the segment boundary between the Mackay and the Thousand Springs segments in the next few miles. Notice the pronounced change in the trend of the range front as we proceed northward.
7.0	15.0	Trail Creek road intersection.
1.2	16.2	(lat 44.08419°N., long 113.84184°W.) Cautiously pull off to the left side (southwest) of the highway.

Stop 3. Overview of Borah Peak Epicenter

This stop provides a good view (fig. 7) of the spatial relations of a number of geologic effects caused by the Borah Peak earthquake. Looking south-southwest, the 1983 epicenter was directly below the low hills on the far side of the valley (about 13 km from where we stand). Turning a little to the east and looking toward the intersection of Trail Creek Road and the highway, we can see general area that was deformed by a lateral spread. The deformation was confined to the lower part of the alluvial fan. Fissures at the head of the lateral spread were subparallel to topography, as much as 1-m wide and 3-m deep, and extended from Trail Creek Road to near Whisky Springs, about 1.5 km to the south (Youd and others, 1985). Most of the fissures were west of the highway, but locally they disrupted the highway grade.

To the southeast, the mountain front swings eastward out of sight as the trend of the Lost River Range front changes direction by about 55°. At this location near Elkhorn Creek, low, uphill-facing scarps formed in 1983, probably due to gravitational failure in response to violent ground shaking (see fig. 11 in Crone and others, 1987). Wallace and Bonilla (1984) identified similar features near the crest of the Stillwater Range, in the general vicinity of the 1954 Dixie Valley earthquake and the 1915 Pleasant Valley earthquake. Interestingly, uphill-facing scarps existed before the 1983 earthquake, and the scarps we see today are the result of more than one earthquake. The uphill-facing scarps are the southernmost ruptures from the 1983 earthquake, and thus define the approximate location of the segment boundary (fig. 7). This earthquake, like many in the intermountain west, produced a unilateral rupture that extended northwestward from the epicenter along the range front, across the flank of Dickey Peak, and beyond the Willow Creek hills to the north.

The structure exposed in the footwall of the Lost River fault at this segment boundary is complex. The zone of deformation is 10-km long (parallel to the Lost River fault) by 2- to 4-km wide (Susong and others, 1990; Janecke, 1993). Although many cross faults (Susong and others, 1990; Janecke, 1993) and subparallel normal faults (Susong and Bruhn,

Figure 7. Panoramic (nearly 360°) view of Thousand Springs Valley from Stop 3. Labeled features are discussed in the text.

1986) are mapped in the footwall near the southernmost ruptures, it is likely that few of them coincide with the segment boundary at hypocentral depths (Janecke, 1993). The prominent northeast-striking Elkhorn Creek, Leatherman Pass, and Mahogany Creek cross faults are far from the epicenter when projected downward (see fig. 4 in Janecke, 1993).

During the Borah Peak earthquake, this segment boundary stopped rupture propagation to the southeast. Aftershocks, which covered a 75 x 10 km area, occurred only north of the main shock (Richins and others, 1987). The segment boundary coincides with a gravity high (Mabey and others, 1974), which is interpreted to be a horst below the modern flat valley floor (Skipp and Harding, 1985). The valley fill is thin over this bedrock block (60 m) compared to elsewhere in the valley (up to 1 km). The horst is expressed at the surface by outcropping Mississippian White Knob limestone of Chilly Buttes.

During the 1983 earthquake, Chilly Buttes was the site of unusual ground-water phenomena. In the flat alluvium surrounding the buttes, violent eruptions of ground water created sand boils, and artesian flow from bedrock on the flanks of Chilly Buttes caused local flooding (Wood, 1985). Water and sand in the sand boils were reported to have erupted as much as 6 m into the air. Remains of these eruptions include at least 47 craters, 19 of which are more that 6 m in diameter, and the largest being about 22 m in diameter and 5-m deep. Some craters apparently existed prior to 1983 (Breckenridge, 1985; Waag, 1985) and at least one was active following the Hebgen Lake earthquake (Youd and others, 1985). Erupting water from fractured bedrock on the flanks of Chilly Buttes (Waag, 1985) required as much as 35 m of artesian head and continued for about 48 hours following the main shock. The large volume of water erupted resulted in localized flooding northwest of where we stand.

Mileage Inc.	Cum.	
		Proceed north on U.S. Highway 93.
2.5	18.7	Old Chilly road.
0.9	19.6	Turn right on Cedar Creek access road (to Borah Peak), just past gravel pit (lat 44.11743°N., long 113.88869°W.). The 1983 scarps near Cedar Creek are visible on the treeless slope at the base of the range beyond the curve in the road. This slope is underlain by a Pinedale-equivalent left-lateral moraine that was left by a glacier that flowed down Cedar Creek.
2.8	22.4	Take right fork in road and park (lat 44.13370°N., long 113.84039°W.).

Stop 4. Birch Springs Landslide and 1983 Fault Scarps on the Thousand Springs Segment

(modified from Crone, 1985)

One of the largest landslides that formed in response to the severe ground shaking is located at Birch Springs. The failure of a Bull Lake-equivalent (?) (K.L. Pierce, 1985, written commun.) moraine resulted in a complex rotational slump, near the headwall, that grades downslope into debris flows. The 100,000-m^3 debris flow covered about 4 hectares; the headwall is about 250-m long and as much as 5-m high. Additional subparallel cracks can be found upslope from the headwall. The upper 50 m of the landslide deposit consists of back-rotated slump blocks, but farther downslope the mobilized material is more disaggregated and within about 100 m of the headwall, the landslide consists of four debris-flow lobes. These debris flows bury the fault scarp showing that they postdate the surface rupture. The velocity of the debris flow was estimated at several tens of meters per hour based on splash marks on trees observed to be 1.2 m above the ground surface (Crone, 1985). Based on pre-1983 aerial photography, a preexisting landslide was present prior to the Borah Peak earthquake (Breckenridge, 1985).

The modern fault scarps also are superimposed on preexisting scarps. One can see the rounded crest of the old scarp above the free face of all the scarps that form the graben near

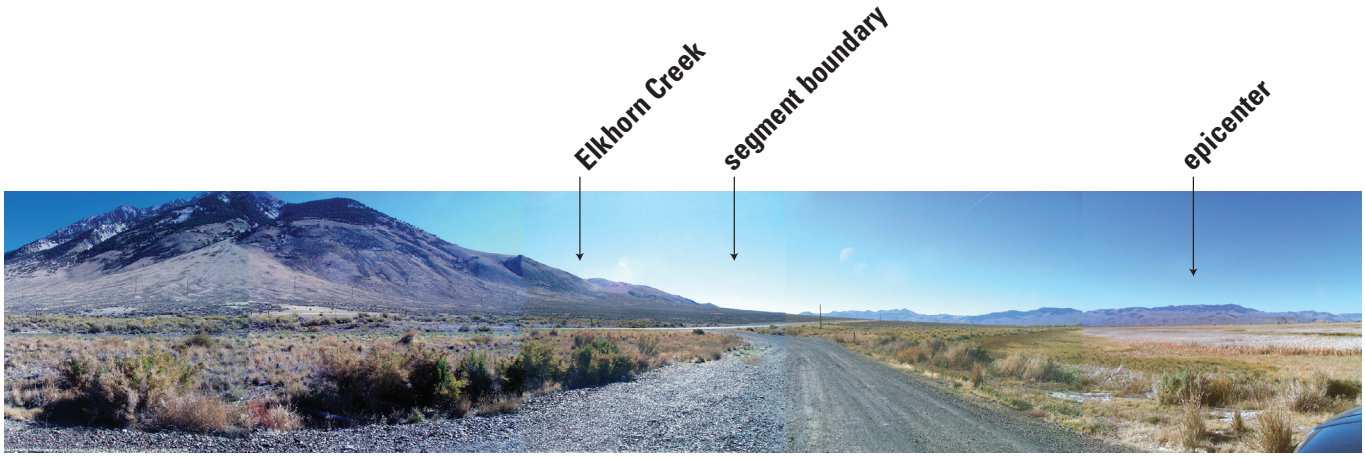

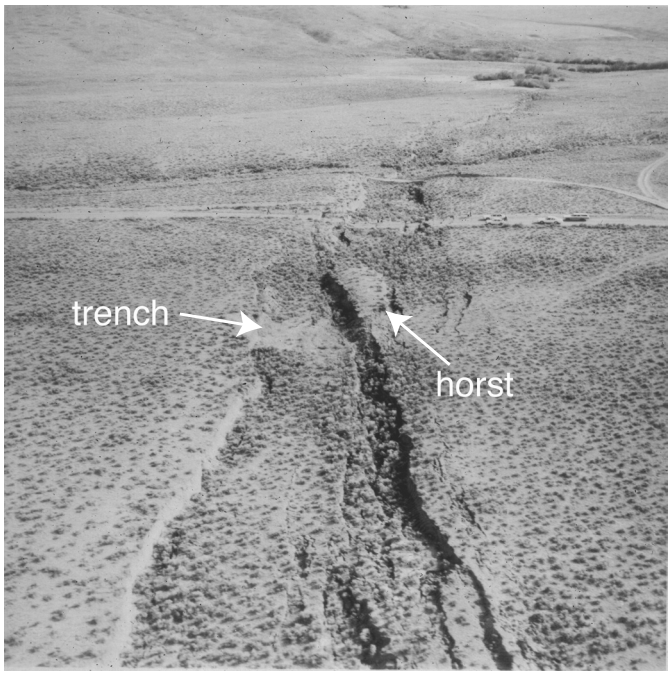

Figure 8. Oblique aerial photograph of surface faulting and location of trench that was excavated before the 1983 earthquake near Doublespring Pass road, view is to the southwest. Note the complex pattern of horsts and grabens that formed on this Pinedale-age alluvial fan. Photograph by R.E. Wallace, November 3, 1983.

the parking area. We will see similar relations, although not necessarily as well expressed, at the next stop to the north. The trail to Borah Peak closely follows the fault scarp; the landslide headwall scarp can be found uphill of the trail.

Mileage Inc.	Cum.	
2.8	25.2	Return to U.S. Highway 93 and proceed north.
1.8	27.0	Turn right onto Doublespring Pass road (lat 44.14020°N., long 113.90488°W.). Two prominent signs are located at a pull out at the northeast corner of this intersection. One describes Borah Peak, which was named for William E. Borah, a U.S. Senator for Idaho from 1907 to 1940. The other sign describes the Borah Peak earthquake.
2.5	29.5	Park at U.S. Forest Service interpretive site. There are picnic facilities and a restroom here.

Stop 5. Doublespring Pass Trenches and Fault Scarps of the Thousand Springs Segment

The Doublespring Pass road crosses the 1983 fault scarps about 2.5 km east of the U.S. Highway 93, where the fault scarps cross the broad alluvial fan of Willow Creek. The scarps are nearly as spectacular today as they were 20 years ago. We will discuss the complex surface rupture at this location and visit the site of two exploratory trenches, one excavated prior to the earthquake, the other after the earthquake. The 1983 scarps span a zone that is as much as 35-m wide and contains prominent horsts, grabens, and stair-step scarps (fig. 8). Individual scarps are just a few centimeters to 5-m high; the largest scarp reported is located about 360 m northwest of the old Doublespring Pass road. Notice as you walk around that some of the cracks are still open to a depth of 1–2 m. The U.S. Forest Service erected an interpretive site where the fault scarps crossed the original Doublespring Pass road (fig. 9). It appears that the scarps have faired far worse inside the fence than outside its perimeter.

The Willow Creek fan generally is thought to have stabilized soon after the most recent glacial cycle (about 15 ka according to Pierce and Scott, 1982). The scarps that cross this fan are composite scarps that result from two surface-rupturing events. This is evident at many locations because the crests of the scarps are rounded (“beveled”) above the abrupt near-vertical free face. This morphology has long been used as evidence of multiple-faulting events. However, it is important to note that, even though several thousands of years (maybe as many as 11 k.y.) elapsed between faulting events, the bevel

Figure 9. Photograph of Doublespring Pass road following the Borah Peak eathquake, view to the northeast. Notice the numerous scarps that distribute deformation over a relatively wide zone. Photograph taken by M.N. Machette (U.S. Geological Survey Archive no. 40) on November 9, 1983.

is only locally preserved on the fault scarps. The relations of significantly different scarp heights on deposits of various ages, however, is clearly demonstrated here, and provide better proof of multiple movements. If you walk over to the modern Willow Creek flood plain, you will see only the 1983 scarp, which is about 2.5-m high on these young fluvial deposits; whereas, on the older (Pinedale-equivalent), higher fan deposits, the scarps are about twice as high.

Trenching studies (fig. 8) conducted at this location are unique. A trench (lat 44.16587°N., long 113.87034°W.) was excavated in 1976 about 45 m northwest of the road (Hait and Scott, 1978; M.H. Hait in Crone, 1985), and during the Borah Peak earthquake, the back-filled trench was exposed in the newly formed near-vertical free faces. The trench was reexcavated and mapped in 1984 (Schwartz and Crone, 1985) because of this unique opportunity. Figure 10 shows simplified trench logs from the two studies. The logs show that faulting in 1983 closely mimicked the amount and style of prehistoric faulting (Schwartz and Crone, 1985). The prominent horst block, which is abruptly truncated by the post-1983 excavation (fig. 8), within the graben was present prior to the Borah Peak earthquake. Displacement reactivated these subsidiary faults and enhanced topographic relief. Stratigraphic relations show that the amounts of 1983 displacements were similar to those associated with the earlier earthquake; total displacement in 1983 was 174–198 cm and 126–150 cm in the prehistoric event (Schwartz and Crone, 1985). These similarities strongly suggest that the prior paleoearthquake had a magnitude that was similar to the 1983 event. Thus, it appears that the model of the characteristic earthquake (Schwartz and Coppersmith, 1984) fits here. We do not know, however, if the temporal characteristics of faulting are as regular as the displacement characteristics.

At the north end of the Willow Creek fan, the surface ruptures extend northward around the east side of a bedrock block known as the West Spring block (Skipp and Harding, 1985; Plate 1 in Crone and others, 1987). Skipp and Harding (1985) offer a couple of explanations for the origin of this block:

> *"The West Spring block contains folded, fractured, and sheared limestones of the Upper Mississippian Scott Peak Formation. These rocks have been dropped down at least 200 m to the west into the Thousand Springs Valley along the Lost River fault zone against folded and sheared beds of the upper part of the Lower Mississippian McGowan Creek Formation. The West Spring block may be either slide block resting in part on valley fill, or a down dropped tectonic sliver caught in a broad zone of range-front faults…..The West Spring block appears to be a part of the Lost River thrust plate, not a structurally higher plate such as the White Knob,*

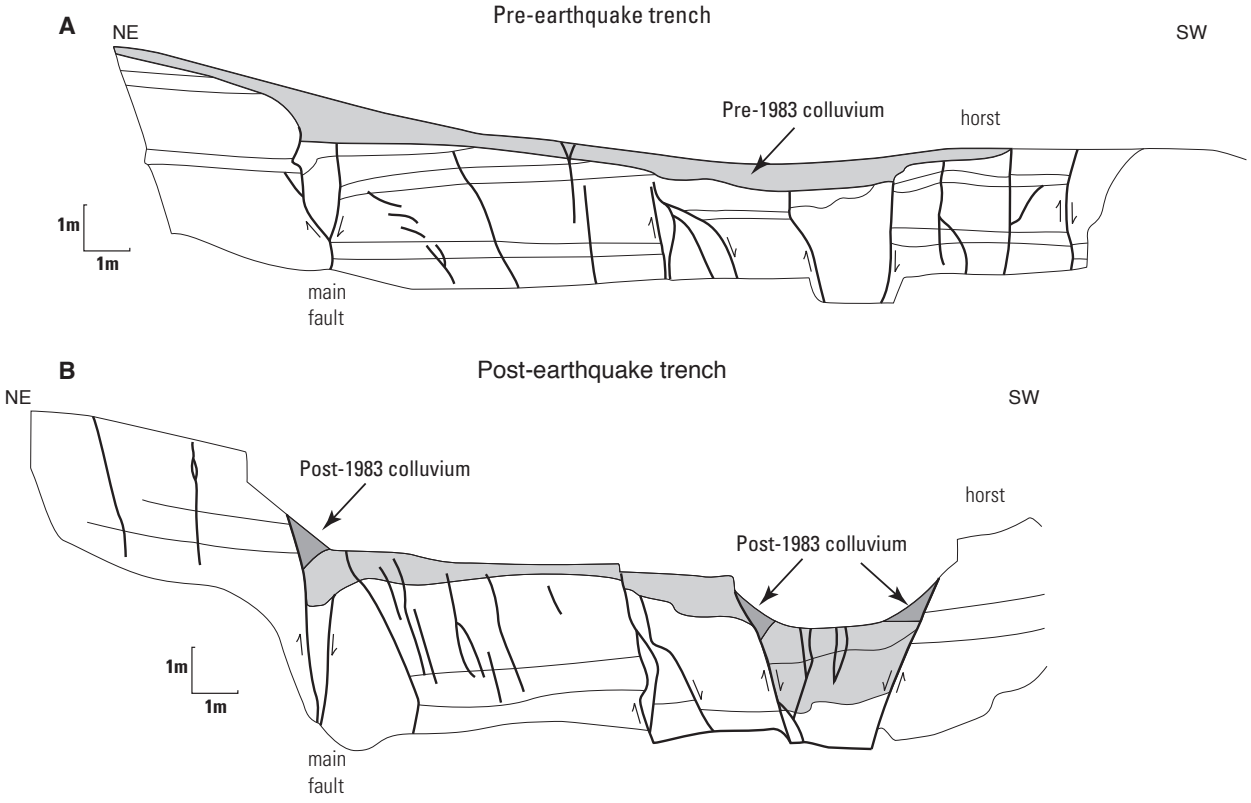

Figure 10. Simplified trench maps from site near Doublespring Pass road. (A) Map of the trench excavated in 1976 by M. T. Hait (modified from Crone, 1985). (B) Map of trench that was excavated in 1984 after the Borah Peak earthquake.

and, in this respect does not resemble slide blocks on the west sides of the Lemhi Range and Beaverhead Mountains (Beutner, 1972; Skipp and Hait, 1977) that are down dropped fragments of structurally higher thrust sheets."

Mileage Inc.	Cum.	
2.5	32.0	Return to U.S. Highway 93 and proceed north.
4.7	36.7	Turn right on Arentson Gulch access road.
0.4	37.1	Park near gate for Stop 6.

Stop 6. Dickey Peak and the Northern End of the Thousand Springs Segment

From this location, the fresh scarps cross the flank of Dickey Peak. They appear as tan lineaments crossing scree slopes fairly high on the mountain face. This is one of the few places along the surface rupture where the fault plane was exposed in bedrock; there were at least two sets of slightly weathered slickensides preserved. None of the slickensides appeared to be fresh enough to be from the 1983 earthquake, but collectively they show that past movements had both left- and right-lateral slip components at this site.

The hills to the north are the Willow Creek hills, and at 2,200 m, they form a drainage divide and are the highest point in the valley floor. They separate the south-flowing Big Lost River and its tributaries in the Lost River Valley from the north-flowing Warm Spring Creek and its tributaries in Warm Spring Valley. This ridge of transverse bedrock hills is believed to be the topographic expression of the northern boundary of the Thousand Springs segment. These hills are only 20 km from the highest point in the Lost River Range, Borah Peak.

Following the Borah Peak earthquake, rupture propagation slowed, and a large number of aftershocks concentrated near the Willow Creek hills. This segment boundary seems to be complex in the subsurface (Bruhn and others, 1991); the aftershocks sequence suggests that the overall geometry of the surface faulting directly reflects structure at depth. Detailed analysis of the aftershocks shows that they occurred in discrete zones less than 1 km in width between 6 and 10 km below the surface (Shemata, 1989). In part, the arrest of the rupture propagating at depth may be controlled by the Mahogany Creek fault, which is mapped as a northeast-trending, normal fault that daylights near the southern boundary of the Thousand Springs segment (Janecke, 1993). Janecke (1993) suggests that if the northeast-striking Mahogany Creek fault dips 50° to the northwest, it would then intersect the Lost River fault at 10–15 km depth near the Willow Creek hills. This interpretation reinforces the concept that 2-dimensional mapping is not sufficient to prove or disprove what structures may control the initiation or termination of rupture; the critical fault intersections are those at seismogenic depth.

Additionally, the sequence of aftershock activity suggests that there were notable differences in rupture propagation in the area near the Willow Creek hills. Twelve hours after the Borah Peak earthquake, intense aftershock activity began in this area, suggesting that strain was concentrated at the segment boundary. All of the largest aftershocks located here had large stress drops (Boatwright, 1985). About one month after the Borah Peak earthquake, the rate of aftershock activity increased to the north along the Warm Spring segment.

The 1983 scarps are obvious across the south side of the Willow Creek hills; here, the rupture diverged northwestward away from the main range front, leaving a 4.8-km-long gap in surface faulting along the Lost River fault (see "1983 Gap" on fig. 4). From a location along one of the tributaries of Arentson Gulch, and within 100 m of the surface rupture on the Willow Creek hills, we have the following eyewitness account:

"Lawana Knox of Challis, Idaho, witnessed the formation of a fault scarp during the M_s 7.3 earthquake of 28 October 1983 along the Lost River Range, Idaho. The earthquake occurred at 8:06 a.m. local time (1406 UTC) while Mrs. Knox was hunting with her husband, William Knox.

Mrs. Knox was sitting at a point along a fork of Arentson Gulch…and was watching the southwest-facing slope down which she expected to see her husband driving elk. As she watched, the fault scarp formed before her eyes. At the closest point, the scarp was about 300 m away, but she could clearly see the scarp for at least 1 kilometer both to the northwest and to the southeast. Mr. Knox was on the hill north of and above the fault scarp.

Mrs. Knox reported that the 1- to 1.5-m-high scarp formed in about 1 second. She reported that the scarp reached its full height quickly, and that it did not appear to adjust up or down later or oscillate up and down while reaching its full height.

Mrs. Knox reported that the scarp did not form until the peak of strong shaking was beginning to subside. Upon being asked how long the strong shaking lasted, Mr. Knox replied, "about a minute." Mrs. Knox disagreed and said, "it might have been a half a minute, but it felt like a lifetime." Both Mr. and Mrs. Knox said the earthquake started with noise and that "the earthquake came from the south, from the direction of Borah Peak." After the first sensations, the ground shook harder and harder, and only after the shaking started to subside or ease did Mrs. Knox see the scarp form."

—from Wallace (1984)

This eyewitness account provides some intriguing information. Wallace (1984) infers from his discussions with Mr. and Mrs. Knox that the fault scarp formed within a few seconds and propagated from northwest to southeast, which is contrary to the direction of rupture propagation along the Lost River fault from southeast to northwest. In addition, he believes this part of the surface rupture occurred maybe 10 seconds after strong shaking began. There are few eyewitness accounts of this nature, and their words provide us with another unique perspective of the earthquake.

Optional Stop. Prehistoric Fault Scarp in the "1983 Gap"

Proceed north on the Arentson Gulch road (you will encounter several gates along the way—Please leave them as you find them). This side trip does not venture far from the highway, but the road is locally impassable when wet.

Mileage Inc.		
		Left turn through gate.
1.6		Gate.
0.6		Stay left.
0.4		Turn right. In 0.1 mi the road will cross the fault scarp and in another 0.2 mi, the northern end of the rupture on the Thousand Springs segment is visible to the right.
0.6		Challis National Forest boundary (lat 44.24678°N., long 113.92425°W.).
0.1		Turn right.
0.2		Prehistoric fault scarp.

This fault scarp did not rupture during the Borah Peak earthquake. We are in a 4.8-km-long gap, the previously mentioned "1983 Gap", between the historic scarps of the Thousand Springs segment and the Warm Spring segment to the north. The scarp here is older than the Holocene scarps of the Warm Spring, Thousand Springs, and the Mackay segments (Crone and others, 1987). Thus, surface rupture of this short part of the fault has not occurred in the past three events on the Warm Spring or Thousand Springs segments. The scarp is 3–5 m high with a maximum slope angle of 9–11°. Based on comparative geomorphology, the scarp is most likely older than 15 ka (Crone and others, 1987).

Mileage Inc.	Cum.	
		Return to U.S. Highway 93 and proceed north.
2.7	39.8	Willow Creek Summit (lat 62.73719°N., long 113.97530°W.).
2.8	42.6	Pull off highway (lat 64.73769°N., long 114.00864°W.)

Stop 7. Overview of Warm Springs Segment

As we look down valley to the north, the end of the 1983 ruptures is less than 1 km south of McGowan Creek at the end of the prominent mountain front. The preponderance of evidence, geologic, geodetic, and seismologic, suggest that rupture of the Warm Spring segment following the Borah Peak earthquake was in the form of secondary slip. The amount of vertical offset (fig. 4) along this segment was substantially less than to the south, scarps were less continuous, and there was one report that indicates movement may have occurred on this segment many hours after the main shock. Most of the reported surface ruptures were on two approximately 3-km-long parts of the fault. The southern one extended from the northern end of the "1983 Gap" to about 1.5 km southeast of Gooseberry Creek. The northern one extended between Gooseberry Creek and McGowan Creek. The southern part of the rupture generally had net vertical offsets of 60–110 cm. Along the northern rupture, net vertical offsets rarely exceeded 20 cm (fig. 4).

To the west of the pull out, small ruptures formed on preexisting scarps of the Lone Pine fault. The Lone Pine fault is antithetic to the Lost River fault and probably intersects it at depth (Jackson, 1994). There has been no geologic characterization of the Lone Pine fault; however, fault scarps are clearly evident along the part of the fault that is not covered by a tree canopy.

Mileage Inc.	Cum.	
		Return to U.S. Highway 93 and proceed north. Turn right on Gooseberry Creek access road.
1.1	43.7	Fence (lat 44.31074°N., long 113.98858°W.).
1.1	44.8	Turn right (lat 44.30039°N., long 114.01429°W.).
1.5	46.3	Fence (lat 44.31074°N., long 113.98858°W.).
1.4	47.7	Gooseberry graben (lat 44.31348°N., long 113.97813°W.).

Stop 8. Characteristics of Scarps on the Warm Spring Segment

The 1983 ruptures on the Warm Spring segment consist of minor, nearly continuous ruptures (<1 m) on prehistoric scarps (up to 5.7-m high) (Crone and Haller, 1991). The morphology of prehistoric scarps on the Warm Spring segment is similar to Holocene scarps on the Mackay segment. Their size suggests that the prehistoric earthquake that formed them typically produced scarps that were much larger than seen in 1983.

At Gooseberry Creek, surface faulting has formed a graben that is similar to the grabens we visited on the Mackay segment and at Doublespring Pass road. The graben here is 0.5-km wide and contains as many as four antithetic and synthetic scarps. Only small (<5 cm), isolated scarps formed in 1983; thus, the vertical offset of 4 m here occurred in prehistoric time.

Two trenches were excavated near the ends of the Warm Spring segment (about 7.5 km apart) that suggest a prehistoric surface-rupturing event occurred shortly before 5.5-6.2 ka (Schwartz and Crone, 1988). No other surface faulting events have occurred since about 12 ka.

Mileage Inc.	Cum.	
		Return to U.S. Highway 93 and proceed north.
1.1	48.8	Entering bedrock exposed in valley near Warm Spring-Challis segment boundary.
1.7	50.5	Entering Grand View Canyon. The highway extends for more than 5 mi through Mississippian McGowan Creek Formation and the Devonian Grand View and Jefferson Dolomites.

Note the pronounced change to a subdued range front with low relief where the road rises to the top of the alluvial-fan sequence. This morphology is typical of the Challis segment. The low hills in the foreground are bounded on both sides by down-to-the-west faults.

The Devil Canyon earthquake (M 5.8) occurred in this general area on August 22, 1984, and is considered to be a late aftershock of the Borah Peak earthquake. Its epicenter is near the segment boundary between the Challis and Warm Spring segments. Jackson (1994) places the epicenter just north of the Challis-Warm Spring segment boundary, near the northern end of the mapped surface rupture of the Borah Peak earthquake. At least 50 aftershocks greater than M 3.0, five greater than M 4.0, and one M 5.0 occurred in the following month (Jackson, 1994); some of the aftershocks were on the Lost River fault and some on the east-dipping Lone Pine fault on the west side of the valley.

Figure 11. View of Challis segment from Hot Springs road, south of Challis, Idaho. Note the subdued topography of the range front, which indicates that the slip rate on this segment of the Lost River fault is considerably lower than the rate on segments to the south.

10.1	60.6	Hot Springs road. Pull off on right provides a good view the Challis segment. Ahead is Challis, the end of the trip.

Stop 9. View of Challis Segment

This view of the Challis segment (fig. 11) illustrates the basis for assigning a low activity rate on the northern Lost River fault. Here the range is characterized by low topographic and structural relief. The fault is not marked by scarps on alluvium, and its location is poorly constrained by the bedrock-alluvium contact; likewise, the faulting history is poorly understood. There is no evidence of late Quaternary (<130 ka) movement (Scott and others, 1985), and the slip rate is suspected to be an order of magnitude lower than other parts of the fault. It is obvious from the overall geomorphology, that the activity rate of this segment is substantially lower than any of the segments to the south.

Summary

The Lost River fault is one of the best-expressed segmented faults in the intermountain west. The Holocene record of surface ruptures on the central three segments of the fault provides a picture of characteristic behavior that indicates thousands of years between faulting events. However, where longer records are available, as for the two southern segments, the most recent faulting events may not be regularly spaced in time and may vary in size and rupture different parts of the fault. The episodic character of surface-rupturing events along the southern segments, and the exceedingly high variability in slip rates over the course of 4–7 events may be the rule rather than the exception. We do not have a similarly long record for the central and northern parts of the fault and, thus their long-term behavior remains unknown.

References

Anderson, A.L., 1934, A preliminary report on recent block faulting in Idaho: Northwest Science, v. 8, p. 17–28.

Bankey, V., Webring, M., Mabey, D.R., Kleinkopf, M.D., and Bennett, E.H., 1985, Complete Bouguer gravity anomaly map of Idaho: U.S. Geological Survey Miscellaneous Field Studies Map MF-1773, 1 sheet, scale 1:500,000.

Baldwin, E.M., 1943, Structure and stratigraphy of the north half of the Lost River Range, Idaho: Ithaca, New York, Cornell University, unpublished Ph.D. dissertation.

Baldwin, E.M., 1951, Faulting in the Lost River Range area of Idaho: American Journal of Science, v. 249, p. 884–902.

Barrientos, S.E., Stein, R.S., and Ward, S.N., 1987, Comparison of the 1959 Hebgen Lake, Montana and the 1983 Borah Peak, Idaho, earthquakes from geodetic observations: Bulletin of the Seismological Society of America, v. 77, p. 784–808.

Beutner, E.C., 1972, Reverse gravitative movement on earlier overthrusts, Lemhi Range, Idaho: Geological Society of America Bulletin, v. 83, p. 839–846.

Boatwright, J., 1985, Characteristics of the aftershock sequence of the Borah Peak, Idaho, earthquake determined from digital recordings of the events: Bulletin of the Seismological Society of America, v. 75, p. 1265–1284.

Breckenridge, R.M., 1985, Identifying active faults by aerial photography—A comparison of the Lost River fault before and after the Borah Peak earthquake of October 28, 1983, *in* Stein, R.S., and Bucknam, R.C., eds., Proceedings of workshop XXVIII on the Borah Peak, Idaho, earthquake: U.S. Geological Survey Open-File Report 85-290, v. A, p. 110–115.

Bruhn, R.L., Yang, Z., Wu, D., and Yonkee, W.A., 1991, Structure of the Warm Spring and northern Thousand Springs fault segments, Lost River fault zone, Idaho—Possible effects on rupturing during the 1983 Borah Peak earthquake: Tectonophysics, v. 200, p. 33–49.

Crone, A.J., 1985, Fault scarps, landslides and other features associated with the Borah Peak earthquake of October 28, 1983, central Idaho—A field trip guide, with a section on the Doublespring Pass road trench by Hait, M.M., Jr.: U.S. Geological Survey Open-File Report 85-290, v. B, 23 p., 3 pls., scale 1:24,000.

Crone, A.J., and Haller, K.M., 1991, Segmentation and the coseismic behavior of Basin and Range normal faults—Examples from east-central Idaho and southwestern Montana, *in* Hancock, P.L., Yeats, R.S., and Sanderson, D.J., eds., Characteristics of active faults: Journal of Structural Geology, v. 13, p. 151–164.

Crone, A.J., Machette, M.N., Bonilla, M.G., Lienkaemper, J.J., Pierce, K.L., Scott, W.E., and Bucknam, R.C., 1987, Surface faulting accompanying the Borah Peak earthquake and segmentation of the Lost River fault, central Idaho: Bulletin of the Seismological Society of America, v. 77, p. 739–770.

Doser, D.I., and Smith, R.B., 1985, Source parameters of the 28 October 1983 Borah Peak, Idaho, earthquake from body wave analysis: Bulletin of the Seismological Society of America, v. 75, p. 1041–1051.

Hait, M.H., Jr., and Scott, W.E., 1978, Holocene faulting, Lost River Range, Idaho: Geological Society of America Abstracts with Programs, v. 10, p. 217.

Haller, K.M., 1988, Segmentation of the Lemhi and Beaverhead faults, east-central Idaho, and Red Rock fault, southwest Montana, during the late Quaternary: Boulder, University of Colorado, unpublished M.S. thesis, 141 p., 10 pls.

Jackson, S.M., 1994, Seismic evidence of conjugate normal faulting—The 1984 Devil Canyon earthquake sequence near Challis, Idaho: Boise, Idaho, Boise State University, unpublished M.S. thesis, 156 p.

Janecke, S.U., 1993, Structures in segment boundary zones of the Lost River and Lemhi faults, east central Idaho: Journal of Geophysical Research, v. 98, no. B9, p. 16,223–16,238.

King, J.J., Doyle, T.E., and Jackson, S.M., 1987, Seismicity of the eastern Snake River Plain region, Idaho, prior to the Borah Peak, Idaho, earthquake—October 1972-October 1983: Bulletin of the Seismological Society of America, v. 77, p. 809–818.

Kirkham, V.R.D., 1927, A geologic reconnaissance of Clark and Jefferson and parts of Butte, Custer, Fremont, Lemhi, and Madison Counties, Idaho: Idaho Bureau of Mines and Geology Pamphlet 19, 47 p., 4 pls.

Livingston, D.C., 1934, Some physiographic features of Idaho: The Compass, v. XIV, no. 4, p. 137–148.

Mabey, D.R., Peterson, D.L., and Wilson, C.W., 1974, Preliminary gravity map of southern Idaho: U.S. Geological Survey Open-File Report 74-78, 1 pl., scale 1:500,000.

Malde, H.E., 1971, Geologic investigation of faulting near the National Reactor Testing Station, Idaho: U.S. Geological Survey Open-File Report, 167 p., 2 pls.

Malde, H.E., 1985, Quaternary faulting near Arco and Howe, Idaho, *in* Stein, R.S., and Bucknam, R.C., eds., Proceedings of workshop XXVIII on the Borah Peak, Idaho, earthquake: U.S. Geological Survey Open-File Report 85-290, v. A, p. 207–235.

Malde, H.E., 1987, Quaternary faulting near Arco and Howe, Idaho: Bulletin of the Seismological Society of America, v. 77, p. 847–867.

Olig, S.S., Gorton, A.E., Bott, J.D., Wong, I.G., Knuepfer, P.L.K., Forman, S.L., Smith, R.P., and Simpson, D., 1995, Paleoseismic investigation of the southern Lost River fault zone, Idaho: Technical report to Lockheed Idaho Technologies Company, Idaho National Engineering Laboratory, Idaho Falls, Idaho, under Contract C93-134020, June 1995, 81 p., 5 pls.

Pierce, K.L., 1985, Quaternary history of faulting on the Arco segment of the Lost River fault, central Idaho, *in* Stein, R.S., and Bucknam, R.C., eds., Proceedings of workshop XXVIII on the Borah Peak, Idaho, earthquake: U.S. Geological Survey Open-File Report 85-290, v. A, p. 195–206.

Pierce, K.L., and Scott, W.E., 1982, Pleistocene episodes of alluvial-gravel deposition, southeastern Idaho, *in* Bonnichsen, B., and Breckenridge, R.M., eds., Cenozoic geology of Idaho: Idaho Bureau of Mines and Geology Bulletin 26, p. 685–702.

Reynolds, M.W., 1979, Character and extent of Basin-Range faulting, western Montana and east-central Idaho, *in* Newman, G.W., and Goode, H.D., eds., Basin and Range symposium and Great Basin field conference: Rocky Mountain Association of Geologists and Utah Geological Association, p. 41– 54.

Richins, W.D., Pechmann, J.C., Smith, R.B., Langer, C.J., Goter, S.K., Zollweg, J.E., and King, J.J., 1987, The 1983 Borah Peak, Idaho, earthquake and its aftershocks: Bulletin of the Seismological Society of America, v. 77, p. 694–723.

Ross, C.P., 1937, Geology and ore deposits of the Bayhorse region, Custer County, Idaho: U.S. Geological Survey Bulletin 877, 166 p.

Ross, C.P., 1947, Geology of the Borah Peak quadrangle, Idaho: Geological Society of America Bulletin, v. 58, p. 1085–1160.

Schwartz, D.P., and Coppersmith, K.J., 1984, Fault behavior and characteristic earthquakes—Examples from the Wasatch and San Andreas fault zones: Journal of Geophysical Research, v. 89, no. B7, p. 5681–5698.

Schwartz, D.P., and Crone, A.J., 1985, The 1983 Borah Peak earthquake—A calibration event for quantifying earthquake recurrence and fault behavior on Great Basin normal faults, *in* Stein, R.S., and Bucknam, R.C., eds., Proceedings of workshop XXVIII on the Borah Peak, Idaho, earthquake: U.S. Geological Survey Open-File Report 85-290, v. A, p. 153–160.

Schwartz, D.P., and Crone, A.J., 1988, Paleoseismicity of the Lost River fault zone, Idaho—Earthquake recurrence and segmentation: Geological Society of America Abstracts with Programs, v. 20, no. 3, p. 228.

Scott, W.E., 1982, Surficial geologic map of the eastern Snake River Plain and adjacent areas, 111° to 115° W., Idaho and Wyoming: U.S. Geological Survey Miscellaneous Investigations Series Map I-1372, 2 sheets, scale 1:250,000.

Scott, W.E., Pierce, K.L., and Hait, M.H., Jr., 1985, Quaternary tectonic setting of the 1983 Borah Peak earthquake, central Idaho: Bulletin of the Seismological Society of America, v. 75, p. 1053–1066.

Shemata, J.E., 1989, New analysis of three-component digital data for aftershocks of the 1983 Borah Peak earthquake, central Idaho—Source parameters and refined hypocenters: Salt Lake City, University of Utah, unpublished M.S. thesis, 126 p.

Skipp, B., and Hait, M.H., Jr., 1977, Allochthons along the northeast margin of the Snake River Plain, Idaho, *in* Heisey, E.L., Norwood, E.R., Wach, P.H., and Hale, L.A., eds., Rocky Mountain thrust belt geology and resources: Wyoming Geological Association, 29th Annual Field Conference, Teton Village, Wyoming, Guidebook, p. 499–515.

Skipp, B., and Harding, S.T., 1985, Preliminary report on geology of Borah Peak area, Idaho, including interpretation of seismic and gravity data, *in* Stein, R.S., and Bucknam, R.C., eds., Proceedings of workshop XXVIII on the Borah Peak, Idaho, earthquake: U.S. Geological Survey Open-File Report 85-290, v. A, p. 657–671.

Smith, R.B., Richins, W.D., and Doser, D.I., 1985, The 1983 Borah Peak, Idaho, earthquake—Regional seismicity, kinematics of faulting, and tectonic mechanism, *in* Stein, R.S., and Bucknam, R.C., eds., Proceedings of workshop XXVIII on the Borah Peak, Idaho, earthquake: U.S. Geological Survey Open-File Report 85-290, v. A, p. 236–263.

Stein, R.S., and Bucknam, R.C., eds., 1985, Proceedings of workshop XXVIII on the Borah Peak, Idaho, earthquake: U.S. Geological Survey Open-File Report 85-290, 686 p.

Stickney, M.C., and Bartholomew, M.J., 1987, Seismicity and late Quaternary faulting of the northern Basin and Range province, Montana and Idaho: Bulletin of the Seismological Society of America, v. 77, p. 1602–1625.

Stover, C.L., 1985, Isoseismal map and intensity distribution for the Borah Peak, Idaho,. earthquake of October 28, 1983., *in* Stein, R.S., and Bucknam, R.C., eds., Proceedings of workshop XXVIII on the Borah Peak, Idaho, earthquake: U.S. Geological Survey Open-File Report 85-290, v. A, p. 401–408.

Susong, D.D., and Bruhn, R.L., 1986, Structure of an earthquake rupture segment boundary in the Lost River fault zone, Idaho—Implications for rupture propagation during the 1983 Borah Peak earthquake [abs.]: Eos, Transactions of the American Geophysical Union, v. 67, no. 44, p. 1107.

Susong, D.D., Janecke, S.U., and Bruhn, R.L., 1990, Structure of a fault segment boundary in the Lost River fault zone, Idaho, and possible effect on the 1983 Borah Peak earthquake rupture: Bulletin of the Seismological Society of America, v. 80, p. 57–68.

Waag, C.J., 1985, Groundwater eruptions and sediment boil formation in the Chilly Butte area, Mt. Borah, Idaho, *in* Stein, R.S., and Bucknam, R.C., eds., Proceedings of workshop XXVIII on the Borah Peak, Idaho, earthquake: U.S. Geological Survey Open-File Report 85-290, v. A, p. 593–611.

Wallace, R.E., 1984, Eyewitness account of surface faulting during the earthquake of 28 October 1983, Borah Peak, Idaho: Bulletin of the Seismological Society of America, v. 74, p. 1091–1094.

Wallace, R.E., and Bonilla, M.G., 1984, Faulting related to the 1915 earthquakes in Pleasant Valley, Nevada: U.S. Geological Survey Professional Paper 1274-A, B.

Wilson, A.B., and Skipp, B., 1994, Geologic map of the eastern part of the Challis National Forest and vicinity, Idaho: U.S. Geological Survey Miscellaneous Investigations Map I-2395, 1 sheet, scale 1:250,000.

Wood, S.H., 1985, Regional increase in groundwater discharge after the 1983 Idaho earthquake—Coseismic strain release, tectonic and natural hydraulic fracturing, *in* Stein, R.S., and Bucknam, R.C., eds., Proceedings of workshop XXVIII on the Borah Peak, Idaho, earthquake: U.S. Geological Survey Open-File Report 85-290, v. A, p. 573-–592.

Youd, T.L., Harp, E.L., Keefer, D.K., and Willson, R.C., 1985, Liquefaction generated by the 1983 Borah Peak, Idaho, earthquake, *in* Stein, R.S., and Bucknam, R.C., eds., Proceedings of workshop XXVIII on the Borah Peak, Idaho, earthquake: U.S. Geological Survey Open-File Report 85-290, v. A, p. 625–644.

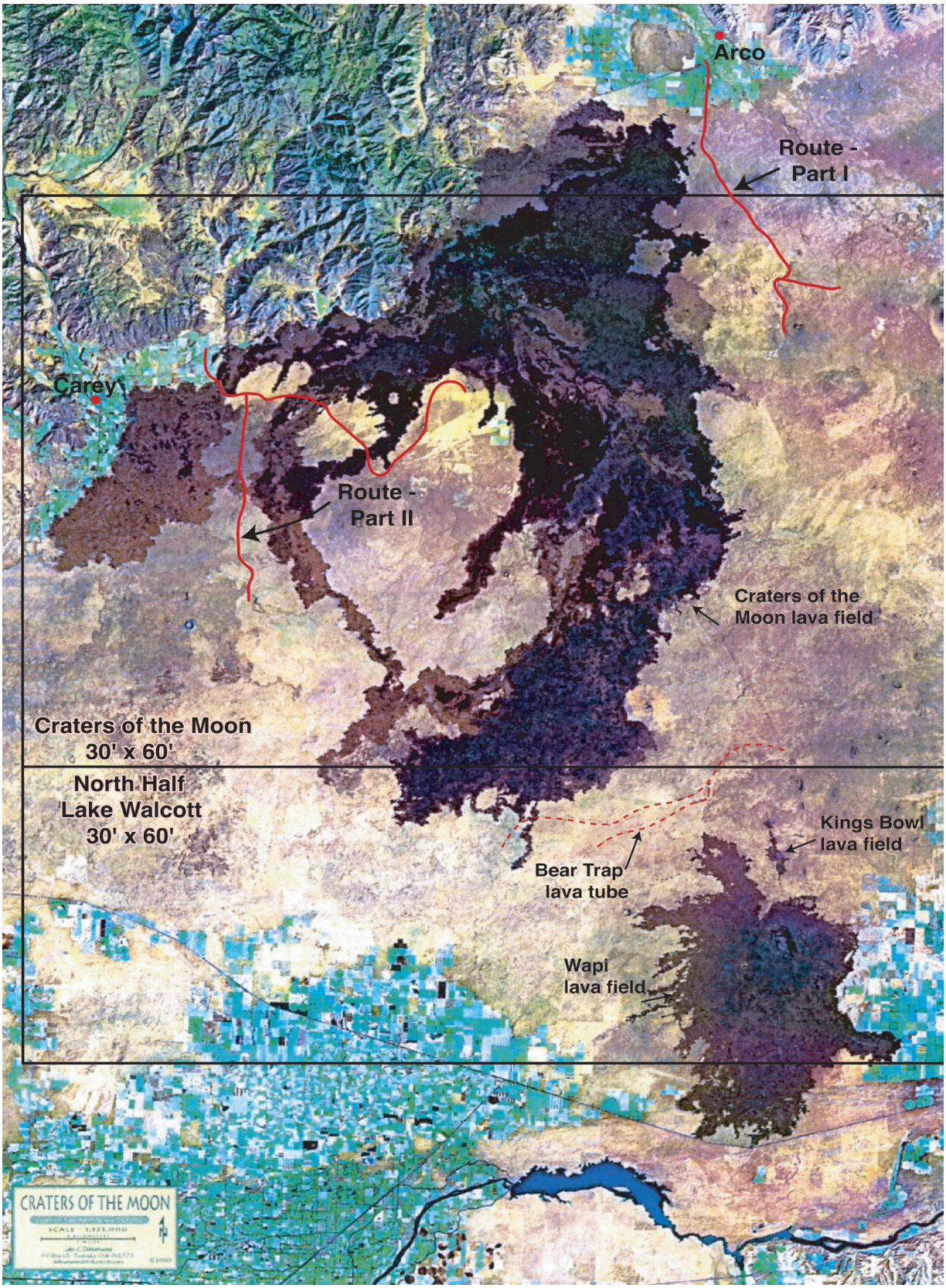

Figure I-1. Landsat-7 image of the Craters of the Moon, Kings Bowl, and Wapi lava fields. Shown on figure are routes of Parts I and II of this road log and boundaries of the Craters of the Moon and the northern half of the Lake Walcott 30′ x 60′ minute quadrangles. Image prepared by John Dohrenwend, P.O. Box 141, Teasdale, Utah, 84773. dohrenwend@rkymtnhi.com.

Geology of the Craters of the Moon 30′ X 60′ Map Area and New Perspectives on Basaltic Volcanism of the Eastern Snake River Plain, Idaho

By Mel A. Kuntz[1], Douglass E. Owen[2], Duane E. Champion[3], Phillip B. Gans[4], Sara C. Smith[5], and Cooper Brossy[5]

Introduction

Basaltic volcanism was a dominant geologic process in the eastern Snake River Plain (ESRP) in Holocene time, as attested by the fact that eight dominantly late Pleistocene and Holocene (<15 ka) lava fields cover about 13 percent of the ESRP.

Because widespread loess deposition essentially terminated at the end of the late Pleistocene, probably owing to abrupt climate change due to retreat of continental and alpine glaciers, the dominantly Holocene lava fields are relatively loess free and have low reflectance in Landsat satellite images (fig. I-1). Three of these lava fields, Craters of the Moon, Kings Bowl, and Wapi, lie along the Great Rift volcanic rift zone. The Great Rift volcanic rift zone is an 85-km-long and 2- to15-km-wide belt of tephra cones, lava cones, shield volcanoes, eruptive fissures and associated tephra deposits, and noneruptive fissures. These three, dominantly Holocene lava fields and the volcanic structures of the Great Rift volcanic rift zone lie within the Craters of the Moon 30' x 60' quadrangle and the northern half of the Lake Walcott 30' x 60' quadrangle (fig. I-1).

The Craters of the Moon National Monument was established by President Coolidge on May 2, 1924. Since 1924, the Monument has been expanded through five presidential proclamations. The most recent and largest expansion of the Monument occurred on November 9, 2000, when President Clinton signed a proclamation enlarging the Monument 13-fold, from 55,000 acres to 715,000 acres. The expanded Monument assures the protection of the entire Great Rift volcanic rift zone. It encompasses all of the Craters of the Moon lava field as well as remote areas that include the Kings Bowl lava field, Wapi lava field, and the Bear Trap lava tube. The Monument is managed cooperatively by the National Park Service and the Bureau of Land Management. The National Park Service has primary management authority over the portion of the Monument that includes the dominantly Holocene lava fields (Craters of the Moon, Kings Bowl, and Wapi). The Bureau of Land Management has primary management authority over the remaining portion of the monument. A Visitor Center, camping facilities, and the best access for sightseeing and hiking in the Craters of the Moon lava field are provided by the National Park Service at the north end of the Monument, located off U.S. Highway 20-26-93 between Arco and Carey.

[1]U.S. Geological Survey, Denver, CO 80225, mkuntz@usgs.gov

[2]Craters of the Moon National Monument and Preserve, Arco, ID 83213

[3]U.S. Geological Survey, Menlo Park, CA 94025

[4]Department of Geology, University of California, Santa Barbara, CA 93106

[5]Bureau of Land Management, Shoshone, ID 83352

Focus of Field Trip

The geologic map of the Craters of the Moon 30' x 60' quadrangle has now been published by the U.S. Geological Survey (Kuntz and others, in press). The map details the northern part of the Craters of the Moon lava field, especially near the Visitor Center and most easily accessible parts of Great Rift volcanic rift zone. This map now places the Craters of the Moon lava field within a larger framework of accurately dated and correlated, pre-Holocene basaltic volcanism in the ESRP.

The Craters of the Moon (COM) 30' x 60' map was published previously as a USGS Open-File map (Kuntz and others, 1994). On this map, the detailed geology of the northern part of the Craters of the Moon lava field was shown, based on detailed mapping, paleomagnetic studies, and radiocarbon dating (see Kuntz and others, 1994, and references therein). On the Open-File map, all surrounding lava fields were identified simply as “pre-Holocene lava fields”, because little accurate and precise radiometric dating had been conducted in this area. With the expansion of the Monument in 2000, funds became available from the National Park Service and the Bureau of Land Management to support additional paleomagnetic studies and $^{40}Ar/^{39}Ar$ dating. The completion of the geologic map of the Craters of the Moon 30' x 60' quadrangle is due in part to these two agencies. We acknowledge their support and encouragement. We hope that the Craters of the Moon quadrangle map and the forthcoming map of the northern half of the Lake Walcott 1:100,000-scale quadrangle will be important contributions for management of the expanded Monument as well as for the broad-scale understanding of the basaltic-volcanic evolution of the ESRP.

The combined field, paleomagnetic, and $^{40}Ar/^{39}Ar$ studies have given detail to the pre-Holocene lava fields that surround and lie within kipukas (areas of older lava flows surrounded

by younger lava flows) of the Craters of the Moon lava field. In addition, these studies now permit a more detailed analysis of the timescales for tectonics and basaltic magmatism for an important part of the ESRP. In a sense, these data can be used to determine the late and middle Pleistocene and Holocene "pulse rate" for basaltic volcanism for the Craters of the Moon lava field and lava fields that surround the Craters of the Moon field. These data show that a major volcanic rift zone, the Borkum rift zone, which contains vents at Sand Butte and Broken Top Butte, was active about 50 ka on the western margin of the Craters of the Moon lava field. A second region of young basaltic volcanism was active about 65–12 ka in the Arco-Big Southern Butte and Rock Corral Butte volcanic rift zones that lie east of the Craters of the Moon lava field (fig. I-1).

The focus of this field trip is to examine the setting of Holocene and late Pleistocene basaltic volcanism in the Craters of the Moon 30' x 60' area. The field-trip guidebook is presented in three parts. Part I will focus on late Pleistocene lava fields that lie east of the Craters of the Moon lava field in the Quaking Aspen Butte-Big Southern Butte area. This area is easily accessible on the Arco-Minidoka road (assuming good weather and dry roads) from 15 to 25 km south of Arco, Idaho. Part II will focus on late Pleistocene basaltic volcanism that lies west of the Craters of the Moon lava field in the Sand Butte-Laidlaw Park area. These latter two areas are easily accessible via the Carey-Kimama and Laidlaw Park roads. Part III will focus on new studies of various aspects of the Holocene basaltic volcanism of the Craters of the Moon lava field.

Travel Recommendations and Warning!

Travel on nonpaved roads in the ESRP is potentially very dangerous. This area is one of the most remote parts of the lower 48 states. You can travel roads in this part of Idaho for days without seeing another vehicle or person.

Type of vehicle, tire type and quality, and weather conditions must all be ideal to attempt travel on the roads described in this field-trip guide. **Four-wheel drive vehicles** with high clearance are strongly recommended. **Tires** should be of good quality; 6-ply and 8-ply tires with strong sidewalls are highly recommended. Typical tires on passenger sedans are much too weak for backcountry roads. If you should have a flat tire on a backcountry road, replace the tire and promptly, but **slowly,** drive to the nearest paved road. Do not tempt fate without a spare tire. Travel should be attempted only in times of **ideal weather conditions** (*i.e.*, when roads are dry and weather forecasts do not include the possibility of rain or snow). Travel on these roads in spring and early summer, when the roads are wet, can easily lead to vehicles becoming stuck in water-saturated, gumbo-like road materials. Backcountry roads typically are constructed of loess and gravel; loess becomes very sticky and slippery when wet. During the summer months and hot weather, it is advisable to travel in an air-conditioned vehicle. Keep windows closed and air conditioning on in order to create positive air pressure in the vehicle to keep out air-borne loess. **Always have a cell phone** in your vehicle. Many backcountry roads in the ESRP do not have cell phone coverage at road level, but coverage generally can be obtained by climbing to the top of a nearby hill or butte. **Always travel with extra food and water**. If you become stranded in the middle of the ESRP, you face a 10–50 km walk to the nearest paved road and some semblance of civilization. Potential problems can be also be alleviated if you also **carry a GPS receiver and maps that contain latitude-longitude and/or UTM coordinates**, such as 1:24,000-scale and 1:100,000-scale USGS topographic maps. If you become stranded, determine your location on a map, determine where roads lead, and how to find the quickest and shortest route to a paved road. In short, vehicle travel on backcountry roads in the ESRP can be enjoyable, educational, and entertaining, but it is not for the faint of heart. Follow these recommended safety precautions.

FIELD-TRIP ROAD LOG

Part I: Pre-Holocene Basaltic Volcanism of the Eastern Part of the Craters of the Moon 30′ x 60′ Quadrangle

The route of Parts I and II of the field trip may be followed on one of several maps, including the Craters of the Moon 30' x 60' topographic map, the Geologic Map of the Craters of the Moon 30' x 60' quadrangle, various USGS 1:24,000-scale topographic maps, and on figure I-1.

Mileage Inc.	Cum.	
0.0	0.0	START: Junction of U.S. Highways 20-26-93 in downtown Arco, Idaho. Proceed south on U.S. Highway 20-26 through Arco. Low flat ground on path of highway is Holocene flood plain of Big Lost River.
1.8	1.8	Cross Big Lost River.
0.3	2.1	Turn south on 3100 West Road (Arco-Minidoka Road).
0.2	2.3	Road rises onto upper Pleistocene, Pinedale-age terrace deposits on west side of Big Lost River. Unit covered by approximately 1–2 m of loess, which is exposed in borrow pit to west (right). Note very flat surface of unit; runways of Arco airport are located on this unit 1.5 km west. Extensive farming of potatoes, hay, and alfalfa for next several kilometers are on loess that covers this unit.

Mileage Inc.	Cum.	
~2.0	~4.3	Gooddales Cutoff (a branch of the Oregon Trail that began at Fort Hall, crossed the ESRP from Springfield, Idaho, to Big Southern Butte, and then traversed the northern side of the Snake River Plain) crosses 3100 West Road at approximately this point. Evidence of the emigrant trail at this locality now is destroyed by farming, but trail ruts can be easily recognized 1.5 km east and about 2 km west of this point.
0.7	5.0	Edge of terrace. Sediment in low area for next 0.6 km is alluvium deposited along a tributary of the Big Lost River that followed contact of the south edge of terrace deposit and basalt flows to the south.
0.4	5.4	Road rises onto basalt flows of the Wildhorse Butte lava field. Vent at Wildhorse Butte is located approximately 9 km south, just slightly east (left) of due south at about 11:30 o'clock on the horizon, just to the right of Big Southern Butte. $^{40}Ar/^{39}Ar$ age for Wildhorse Butte lava field is 325±10 ka.
1.0	6.4	Cattle guard and kiosk that describes the newly expanded, NPS-BLM, jointly-managed Craters of the Moon National Monument.
0.4	6.8	Bear left (southeast) and stop within 100 feet of the road junction for Stop I-1.

Stop I-1. Fault Scarp

Approximately 100–200 yards to the northeast is a fault scarp in flows correlated with Wildhorse Butte flows (325±10 ka) having steep, southwest-facing scarps, and displacement to the southwest. Total displacement on the fault ranges from about 5 m to the northwest, gradually decreasing to about 1 m to the southeast. Note that there is a small amount of drag of the upper surface toward the scarp face. This is a remarkably linear feature when viewed on aerial photos. The fault is parallel to the Arco segment of the Lost River range-front fault and to faults in the Box Canyon area of the Big Lost River, which is located about 8 km northeast of this stop (see Kuntz and others, 1994). Kuntz and others (2002) interpreted faults in the Box Canyon area to be of tectonic origin and that represent extensions onto the Snake River Plain of the Lost River range-front fault. A similar origin is postulated for this fault scarp. Smith and others (1989, 1996) and Hackett and Smith (1992) believe the faults in the Box Canyon area are related to dike-emplacement processes. The two different origins for the faults have significant implications for volcanic-hazard and seismic-hazard evaluations for present-day and future reactor and radioactive waste-burial sites at the Idaho National Engineering and Environmental Laboratory.

Mileage Inc.	Cum.	
2.5	9.3	Sixmile Butte shield volcano directly to the left at 9:00 o'clock, vent is 1.5 km away. Vent area for Quaking Aspen Butte shield volcano lies straight ahead, approximately 8 km distant. Wildhorse Butte vent area is approximately 3 km distant in a south-southwest direction (about 1:30 o'clock).
4.6	13.9	Road Junction. Bear straight ahead. Tincup Butte is directly to east (9:00 o'clock), Fingers Butte is to the right at 2:30 o'clock. Sunset Ridge is at 11:00 o'clock.
0.4	14.3	Note steep flow front of pahoehoe flows from Fingers Butte to right. The $^{40}Ar/^{39}Ar$ age of the Fingers Butte lava field is 57±20 ka. The road follows Fingers Butte flows (on right) for about 3 km.
0.8	15.1	Road Junction. Bear right toward "Bear Trap Cave" on sign.
1.1	16.2	Cattle guard. Vent area for Fingers Butte lava field to right at 3:00 o'clock, 1.8 km away.
0.9	17.1	Road to left. Wooden post with no sign marks junction. This road leads to vent area for Quaking Aspen Butte lava field. This road is rough and lined with sagebrush that will scratch vehicle doors. Do not attempt this road without 4WD.
2.1	19.2	Cattle Guard.
0.4	19.6	Stop I-2 is at a high point on the road on the west flank of the Quaking Aspen Butte lava field. At the end of the stop, turn vehicles around and head back north on the Arco-Minidoka road.

Stop I-2. Viewscape of the Rock Corral Butte Volcanic Rift Zone and the Southeast Margin of the Craters of the Moon Lava Field

The stop is chosen for its view to the east, south, and west. Many vent areas on the east side of the Craters of the Moon lava field are visible from this spot. From east to south to west, the major vents are:

•**Rock Corral Butte.** A large shield volcano on Rock Corral Butte volcanic rift zone. $^{40}Ar/^{39}Ar$ age of the rock Corral Butte lava field is 55±12 ka.

•**Serviceberry Butte.** A large shield volcano. $^{40}Ar/^{39}Ar$ age of the Serviceberry Butte lava field is 120±12 ka.

•**Split Top Butte.** A large shield volcano. $^{40}Ar/^{39}Ar$ age of the Split Top Butte lava field is 113±10 ka. Most flows from this vent area flow to the east into the Blackfoot 1:100,000-scale quadrangle.

•**Mosby Butte.** A large shield volcano on the southern margin of the Craters of the Moon 1:100,000-scale map. $^{40}Ar/^{39}Ar$ age of the Mosby Butte lava field is 265±30 ka.

•**Horse Butte.** Horse Butte is one of the largest, young shield volcanoes in the area southeast of the Craters of the Moon lava field. It has an awe-inspiring vent that is 1.1-km long, 700-m wide, and 90-m deep. Horse Butte is the source vent for the Bear Trap Cave lava tube-skylight-rootless vent system. Horse Butte flows extend about 35 km north and west from the source vent. The Bear Trap Cave lava-tube system extends about 31 km from Horse Butte, making it the longest lava tube-skylight-rootless vent system in the ESRP.

•**Rattlesnake Butte.** Rattlesnake Butte is a small cinder cone 40-m high that is on the Vent 5149–Rattlesnake Butte eruptive-fissure system. The northwestern part of the eruptive-fissure system is represented by four small, aligned kipukas of cinder deposits that are completely surrounded by the Blue Dragon flows of the Craters of the Moon lava field.

•**Pratt Butte.** A large shield volcano. Only proximal flows are exposed. Medial and distal flows are covered by younger flows. $^{40}Ar/^{39}Ar$ age of the Pratt Butte lava field is 263±20 ka.

•**Blacktail Butte.** This vent area, a fissure-dominated, cinder-cone complex, is the southernmost cinder-cone vent area of the Craters of the Moon lava field. Age of flows from this vent area is about 4,300 ^{14}C yr BP.

•**Quaking Aspen Butte.** The vent area for this lava field lies behind (northeast of) the viewpoint about 2 km. Quaking Aspen Butte shield volcano is one of the largest in the ESRP. Quaking Aspen Butte flows have not been dated by $^{40}Ar/^{39}Ar$ methods, but Quaking Aspen Butte flows partly cover the Coyote Butte eruptive-fissure center in the Arco-Big Southern Butte volcanic rift zone, which has been dated at 64±20 ka.

Mileage Inc.	Cum.	
4.3	23.9	Junction. Turn right to "Quaking Aspen Butte airstrip."
1.3	25.2	Cattle guard.
0.7	25.9	Park for Stop I-3. At the end of the stop, turn vehicles around and head back (west) toward Arco-Minidoka road.

Stop I-3. Viewscape of the Arco-Big Southern Butte Volcanic Rift Zone, Big Southern Butte, and Rock Corral Butte Area

The $^{40}Ar/^{39}Ar$ age of Coyote Butte, a fissure-dominated eruptive center, is 64±20 ka, demonstrating that basaltic volcanism is a recent and major process in the Arco-Big Southern Butte volcanic rift zone. Middle Butte and East Butte (hidden behind Middle Butte) are visible on the horizon to the left of Big Southern Butte. Middle Butte has a cap of olivine basalt dated at approximately1 Ma. No rhyolite is exposed on flanks of Middle Butte, but geophysical data suggest that rhyolite forms the core of the Butte. Big Southern Butte consists of two, coalesced cumulo domes. The main, central part of the dome consists of spherulitic, flow-banded rhyolite in the core and autoclastic breccia and sugary rhyolite that represent deformed crust above the flow-banded core. The age of the flow-banded, central part of the dome is 309±10 ka. The flow-banded rhyolitic core uplifted and tilted 45° northeastward a 350-m-thick section of basaltic flows on the northeast flank of the dome. Spear and King (1982) and Fishel (1993) suggest that this section is an uplifted and tilted flap of basalt flows of the predome surface of the ESRP. About 20 individual flows and flow units are present in the flap. Most flows are olivine basalts and evolved olivine basalts; the uppermost flow is ferrolatite from Cedar Butte, which is located out of sight behind and about10 km east of Big Southern Butte. The age of Cedar Butte is 400±19 ka (Kuntz and others, 1994). A massive, aphyric, sugary-textured, curved rhyolite "dike" forms a carapace over the flow-banded rhyolite on the west and southwest sides of the dome. This northwestern part of the dome is dated at 294±15 ka (Kuntz and others, 1994). Big Southern Butte is 6.5 km in diameter, rises 760 m above the surrounding flat surface, and has an exposed volume of about 8 km^3. Spear and King (1982) suggest that Big Southern Butte formed in several stages, including initial sill and laccolith stages at depth, followed by extrusion and growth of two endogenous domes on the surface. East Butte, Middle Butte, and Big Southern Butte were prominent landmarks for early travelers and explorers in the ESRP; they were referred to as the "Trois Tetons" and the "Three Buttes" in early descriptions of the area (*e.g.*, Fremont, 1845), whereas the Teton Mountains were referred to as the "Pilot Knobs." Rock Corral Butte can be observed on the horizon to the south (right) of Big Southern Butte. The $^{40}Ar/^{39}Ar$ age of Rock Corral Butte lava field is 55±12 ka.

Mileage Inc.	Cum.	
2.0	27.9	Junction of Quaking Aspen Butte airstrip road and Arco-Minidoka road. Turn right (north) toward Arco.
15.9	43.8	Junction, Arco-Minidoka Road (3100 E.) and U.S. Highway 20-26. Turn right.

2.1	45.9	END. Intersection of U.S. Highways 93 and 20-26 at stoplight in downtown Arco, Idaho.

Part II: Pre-Holocene Basaltic Volcanism of the Western Part of the Craters of the Moon 30′ x 60′ Quadrangle

Mileage Inc.	Cum.	
0.0	0.0	START. Begin field trip at Texaco station at Adamson's Market (west side) and the Carey Sport Shop (east side) of U.S. Highway 20-26 in downtown Carey, Idaho.
0.7	0.7	Park in lot on right just past the Loading Chute Restaurant for Stop II-1.

Stop II-1. Fault in Basalt At Carey

Across road on northwest side is a fault in basalt at Carey. $^{40}Ar/^{39}Ar$ age of flow is 4.20±0.02 Ma. The scarp at the road level is about 7-m high; about 1.5 km northwest, the scarp is about 10-m high. Note that basalt flow dips about 2° to the southeast, toward the Snake River Plain.

Mileage Inc.	Cum.	
1.1	1.8	Carey Lake on right (south). Lake formed by damming of springs that lie just north of road by Carey flows of the Craters of the Moon lava field (radiocarbon age 12,010±150 ^{14}C yr BP; table 1).
0.7	2.5	Shield volcano on horizon at 1:00 o'clock is Laidlaw Butte. Laidlaw Butte is one of the highest shield volcanoes on the ESRP, rising about 275 m above surrounding, younger flows. Flows of this shield are characterized by extremely coarse texture containing plagioclase crystals as long as 3 cm. The relatively high viscosity of the lava probably caused "piling up" of flows near the vent and creation of steep shield flanks.
3.1	5.6	Gravel pits are in alluvial fan deposits of Fish Creek. Alluvial deposits lie on flows of the Fish Creek Reservoir lava field. Vent for flows is at Fish Creek Reservoir and lies about 8 km north of highway.
1.5	7.1	Turn right (south) on Carey-Kimama road (Laidlaw Park road). Fish Creek Reservoir flows on right.
0.2	7.3	Gravel pits on left are in alluvial-fan deposit of Fish Creek.
1.0	8.3	Intersection. Interpretive kiosk is for Craters of the Moon National Monument. Turn left (east).
0.1	8.4	Road rises onto loess-covered pahoehoe (Hawaiian term for basaltic lava flow having billowy, ropy surfaces) flow of unknown age and unknown source vent. Source vent probably east of this point.
0.7	9.1	Road curves to right and rises onto pahoehoe of the Carey flows of the Craters of the Moon lava field (radiocarbon age 12,010±150 ^{14}C yr BP; table 1). Contrast lack of loess cover on Carey flows here with flows observed 0.7 km back to west.
0.4	9.5	Collapse pits in Carey pahoehoe flows to left and right of road.
0.8	10.3	Road drops off Carey flows onto older flows in Paddelford Flat. Paddelford Flat is a kipuka surrounded by flows of the Craters of the Moon lava field. Note that flows here are loess covered and very smooth. Excavation site for radiocarbon samples for dating Carey flows lies about 10 m north of road at this location.
1.0	11.3	Road intersection. Turn right (south) onto Carey-Kimama road.
0.5	11.8	Road rises onto pre-Holocene pahoehoe flows in south part of Paddelford Flat. Even though pre-Holocene, these flows are very young, probably 40–20 ka.
0.6	12.4	Flow fronts for pahoehoe flows from here and for several kilometers.
3.9	16.3	Road rises onto north edge of Carey flow.
0.8	17.1	South edge of Carey pahoehoe flows. Wagon Butte to right at 2:00 o'clock. $^{40}Ar/^{39}Ar$ age of Wagon Butte is 120±25 ka. Laidlaw Butte shield volcano to left at 10:00 o'clock. $^{40}Ar/^{39}Ar$ age of Laidlaw Butte lava field is 425±25 ka.

Table 1. Radiocarbon ages of lava flows in the Craters of the Moon and Quaking Aspen Butte lava fields of the eastern Snake River Plain, Idaho.

[Type of sample: sa = charred sediment pretreated by sieving and acid leaching only; sdda = charred sediment pretreated by dissaggregation-deflocculation-acid method; saaa = charred sediment pretreated by sdda method and by acid-alkali-acit pretreatment; ca = charcoal leached with dilute HCI acid only; caaa = charcoal pretreated by acid-alkali-acid method. For lab number, prefit Tx refers to University of Texas (Valastro and others, 1972); prefix W refers to samples analyzed at the USGS Radiocarbon Laboratory, Reston, Va. Prefix USGS refers to samples analyzed at the USGS Radiocarbon Laboratory, Menlo Park, Calif. Radiocarbon measurements were made by the standard acetylene gas counting method at the USGS Radiocarbon Laboratories, Reston, Va., and Menlo Park, Calif. Sample activities were not corrected for isotope fractionation by a ^{13}C measurement. The ages were calculated relative to the U.S. National Bureau of standards oxalic acid standard activity (Stuiver and Polach, 1977). See Kuntz and others (1986) for details of radiocarbon dating methods and data.]

Lava fields, lava flows, and eruptive periods	Sample pretreatment	Field number	Lab number or reference	^{14}C date (yr B.P.)	Mean or oldest age (yr B.P.)
		CRATERS OF THE MOON LAVA FIELD			
Eruptive period A					
Broken Top				Undated	
Blue Dragon	ca	K79-C5	W-4466	1,670±60	
	caaa	K79-C5	W-4578	2,030±80	
	caaa		Tx-899	2,110±90	
	caaa		Tx-900	2,050±80	2,076±45
	caaa		Tx-901	2,200±130	
Trench Mortar Flat	caaa		Tx-1157	2,210±80	
	caaa		Tx-1158	2,240±80	
	caaa		Tx-1159	2,250±80	
	caaa		Tx-1160	2,310±70	2,205±25
	caaa		Tx-1161	2,130±80	
	caaa		Tx-1162	2,270±80	
	caaa		Tx-1163	2,140±60	
	ca	K79-C3	W-4413	2,100±60	
	caaa	K79-C6	W-4581	2,180±70	
North Crater				Undated	
Big Craters	ca	K80-C1	W-5342	2,400±300	2,400±300
Serrate				Undated	
Devils Orchard				Undated	
Highway				Undated	
Eruptive period B					
Vermillion Chasm				Undated	
Deadhorse	sdda	K78-S55	W-4259	4,300±60	4,300±60
Devils Cauldron	sdda	K78-S56	W-4287	2,820±90	
	saaa	K78-S56	W-4339	3,660±60	3,660±60
Minidoka	sdda	K78-S58b	W-4267	2,650±50	
	saaa	K78-C7	W-4447	3,510±100	4,510±100
Black Top				Undated	
Eruptive period C					
Indian Wells north				Undated	
Indian Wells south				Undated	
Sawtooth	saaa	K78-S67	W-4370	6,020±160	6,020±160
South Echo				Undated	
Sheep Trail Butte				Undated	
Fissure Butte				Undated	

Table 1. Radiocarbon ages of lava flows in the Craters of the Moon and Quaking Aspen Butte lava fields of the eastern Sna Plain, Idaho.—Continued

Lava fields, lava flows, and eruptive periods	Sample pretreatment	Field number	Lab number or reference	^{14}C date (yr B.P.)	Mean or olde (yr B.P.)
Sentinel				Undated	
Eruptive period D					
Silent Cone				Undated	
Carey Kipuka	sdda	K78-S64	W-4310	3,860±120	
	saga	K78-S64	W-4592	6,600±60	6,600±60
Little Park	sdda	K78-S66	W-4260	3,960±90	
	saga	K78-S66	W-4587	6,500±60	6,500±60
Little Laidlaw Park				Undated	
Eurptive period E					
Grassy Cone	saga	K78-S60	W-4385	6,670±100	
	saga	K79-C12	W-4488	7,360±60	7,360±60
Laidlaw Lake	saaa	K79-C9	W-4511	7,470±80	7,470±80
Lava Point	saaa	K78-S68	W-4497	7,840±140	7,840±140
Eruptive period F					
Pronghorn	sdda	K78-S73	W-4271	6,820±60	
	saga	K78-S73	W-4586	10,240±120	10,240±120
Bottleneck Lake	sdda	K78-S72	W-4291	5,230±110	
	saaa	K78-S72	W-4343	7,900±100	
	sdda	K78-S71	W-4280	9,330±120	
	sdda	K78-S71	W-4305	11,000±100	11,000±100
Heifer Reservoir	sdda	K78-S53b	W-4306	9,330±120	
	saaa	K78-S54	W-4583	10,670±150	10,670±150
Eruptive period G					
Sunset	sdda	K78-S58c	W-4270	3,270±80	
	sdda	K76-C4A	W-3674	11,120±120	
	ca	K78-S77	W-4296	12,010±150	12,010±150
Carey	sdda	K78-S62	W-4235	4,310±80	
	sdda	K78-S61c	W-4301	6,500±110	(-12,000)
Lava Creek	saaa	K79-C11	W-4478	11,970±120	
	saaa	K79-C10	W-4476	12,760±150	12,760±150
Eruptive period H					
Kimama	saaa	K78-S75	W-4387	13,900±400	
	saaa	K79-C8	W-4473	15,100±160	15,100±160
Bear Den Lake				Undated	
Baseline				Undated	
Little Prarie				Undated	
Lost Kipuka				Undated	
No Name				Undated	
Brown Flow				Undated	
		QUAKING ASPEN BUTTE LAVA FIELD			
Quaking Aspen Butte	sa	K77-C5	W-3918	>40,000	>40,000

2.6	19.7	Sign "Leaving National Monument."
0.3	20.0	Enter flows of Spud Butte-Broken Top Butte flow complex. $^{40}Ar/^{39}Ar$ age of Broken Top lava field is 57±30 ka.
3.2	23.2	Drop into 300-m-wide lava channel, having leveed walls as high as 10 m. This channel extends 2.5 km north, west, and south from main vent at "The Blow Out" lava field. A rafted block has been stranded in the channel to the left (east).
0.3	23.5	Note levees on south side of channel.
0.9	24.4	Turn onto dirt road on left. Travel 0.1 mi and stop. Do not travel 0.2 mi!
0.1	24.5	Following Stop II-2, return 0.1 mile to main road (Carey-Kimama road), turn right (north), and retrace route north for about 13.0 mi to the intersection of the Laidlaw Park and Carey-Kimama roads in Paddelford Flat.

Stop II-2. Vent Area for "The Blow Out"

Broad, low area directly east is a lava lake. Note walls of lake are 20- to 25-m high. The walls of the lava lake are made up of thin layers of shelly pahoehoe. Note the local frothy character of these flows and that individual flows are made up of interlayered dense and vesicular flow units. These variably-textured flow units represent different conditions of overflow of the lava lake: dense layers represent overflow or explosion of degassed lava from lake, vesicular layers represent overflow of more gas-charged lava. A 100-m-wide, 4.3-km-long lava channel extends east-southeast of the southern end of the lava lake. At the left (north end) of the lava lake is the main vent for "The Blow Out." This vent is a circular depression, 70-m deep and 300-m wide. The $^{40}Ar/^{39}Ar$ age of "The Blow Out" lava field is 116±15 ka. Looking *south* from this location, note Vent 4792 shield volcano at about 5:30 o'clock, about 3 km distant, and Wildhorse Butte ($^{40}Ar/^{39}Ar$ age <50 ka) shield volcano at about 6:00 o'clock (due south), about 10 km distant. In looking *west* from this location, note Sand Butte (tephra cone), Broken Top, and Spud Butte (from left to right; south to north) on the horizon. The vents for these three lava fields are aligned along a 15-km-long, north/south-trending, eruptive-fissure system. These three lava fields have the same paleomagnetic directions, which strongly suggest that they formed contemporaneously. The age for one of these lava fields, the Broken Top field, is 57±30 ka, thus this volcanic rift zone was active at about 60 ka. Sand Butte is a circular tephra cone about 1,400 m in diameter. The cone has a north-south elongated depression about 700 m in diameter; the cone walls are about 100-m high. The cone consists of well-bedded, locally agglutinated ash and palagonitized sideromelane deposited by hydrovolcanic eruptions during the later stages of volcanic activity at Sand Butte. In looking due *north* from this location, note foothills of the Pioneer Mountains, then, progressively to the right (south) are cinder cones (including Grassy, Sunset, Big Craters, Big Cinder Butte, among others) of the northern part of the Craters of the Moon lava field and the Great Rift volcanic rift zone, Laidlaw Butte (large shield volcano), Big Southern Butte, and Bear Den Butte (the cinder cone for the Bear Den Butte lava field. The $^{40}Ar/^{39}Ar$ age of Bear Den Butte lava field is 58±10 ka.

Mileage Inc.	Cum.	
13.0	37.5	Junction. Laidlaw Park and Carey-Kimama roads. Turn right (east). Vents that caused diversion of Carey flows and created Paddelford Flat kipuka are at 11:00 o'clock, about 3 km distant.
1.6	39.1	Tongue of Carey pahoehoe to left (north), about 1 km away.
0.4	39.5	Channel in Paddelford Flat flows.
0.2	39.7	Road rises onto Grassy Cone rough-surfaced pahoehoe flow. This is not an a' a (Hawaiian term for basaltic lava flows typified by rough, jagged, clinkery, spinose surface) flow. Surface roughness here is due to collapse of pahoehoe-flow surfaces. Note that plates consist of broken, ropy pahoehoe. Age of Grassy Cone flows is 7,360±60 ^{14}C yr BP (table 1).
0.5	40.2	Big Cinder Butte in Craters of the Moon lava field at 11:30 o'clock on the horizon.
0.9	41.1	Kipuka in Grassy Cone pahoehoe flows.
1.1	42.2	Road drops off Grassy Cone flows into Little Park, another of the large kipukas on the west side of the Craters of the Moon lava field. Vents for Little Park pahoehoe flows are at 10:00 o'clock to left (north).
1.2	43.4	Channel in pahoehoe flows of Little Park.
2.1	45.5	Road ascends steep flow front of Little Park a' a flow. This is the first of several true a' a flows in the Little Park-Laidlaw Park area that are encountered on or near the Laidlaw Park road. Age of Little Park a' a flow is 6,500±60 ^{14}C yr BP (table 1).
0.3	45.8	Park for Stop II-3.

Stop II-3. Little Park A′ A Flow

This stop provides the easiest access to an a' a flow of the Craters of the Moon lava field. In the Craters of the Moon lava field, pahoehoe flows have a typical partial chemical composition as that given for the Carey flow, and a' a flows have compositions similar to or slightly more silicic than the Little Park a' a flow. Partial chemical analyses (in percent) for Carey pahoehoe flow and Little Park a' a flow are given below:

	Carey pahoehoe	Little Park a' a
SiO_2	47.22	49.46
Al_20_3	13.46	14.28
Fe_2O_3	0.89	1.14
FeO	14.93	13.55
MgO	3.91	3.08
CaO	8.24	6.49
Na_2O	3.47	4.28
K_2O	1.94	2.30

Note the very slight, but significant differences in the compositions of the two flows that lead to such marked differences in flow type. There is only a 2 percent difference in silica, total iron is about the same, lime is significantly lower in the a' a flow, magnesia is slightly lower in the a' a flow, and the total alkalis are approximately equal. Evidently, the slightly higher silica and lower magnesia and lime must have a pronounced effect to increase the viscosity of the a' a lavas.

At this locality, examine the character of the a' a flows. Look for spiny fragments of lava, accretionary lava balls, and note the density of fragments. Most a' a flows contain prominent flow ridges that are perpendicular to and convex toward the direction of flow movement, much like the ogives that characterize the surfaces of glaciers. A' a flows also contain longitudinal furrows and cracks that are roughly parallel to the direction of flow movement. These furrows and cracks are the surface expression of vertical or near vertical shear planes that separate the a' a flow into longitudinal lobes that moved at different rates with respect to one another. The flow ridges and furrows/cracks may not be visible from ground level, but they are obvious on air photos. It is extremely difficult to walk on a' a flows. Be careful!

Mileage Inc.	Cum.	
0.3	46.1	Drop down steep flow front of Little Park a' a flow and cross cattle guard. Road enters Laidlaw Park.
2.6	48.7	Ant Butte Junction. Turn left (north).
0.1	48.8	Cattle guard. Bear right.
1.0	49.8	Ant Butte cinder cone ahead on left. Ant Butte is local source of cinders for road aggregate.
1.6	51.4	Big Blowout Butte on left. Road passes through neck of lava lake that extends southeast from vent crater for distance of about 1 km. $^{40}Ar/^{39}Ar$ age of Big Blowout Butte lava field is 210±15 ka.
1.8	53.2	Road crosses eruptive fissure for Hollow Top lava field. Vent is difficult to discern at road level but is obvious on air photos. Hollow Top is undated.
0.4	53.6	Landing strip to left.
1.0	54.6	Note steep flow fronts for Little Park and Indian Wells South a' a flows to left (north) of road about 0.8 km distant. Road begins relatively steep ascent of west flank of Snowdrift Crater shield volcano. Note the very smooth character of flows that make up west flank of Snowdrift Crater shield volcano, due largely to a significantly thick (~1–3 m) mantle of loess and eolian sand. If the road is dry, you will notice the loess as it fills the air behind vehicles ahead. Be sure to roll up windows.
1.6	56.2	Dirt road on left. Turn left, go 0.1 mi. Do not go 0.2 mi!
0.1	56.3	Following Stop II-4, turn vehicles around and retrace route back across Laidlaw Park, Little Park, Paddelford Flat and the Carey pahoehoe flow to the junction of the Carey-Kimama/ Laidlaw Park road and U.S. Highway 20-26.

Stop II-4. Snowdrift Crater

Snowdrift Crater is the vent for the Snowdrift Crater shield volcano. This shield rises about 90 m above surrounding, younger flows on the west. The vent area is a N. 45° W.-trending depression 1,500-m long, that consists of two craters: northwestern crater is circular and 35-m deep and southeastern crater is elongated and 55-m deep. Crater walls consist of well-layered shelly pahoehoe. The $^{40}Ar/^{39}Ar$ age of Snowdrift Crater lava field is 480±50 ka. Little Laidlaw Park a' a flows of the Craters of the Moon lava field lap up onto the east flank of Snowdrift Crater to within 25 m of summit. Because of its height, Snowdrift Crater shield volcano formed a significant edifice that impeded the southward movement of a' a flows of eruptive periods C and D of the Craters of the Moon lava field and created the large kipuka known as Laidlaw Park. From this locality, large cinder cone on horizon directly north, about 6 km distant, is Big Cinder Butte, the source vent for Indian Wells North, Indian Wells South, and Sawtooth a' a flows. To

the northeast (about 1:30 o'clock) is North Laidlaw Butte, about 2 km distant. North Laidlaw Butte is a kipuka cinder cone that is completely surrounded by Indian Wells North and Sawtooth a' a flows. North Laidlaw Butte is relatively old, as shown by its significant cover of loess.

Mileage Inc.	Cum.	
22.7	79.0	Junction, Carey-Kimama/Laidlaw Park road and Highway 20-26. Turn left (west) on U.S. Highway 20-26 to return to Carey. Turn right (east) on U.S. Highway 20-26 to return to Visitor Center at Craters of the Moon National Monument and/or Arco, Idaho.

Part III. Craters of the Moon Lava Field and the Northern Part of the Great Rift Volcanic Rift Zone

Introduction to the Developed Portion of the Craters of the Moon National Monument and Preserve

Craters of the Moon National Monument was originally set aside by President Calvin Coolidge in 1924 to preserve, for both present and future generations, what was described as "a weird and scenic landscape peculiar to itself." On November 9, 2000, President Bill Clinton increased the size of the original Monument 13-fold and assigned joint management of the expanded Monument to the National Park Service and the Bureau of Land Management. As a result, approximately 750,000 acres (1,100 mi^2) of the area surrounding the Great Rift has been withdrawn from extractive operations (with the exception of existing authorized materials sites within the Monument) and limits mechanized travel within the Monument to roads. Outside the Monument, rock collecting and other extractive operations are permitted, and travel is not as restricted. Almost all of the Great Rift volcanic rift zone, which is the best-developed example of a volcanic rift zone on the ESRP, lies within the Monument. Of the eight geologically young lava fields found on the ESRP, the Monument encompasses the three youngest. Therefore, these three lava fields are some of the least altered by natural processes, making them some the best places for observing geologic features associated with basaltic volcanism on the ESRP. The Monument now includes all but the northern-most part of the Craters of the Moon (COM) lava field, the largest, dominantly Holocene basaltic lava field in the lower 48 states. Monument designation thus provides a long-term beneficial impact to ESRP geologic resources by not only protecting and preserving a sizeable part of the ESRP geology for future generations to enjoy, but also by preserving and protecting some of the best geologic examples of basaltic volcanism within the continental United States.

Mileage Inc.	Cum.	
0.0	0.0	**STOP III-1. CRATERS OF THE MOON VISITOR CENTER.** When you arrive at the Visitor Center, take a few minutes to look at the exhibits and use the restrooms. Road log will follow route on figure III-1.

LUNCH: Maintenance Shop. We will be using the woodshop in the maintenance building behind the Visitor Center for lunch while viewing animations that help explain some of the geology within the developed part of the Monument. These animations are being created by Idaho BLM staff (Antonia Hedrick, Cooper Brossy, and Sara C. Smith) in collaboration with the Educational Multimedia Visualization Center, Dr. Tanya Atwater's animation laboratory at University of California at Santa Barbara.

Trip leaders will be on hand to answer questions during lunch. A 20-page general overview of the Monument geology will be passed out at lunch, along with a 10-page description of the recent rafted-block investigation.

Mileage Inc.	Cum.	
0.2	0.2	Entrance Station.
0.2	0.4	Entrance to Campground. The block-a' a trachyandesite flow in the campground is one of the most silica-rich flows (63 percent silica) of the COM lava field, and it is considered to be part of the undated Highway flow (table 1). The Highway flow will be discussed at Stop III-2.
0.3	0.7	Turnout on right for North Crater flow interpretive trail. Continue on loop road.
0.1	0.8	Park at turnout for Stop III-2.

Stop III-2. Turnout Located at East Flank of North Crater

This trailhead is the start of the North Crater-to-Spatter Cones trail. We will be hiking a few hundred meters on this steep cinder trail to a good overlook of the area. Binoculars and/or cameras with a telephoto lens will be an advantage. A brief discussion of the pressure or flow ridge to the north and its attendant examples of squeeze-ups will be contrasted to

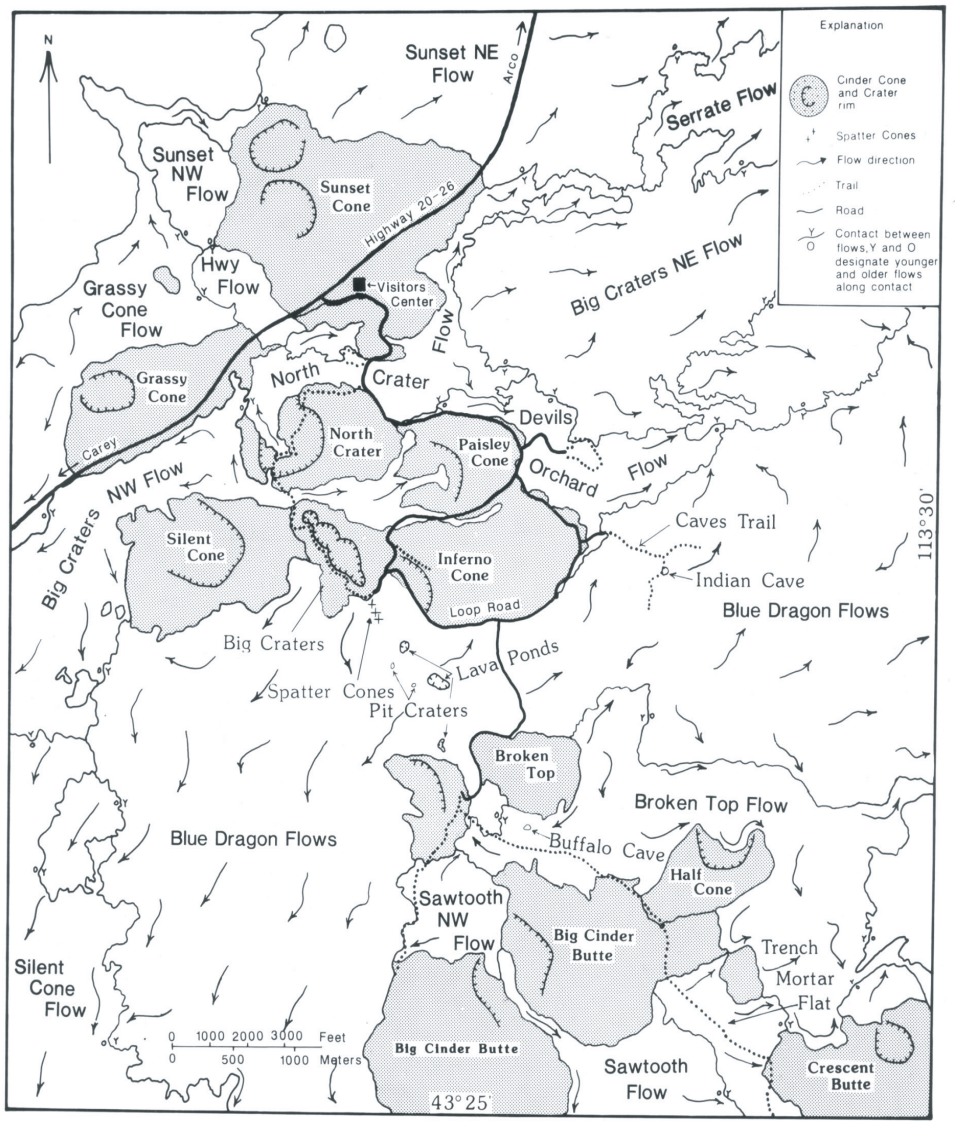

Figure III-1. Area around Craters of the Moon Loop Drive.

other similar features in other parts of the Monument. The trail continues for about 2 km to where it joins the paved trail at the south rim of Big Craters cinder-cone complex.

Stop III-3. Geologic Features at North Crater and Vicinity

Look to the north and notice the sharp drop-off just below the campground, this is the "Highway fault." You can trace the fault off into the distance to the west. The very jagged lava flow nestled between Sunset Cone and Grassy Cone is the Highway flow (fig. III-1). The blocky lava flow that the campground is built on also is a part of this flow. The Highway fault likely represents a collapse scarp that formed because of the large volume of lava that was poured out from the magma chamber (possibly beneath ancestral North Crater cinder cone) in a series of flows. The hill north of the North Crater Flow Trail parking area is either a remnant of North Crater, a very large rafted block, or possibly a part of another old cone.

The area around North Crater cinder cone and the Visitor Center is one of the more complex areas in the Craters of the Moon lava field, and the North Crater Trail provides a good vantage point to view this area. About 2,300 yr ago, this area may have looked very different than it does today. Specifically, North Crater and the small flank cone behind the fee/entrance booth on the southeast side of Sunset Cone probably were larger, and another cone or cones may have existed to the north of North Crater (see fig. III-2). Five lava flows, the Highway, Devils Orchard, Serrate, Big Craters Northeast, and North Crater flows, erupted from vents in the area (see fig. III-3). Three of these flows, the Highway, Devils Orchard, and Serrate flows, are particularly high in silica, 54–64 weight percent (Kuntz and others, 1986). They erupted violently and were viscous enough to break apart cinder cones and carry the pieces as far as 13 km to the northeast (see fig. III-3). These pieces of broken cinder cones, carried by lava flows like icebergs in ocean currents, are termed "rafted blocks." As rafted blocks were carried by lava flows, they broke up into smaller pieces and became incorporated into the transporting flow. Later, younger flows buried many of them. Only the largest and most coherent blocks, which poke through the younger lava flows, are easily seen (see fig. III-4 for distribution of rafted blocks). The North Crater Flow Trail and Devils Orchard Nature Trail provide excellent closeup views of rafted blocks, while the viewpoint atop Inferno Cone offers a panorama of the tremendous scale and extent of rafted blocks.

For a more in-depth discussion of the existence of now absent (destroyed?) cinder cones, the duration and timing of the lava flows, and the process of block rafting, consult the handout from lunch or see *The North Crater Neighborhood—More complex than Mr. Rogers'* on the Monument web site: *http://data2.itc.nps.gov/nature/documents/field%5Ftrip%5Ftext%5F2%2D1%2Epdf.*

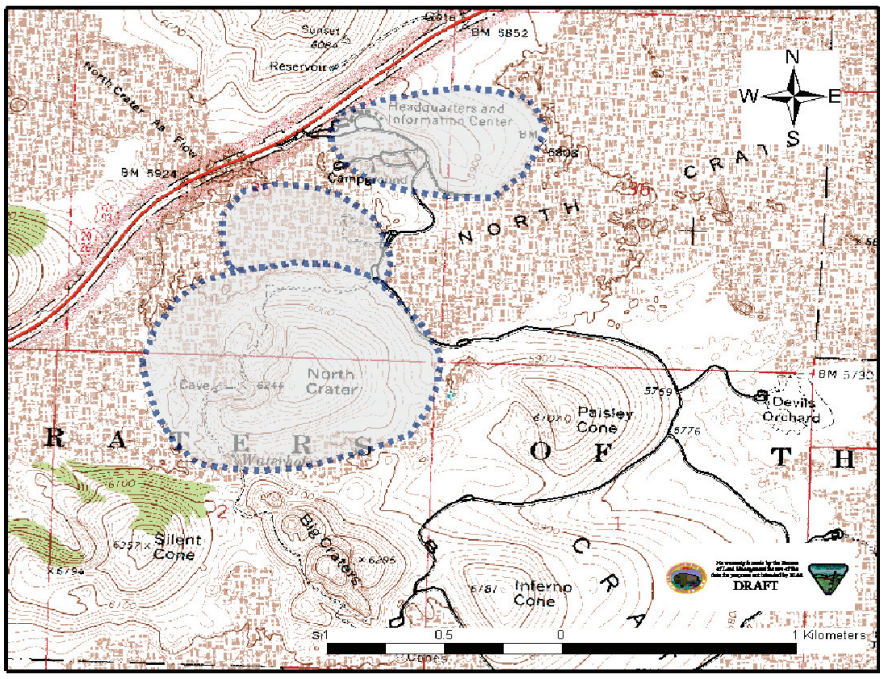

Figure III-2. Portion of Inferno Cone USGS 7.5 minute topographic quadrangle showing the extent and location of present-day North Crater, a possible paleo-North Crater and possible cousins of North Crater prior to block rafting events.

Reconstruction of North Crater by adding the volume of material rafted from the North Crater area to the current North Crater creates a paleo-North Crater that is much larger than present-day North Crater. At minimum, the volume of rafted material is 46×10^6 m^3. The volume of the breach in North Crater is only 1.2×10^6 m^3. Adding the rafted material (46×10^6 m^3) to the current North Crater (42×10^6 m^3) suggests paleo-North Crater may have been as large as 88×10^6 m^3. The radius and height of this large paleo-North Crater would have been, respectively, nearly 200 m greater in diameter and 40 m higher than the modern North Crater. It would have extended from North Crater's current position north to U.S. Highway 20/26/93 and east to the campground. Since the North Crater area has had a prolonged and complex eruptive history, it is possible that several smaller paleo-North Craters existed through time, each being built, partially or completely destroyed by explosive events, and then rebuilt.

If you proceed along the North Crater trail between 1.3 and 1.6 km, you will have the opportunity to see some of the xenoliths associated with North Crater. The most common type of xenolith is composed of pumiceous glass that stands out in stark contrast to the basalt because of its whitish color. The pumice may be related to the rhyolitic rocks formed during eruptions that occurred on the ESRP prior to basaltic volcanism, to Eocene-age rocks of the Challis Volcanic Group, to Mississippian sedimentary rocks, or to Tertiary intrusive rocks. Less common are granulitic xenoliths, thought to represent material from the cratonic basement. Least common are xenoliths from Eocene Challis volcanic rocks.

At about 1 km from the trailhead, the trail climbs steeply up from the North Crater pahoehoe flow in the most recently active vent area for North Crater. Watch for boulders of very dense glass-like basalt. This material is tachylyte, the basaltic equivalent of obsidian.

At approximately 2.9 km, you will pass by an eruptive fissure on your left, which looks like a deep, elongate trench. This fissure is one of the eruptive centers for the Big Craters

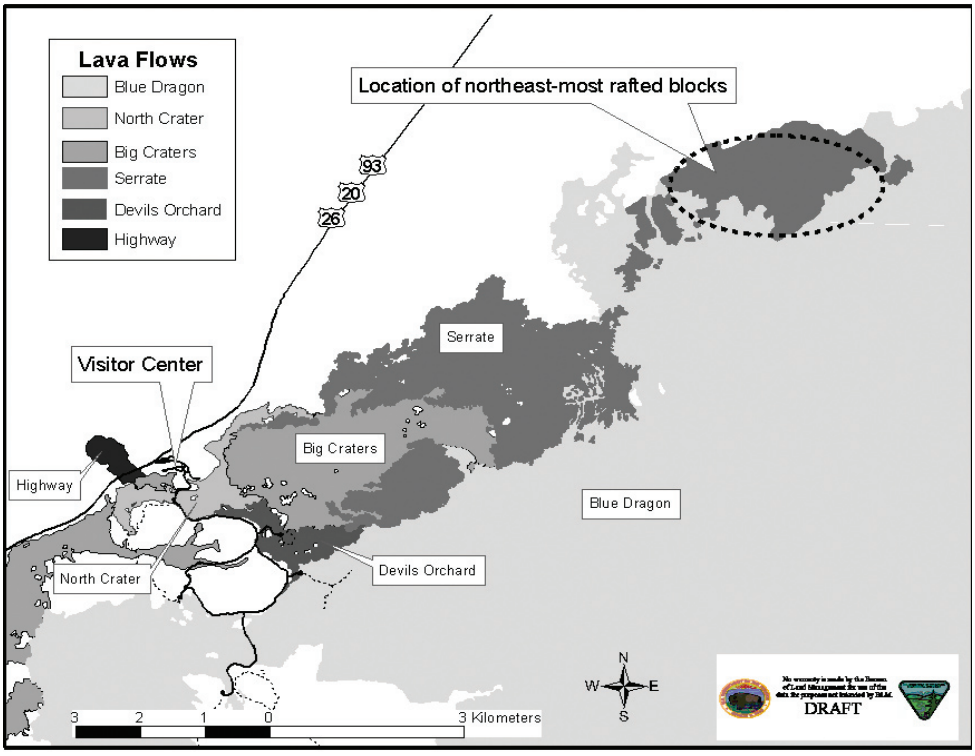

Figure III-3. Map showing extent of lava flows and the location of northeastern most rafted blocks.

flow of eruptive period A. Just beyond the eruptive fissure, the trail begins to climb Big Craters, which consists of at least nine nested cones that indicate a complicated eruptive history. Please watch your footing as you peer into the cones.

End of Stop III-2. Return to vans. Continue on loop road.

Mileage Inc.	Cum.	
0.4	1.2	Big Craters flow to right mantles the western flank of Paisley Cone. The fissure vents for these pahoehoe hawaiite flows are located between North Crater and Big Craters and on the north flank of Big Craters. For the next 2 km, the loop road follows the north, east, and south flanks of Paisley Cone, assumed to have an age of about 6 ka (see table 1).
0.2	1.4	Devils Orchard flow on left. This heavily cinder-covered, block-a' a trachyandesite flow was thought by early workers to be quite old. However, it correlates with the Highway and Serrate flows, approximately 2.3 ka (table 1). The Serrate, Devils Orchard, and Highway flows are considered to be about 2,300 yr based on stratigraphic and paleomagnetic data (see table 1).
0.4	1.8	Entrance to Devils Orchard Interpretive Trail on left. Continue on loop road.
0.1	1.9	Intersection with one-way loop drive. Bear right.
0.2	2.1	Tongue of Big Craters flow. Looking left in the valley between Paisley Cone (on right) and Inferno Cone (on left) is a small lobe of the Big Craters flow. Inferno Cone is directly south on the left. Big Craters area is west (straight ahead), and North Crater is to north (on the right, see fig. III-1).

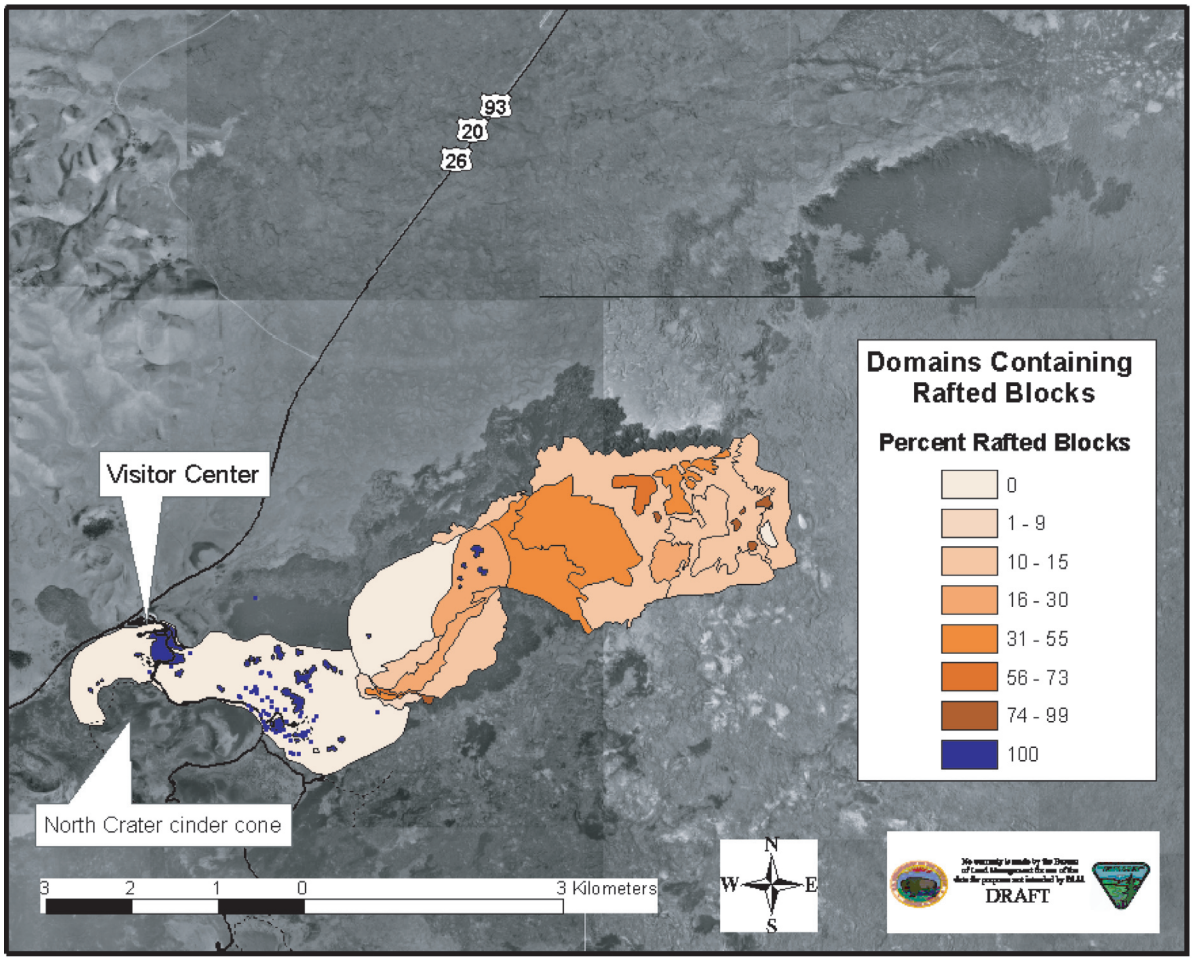

Figure III-4. Digital air photo showing locations of domains of rafted material.

0.6 2.7 Turnout to Inferno Cone parking lot. Inferno Cone is undated, but assumed to be about 6 ka (see table 1). Although not a stop for this road log, visitors may want to hike the trail to the top of Inferno Cone. At the top of Inferno Cone, facing north, geographic features to be noted, in a clockwise direction, are: 9:30 to 10:00 o'clock, Big Craters nested cinder cone complex; 10:30 o'clock, Grassy Cone; 11:00 o'clock, North Crater; 12:00 o'clock, Sunset Cone (directly behind the Visitor Center with the Pioneer Mountains in the far background); and 1:00 o'clock, Paisley Cone. The profile against the mountains of the vegetated surface of the Sunset flow is visible beyond Paisley Cone. On the near side of the Sunset flow is the Serrate flow that extends to the east (right) as far as Round Knoll, a grass-covered kipuka (at 2:30 o'clock) of older Snake River Plain lava flows and cinders**.** The very large butte to the east is Big Southern Butte. To the left of Big Southern Butte are East (left) and Middle (right) Buttes that appear to be one butte from this perspective. Low shield volcanoes are clearly visible to the left and right of the buttes. The eastern part of the vast Blue Dragon flow is in the foreground.

To the southwest is a big cinder cone, called Big Cinder Butte, which is the largest cinder cone in the Monument. At 11:00 o'clock, the two easternmost cinder cones in this direction are Half Cone in the foreground and Crescent Butte, with its distinctive crescent shape. In the background is the dark, saddle-shaped cone, Blacktop Butte, the most southerly cone along the northern part of the Great Rift, and about 20 km away. Many of the more than 25 cinder cones in the COM lava field can be seen from this vantage point, but they are too numerous and closely spaced to differentiate.

From the southwest rim, one may observe the vent and "plumbing system" responsible for the eruption of the vast eastern lobe of the Blue Dragon flow, the largest of all flows of eruptive period A. The "plumbing system" consists of an eruptive fissure, located in the southern part of Spatter Cones–Big Craters area, pit craters, such as Crystal Pit, that overlie the southern end of the eruptive fissures; perched lava ponds, such as Big Sink, that are located on the upper part of a lava tube system that extends east and south of the eruptive fissure; and a lava-tube system that contains numerous skylight entrances into the tubes (Cave area, see fig. III-1). Farther east are rootless vents or hornitos, where lava moving through the tube system was extruded through openings in tube ceilings. Also visible directly south, beyond Big Sink and Lava Cascades, is Broken Top cinder cone and the area to be visited in Stop III-3. Several 2.1-ka fissures slice across the northeast and southwest sides of Broken Top. Source vents for the youngest flow in the COM lava field, the Broken Top lava flow, are on the eruptive fissure on the east and northeast flanks of Broken Top.

0.2 2.9 Spatter Cones-Big Craters Area. At this area, one can view the eruptive features and vent areas along a part of the Great Rift that was active about 2.1 ka, producing the Blue Dragon flow. A segment of the Great Rift about 10-km long that extends from North Crater southeast to the Watchman cinder cone (fig. III-1) was active at various times during the latest eruptive period of the COM lava field. The vents in the area produced about 3.5 km^3 of lava that now covers about 20 percent of the COM lava field. At about the same time, a rift segment of comparable length was active and formed the Kings Bowl and Wapi lava fields in the southern part of the Monument. The Spatter Cones formed in the waning activity along a short, 1-km-long eruptive fissure that extends southeast from the south end of Big Craters. Most of the lava that forms the extensive Blue Dragon flow was erupted from the Great Rift in the Spatter Cones-Big Craters area. Take the trail to the west that ascends to the southern end of Big Craters. Big Craters is a nested cinder cone complex that contains at least nine cones. On the southwest rim, agglutinated spatter material mantles the inner wall of the south-southeast parts of the complex. The mantle drapes over the rim of the complex and covers the outer wall. About 100 m north along the trail, remnants of a lava lake lie along the north wall of the inner crater. Just south of the lava lake remnant, the crest of a small cinder cone has a red streak aligned parallel to the eruptive fissure. Late-stage corrosive steam from the fissure oxidized the black cinders. Lava issued from several satellite vents at the base of Big Craters flow complex along its western (left) flank and traveled to the southwest. Additional nested craters are viewed in the Big Craters complex along the trail. As the trail descends the west slope of Big Craters, it passes near small craters on the west flank of the complex.

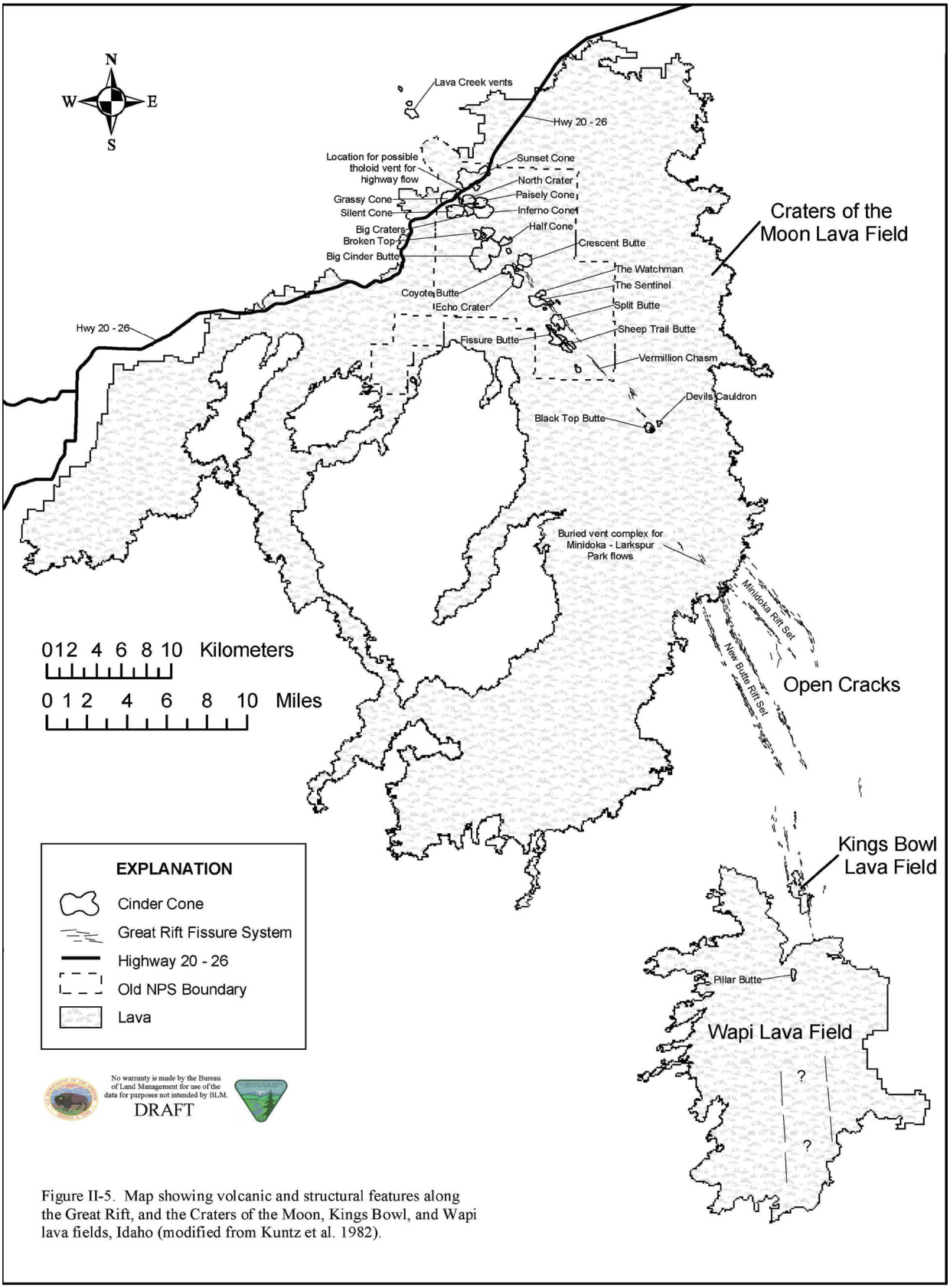

Figure II-5. Map showing volcanic and structural features along the Great Rift, and the Craters of the Moon, Kings Bowl, and Wapi lava fields, Idaho (modified from Kuntz et al. 1982).

Figure III-5. Map showing volcanic and structural features along the Great Rift volcanic rift zone, and the Craters of the Moon, Kings Bowl, and Wapi lava fields, Idaho (modified from Kuntz and others, 1992).

Where the trail flattens out, it passes near a few small fissures to the left of the trail. The trail crosses eruptive fissures, source vents for the Big Craters flows, in the area between the Big Craters complex and the southwest flank of North Crater. Big Craters flows traveled both east and northwest from this area. This lava has an olivine-green to greenish-brown crust, which is useful in distinguishing Big Craters flows in areas where they abut younger and older flows. The trail continues on and was described to this point under Stop III-2.

0.1 3.0 Vent for Inferno Cone. Vent area lies between the small spatter rampart and the low cinder mounds just south of the road and has been in filled by the Blue Dragon flow.

0.1 3.1 Big Cinder Butte on horizon. Blue Dragon slabby pahoehoe lies to the right between the road and the Spatter Cones. The west and south flanks of Inferno Cone are to the left.

0.5 3.6 Intersection to Tree Molds parking lot. Turn right.

0.3 3.9 Lava Cascades Turnout. Here, Blue Dragon lava flowed in a radial pattern from Big Sink, a perched lava pond. The pond is about 100-m long; when the pond drained back into the tube system, the still plastic pond crust draped down to form a depression about 15-m deep inside the levees that had formed at the edges of the pond.

0.3 4.2 Blue Dragon flow slosh-slab. On the left is a slab of Blue Dragon lava flow that mantles the lower north side of Broken Top. Either the flow was considerably inflated as it passed this site or the lava flow "sloshed" up onto the side of the cone as it changed direction to flow east. There are several other "slosh slabs" present in the Monument, some of which do not seem to be explained by either of these two mechanisms.

0.5 4.7 Crossing Blue Dragon slabby pahoehoe flow. Slabby pahoehoe is made up of jumbled plates or slabs of broken pahoehoe crust.

0.1 4.8 Park in Tree Molds parking lot for Stop III-3. Take a short break to visit restrooms. Hike about 2.5 km starting at Broken Top Loop trail. Following the stop, return to the parking lot and drive back to the loop road. Turn right on loop road.

Figure III-6. Aerial view of Broken Top cinder cone. Note slumping on top left side of cone; eruptive and noneruptive fissures (center of photo), and well-developed pressure plateau (lower part of photo).

Stop III-3. Eruptive Fissures, Tension Cracks, and Eruption of Broken Top and Blue Dragon Flows at 2.1 Ka

The geology of the ESRP is characterized by Hawaiian-type basaltic volcanism, where eruptive fissures and dike emplacement features, such as tension cracks or noneruptive fissures, dominate the earliest stages. Flows of the COM lava field erupted from fissures and vents along the Great Rift, one of approximately nine described Pleistocene-Holocene, large-scale (>20 km) volcanic rift zones on the plain (fig. III-5; Kuntz and others, 1992). Faults, which are dike-emplacement features typically aligned with tension cracks in other examples of basaltic volcanism, rarely are seen within the volcanic rift zones on the ESRP. However, faults are found at the margins of the plain in the Arco-Big Southern Butte and Spencer-High Point volcanic rift zones (Kuntz and others, 1992, 2002; Hackett and Smith, 1992; Smith and others, 1996). Because of their locations, these faults are thought to be tectonic in nature rather than dike related, and therefore, part of the collinear extensions of the major, range-front faults for the Basin and Range mountains on the northern edge of the ESRP (Kuntz and others, 2002).

The Great Rift consists of several major sets of tension cracks from north to south, respectively: COM lava field, Open Crack rift set, which consists of two rift-sets (New Butte and Minidoka), and the Kings Bowl lava field (fig. III-5). Within the COM lava field, there are numerous unnamed tension cracks and eruptive fissures related to cinder cone formation and lava flow eruptions. There are no known range-front faults located at the northern edge of the ESRP along the northwest trend of the Great Rift. However, there are mapped faults of appropriate trend located 1.2 km west of the Great Rift northwest of Grassy Cone. The drainage of Little Cottonwood Creek is on trend with the extension of the Great Rift that gives rise to the vent area for the Lava Creek flows. The Lava Creek flows, approximately 12 ka, are part of the COM lava field and represent the northernmost known extension of the Great Rift volcanic rift zone (Kuntz and others, 1992). We will discuss the tension cracks and eruptive fissures of the Great Rift associated with Broken Top, Big Cinder Butte, and Trench Mortar Flat at this stop.

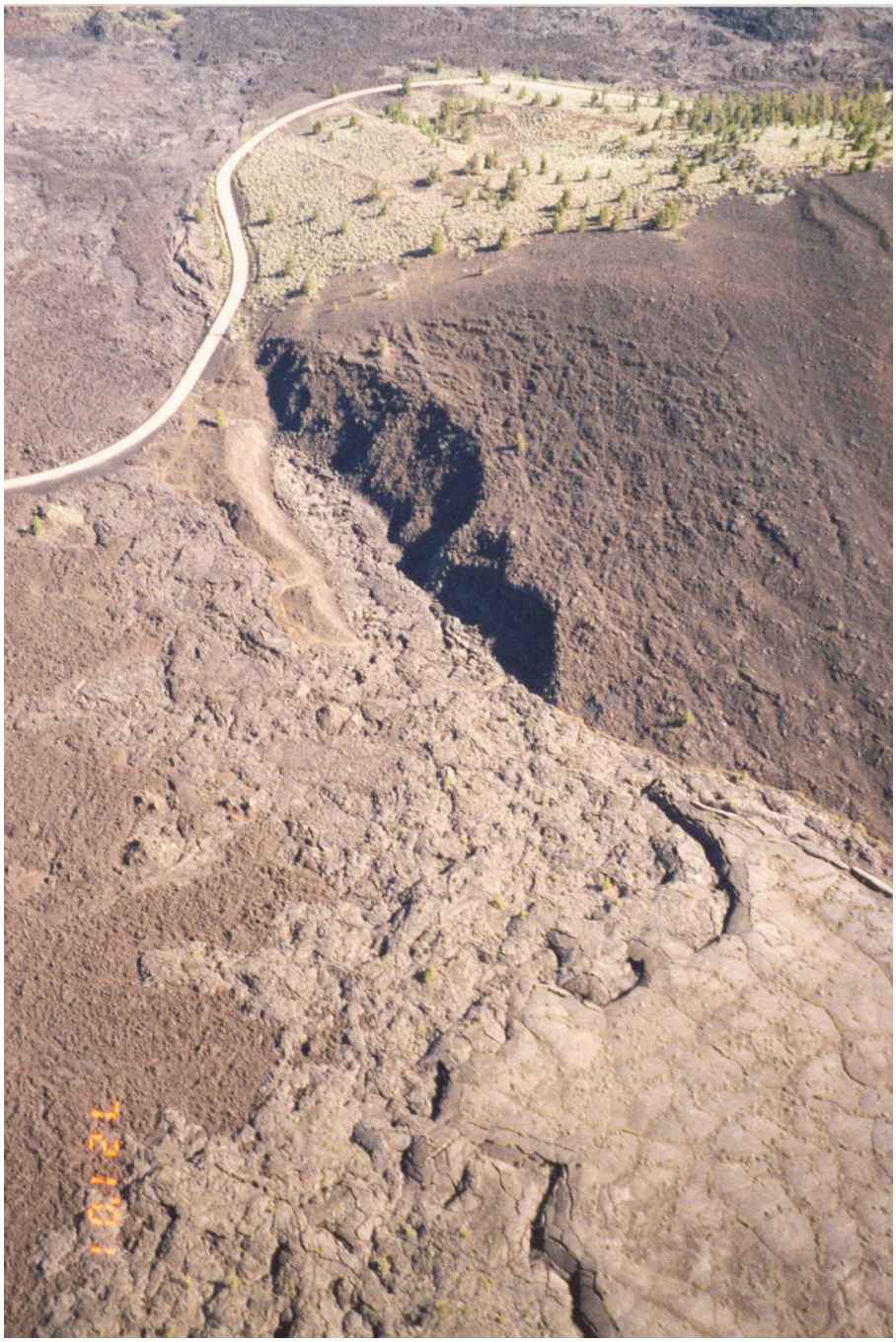

Figure III-7. Aerial view of Broken Top cinder cone. Note breakouts from pressure plateau of Broken Top pahoehoe flow (center right) that form lava toes on top of Blue Dragon flow (along left edge of photo).

We will be hiking about 2.5 km. Start by following the Broken Top loop trail, then cut cross-country over a pressure plateau and a cinder flat to look at eruptive and noneruptive fissures.

Follow the sidewalk east to where it "T's" into the main trail loop and turn right; do not take the trail to the left, which ascends Broken Top. The trail to the right parallels a fissure, which was the main source vent for Broken Top. This eruptive fissure has been partially in-filled by a tongue of the Blue Dragon flow. Follow the trail along the spatter rampart to the southeast then across the surface of the Blue Dragon flow. The southwest-facing wall of the eruptive fissure is heavily mantled with spatter and bombs that were erupted from the fissure. Many faults that trend parallel to the Great Rift cut the west side of Broken Top and slumping was active into the eruptive fissure (see fig. II-6). Walk along the trail to the contact of Broken Top flow with the Blue Dragon flow. Blue Dragon lava in this area is spiny pahoehoe, which forms from very thick, pasty lava. Spiny pahoehoe contains elongated gas bubbles on the surface that form spines, hence the name. The pahoehoe toes of the Broken Top flow that lie on top of the Blue Dragon flow broke out of the pressure plateau visible to the east (see fig. III-7). The Broken Top flow, though not dated, is stratigraphically younger than the Blue Dragon flow (~2.1 ka) and, therefore, the youngest flow in the COM lava field. Pressure plateaus may form from the sill-like injection of new lava beneath the crust of an earlier sheet flow that had not completely solidified.

After looking at classic lava-inflation structures, we will climb up onto the pressure plateau, follow the edge, and look at fissures visible from this vantage point. Hike may end while studying fissures most likely related to the 2.1-ka events associated with Trench Mortar Flat.

If time permits, we will make a quick stop at Buffalo Caves, in the Broken Top flow, and discuss lava-tube formation and hot and cold tube collapses. Buffalo Caves show many interesting features, such as lava stalactites, curbs (showing successive flow levels on the cave walls), ropes (showing flow direction), and stacked tubes.

If you follow the cairns east from Buffalo Caves to the intersection with the Wilderness Trail, you can turn left and make a loop up and over Broken Top. When you reach the Wilderness Trail, there also are good examples of shelly pahoehoe just to the east of the trail. Shelly pahoehoe forms from highly gas-charged lava, often near vents or tube skylights. Shelly pahoehoe contains small, open tubes, blisters, and thin crusts. Crusts here are about 10-cm thick, but in other parts of the Monument, they are as little as 2–3-cm thick. Also, just to the east of the trail, small chunks of agglutinated cinders can be found that were being transported away by the lava flow. Overlooks along the trail on the north and west sides of Broken Top provide insight into the plumbing system earlier described for the Blue Dragon flow (2.7 Inferno Cone Turnout). Figure III-8 is an aerial view showing the plumbing system that was described.

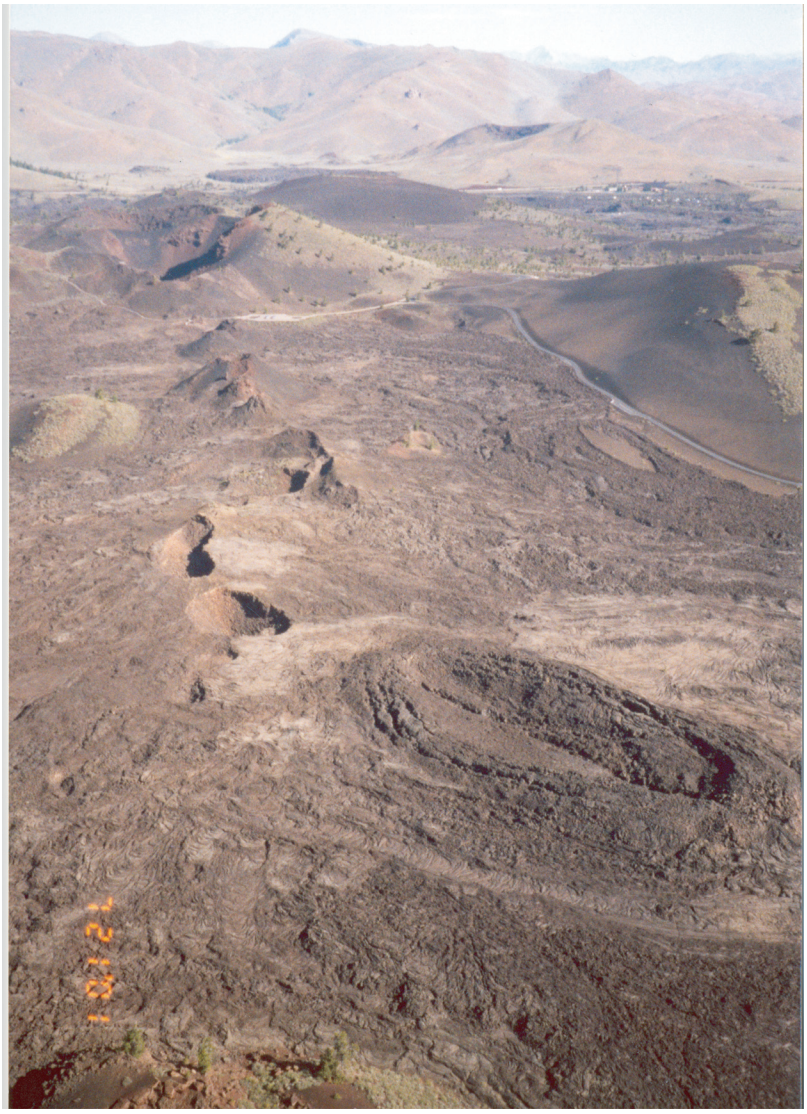

Figure III-8. Aerial view of the northern part of the Great Rift volcanic rift zone. From upper left to lower right: Pioneer Mountains, Big Craters cinder cone complex, Spatter Cones, pit craters, Little Sink (collapsed lava pond).

For teachers or others who are interested, there is 60-page teachers' guide to Broken Top Loop available on the Schools and Education section of the park web page.

Mileage Inc.	Cum.	
0.0	6.7	Road to Caves Area on right; continue straight on loop road.
0.2	6.9	Devils Orchard blocky lava flow on right.
0.3	7.2	Intersection with the two-way portion of the loop road; turn right.

0.1	7.3	Entrance into Devils Orchard spur road; continue on loop road.
1.7	9.0	Visitor Center

References

Fishel, M.L. 1993, The geology of uplifted rocks on Big Southern Butte—Implications for the stratigraphy and chemistry of the eastern Snake River Plain, Idaho: Pocatello, Idaho State University, unpublished M.S. thesis, 178 p.

Fremont, Brevet Captain John C., 1845, Report of the exploring expedition to the Rocky Mountains in the year 1842 and to Oregon and north California in the years 1843–1844: Washington, D.C., Blair and Rives, first edition, 583 p.

Hackett, W.R., and Smith, R.P., 1992, Quaternary volcanism, tectonics, and sedimentation in the Idaho National Engineering Laboratory area, *in* Wilson, J.R., ed., Field guide to geological excursions in Utah and adjacent areas of Nevada, Idaho, and Wyoming: Utah Geological Survey Miscellaneous Publications 92-3, p. 1–18.

Kuntz, M.A., Skipp, B., Champion, D.E., Gans, P.B., and Van Sistine, D., in press, Geologic map of the Craters of the Moon 30' x 60' quadrangle, Idaho: U.S. Geological Survey Miscellaneous Investigations Map, scale 1:100,000.

Kuntz, M.A., Anderson, S.R., Champion, D.E., Lanphere, M.A., and Grunwald, D.J., 2002, Tension cracks, eruptive fissures, dikes, and faults related to late Pleistocene-Holocene basaltic volcanism and implications for the distribution of hydraulic conductivity in the eastern Snake River Plain, Idaho, *in* Link, P.K., and Mink, L.L., eds., Geology, hydrology, and environmental remediation-Idaho National Engineering and Environmental Laboratory, eastern Snake River Plain, Idaho: Geological Society of America Special Paper 353, p. 111–133.

Kuntz, M.A., Skipp, B.A., Lanphere, M.A., Scott, W.E., Pierce, K.L., Dalrymple, G,B., Champion, D.E., Embree, G.F., Page, W.R., Morgan, L.A., Smith, R.P., Hackett, W.R., Rodgers, D.W., 1994, Geologic map of the Idaho National Engineering Laboratory and adjoining areas, eastern Idaho: U. S. Geological Survey Miscellaneous Investigations Series Map I-2340, scale 1:100,000.

Kuntz, M.A., Covington, H.R., and Schorr, L.J., 1992, An overview of basaltic volcanism of the eastern Snake River Plain, Idaho, *in* Link, P.K., Kuntz, M.A., and Platt, L.B., eds., Regional geology of eastern Idaho and western Wyoming: Geological Society of America Memoir 179, p. 227–267.

Kuntz, M.A., Champion, D.E., Spiker, E.C., Lefebvre, R.E., 1986, Contrasting magma types and steady-state, volume-predictable, basaltic volcanism along the Great Rift, Idaho: Geological Society of America Bulletin, v. 97, p. 579–594.

The North Crater Neighborhood—More complex than Mr.Rogers', *http://data2.itc.nps.gov/nature/documents/field%5Ftrip%5Ftext%5F2%2D1%2Epdf*.

Smith, R.P., Hackett, W.R., and Rodgers, D.W., 1989, Geologic aspects of seismic-hazard assessment at the Idaho National Engineering Laboratory, southeastern Idaho, *in* Proceedings, Second Department of Energy Natural Phenomena Hazards Mitigation Conference: Livermore, California, Lawrence Livermore National Laboratory, p. 282–289.

Smith, R.P., Jackson, S.M., and Hackett, W.R., 1996, Paleoseismology and seismic hazard evaluations in extensional volcanic terrains: Journal of Geophysical Research, v. 101, p. 6277–6292.

Spear, D.B., and King, J. S., 1982, The geology of Big Southern Butte, Idaho, *in* Bonnichsen, B., and Breckenridge, R.M., eds., Cenozoic geology of Idaho: Idaho Bureau of Mines and Geology Bulletin 26, p. 395-404.

Stuiver, M., and Polach, H.A., 1997, Reporting of ^{14}C data: Radiocarbon, v. 19, p. 355—363.

Valastro, S., Jr., Davis, E.M., and Zarela, A.G., 1972, University of Texas radiocarbon ages: Radiocarbon, v. 14, p. 468—470.

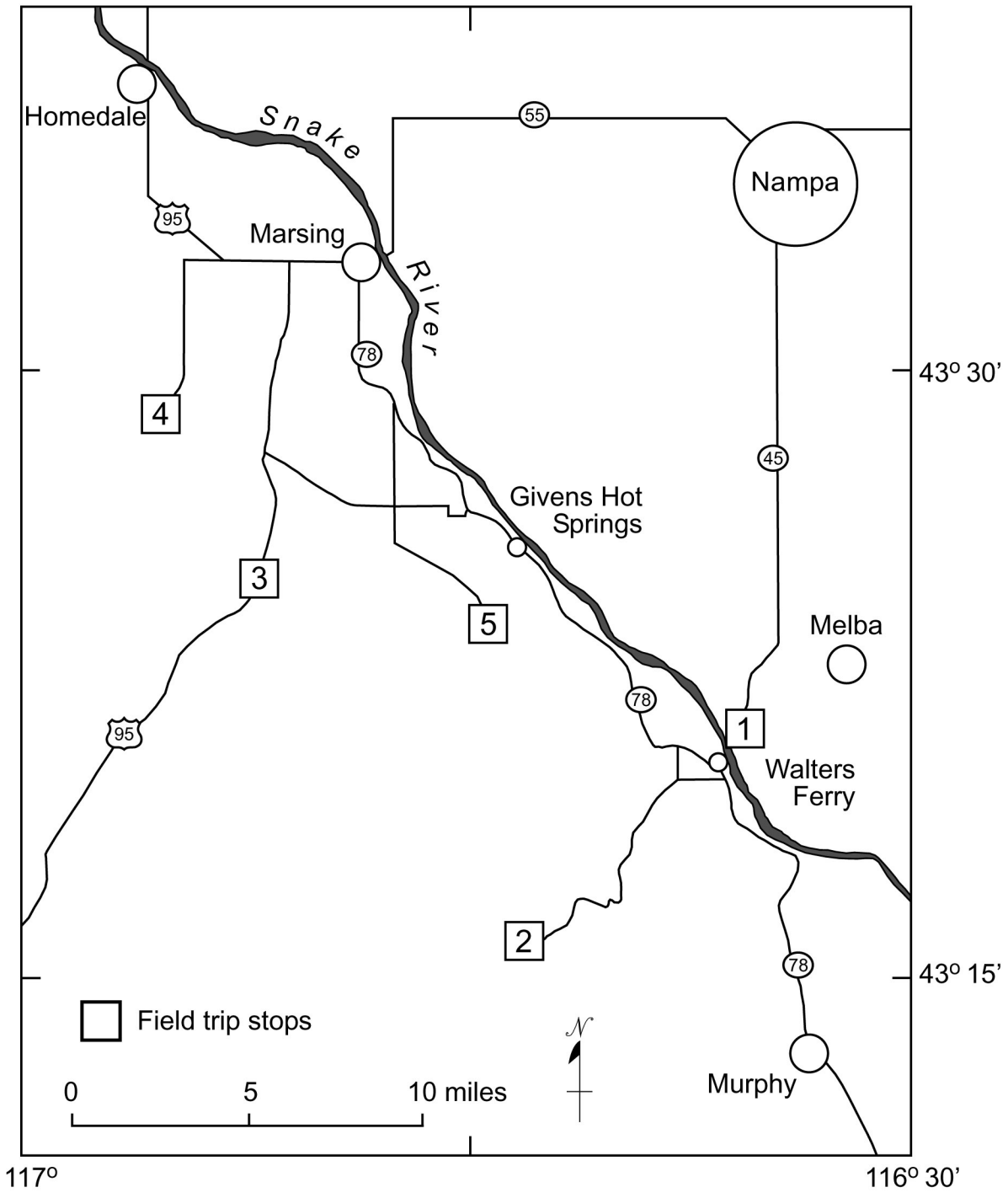

Figure 1. Route map for day 1 and day 2 of this field-trip guide for the Owyhee Front rhyolite field.

Miocene Snake River Plain Rhyolites of the Owyhee Front, Owyhee County, Idaho

By Bill Bonnichsen[1], Mike McCurry[2], and Martha M. Godchaux[1]

Introduction

The rhyolite units of the Owyhee Front are discontinuously exposed along the front for more than 40 km (25 mi) between southwest of Homedale to southwest of Murphy, Idaho. In this field-trip guide, the route to the principal rhyolite units of the Owhyee Front is shown in figure 1. The Owyhee Front region lies along the southwest margin of the western Snake River Plain (fig. 2). From northwest to southeast, the principal rhyolite units are the Jump Creek rhyolite lava-flow field, the Wilson Creek ignimbrite, the Cerro el Otoño dome field, and the Reynolds Creek rhyolite lava flow (fig. 3). This group of rhyolite units seems to have been erupted a short time after the western Snake River Plain graben started to form, and the units range between 11.7 and 10.6 Ma in age. The western Snake River Plain is a complex graben that has evolved over the past 11 or 12 m.y. and seems to be a subsidiary tectonic feature in which northeast-southwest extension accompanied the development of the main Snake River Plain-Yellowstone hot-spot trend (Bonnichsen and others, 1989; McCurry and others, 1997). Starting before the eruption of the Owyhee Front rhyolite units and continuing until about 2 m.y. ago, the western Snake River Plain graben held a large, deep lake generally known as Lake Idaho (Jenks and Bonnichsen, 1989; Wood and Clemens, 2002). It is unknown if this lake was continuously present in the graben, or if it was absent at times.

In the Owyhee Front region the geologic units that are older than the rhyolites of the Owyhee Front are the Cretaceous Silver City Range granitic rocks, the Eocene Rough Mountain felsic volcanics, the Oligocene Salmon Creek volcanics, the Miocene Silver City basaltic, intermediate, and silicic volcanics, the Miocene sediments and tuffs of the Sucker Creek Formation, and the Miocene rhyolitic rocks affiliated with the formation of the Owyhee-Humboldt eruptive center of the Snake River Plain hot-spot track (Ekren and others, 1981; Bonnichsen and Kauffman, 1987; Bonnichsen and Godchaux, 2002). The major rock groups younger than the Owyhee Front rhyolite units include the Miocene, Pliocene, and Pleistocene basalt units associated with the evolution of the western Snake River Plain graben, and Miocene and Pliocene lake and stream sediments of the Poison Creek, Chalk Hills, and Glenns Ferry Formations of the Idaho Group (Ekren and others, 1981; Jenks and Bonnichsen, 1989; McCurry and others, 1997; Bonnichsen and Godchaux, 1998 and 2002).

Rhyolite Units of the Owyhee Front

The Owyhee Front rhyolite units, although erupted within a time window of about a million years, are somewhat diverse in character. The most voluminous group is the lava flows of Jump Creek rhyolite field. These flows erupted from several vents to form a series of partially merged rhyolite lava-flow fields covering the western two-thirds of the Owhyee Front region (fig. 3), west of where any of the Cretaceous granitic rocks are exposed, as mentioned by Godchaux and Bonnichsen (2002). The various Jump Creek rhyolite flows are rich in large phenocrysts, especially plagioclase, and range from the oldest to the youngest rhyolite units known along the front.

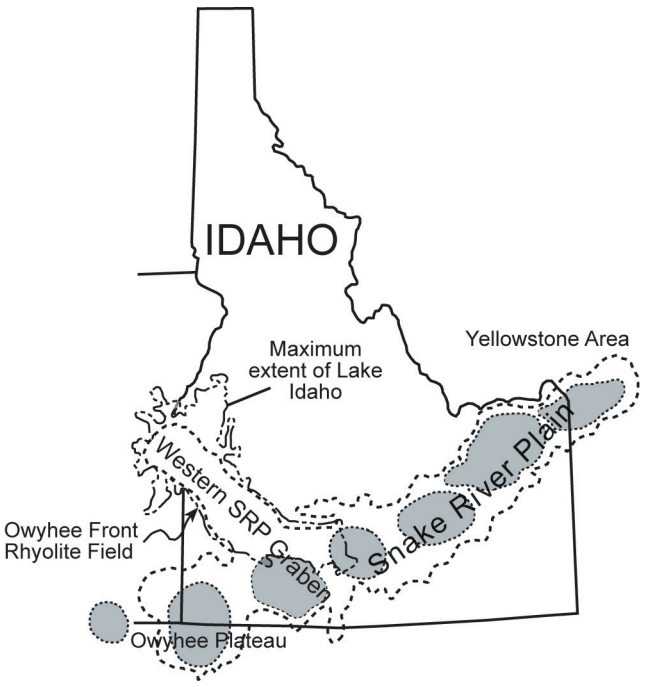

Figure 2. Location of the Owyhee Front rhyolite field in relation to other features of the Snake River Plain volcanic province.

[1]927 East 7th Street, Moscow, ID 83843; billb@uidaho.edu; mgodchau@mtholyoke.edu

[2]Department of Geosciences, Idaho State University, Pocatello, ID 83209; mccumich@isu.edu

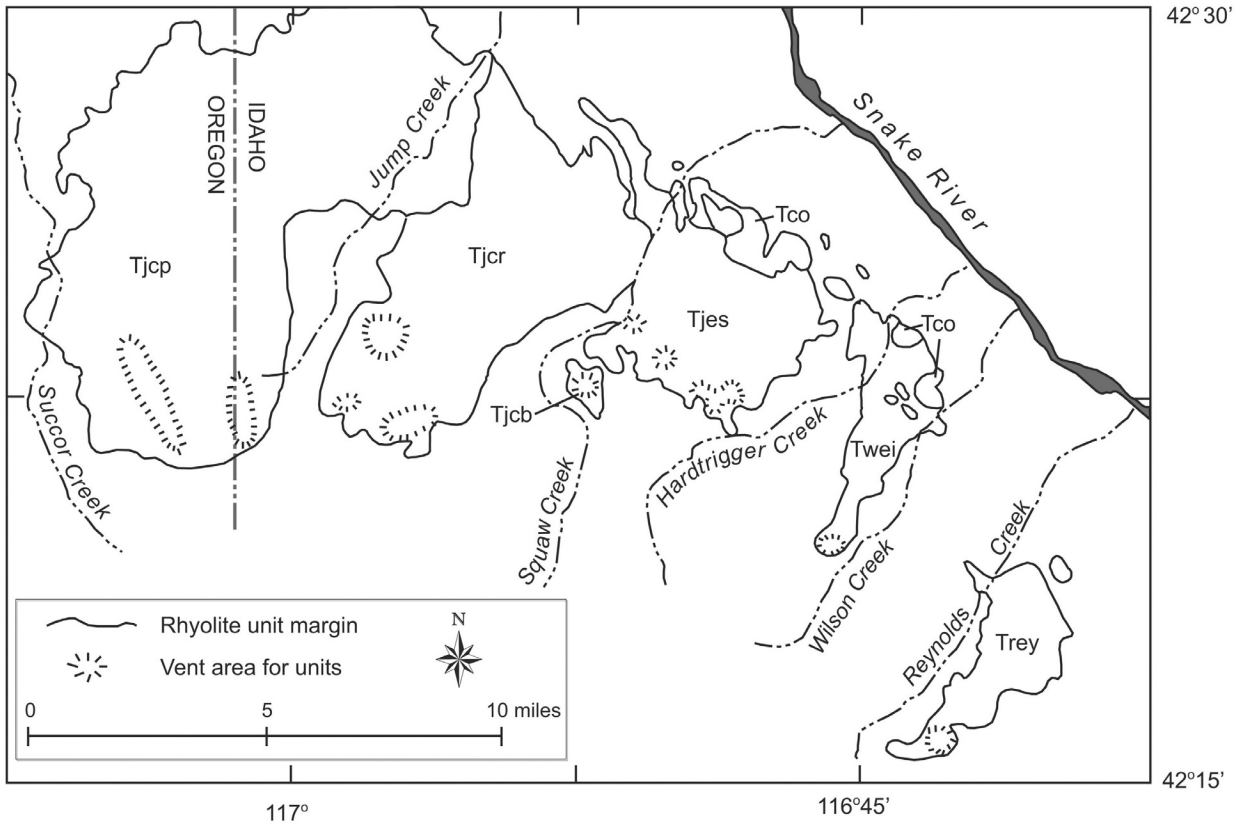

Figure 3. Geologic map outlining the individual rhyolite units in the Owyhee Front rhyolite field of Idaho and Oregon. Symbols used for segments of the Jump Creek rhyolite are: Tjcp—Pole Creek Top segment, Tjcr—Rockville segment, Tjcb—Buck Mountain segment, and Tjcs—Shares Snout segment. Other symbols are: Trey—Reynolds Creek rhyolite lava flow, Twci—Wilson Creek ignimbrite, Tco—Cerro el Otoño dome field.

The other units, the Wilson Creek ignimbrite, the Reynolds Creek rhyolite lava flow, and the Cerro el Otoño dome field, are less voluminous than, and lie east of, the Jump Creek rhyolite field. These eastern units include materials that were erupted as lava flows, ignimbrites, and domes. The phenocryst contents and sizes of these smaller, more easterly units are considerably less than in the flows of the Jump Creek rhyolite, and are dominated by sanidine. Also, the compositions of the eastern units tend toward being high-silica rhyolite, whereas the compositions of the Jump Creek flows tend toward low-silica rhyolite (table 1). Additionally, there are large differences in the minor element contents of these two groups of rhyolite. These differences probably are largely correlative with the differences in phenocryst contents of the two groups of units.

The time interval during which the Owyhee Front rhyolite units were erupted falls within the same time interval that many of the much larger high-grade ignimbrites and rhyolite lava flows were forming in the Bruneau-Jarbidge eruptive center, located to the southeast in the region where the western Snake River Plain merges into the main Snake River Plain hot-spot track (fig. 2). The most voluminous of the rhyolitic ignimbrites erupted from the Bruneau-Jarbidge center in the 12.0 to 10.8 Ma time interval. This is the time interval during which most of the regional collapse associated with the eruption of those huge ignimbrites occurred. Some Bruneau-Jarbidge units, including the earliest ignimbrites, are a little older than the Owyhee Front rhyolite units and others, including most of the rhyolite lava flows, are somewhat younger, but the bulk of the Bruneau-Jarbidge volcanism coincides in time with the Owyhee Front volcanism (Bonnichsen, 1982a, 1982b; Bonnichsen and Citron, 1982; Bonnichsen and Kauffman, 1987; Hart and Aronson, 1983; Armstrong and others, 1980; Perkins and others, 1995; B. Bonnichsen, unpublished data; New Mexico Geochronological Research Laboratory, unpublished reports). Overlap in ages, and similarities in bulk chemical composition and phenocryst mineralogy (*e.g.*, Bonnichsen and Citron, 1982), argues that the origin of the rhyolitic magmas that gave rise to the Owyhee Front rhyolite units, at least in part, may have been related to the same tectonic and magmatic events that gave rise to the silicic magmas that erupted in the Bruneau-Jarbidge region immediately southeast of the western Snake River Plain graben. Conversely, the rhyolite units in the older Owyhee-Humboldt region and younger eastern Snake River Plain region (fig. 2) do not overlap in time with the Owyhee Front rhyolite units.

Table 1. Chemical analyses of Owyhee Front rhyolite samples, southwestern Idaho. Analyses by x-ray fluorescence at Washington State University GeoAnalytical Laboratory.

Sample	**1**	**2**	**3**	**4**	**5**	**6**	**7**	**8**	**9**	**10**
	I-3849	**I-3747**	**I-3478**	**I-3673**	**I-3846**	**I-3664**	**I-3804**	**I-3672**	**I-3246**	**I-3715**
Unit	Jump Ck. Pole Ck. Tp segment	Jump Ck. Rockville segment	Jump Ck. Buck Mtn. segment	Jump Ck. Shares Sn segment	Reynolds Ck. lava flow	Wilson Ck. ignimbrite	Wilson Ck. ignimbrite	Cerro el Otoño Hill 3036	Cerro el Otoño Hill 2471	Cerro el Otoño Hill 2781
Wt.%										
SiO_2	69.82	72.98	69.52	71.77	75.11	77.41	75.37	78.89	77.38	80.49
Al_2O_3	14.28	13.11	14.04	14.05	12.49	12.39	12.32	11.63	11.21	10.64
TiO_2	0.50	0.44	0.48	0.50	0.22	0.10	0.12	0.09	0.09	0.07
FeO	3.53	3.15	3.21	3.17	2.03	0.96	1.45	0.94	0.73	0.72
MnO	0.07	0.07	0.08	0.03	0.01	0.01	0.02	0.01	0.01	0.01
CaO	1.67	1.48	1.80	1.29	0.90	0.26	0.61	0.10	1.13	0.22
MgO	0.63	0.40	0.43	0.21	0.28	0.02	0.33	0.08	0.00	0.07
K_2O	4.34	4.08	4.65	4.71	5.08	5.08	5.55	4.79	4.69	4.28
Na_2O	3.96	3.76	3.89	3.92	3.31	3.71	2.53	3.70	3.80	3.19
P_2O_5	0.13	0.12	0.14	0.14	0.07	0.03	0.05	0.02	0.03	0.02
Total	98.93	99.58	98.24	99.78	99.50	99.96	98.36	100.25	99.06	99.71
ppm										
Ni	7	4	0	4	5	6	11	10	3	6
Cr	0	0	0	0	0	0	0	1	3	0
Sc	8	7	7	4	4	1	3	7	5	3
V	11	21	20	13	33	11	5	0	4	0
Ba	2063	1874	1945	1930	1477	27	71	14	20	15
Rb	87	82	91	97	150	155	150	176	171	143
Sr	290	246	286	227	73	7	36	7	19	10
Zr	558	483	485	517	362	210	213	282	288	172
Y	51	48	49	56	39	39	65	86	72	39
Nb	44	39	41	42	41	55	53	78	74	53
Ga	21	17	22	21	19	20	20	23	26	21
Cu	3	0	1	2	2	0	3	0	0	0
Zn	117	92	103	99	72	65	91	120	35	41
Pb	22	23	26	24	28	29	30	38	16	22
La	89	71	85	82	100	64	68	52	31	89
Ce	164	139	140	134	180	101	127	119	72	100
Th	11	10	18	13	26	14	12	19	7	13

Jump Creek Rhyolite Field

The Jump Creek rhyolite field consists of several lava flows, which erupted from a series of vents that form an east-west elongate zone located several miles south of the margin of the western Snake River Plain graben. The field consists of three principal subdivisions that partially are separated by intervening zones of older rocks. From southeast to northwest these subdivisions are the Shares Snout segment, the Rockville segment, and the Pole Creek Top segment (fig. 3). These segments become larger and younger toward the northwest. In addition, there is the small Buck Mountain segment located just off the southwest margin of the Shares Snout segment. As far as we know, all of the Jump Creek rhyolite was erupted in the form of lava flows. These lavas mainly flowed northeastward from their vents, down the regional slope that existed at that time. At some localities, the flow went over relatively steep ground, perhaps a combination of fault and erosional escarpments, to form zones of large-scale fragmentation and folding. To date, no ignimbrites have been encountered in the Jump Creek rhyolite field, although some spatter accumulations have been found. The zone of vents for the Jump Creek rhyolite field appears to have been on land when the flows were erupted. However, many of the flows ran out into the Miocene version of Lake Idaho, resulting in significant amounts of brecciation and silicification of their more distal parts.

All the flows of the Jump Creek rhyolite field are rich in large phenocrysts, dominated by plagioclase and accompanied by smaller amounts of quartz, alkali feldspar, and pyroxenes. Many plagioclase phenocrysts are more than a centimeter long and some as long as 2 cm have been encountered. Some of the phenocrysts are composite, with alkali feldspar overgrowths on plagioclase, or symplectic intergrowths of feldspars and quartz. Ekren and others (1981, 1984) presented the following petrographic summary for the Jump Creek. Phenocrysts constitute 12–23 percent of the rocks, of which plagioclase (An 33) constitutes 54–88 percent of the phenocrysts, alkali feldspar 0–20 percent, quartz 0–10 percent, ferrohypersthene 6–13 percent, clinopyroxene trace to 4 percent, and traces

of zircon, apatite, and olivine. Table 1 presents an analysis from each of the segments of the Jump Creek field. All are quite similar in being relatively low in silica and with quite high contents of Ba, Sr, and Zr, and low Rb, in comparison to samples of the other Owyhee Front rhyolite units.

The Shares Snout segment extends for about 6 km SW.-NE. by about 8 km NW.-SE. and typically ranges from 100- to 200-m thick (fig. 3). Its volume likely is in the range of 3–10 km^3. A sample collected from the Shares Snout vent area gave an Ar-Ar date on sanidine of 11.69±0.06 Ma (New Mexico Geochronological Research Laboratory, unpublished report). Buck Mountain, which probably should be considered as part of the Shares Snout segment, is small in comparison to the other parts of the Jump Creek rhyolite field, with a volume probably in the range of 0.2–0.4 km^3. A sample collected from the Buck Mountain vent gave an Ar-Ar date on sanidine of 11.56±0.25 Ma (New Mexico Geochronological Research Laboratory, unpublished report).

The Rockville segment extends about 12 km SW.-NE. by about 6 km NW.-SE. and typically ranges from 50- to 200-m thick (fig. 3). Its volume likely is in the range of 5–15 km^3. Armstrong and others (1980) give a K-Ar date on sanidine of 11.1±0.2 Ma for a Rockville segment sample.

The Pole Creek Top segment extends about 20 km SW.-NE. by about 10 km NW.-SE. and typically ranges from 100- to nearly 300-m thick (fig. 3). Its volume probably is somewhere in the 20–50 km^3 range. Ferns and others (1993) and Cummings and others (2000) cite a K-Ar date of 10.6±0.3 Ma for a sample from the Pole Creek Top segment.

Reynolds Creek Rhyolite Lava Flow

The Reynolds Creek rhyolite unit (fig. 3) is a lava flow that erupted from a vent along the Owyhee Front and ran northeastward for several kilometers, to where its leading edge entered Lake Idaho. The vent area is in sec. 8, T. 2 S., R. 3 W., and consists of a west-northwest-trending ridge about 0.4-km long that extends across the flow. The flow was erupted into, and appears to have filled, a valley that contained the middle Miocene precursor of Reynolds Creek. The western part of the flow has subsequently been eroded away by Reynolds Creek, as the stream was reestablished near its original course. The Reynolds Creek lava flow is 9- to 10-km long and varies from only about 0.2-km wide at its southwestern end to nearly 4-km wide near its northeastern extent. It varies from less than 50-m to nearly 150-m thick. Its present volume would be in the 2.5–3.5 km^3 range, and its original volume would not have been more than twice that. Thus, it is one of the smallest rhyolite lava flows in the Snake River Plain system, as most contain between 10 and 100 km^3 of material. Throughout most of its length, the Reynolds Creek lava flow consists of fresh rhyolite. Most is devitrified, but at the flow base, and sporadically at the flow top, black vitrophyre is preserved. At the north end of the flow, however, there has been extensive silicification of the Reynolds Creek rhyolite. This, in conjunction with the observation that the flow there has been broken into several large blocks that appear to have been rotated from their original orientations, suggests that the flow ran out into standing water of the Miocene version of Lake Idaho. This is consistent with the nature of several other rhyolite units that were erupted along the Owyhee Front at about the same time (Godchaux and Bonnichsen, 2002).

The Reynolds Creek lava flow erupted at about 11.48±0.09 Ma (sanidine Ar-Ar date, New Mexico Geochrological Research Laboratory, unpublished report), which is in good agreement with an earlier age determination of 11.4±0.6 Ma (sanidine K-Ar date, Armstrong and others, 1980). The Reynolds Creek unit generally contains small sanidine, quartz, and plagioclase phenocrysts, accompanied by traces of pyroxene and zircon. Ekren and others (1981) report 16 percent phenocrysts, in which sanidine constitutes 63 percent, quartz 29 percent, plagioclase 7 percent, and pyroxene pseudomorphs 1 percent, accompanied by traces of zircon. The phenocrysts tend to be larger and more abundant in this unit than in the Wilson Creek or Cerro Otoño units, but not nearly as large or as abundant as in the Jump Creek rhyolite. An analysis of a typical Reynolds Creek sample is given in table 1. This sample indicated the Reynolds Creek to be high in silica, similar to the Wilson Creek and Cerro Otoño units, but to have a Ba, Sr, Rb, and Zr contents in between the Jump Creek and the other units.

As indicated above, we believe the Reynolds Creek rhyolite unit is a lava flow that erupted from a vent area near its southeastern terminus, and it flowed northeastward mainly confined to a paleovalley. Contrary to this view, Ekren and others (1984, p. 41) suggested the Reynolds Creek rhyolite is a welded tuff that had erupted from within the Snake River Plain and flowed southwestward, upslope, away from the Plain, following the paleodrainage. They considered it to be part of a larger welded-tuff unit, which they refer to as the tuff of Browns Creek. Our interpretation that the unit is a lava flow, rather than a welded tuff, precludes it from being part of the tuff of Browns Creek as they describe it, even though the rhyolite constituting the Browns Creek unit is petrographically and geochemically similar to our Reynolds Creek lava flow. Our interpretation is that the Reynolds Creek lava flow is of clastigenic eruptive origin, rather than being an ignimbrite. We believe it was erupted mainly as molten material, perhaps accompanied by some partially solidified rhyolitic lava that was flung into the air at the site of the vent by the force of expanding gasses. These molten fragments fell back and coalesced to form lava that flowed many kilometers from the vent. We suggest that this lava flowed as a nonparticulate silicate liquid, rather than as particles enclosed within a gaseous medium.

Fragmentation of the magma as it ascended and erupted was the cause of the clastigenic nature of the eruption of the Reynolds Creek lava flow. We do not know how much of the gas responsible for the fragmentation of the ascending magma was derived from within the magma itself and how much was

from water that gained access to the vent area from sources external to magma. Given that the venting of the flow appears to have occurred in a paleodrainage, it may be that some of the gasses responsible for the explosive character of the eruption were derived from surface sources. If so, then it would be reasonable to think of the eruption mechanism of the Reynolds Creek rhyolite to be partially phreatomagmatic in character.

At some localities, in its northern reaches there is a bona fide welded ignimbrite, on the order of 30-m thick, that occurs stratigraphically beneath the Reynolds Creek lava flow. This ignimbrite is petrographically similar to the rhyolite of the overlying lava flow, but it contains abundant lithic and flattened-pumice clasts, especially in its lower part. Neither the areal extent nor the source of this ignimbrite has been determined. It appears to be quite limited in its distribution, however. Its very existence raises the possibility that during the first phase of the Reynolds Creek rhyolite, an authentic ignimbrite was produced. However, the fact remains that most of material that erupted and which gave rise to the Reynolds Creek flow was truly lava and not explosively derived shards and pumice that traveled as an ignimbrite.

Wilson Creek Ignimbrite

The Wilson Creek ignimbrite extends about 9 km SW.-NE. from its vent area at Wilson Bluff at the southwest end of its flow field down into the western Snake River Plain graben and varies in width considerably. It has a probable volume somewhere in the range of 2–4 km^3. Its vent area apparently was on land but evidently within a palaeodrainage, whereas the distal parts of the unit appear to have been emplaced subaqueously. Contrary to our view, Ekren and others (1984, p. 40) suggested that the source of Wilson Creek unit was in the Snake River Plain and that it flowed southwestward up a paleodrainage and eventually filled it. However, we find the field evidence at the southwestern end of the unit to be so compelling that we believe Wilson Bluff is the vent and that the unit flowed northeastward down the paleodrainage, not southwestward.

The Wilson Creek ignimbrite is a very complex unit, showing wide variation in the nature of materials it contains. There generally seem to be four types of material, probably deposited as a magmatic eruptive time sequence, rather than lateral facies, although it is not yet clear if all of these lithotypes stem from the same eruptive sequence from the Wilson Bluff vent. The oldest deposits are a block and ash mixture with mainly vitrophyric blocks ranging to more than a meter across in a vitric-ash matrix. The next oldest materials are low- to middle-grade ignimbrites that, in places, contain significant amounts of pumice and vesicular vitrophyre clasts. These materials grade upwards and toward the core of the unit to densely welded and devitrified, high-grade rheomorphic ignimbrite with a general lack of lithic inclusions or flattened pumices, and with abundant incipient to large lithophysal cavities. These dense devitrified materials probably were deposited in the central part of the paleochannel and are of considerable, but unknown thickness, perhaps in excess of 100 m. It appears that some of the densely welded core material of the Wilson Creek ignimbrite flowed out into the boundary zone along the Owyhee Front-western Snake River Plain graben, which was partially submerged, to form large blocks in the downflow part of the unit, evidently where the material had been emplaced on incompetent sediments in the lake-margin environment. Lastly, in the first couple of miles downflow (northeast) from the vent area, the unit has a greater thickness of material than elsewhere. This shows up as an elongate lump rising 100 m or so higher than the rest of the longitudinal profile of the unit's generally graded upper surface. We have not detected any sort of cooling break (*e.g.,* a vitrophyre or unwelded ash layer) between this material on top of the unit and the high-grade ignimbritic part of the unit beneath it. Although it is speculation at this point, it may be that this lump actually is clastigenic lava rather than high-grade ignimbrite, which represents the final stage of the eruption.

The block and ash deposits and the vesicular vitrophyre inclusions in the low-grade ignimbrite suggest that the formation and then collapse of early domes or spines may have been part of the eruptive sequence. In the lower part of the non-welded ignimbritic deposits at Wilson Bluff, there are clasts of a variety of older lithologies incorporated in the ignimbrite. Similarly, at higher stratigraphic levels on the bluff there are similar clasts interstratified with the welded ignimbrite. These foreign clasts very likely represent the results of phreatomagmatic explosions that accompanied the early phases of the eruption, as ground water and water in the drainage were heated to steam and blew up the preexisting ground at the eruption site. Finally, along parts of the western margin of the unit there are low-grade ignimbritic materials that have undergone considerable silicification and chloritization; these materials might be portions of the Wilson Creek ignimbrite that were flooded by streamwater while still hot, right after their deposition, or they might be of an earlier age and unrelated to the Wilson Creek unit.

Two Ar-Ar age determinations on sanidines from the Wilson Creek ignimbrite yield dates that are in good agreement. One is 11.42±0.08 Ma for a welded, but non-rheomorphic, ignimbrite from the east side of the unit. The other is 11.34±0.11 Ma for welded ignimbrite from the vent area (New Mexico Geochronological Research Laboratory, unpublished reports). A third Ar-Ar date on sanidine of 11.41±0.05 Ma (New Mexico Geochronological Research Laboratory, unpublished report) from a rhyolite locality (Hill 2597), which might either be part of the Wilson Creek ignimbrite or part of the Cerro el Otoño dome field from within the Snake River Plain, also is in good agreement. The Wilson Creek ignimbrite typically contains only a few percent of small phenocrysts, dominantly sanidine and quartz. Ekren and others (1981) give these data on phenocryst content of the unit: total phenocryst content is 4–5 percent, of which sanidine is 50–68 percent, and quartz is 32–50 percent, and these are accompanied by

traces of clinopyroxene and zircon. Two analyzed samples of the Wilson Creek ignimbrite are included in table 1 and show high silica contents and a paucity of Ba and Sr relative to the Jump Creek and Reynolds Creek units, and show lower Zr but higher Rb abundances than in those units. The composition of the Wilson Creek ignimbrite basically is indistinguishable from that of the Cerro el Otoño samples (table 1).

Cerro el Otoño Dome Field

Along the boundary between the Snake River Plain and the Owyhee Front is a series of small rhyolitic bodies that has been referred to as the Cerro el Otoño dome field (fig. 3). The Cerro el Otoño dome field appears to extend along the margin of the Owyhee Front for 11–13 km (7–8 mi). All of these bodies are small, with dimensions typically in the tens to hundreds of meters, and the volume of the entire field likely is to add up to less than a cubic kilometer of rhyolite. Most of the bodies show considerable silicification suggesting they were intruded and extruded into a lake-margin environment. Some of them have sheared to peperitic margins, evidently formed where viscous lava or magma pushed up through wet sediments, and spatter accumulations have been found at their margins. Locally, some have incorporated bits of sediment, mainly sandstone, near their margins as they were intruded or have pushed the overlying sediments up and deformed them into folds. The form of these bodies range from elongate dikes with steep margins, and are wide but short, to layered deposits that have small areal dimensions. These relations indicate that a combination of limited lateral flowage to form tholoids and the accumulation of fragmental material to form spatter rings were involved in the emplacement of these bodies.

The rhyolite of the Cerro el Otoño bodies is essentially the same as that of the Wilson Creek ignimbrite in its phenocryst assemblage and composition (table 1). Consequently, distinguishing between the dikes, domes, and tholoids of the Cerro el Otoño field and the foundered blocks of the Wilson Creek ignimbrite has been difficult; the problem is further compounded by later faulting along the margin of the Owyhee Front. Two Ar-Ar sanidine dates have been obtained from unequivocal Cerro el Otoño localities. These are 11.14±0.03 Ma for Hill 2471 and 11.03±0.07 Ma for Hill 3036 (New Mexico Geochronological Research Laboratory, unpublished reports). The age of the Cerro el Otoño dome field may be younger than that of the Wilson Creek ignimbrite or, with the 11.41-Ma date cited above for Hill 2597 (which either is part of the Cerro el Otoño dome field or part of the Wilson Creek ignimbrite), it is possible the age of the dome field overlaps the time of emplacement for the Wilson Creek ignimbrite.

The largest rhyolite body in the Cerro el Otoño dome field is the Cerro el Otoño body itself, located at Hill 3036, mainly in sec. 30, T. 1 N., R. 3 W. This body consists of an early-formed spatter ring filled with a small dome or tholoid of rhyolite that filled the crater, which formed during the eruption of the spatter. Most of the spatter was deposited on the inner wall of the crater, but more distal, thinner and outward-dipping beds of spatter also occur as erosional remnants as much as a few hundred meters from the main deposits. The Cerro el Otoño spatter and dome complex measures about 1 km E.-W. and about 0.8 km N.-S. and has a minimum volume of about 0.2 km^3. Its northeastern part has been downfaulted to a position too deep to be observed, so the total extent and volume of this body are unknown. The eruption of the Cerro el Otoño spatter and dome complex, like that of the other bodies in the dome field, seems to have been a combination of magmatic extrusion of quite viscous rhyolite to form the dike, dome, and tholoid forms, and fragmentation of some lavas, by some combination of magmatic and phreatic processes, to form the spatter accumulations.

Road Log and Stop Descriptions

The following 2-day field trip has been designed to bring participants to instructive places in each of the major rhyolite units in the Owyhee Front region and to demonstrate the nature of some of the rhyolite vents, ignimbrites, clastigenic lavas, spatter deposits, and domes that have been produced by the various magmatic and phreatomagmatic eruptions that shaped the Owyhee Front rhyolite field.

General Plan

On Day 1, drive from Boise to Walters Ferry for an overview of the Owyhee Front at Stop 1. Then drive to the vent area of the Reynolds Creek rhyolite, which will be Stop 2. After this, drive to Givens Hot Springs for lunch. After lunch, drive to the French John Hill area to inspect various features of the Jump Creek rhyolite, which will be Stop 3. Then return to Boise via Marsing and Nampa. The road log for Day 1 starts at Walters Ferry and ends at the intersection of Highways 95 and 55, two miles west of Marsing.

On Day 2, drive from Boise through Nampa and Marsing to the junction of Highways 95 and 55. Drive west and south on rural roads to the Jump Creek Falls Park area for Stop 4 to examine the silicification and brecciation that affected the Jump Creek lava flows when they ran into water impounded in an early stage of Lake Idaho. Then return to Highway 95 and follow it east and south to Sommercamp Road. Follow Sommercamp Road east, then Clark Road south, and finally the unimproved powerline access road southeastward to the mouth of Hardtrigger Creek canyon for Stop 5, which will be a tour of the Wilson Creek lava-like ignimbrite and the Cerro el Otoño dome and spatter ring. Return to Marsing via Clark Road and Highway 78, then on to Boise via Highways 55 and I-84. The road log for Day 2 starts at the junction of Highways 95 and 55, 2 mi west of Marsing where the Day 1 road log stopped, and ends at Marsing.

First Day

Mileage Cum.	Inc.	
0.0	0.0	Start trip at intersection of 3rd Street and 12th Avenue in downtown Nampa. Drive southwest on Highway 45, headed for Murphy.
17.5	17.5	Stop 1 at parking lot of Dan's Ferry Service on Highway 45 at the community of Walters Ferry.

Stop 1. View of Owyhee Front and Other Nearby Geologic Features

From the parking lot of Dan's Ferry Service on Highway 45 at the community of Walters Ferry, just north of the Snake River (Walters Butte 7.5-minute quadrangle), good views of the Owyhee Front can be seen. From southeast to northwest, some of the prominent features that can be seen on the southwestern skyline are Hayden Peak in the Silver City Range, the northeast end of the Reynolds Creek rhyolite lava flow, and Soldier Cap Butte and Wilson Peak that are made of granitic rocks overlain by the lower basalt of the Silver City volcanics.

In the immediate vicinity of Walters Ferry are the Hat Butte ferrobasalt, which forms the canyon rim to the north; the Grouch Drain maar that cuts the Hat Butte ferrobasalt near the top of the grade where Highway 45 starts down into the Snake River Valley; the Glenns Ferry Formation lake beds deposited during the latter life of Lake Idaho; and the Bonneville Flood deposits that include the gravel deposits immediately north of Dan's Ferry Service, as well as the rounded basalt boulders scattered through the fields along the southwest side of the Snake River. These and other volcanic and sedimentary units in the Walters Ferry region, are described on the geologic map of Bonnichsen and Godchaux (1998).

Mileage Cum.	Inc.	
		Drive south from Stop 1, across the Snake River, on Highway 45. Once across the river veer left at the road fork onto Highway 78, toward Murphy.
19.0	1.5	Turn onto Reynolds Creek Road and continue generally southwestward.
28.6	9.6	Park alongside the road at the mouth of the unnamed box canyon for Stop 2.

Stop 2. Vent Area of Reynolds Creek Rhyolite Lava Flow

(sec. 8, T. 2 S., R. 3 W.; Wilson Peak 7.5-minute quadrangle)

Walk about 0.3 mi west of the road into the little box canyon, then climb up the back of the canyon to the rim. Later, walk another 0.4 mi westward to the west side of the Reynolds Creek lava flow to look into the canyon of Reynolds Creek. Examine the features of interest (Stops 2A, 2B, 2C, and 2D) along the walk.

Stop 2A. Dipping Layer of Welded Pyroclastic Rocks Beneath the Lava Flow

Exposed in the slope at the head of the box canyon, downslope from the dike complex on the east side of the vent area, is a moderately dipping layer of welded pyroclastic material a few meters thick (fig. 4). At its base, this layer has a fragmental zone, which suggests that part of the emplacement process involved downslope avalanching of erupted material. The fragmental material is overlain by vitrophyre containing streamlined glassy clasts of the same composition in a layered matrix that originally was of finer grain size (fig. 5). This layer, which might have been deposited from a small debris avalanche of very hot particulate material and enclosed partially molten clasts, is limited in its distribution to the vicinity of the vent area, rather than representing an ignimbrite of large extent. This thin layer may have been a precursor to one of the eruptions that led to the development of the Reynolds Creek lava flow, or it may be material that was expelled from a portion of the flow after it had been erupted, perhaps by steam explosions. We don't know if this pyroclastic layer formed at the beginning or the eruption sequence, or sometime later during the development of the lava flow.

Stop 2B. Complex of Near-Vertical Feeder Dikes at East End of Vent Area

Exposed near the canyon rim at the head of the box canyon are a series of parallel rhyolite dikes that form the east end of the vent area of the Reynolds Creek rhyolite lava flow. These dikes generally trend east-west and are as much as a few meters thick (fig. 6). Some are composed of vitrophyre, and others have been partly to completely devitrified. They tend to be subparallel and may be a series of feeder zones through which lava was expelled as the flow developed. Scattered about in the vent area are accumulations of rhyolite that have a fragmental texture. These accumulations are considered to have accumulated by the coalescence of individual blobs of rhyolitic spatter that vary in size from a millimeter to several centimeters across that were thrown into the air during the eruption. In some instances, the individual spatter clots are quite distinguishable and only seem to have undergone flattening (fig. 7). In other instances, the blobs have merged

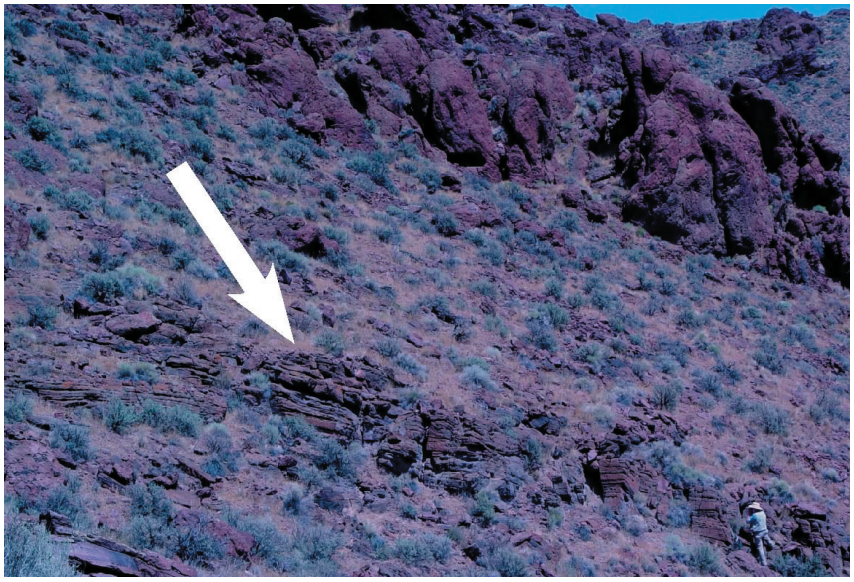

Figure 4. Dipping layer of welded pyroclastic material (arrow) beneath rhyolitic lava and spatter accumulations in the vent area of the Reynolds Creek rhyolite lava flow.

and undergone mass flowage to produce inclined layers of flow-layered and folded rhyolite with abundant secondary gas cavities (fig. 8).

The presence of these preserved spatter accumulations may indicate that substantial amounts, if not basically all, of the material that coalesced and flowed away from the vent to form the rhyolite lava flow erupted as particles or clots of lava, rather than simply welling up and out of the feeder dikes as a nondisrupted flow of liquid silicate melt. If so, then the rhyolite flow should be considered as having a clastigenic mode of eruption, perhaps similar to many basalt flows that have been shown to coalesce from clots of liquid basalt thrown into the air in vent areas, sometimes in the form of spectacular fire fountains. In the case of the Reynolds Creek rhyolite eruption, however, we don't at this time know how high the material may have been thrown from the vent. Nor do we know to what extent the explosive character was the result of the expansion of original gasses in the magma, rather than the result of surface waters that might have been incorporated into the magma or lava and then expanded to steam causing phreatomagmatic explosions that hurled some of the rhyolitic lava about.

Stop 2C. View Point into Reynolds Creek Canyon at West End of Vent Area

After walking along the top of the vent area, which is the ridge proceeding west-northwest from the dike complex of Stop 2B, you will come to the western side of the Reynolds Creek lava flow. This ridge extending across the flow is thought to be the general area from which the Reynolds Creek lava erupted and was the highest part of the flow at that time. This lava evidently filled a paleocanyon, with most of the material flowing northward as much as about 8 km (5 mi) toward the lake that occupied the incipient western Snake River Plain graben. A small amount of the lava flowed westward about 2 km (1.2 mi) to fill the paleocanyon as far upstream as the lava would flow. The western side of the flow seems to have been eroded back some from its original extent by downcutting of Reynolds Creek to form the 350-m-deep (1200-ft-deep) canyon. Across the canyon, the rocks are granite. The rocks below the Reynolds Creek rhyolite lava flow on this (east) side of the stream may be part of the lower basalt of the Silver City area (unit Tlb of Ekren and others, 1981) or part of the older Salmon Creek volcanics.

Stop 2D: Flow Ridges on Top of Reynolds Creek Flow

On the way back to the east side of the vent area turn to the north, where several flow ridges (ogives) are preserved at the top of the lava flow. Their curvature, convex away from the proposed vent area, is consistent with flowage to the north, away from the dikes. The exact origin of these ridges is not

Figure 5. Close-up view of the welded pyroclastic layer shown in Figure 4. Note the dark-colored, glassy lensoidal structures (arrow). They probably are flattened lava clots rather than pumices.

known. They might simply be folds in the upper few meters of the lava flow. However, it is possible that they are ramped-up zones that formed in the rigid top of the flow, or they might have been formed some other way. It would take examination of the third dimension to obtain a clearer picture of their character and origin.

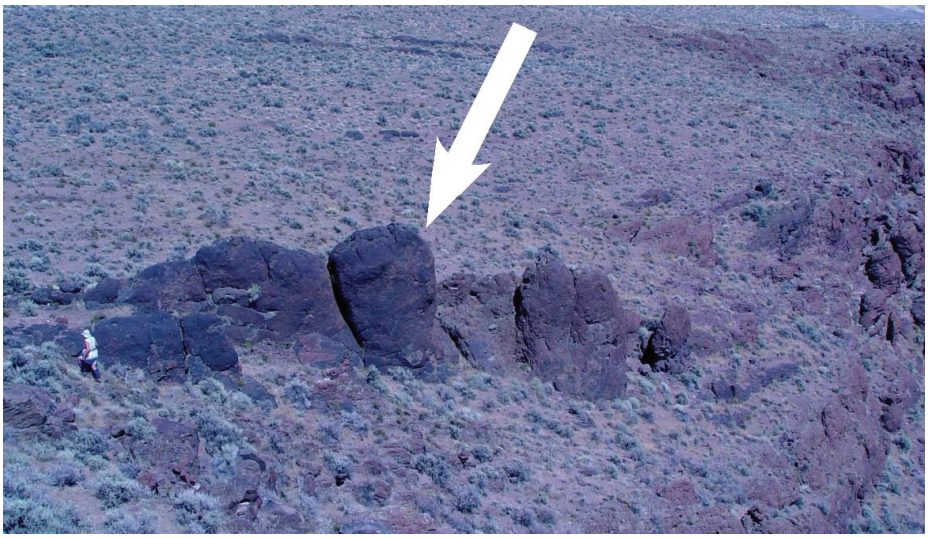

Figure 6. Vertical dike of glassy, somewhat fragmental, rhyolite in the vent area of the Reynolds Creek rhyolite lava flow (arrow).

Mileage Cum.	Inc.	
		When finished at Stop 2, return to the vehicles and retrace the route northeastward on Reynolds Creek Road.
32.9	4.3	View of an unnamed welded ignimbrite that occurs beneath the Reynolds Creek rhyolite lava flow exposed on the west (left) side of the road.
36.9	4.0	Turn north (left) at intersection onto the unnamed road and proceed north, past the defunct ostrich ranch, to join Highway 78.
37.9	1.0	Highway 78. Turn northwest (left) onto the highway and proceed to Givens Hot Springs.
45.0	7.1	Givens Hot Springs natatorium and picnic grounds, a good place to stop for lunch. Afterwards, continue driving northwestward on Highway 78 to its intersection with Sommercamp Road.
48.1	3.1	Sommercamp Road intersection. Turn southward (left) onto Sommercamp Road, and follow it through its turns then westward to its junction with Highway 95.
55.1	7.0	Junction with Highway 95. Turn south (left) onto the highway.
59.5	4.4	Pull off road at the Owyhee Country scenic view turnout and park for Stop 3.

Stop 3. Emplacement and Deformation of Jump Creek Rhyolite Lava Flows in French John Hill Area along Highway 95 and View of Buck Mountain Volcano

(sec. 19, T. 1 N., R. 4 W.; Opalene Gulch 7.5-minute quadrangle)

The various points of interest here (Stops 3A, 3B, 3C, and 3D) can be reached by first walking east of the highway to the overview into the canyon of Squaw Creek, then to the long road cut north of the Owyhee Country viewpoint parking area, then to the other big road cut southwest of the parking area, and finally to the viewpoint farther southwest along the highway for an excellent view of the Buck Mountain volcano.

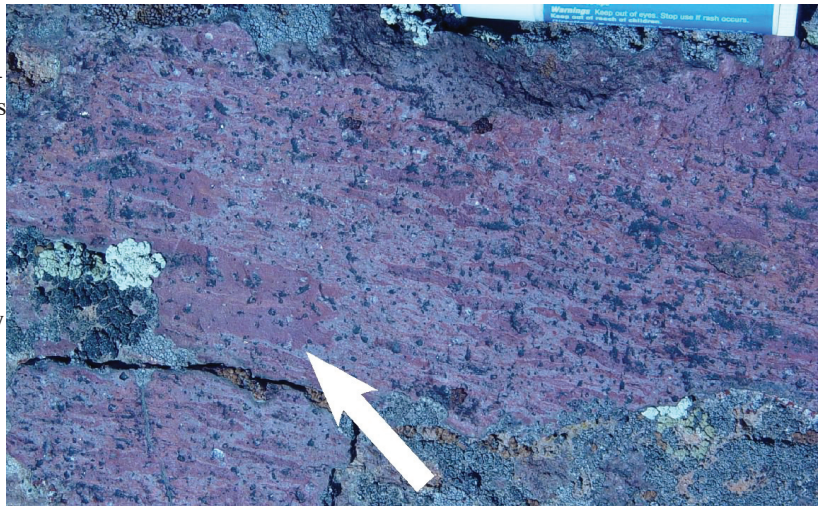

Figure 7. Flattened millimeter- to centimeter-sized spatter blobs (arrow) in the vent area of the Reynolds Creek rhyolite lava flow.

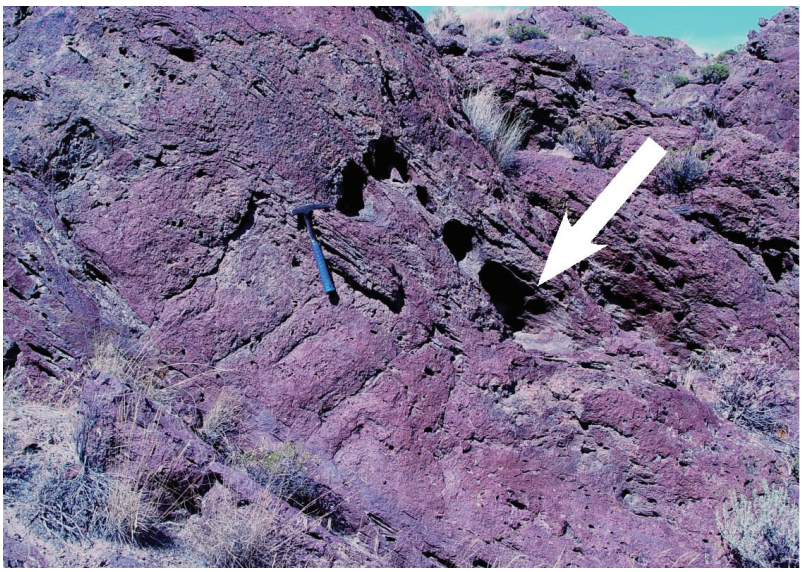

Figure 8. Spatter that merged, flowed, and became folded as it accumulated in the vent area of the Reynolds Creek rhyolite lava flow. Note the large gas cavities that are associated with the hinge zones of the folds (arrow).

Stop 3A: Boundary Zone Between the Rockville and Shares Snout Segments of the Jump Creek Rhyolite Field in Squaw Creek Canyon

The features in Squaw Creek canyon include the eastern margin of the Rockville segment of the Jump Creek rhyolite field, which generally is exposed along the west side of the canyon, and the western margin of the Shares Snout segment, which generally is exposed along the east side of the canyon. The paleo-Squaw Creek drainage evidently was established along the zone where these two segments of the Jump Creek rhyolite field abutted, and then the stream incised along that course. On the east side of Squaw Creek canyon, a little upstream from this viewpoint, is one of the probable vents of the Shares Snout segment. Exposed beneath the Jump Creek rhyolite are sediment and volcanic ash beds of the Sucker Creek Formation.

Stop 3B: Strongly Fractured Rhyolite Along Highway North of Owyhee Country Viewpoint

Walk along the highway north of the viewpoint and examine the walls of the long road cut. The rhyolite here is part of the Rockville segment and appears to be part of the devitrified interior of the unit. The rhyolite is pervasively fractured, with many joints having a vertical orientation, and a lesser number having subhorizontal or inclined orientations. Several near-vertical faults cut this mass of rhyolite, and at one locality a kink-band structure (fig. 9) can be seen to have developed in the near vertical joints. It is our interpretation that most of the joints, especially the abundant near-vertical ones, formed in this rhyolite mass after it had been crystallized and partly to completely cooled but still during the emplacement episode of the flow. The high concentration of near-vertical joints cutting the rhyolite here is unusual for a Snake River Plain rhyolite unit and probably suggests some special structural circumstances during the emplacement of this unit, or shortly afterwards. Relations we will examined in the road cut along the highway to the south (Stop 3C) may provide some insight as to why this rhyolite is so fractured.

Stop 3C: Chaotic Megabreccia Zone in Rhyolite Along Highway South of Owyhee Country Viewpoint

Walk along the highway south of the Owyhee Country viewpoint through the quarter-mile-long road cut in the lower part of the Rockville segment of the Jump Creek rhyolite and what evidently were sediment beds beneath the rhyolite that have been extremely disrupted (fig. 10). This occurrence rightfully can be referred to as a chaotic megabreccia, a non-genetic term for

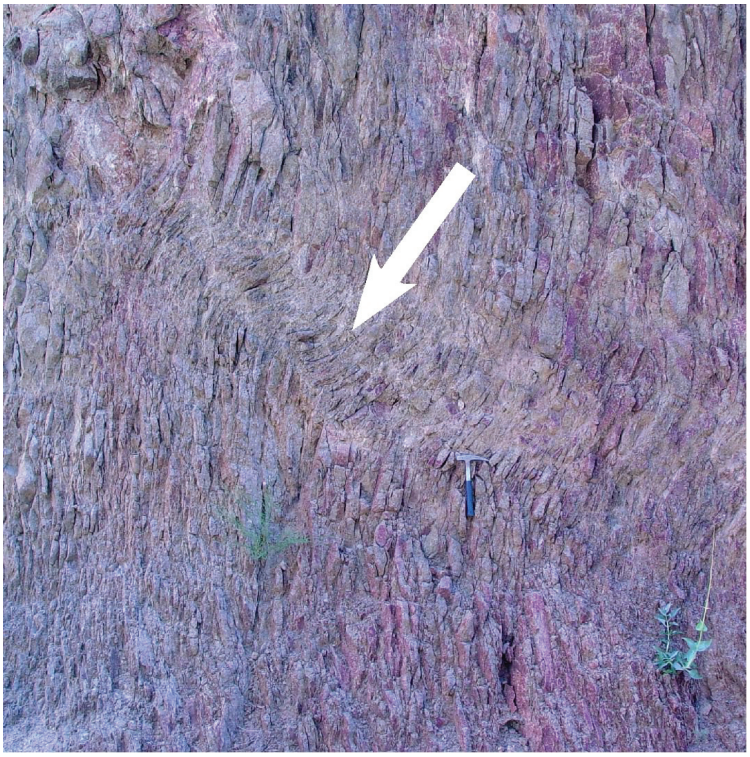

Figure 9. A kink-band zone (arrow) that occurs in a pervasively jointed exposure of devitrified Jump Creek rhyolite along U.S. Highway 95 in the French John Hill area.

Figure 10. A chaotic megabreccia that formed where a Jump Creek rhyolite lava flow may have loaded and mixed with the underlying sedimentary beds, exposed along U.S. Highway 95 in the French John Hill area.

this messy mixture of rhyolite and disrupted sediments. Within this zone much of the rhyolite is vitrophyre that has been fragmented. In some instances, the fragments are intimately mixed with disrupted sedimentary materials. The sediments are a section of fine-grained to cobble-sized materials that initially might have been stream, and perhaps lacustrine, deposits that probably are part of the Sucker Creek Formation or younger deposits eroded and redeposited from that formation. At this locality, these sediments have been thoroughly scrambled and disrupted from their presumed original subhorizontal attitude. Numerous faults cut the sediments and the rhyolite, separating various packages of materials. A plausible interpretation for the origin of this chaotic megabreccia is that this portion of the Rockville segment lava flow cascaded over steep terrain and broke up in the process. It may have flowed into a small paleocanyon along or near the present day position of Squaw Creek. On the slope to the west of this exposure, but out of view from the highway, the lava flow can be seen to steepen in dip as the highway is approached, as if this flow unit plunged into a paleocanyon, supporting the interpretation offered. As the leading edge of the hot, but fragmented, rhyolite filled the paleocanyon it probably loaded the previously deposited, but generally incompetent, package of sediments. This loading probably also disrupted the sediments and caused their upwards diapiric flow into the base of the fragmented rhyolite and the intermixing of the two types of materials. The evidence in this road cut for rhyolite loading of underlying incompetent sediments also may explain the highly fractured rhyolite in the road cut to the north (Stop 3B); it is likely that the rhyolite there was deposited above similar incompetent materials.

Stop 3D. Buck Mountain Volcano

From the highway pullout and parking area south of the chaotic megabreccia road cut one can see, at a distance of about 2.5 km (1.5 mi) due south, a hill named Buck Mountain (fig. 11). Buck Mountain is a small volcano composed of Jump

Figure 11. View, looking south from U.S. Highway 95, into the crater area of the Buck Mountain volcano.

Creek rhyolite, which has been dissected only a little since it formed about 11.56 Ma. The volcano was constructed above deposits of the Salmon Creek volcanics, the Sucker Creek Formation, and the lower basalt of the Silver City area (units Tab, Tsu, and Tlb of Ekren and others, 1981). From this location one can see directly into its breached crater area, where inward-dipping layers of rhyolite are exposed. Examination of the Buck Mountain volcano shows that it consists mainly of stubby lava flows, spatter accumulations, and masses of volcanic breccia. Evidently, lava flows did not extend away from this volcano for distance much greater than its current extent.

Mileage Cum.	Inc.	
		After visiting the points of interest at Stop 3 retrace your route northward on Highway 95 to its junction with Highway 55.
69.7	10.2	Junction of Highways 95 and 55. Day 1 road log ends here. From here, turn east (right) and follow Highways 55 and I-84 back to Boise through Marsing and Nampa.

Second Day

Mileage Cum.	Inc.	
0.0	0.0	Start Day 2 trip at intersection of Highways 95 and 55 where the road log for the first day stopped. Stop in the parking lot at this intersection for a view of the Owyhee Front to the southwest, where the Jump Creek lava flows have been truncated by faulting. Then proceed westward on Highway 95 to where the highway starts curving to the right.
1.9	1.9	Turn left from Highway 95 onto Cemetery Road.
3.1	1.2	Turn left from Cemetery Road onto Jump Creek Road.
6.8	3.7	Sharp turn to the west (right) along Jump Creek Road.
8.3	1.5	Follow Jump Creek road southward to parking lot for Jump Creek Falls Park for Stop 4.

Stop 4. Character of Jump Creek Rhyolite in Vicinity of Jump Creek Falls Park

(sec. 27, T. 2 N., R. 5 W., Jump Creek Canyon 7.5-minute quadrangle)

Much of the Jump Creek rhyolite in this area was emplaced in water and was extensively silicified and brecciated during emplacement. It was subsequently faulted during continued downdropping of the western Snake River Plain

Figure 12. View, looking south, of the mouth of Jump Creek Canyon near the margin of the Owyhee Front. Photograph illustrates the massive interior of the Jump Creek rhyolite.

Figure 13. Jump Creek Falls where the stream cascades down a wall of massive devitrified Jump Creek rhyolite.

graben along the Owyhee Front. The pervasive brecciation and silicification of the rhyolitic lava and other points of interest(Stops 4A, 4B, and 4C) can be seen by first walking south along Jump Creek for 0.2 mi to Jump Creek Falls, and then going to the small sandstone-capped hill located about 0.5 mi north of the park.

Stop 4A. Brecciation and Silicification of Rhyolite along Jump Creek Falls Trail

At the boundary between the Owyhee Front and the western Snake River Plain, which essentially passes through the parking lot of Jump Creek Falls Park, the Jump Creek rhyolite flows are cut off by faults. At the faults, the stream emerges from a deep, narrow canyon cut in rhyolite flows onto a plain, where post-rhyolite lake sediments have been deposited (fig. 12). The Jump Creek lavas along the front have been fragmented and silicified by interaction with the water of the lake. Along the trail between the parking lot and the waterfall, the Jump Creek rhyolite has been broken into large and small fragments. Between the fragments, and commonly cementing them, are veins and masses of secondary silica, mainly chalcedony. The brecciation probably occurred as the rhyolite entered the lake, because it would have flowed down across steep slopes and cooled rapidly by immersion in the lake. The silicification probably represents silica dissolved from the brecciated rhyolite that was reprecipitated in fractures as the rhyolite cooled. At the parking lot, note the sediments exposed along the road. These materials provisionally are assigned to the Chalk Hills Formation and are thought to have been deposited against the front after the Jump Creek rhyolite flows were offset by faults. Downstream from the parking lot, the rhyolite exposed along Jump Creek becomes more and more pervasively brecciated and silicified.

Stop 4B: Jump Creek Falls and Massive Rhyolite in the Lava Flow Interior

At Jump Creek Falls (fig. 13) the rhyolite is not brecciated, although it is pervasively jointed. The style of jointing in the wall of rhyolite at the waterfall is typical of the devitrified interior portions of large rhyolite lava flows. A probable normal fault cuts across the canyon at the site of the waterfall. Several other normal faults, with mainly north-side-down displacements, occur between the waterfall and the parking lot area. The waterfall is slightly greater than 10 m in height.

Mileage
Cum. Inc.

When finished at the Park, drive back out of the parking area and proceed to the hill near the road, about one-half mile to the north, for Stop 4C.

8.9	0.6	Stop by the gate in the fence on the east (right) side of road, cross the fence, and walk about 0.1 mi east to the top of the hill.

Stop 4C: Pervasively Fragmented and Silicified Rhyolite and Overlying Sandstone Containing Rhyolite Clasts

At the top of the hill are beds of sandstone that conformably overlie rhyolite (fig. 14). At this locality, the upper part of the rhyolite consists of a mass of small silicified and bleached fragments. The sandstone contains thin interlayers of these fragments and, although the contact between the fragmental rhyolite and the sandstone is abrupt, it would appear to be a transition without a significant time break. Rather, it seems that after the fragmental rhyolite had flowed into its present position the deposition of sand, perhaps representing a near-shore environment in the lake, commenced. This hill may mark the position of a small horst that developed in the Owyhee Front zone prior to deposition of the Chalk Hills Formation sediments and prior to deposition of the sandstone capping the hill. Additional sandstone occurs at the northern base of this hill where the beds are downfaulted.

Mileage Cum.	Inc.	
		After finishing at Stop 4, retrace your route to the junction of Highways 95 and 55.

Figure 14. Sandstone beds lying on the fragmental and altered top of the Jump Creek rhyolite. This part of the rhyolite flow was emplaced subaqueously and the sandstone probably was deposited soon afterwards.

16.6	7.7	Junction of Highways 95 and 55. Turn south (right) on highway and proceed to the Sommercamp Road junction.
22.4	5.8	Junction of Highway 95 and Sommercamp Road. Turn east (left) on Sommercamp Road.
23.2	0.8	The hill to the south (right) is Elephant Butte. It is an outlier of the Shares Snout segment of the Jump Creek rhyolite field preserved either as a slide block or as a remnant of a small horst.
23.7	0.5	The well exposed and slightly deformed sediments to the north (left) as we drive down this grade probably are part of the Chalk Hills Formation of the Idaho Group. These were deposited in Lake Idaho during the latter part of the Miocene. In this region the Chalk Hills Formation sediments overlie outliers of the Owyhee Front rhyolite field and have basaltic ash and subaqueously emplaced basalt flows intercalated within them. The hill south of the road is Hill 3180; it is another outlier of Jump Creek rhyolite of the Shares Snout segment. This rhyolite body is cut by veins of chalcedony and has tilted beds of sandstone lying on its flanks. These sandstones, which we believe belong to the Poison Creek Formation, are older than the Chalk Hills Formation sediments by the road that are noted above.
27.3	3.6	Junction of Sommercamp and Clark Roads. Turn south (right) on Clark Road and follow it south for a mile to where it forks at the powerline.
28.3	1.0	South end of Clark Road where the road forks by the powerline. Take the left fork and follow the unimproved powerline access road generally southeastward for about 3.5 mi to the mouth of Hardtrigger Creek.
29.5	1.2	Pass through a small, northward-plunging anticline that deforms sandstone beds in this area. This sandstone probably is part of the Poison Creek Formation. The anticline may have been uplifted by a still-hidden rhyolite body that punched up from below, but did not reach the surface. The elongation of this anticline is nearly on line with the dike-like rhyolite mass immediately to the northwest (Hill 2597) that was emplaced at 11.41 Ma and which may be either part of the Wilson Creek ignimbrite or part of the Cerro el Otoño dome field.

30.3	0.8	Turnoff from road to the left near the power-line. Look carefully to find this turnoff. Turn sharply to the left on it, rather than proceeding straight.
31.0	0.7	Go through gate and continue southeastward after driving up the short grade.
31.8	0.8	Parking area at the mouth of Hardtrigger Creek canyon, Stop 5.

Stop 5. Rheomorphic Core of the Wilson Creek Ignimbrite and the Cerro El Otoño Spatter and Dome Complex, Lower Canyon of Hardtrigger Creek

(sec. 30, T. 1 N., R. 3 W., Givens Hot Springs 7.5-minute quadrangle)

The parking area at the mouth of Hardtrigger Creek canyon is a good place for lunch. Afterwards, the features of interest can be visited on foot. Walk south for about 0.4 mi along the stream course to see the various facets of the Wilson Creek ignimbrite (Stops 5A and 5B). Then climb up the slope on the east side of the stream course to the base of the cliff, where the spatter ring of the Cerro el Otoño dome (Stop 5C) is exposed above the Wilson Creek unit. Follow this cliff northward about 0.2 mi, then climb up to the top of the dome and walk about 0.5 mi southeastward, across its top (Stop 5D). Then continue to the occurrence of silicified boulders, cobbles, and sandstone on the southeast side of the dome (Stop 5E). After this, follow the southern lower flank of the dome westward to Hardtrigger Creek and follow the stream course northward back to the vehicles, a distance of about a mile.

Stop 5A. Rheomorphic Core of Wilson Creek Ignimbrite

On the walk through the lower canyon of Hardtrigger Creek, an excellent view of the core of this densely welded rheomorphic ignimbrite can be observed. It is somewhat lava-like in many ways due to post-emplacement rheomorphic adjustments. One of the characteristics of the Wilson Creek unit is the presence of lithophysal cavities, some of which are quite large and complex in this area (fig. 15). In this area, it is notable that many of these cavities appear to have been tilted as much as 90 degrees from their original orientations; we attribute this to post-emplacement rheomorphic flowage of the entire rhyolitic mass that forms the core of the ignimbrite. Most commonly, lithophysal cavities such as those in this unit, form with their arched side convex-upwards. Also, note that the rhyolite in this canyon shows well-developed layering. Although some of this layering may be due to flowage during later deformation of the ignimbrite. It also is probable that some of the layering and its small-scale deformation is original and was produced as the flowing ignimbrite made the transition to a continuous mass of silicate liquid that continued to flow, deform, and expel gasses, some of which remained trapped as gas cavities. That is, as the flow underwent progressive aggradation such as described by Branney and Kokelaar (1992, 2002) layering was produced that had a subhorizontal attitude. En masse flowage after progressive aggradation of the entire core of the Wilson Creek unit then tilted and deformed the depositional layering to steep attitudes, as can be observed in the walls of the canyon. The en masse flowage here is not like that in a lava flow where the material may flow many kilometers but is instead of more limited distance. Distances indicated here were just enough to tilt the layering and enclosed lithophysal cavities, which would not require distances of more than a hundred meters.

Stop 5B. Vitrophyre and Breccia at Top of Wilson Creek Ignimbrite

The glassy rocks exposed upstream, about 0.4 mi from the parking area at the mouth of Hardtrigger Creek canyon, vary from dense vitrophyre to perlite and commonly are vesicular. Locally, lithic fragments have been found within this outcrop area. These materials, based on their locations, appear to be a part of the Wilson Creek unit that was rapidly cooled. It probably is part of either the base or the side of the unit.

Stop 5C. Thick Accumulation of Inner-Crater-Wall Spatter at West Side of Cerro el Otoño Dome

Figure 15. Lithophysal gas cavities developed in the devitrified, high-grade, rheomorphic core of the Wilson Creek ignimbrite in the lower canyon of Hardtrigger Creek.

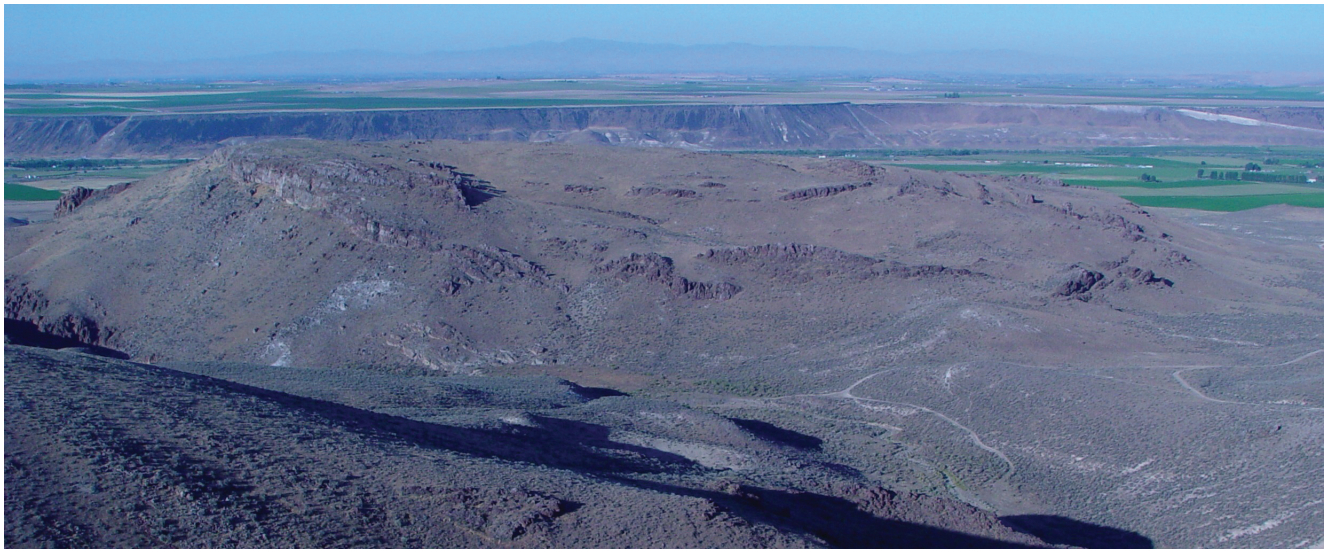

Figure 16. View looking northeast at the Cerro el Otoño dome (Hill 3036). The escarpment on the west side of the dome (left side of view) is an accumulation of rhyolitic spatter. Note the arcuate ridges on the top of the dome.

Figure 17. Dipping rhyolitic spatter layers that were deposited on the inner crater wall of the Cerro el Otoño spatter ring and dome complex.

The Cerro el Otoño spatter and dome complex sits on the Wilson Creek ignimbrite and is thought to have erupted up through that unit, perhaps through a dike along the northeast side of the complex. The oblique view of the complex taken from the southwest (fig. 16) clearly shows an accumulation of bedded, partially agglutinated, spatter, about 30-m thick (fig. 17), on the west side of the complex, where it is cut by Hardtrigger Creek canyon. Layering within this spatter dips eastward toward the central part of the complex and is interpreted to have been deposited on the inner wall of a crater. Such inward-dipping spatter deposits occur all around the western, southern, and eastern sides of the complex, but not to the north because a fault has displaced the northern part of the complex beneath the surface. At places, the spatter that accumulated on the inner crater wall appears to have been flowing back into the crater as it solidified. Farther away from the dome, erosional remnants of thinner-layered outer-wall spatter accumulations have been observed.

Notable within the spatter deposits that occur low in the section, on both the west and east sides of the complex, are accumulations as much as a meter thick consisting of small, pea-sized, semispherical drops (fig. 18), many of which have devitrified to reddish-brown spherulites. We refer to these deposits as the “brown pea” horizon and tentatively conclude that the rounded particles were silicate melt drops that, after having been erupted into the air, quenched sufficiently before they landed so that their spherical shapes were preserved. Also, the rate of accumulation would have been sufficiently slow so that the individual drops were not flattened but only sintered together. Microscopic examination of the textural arrangement of the drops (fig. 19) reveals that many had merged into an polygonal equilibrium fabric prior to any devitrification. Others, however, are separated by a glassy matrix, which probably originally was dust. In many, instances

Figure 18. Layers of devitrified, semispherical spatter droplets that accumulated to form the "brown pea" horizon within the spatter ring portion of the Cerro el Otoño spatter ring and dome complex.

Stop 5D: Traverse Across Top of Cerro el Otoño Dome

In traversing across the top of the dome, you will find that the rhyolite is fairly massive to flow-layered in character and much is devitrified. At many localities, fragmental zones and thoroughly silicified horizons are present in the interior of the dome. Also, as can be seen in figure 16, on the top of the dome is a series of concentric arcuate ridges that are convex toward the southeast. These ridges may be the result of flowage of material from a vent area in the northern part of the dome, or they may be resistant layers of rhyolite that perhaps are more silicified than other parts and represent the sequential accumulation of material as the crater was filled. At several localities in the upper part of the dome, there are thoroughly fragmented silicified zones, which probably represent hydrothermal chimneys that vented high-pressure steam.

the boundaries of the spherulites do not extend all to the way to the drop margins (Godchaux and Bonnichsen, 2002). At present it is not known if the explosive conditions that led to the formation of melt drops, which were quenched in the atmosphere, were due only to the escape of magmatic gasses, or due to meteoric water that gained access to lava in the crater, causing explosive activity that was partially, or wholly, phreatomagmatic in character. The fact that we find the results of such eruptions located in an environment that we believe was at the shore of a large lake, however, leads us to suspect that phreatomagmatic activity played an important part in the origin of the "brown pea" accumulations.

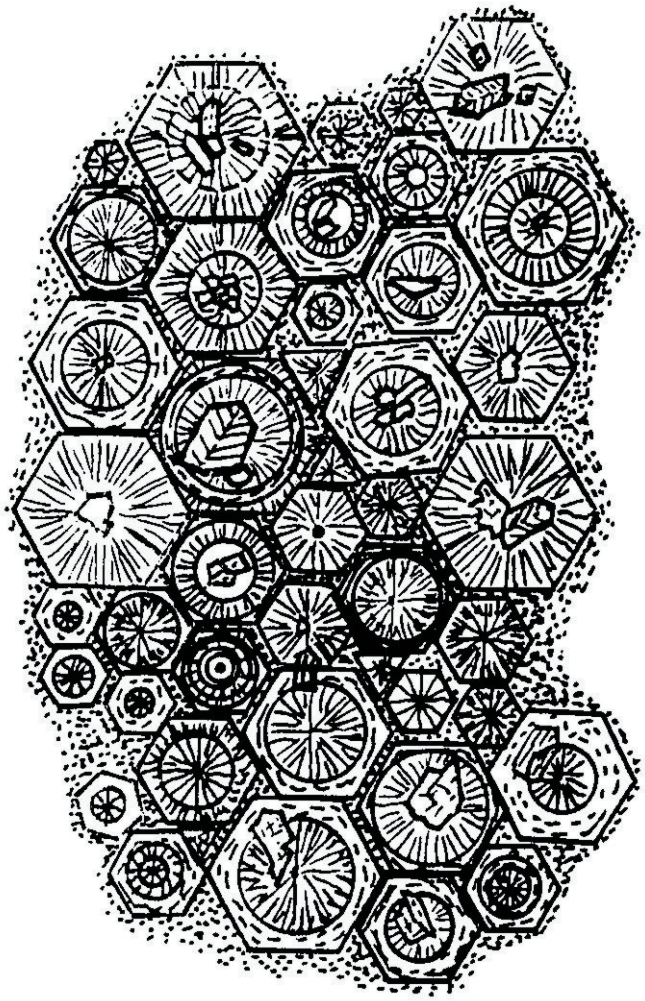

Figure 19. Sketch illustrating annealing and devitrification textures encountered in the "brown pea" horizon of the Cerro el Otoño spatter ring and dome complex. Circles represent spherulites developed in glassy droplets that merged to give an annealed fabric (hexagonal shapes). Stippled areas represent glassy areas that are interstitial to the droplets and may have initially been glassy dust. In the spherulites the radial patterns represent fibrous crystals. Dashed zones outside of the spherulite rims are microperlitic glass that did not devitrify. Small crystals of feldspar, other minerals, and tiny vesicles were present in some of the original droplets and have been enclosed by the spherulites.

Stop 5E. Silicified Sediments Deposited on East Side of Cerro el Otoño Dome

In the southeastern part of the dome, perched high on its side, is a thoroughly silicified sedimentary deposit that evidently was deposited in a stream channel after the dome formed. The deposit has resisted erosion because of its extremely durable character. The deposit grades upwards from rounded boulders and cobbles in its lower part to sandstone in its upper part. Although silicification of the deposit may have occurred while the dome was cooling, it also is possible that it was silicified much later, perhaps coinciding with the emission of hot springs along the Owyhee Front during the episode of faulting and subaqueous basaltic volcanism that occurred in the western Snake River Plain graben 7 to 9 m.y. ago (Bonnichsen and Godchaux, 2002).

Mileage Cum.	Inc.	
		After walking back to the vehicles, retrace your route along the powerline access road to the junction with the south end of Clark Road, follow it north to Highway 78, turn to the northwest (left) on the highway and follow it to the junction with Highway 55 in Marsing.
35.3	3.5	Rejoin Clark Road and drive north.
38.4	3.1	Junction with Highway 78. Turn to the northwest (left).
44.1	5.7	Junction with Highway 55 by the Snake River Market in Marsing. This is the end of the road log for the second day. Turn east (right) on Highway 55 and follow it, via Nampa, back to Boise.

Acknowledgments

We would like to thank all of our colleagues who, while in the field with us, made many helpful suggestions about the nature and origin of the rhyolites that are described in this field guide. In particular we take delight in thanking Craig White, Curtis Manley, John Wolff, Scott Boroughs, Janet Sumner, Mary O'Malley, Spencer Wood, Jocelyn McPhie, and Nancy Riggs. We also would like to thank the institutions that we now or previously worked for, the Idaho Geological Survey at the University of Idaho, the Department of Geosciences at Idaho State University, and the Department of Earth and Environment at Mount Holyoke College, for their support and encouragement over the years. Our thanks for the financial support that funded this research and gave us the knowledge to prepare this guide goes to the Idaho Geological Survey and the STATEMAP program of the U.S. Geological Survey.

References

Armstrong, R.E., Harakal, J.E., and Neill, W.M., 1980, K-Ar dating of Snake River Plain (Idaho) volcanic rocks—New results: Isochron/West, v. 27, p. 5–10.

Bonnichsen, B., 1982a, The Bruneau-Jarbidge eruptive center, southwestern Idaho, *in* Bonnichsen, B., and Breckenridge, R.M., eds., Cenozoic geology of Idaho: Idaho Bureau of Mines and Geology Bulletin 26, p. 237–254.

Bonnichsen, B., 1982b, Rhyolite lava flows in the Bruneau-Jarbidge eruptive center, southwestern Idaho, *in* Bonnichsen, B., and Breckenridge, R.M., eds., Cenozoic geology of Idaho: Idaho Bureau of Mines and Geology Bulletin 26, p. 283–320.

Bonnichsen, B., Christiansen, R.L., Morgan, L.A., Moye, F.J., Hackett, W.R., Leeman, W.P., Honjo, N., Jenks, M.D., and Godchaux, M.M., 1989, Excursion 4A: Silicic volcanic rocks in the Snake River Plain-Yellowstone Plateau province: New Mexico Bureau of Mines and Mineral Resources Memoir 47, p. 135–182.

Bonnichsen, B., and Citron, G.P., 1982, The Cougar Point Tuff, southwestern Idaho and vicinity, *in* Bonnichsen, B. and Breckenridge, R.M., eds., Cenozoic geology of Idaho: Idaho Bureau of Mines and Geology Bulletin 26, p. 255–281.

Bonnichsen, B., and Godchaux, M.M., 1998, Geologic map of the Walters Butte quadrangle, Ada, Canyon, and Owyhee Counties, Idaho: Idaho Geological Survey Geological Map GM-21, 1:24,000.

Bonnichsen, B., and Godchaux, M.M., 2002, Late Miocene, Pliocene, and Pleistocene geology of southwestern Idaho with emphasis on basalts in the Bruneau-Jarbidge, Twin Falls, and western Snake River Plain regions, *in* Bonnichsen, B., White, C.M., and McCurry, M., eds., Tectonic and magmatic evolution of the Snake River Plain volcanic province: Idaho Geological Survey Bulletin 30, p. 233–312.

Bonnichsen, B., and Kauffman, D.F., 1987, Physical features of rhyolite lava flows in the Snake River Plain volcanic province, southwestern Idaho, *in* Fink, J.H., ed., The emplacement of silicic domes and lava flows: Geological Society of America Special Paper 212, p. 119–145.

Branney, M.J., and Kokelaar, B.P., 1992, A reappraisal of ignimbrite emplacement—Progressive aggradation and changes from particulate to non-particulate flow during emplacement of high-grade ignimbrite: Bulletin of Volcanology, v. 54, p. 504–520.

Branney, M.J., and Kokelaar, B.P., 2002, Pryoclastic density currents and the sedimentation of ignimbrites: Geological Society of London Memoir 27, 143 p.

Cummings, M.L., Evans, J.G., Ferns, M.L., and Lees, K.R., 2000, Stratigraphic and structural evolution of the middle Miocene synvolcanic Oregon–Idaho graben: Geological Society of America Bulletin, v. 112, p. 668–682.

Ekren, E.B., McIntyre, D.H., and Bennett, E.H., 1984, High-temperature, large-volume, lavalike ash-flow tuffs without calderas in southwestern Idaho: U.S. Geological Survey, Professional Paper 1272, 76 p.

Ekren, E.B., McIntyre, D.H., Bennett, E.H., and Malde, H.E., 1981, Geologic map of Owyhee County, Idaho, west of longitude 116 degrees W: U.S. Geological Survey Miscellaneous Investigations Series Map I-1256, 1:125,000.

Ferns, M.L., Evans, J.G., and Cummings, M.L., 1993, Geologic map of the Mahogany Mountain 30 x 60 minute quadrangle, Malheur County, Oregon, and Owyhee County, Idaho: Oregon Department of Geology and Mineral Industries Geological Map Series GMS-78, 1:100,000.

Godchaux, M.M., and Bonnichsen, B., 2002, Syneruptive magma-water and posteruptive lava-water interactions in the western Snake River Plain, Idaho, during the past 12 million years, *in* Bonnichsen, B., White, C.M., and McCurry, M., eds., Tectonic and magmatic evolution of the Snake River Plain volcanic province: Idaho Geological Survey Bulletin 30, p. 387–434.

Hart, W.K., and Aronson, J.L., 1983, K-Ar ages of rhyolites from the western Snake River Plain area, Oregon, Idaho, and Nevada: Isochron/West, v. 36, p. 17–19.

Jenks, M.D., and Bonnichsen, B., 1989, Subaqueous basalt eruptions into Pliocene Lake Idaho, Snake River Plain, Idaho, *in* Chamberlain, V.E., Breckenridge, R.M., and Bonnichsen, B., eds., Guidebook to the geology of northern and western Idaho and surrounding area: Idaho Geological Survey Bulletin 28, p. 17–34.

McCurry, M., Bonnichsen, B., White, C., Godchaux, M.M., and Hughes, S.S., 1997, Bimodal basalt-rhyolite magmatism in the central and western Snake River Plain, Idaho and Oregon, *in* Link, P.K., and Kowallis, B.J., eds., Proterozoic to recent stratigraphy, tectonics, and volcanology, Utah, Nevada, southern Idaho, and central Mexico: Brigham Young University Geological Studies, v. 42, part 1, p. 381–422.

Perkins, M.E., Nash, W.P., Brown, F.H., and Fleck, R.J., 1995, Fallout tuffs of Trapper Creek, Idaho—A record of Miocene explosive volcanism in the Snake River Plain volcanic province: Geological Society of America Bulletin, v. 107, p. 1484–1506.

Wood, S.H., and Clemens, D.M., 2002, Geologic and tectonic history of the western Snake River Plain, Idaho and Oregon, *in* Bonnichsen, B., White, C.M., and McCurry, M., Tectonic and magmatic evolution of the Snake River Plain volcanic province: Idaho Geological Survey Bulletin 30, p. 69–103.